DISS. ETH No. 16970

Associated MSSM Higgs Production with Heavy Quarks: SUSY-QCD Corrections

&

Impact of A_0 on the mSUGRA Parameter Space

A dissertation submitted to
ETH Zurich

for the degree of
Doctor of Natural Sciences

presented by
Petra Häfliger
Dipl. Phys. ETH
born July 13th, 1976
citizen of Luzern (LU)

accepted on the recommendation of
Prof. Dr. Felicitas Pauss, examiner
PD Dr. Michael Spira, co-examiner

2006

Abstract

The associated neutral Higgs production with heavy quarks in the framework of the minimal supersymmetric extension of the Standard Model (MSSM) is an important process at e^+e^- colliders as well as at hadron colliders. It allows to measure the top Yukawa coupling and, for the bottom quark final state, the tanβ parameter of the MSSM. At the Large Hadron Collider (LHC) the associated neutral MSSM Higgs production with bottom quarks is the dominant Higgs production process for large tanβ values. The leading order (LO) cross sections are plagued by large uncertainties due to the scale dependence. The next to leading order (NLO) corrections within Quantum Chromodynamics (QCD) significantly stabilise the theoretical predictions. However, NLO supersymmetric QCD (SUSY-QCD) corrections, which are the subject of this thesis, are needed to reduce the uncertainties further. In e^+e^- collisions they turn out to range within 10−20% and are thus important for a future International Linear Collider (ILC). At the LHC and the Tevatron these corrections can amount up to 50%. Therefore, including NLO SUSY-QCD corrections can strongly enhance or reduce the predicted cross sections of associated Higgs production with heavy quarks at hadron colliders.

The MSSM based on minimal supergravity models (mSUGRA) provides an excellent cold dark matter (CDM) candidate with the lightest supersymmetric particle, the neutralino. The allowed mSUGRA parameter space can be significantly reduced, if the experiment limits on the CDM relic density, obtained with the WMAP satelite, are taken into account. The impact of the scalar trilinear coupling A_0 on the CDM relic density is explored in this thesis. With a vanishing A_0 and fixed tanβ values, the range of allowed mSUGRA models in the $m_0 - m_{1/2}$ plane shrinks to narrow lines, the WMAP strips. By using fixed but non-vanishing trilinear couplings within ± a few TeVs these lines are shifted significantly in the $m_0 - m_{1/2}$ plane.

Zusammenfassung

Die neutrale Higgs Produktion zusammen mit schweren Quarks in der minimalen supersymmetrischen Erweiterung des Standard Modells (MSSM) ist sowohl für e^+e^- Beschleuniger als auch für Hadron Beschleuniger ein wichtiger Prozess. Er erlaubt, die Top Yukawa Kopplung und für Bottom Quarks im Endzustand den Parameter tanβ des MSSM zu messen. Am Large Hadron Collider (LHC) ist die neutrale Higgs Produktion zusammen mit Bottom Quarks der dominante Higgs Produktions Prozess für grosse tanβ Werte. Die Wirkungsquerschnitte in führender Ordnung (LO) weisen grosse Unsicherheiten aufgrund der Skalenabhängigkeit auf. Die nächst höheren (NLO) Korrekturen innerhalb der Quanten-Chromodynamik (QCD) stabilisieren die theoretische Vorhersage deutlich. Trotzdem sind NLO supersymmetrischen QCD (SUSY-QCD) Korrekturen, welche das Thema dieser Arbeit sind, notwendig, um die Unsicherheiten weiter zu reduzieren. In e^+e^- Kollisionen stellt sich heraus, dass sie von der Grössenordung 10–20% sind und daher für einen zukünftigen Internationalen Linearbeschleuniger (ILC) von Bedeutung. Am LHC und am Tevatron betragen diese Korrekturen bis zu 50%. Daher können die vorhergesagten Wirkungsquerschnitte für die neutrale Higgs Produktion zusammen mit schweren Quarks an Hadron Beschleunigern durch einbeziehen der NLO SUSY-QCD Korrekturen stark erhöht oder reduziert werden.

Das MSSM basierend auf minimalen Supergravitations Modellen (mSUGRA) bietet mit dem leichtesten supersymmetrischen Teilchen, dem Neutralino, einen ausgezeichneten Kandidaten für die kalte dunkle Materie (CDM). Der mSUGRA Parameterraum kann durch die Grenzen an die CDM Dichte, welche aus den Daten des WMAP Satelliten abgleitet werden können, deutlich reduziert werden. Der Einfluss der skalaren trilinearen Kopplung A_0 auf die CDM Dichte wird in dieser Arbeit untersucht. Für einen verschwindenden A_0 und einen festen tanβ Wert schrumpft das erlaubt Gebiet in der $m_0 - m_{1/2}$ Ebene zu schmalen Linien, den WMAP Streifen. Unter der Verwendung fester, aber nicht verschwindenden trilinearen Kopplungen innerhalb $\pm$ einiger TeV's werden diese Linien in der $m_0 - m_{1/2}$ Ebene signifikant verschoben.

Contents

Chapter 1

Introduction

The predictions based on the Standard Model (SM) of elementary particle physics [1, 2] have been widely tested and are in excellent agreement with the data. Its only not yet experimentally established part is the Higgs sector which has been introduced to hide the electroweak symmetry. Thereby, the masses of the gauge bosons and fermions are generated. Although the Higgs mass is not predicted by the theory, an upper and a lower bound can be derived. Furthermore, the LEP2 (e^+e^- collider at $\sqrt{s} = 209$ GeV) data analyses lead to a lower limit of 114.4 GeV at 95% CL.

Despite its impressive success, the SM cannot describe physics up to the Planck scale. Supersymmetry (SUSY) [3] or theories including large extra dimensions [4] are possible candidates for theories beyond the SM. The minimal supersymmetric extention of the SM, the MSSM [5], contains the minimal possible particle content including three neutral and two charged Higgs bosons. The SM particles and their superpartners have exactly the same quantum numbers, except for the spin which differs by 1/2. Since, for example, no superpartner of the electron with a mass of 511 keV has been found, SUSY has to be broken. The mechanism behind this breaking is not yet unterstood. It is usually assumed that the SUSY breaking occurs at a high energy scale. Different breaking models contain different messenger particles, which mediate the breaking effects down to the electroweak scale.

The SM Higgs boson as well as the neutral MSSM Higgs bosons are mainly produced by gluon fusion in hadronic collisions. Additionally, the vector-boson fusion can play an important role in the SM, due to the two additional quarks in the final state. They offer the opportunity to reduce the background significantly. In the MSSM this is an important channel for the light scalar Higgs boson at its upper mass bound as well as for the heavy scalar Higgs boson at its lower mass bound.

Vector-boson fusion and the Higgs-strahlung process dominate the SM and the scalar MSSM Higgs bosons production in e^+e^- collisions. Pair production may play a significant role for the scalar MSSM Higgs bosons, while this is the only relevant production channel for the pseudoscalar Higgs boson, in leading order.

The branching ratios of the SM Higgs boson are completely determined, once the Higgs mass is fixed. The decay channels in the MSSM exhibit a more complicated structure, since they also depend on other parameters than the Higgs masses. The Higgs bosons in both theories can be discovered in their whole mass ranges at the LHC (pp collider at $\sqrt{s} = 14$ TeV). At the Tevatron ($p\bar{p}$ collider at $\sqrt{s} = 2$ TeV), the chance to exclude or discover Higgs bosons is small, since the required integrated luminosity exceeds the expected one. If the LHC finds one or more Higgs bosons, their properties can be explored very precisely at a future ILC (planned e^+e^- collider at $\sqrt{s} \lesssim 1$ TeV).

The associated Higgs production with top quarks can play a crucial role in exploring the light scalar MSSM Higgs boson at the LHC. It provides a good channel to study the top Yukawa coupling. The bottom quark final state can be very important, particularly for large tanβ, due to the enhanced Yukawa couplings to down-type fermions. The leading order (LO) predictions for the cross sections of associated neutral MSSM Higgs production with heavy quarks are plagued by large uncertainties originating from the strong dependence on renormalisation and factorisation scales. Including the next to leading (NLO) corrections within Quantum Chromodynamics (QCD) significantly stabilises the theoretical predictions. However, NLO SUSY-QCD corrections are needed to further reduce these uncertainties. Moreover, they can be large.

At the ILC, the cross section of associated Higgs production with top quarks ranges about two orders of magnitude below the dominant Higgs production process. Nevertheless, it can be measured with an accuracy of some 5%. Thus, this process is one of the most promising channels to measure the top Yukawa coupling with high precision, for the Higgs masses below the top threshold. For large tanβ values, the bottom quark final state offers a possibility to measure tanβ. Since the observables at e^+e^- collisions can be measured with high accuracy, it is mandatory to include higher order corrections.

R-parity conserving SUSY models provide an excellent cold dark matter candidate (CDM), since the lightest SUSY particle, the LSP, is stable. Different SUSY breaking models contain different LSPs, e.g., the lightest neutralino in mSUGRA models. Via the influence of the LSP annihilation cross section on the CDM relic density, the experimental limits on this density, obtained from the WMAP satelite, can constrain the mSUGRA parameter space. The SUSY breaking trilinear scalar coupling A_0 has a strong impact on the annihilation cross section and thereby on the presently allowed mSUGRA parameter space.

This thesis is organised as follows: after a short introduction to the Standard Model, Supersymmetry is described in the main part of Chapter 1. The phenomenology of Higgs boson production and decays at different colliders is discussed in Chapter 2. In Chapter 3 techniques used to perform the calculations are introduced. The NLO SUSY-QCD corrections to associated Higgs production at the ILC are described in detail in Chapter 4, while the corrections at hadron colliders are treated in Chapter 5. The effects of varying the soft breaking trilinear scalar coupling constant A_0 on the allowed mSUGRA parameter space are discussed in Chapter 6. The conclusions are drawn in Chapter 7. Some details are explained in the Appendix.

1.1 The Standard Model

The Standard Model ([1, 2] and e.g. [6] for a review) consists of three components:

1. Matter: The basic constituents of *matter* are the fermionic leptons and quarks (Table 1.1). Both appear in three generations of identical structure[1]:

- Leptons: electrons (e^-), muons (μ^-) and taus (τ^-) with electric charge $Q = -1$ and the electrically neutral associated neutrinos (ν_e, ν_μ and ν_τ).
- Quarks: up (u), charm (c) and top (t) quarks with electric charges $Q = 2/3$, down (d), strange (s) and bottom (b) quarks with $Q = -1/3$.

	particles			quantum numbers				
field	1.gen	2.gen	3.gen	$SU(3)_c$	$SU(2)_L$	I_3	Q	Y
f_L	$\begin{pmatrix} \nu_e \\ e^- \end{pmatrix}_L$	$\begin{pmatrix} \nu_\mu \\ \mu^- \end{pmatrix}_L$	$\begin{pmatrix} \nu_\tau \\ \tau^- \end{pmatrix}_L$	1	2	$1/2$ $-1/2$	0 -1	-1
	$\begin{pmatrix} u \\ d \end{pmatrix}_L$	$\begin{pmatrix} c \\ s \end{pmatrix}_L$	$\begin{pmatrix} t \\ b \end{pmatrix}_L$	3	2	$1/2$ $-1/2$	$2/3$ $-1/3$	$1/3$
f_R	e_R^-	μ_R^-	τ_R^-	1	1	0	-1	-2
	u_R	c_R	t_R	3	1	0	$2/3$	$4/3$
	d_R	s_R	b_R	3	1	0	$-1/3$	$-2/3$

Table 1.1: *Fermionic particle content of the SM.*

Each generation consists of a lefthanded $SU(2)_L$ doublet f_L with weak isospin $I = 1/2$ and a righthanded $SU(2)_L$ singlet f_R with $I = 0$. Every quark appears in three different colour states, it belongs to a $SU(3)_c$ triplet, while the leptons are colourless $SU(3)_c$ singlets. The hypercharge Y is related to the electric charge Q and the third component of the weak isospin I_3 by the Gell-Mann-Nishijima relation $Q = I_3 + Y/2$. These fermions and their antiparticles[2] have all been experimentally identified [7].

2. Forces: Four different *forces* act between leptons and quarks (Figure 1.1). The electromagnetic and the weak interactions can be unified as the electroweak interactions [1].

[1]Neutrino-experiments using atmospheric, solar as well as ν from reactors have demonstrated that also neutrinos are massive, thus they should have a righthanded component as well. However, in the SM they are defined to be massless.

[2]For each particle exists an associated antiparticle with identical quantum numbers, but opposite charge.

The physical mass eigenstates $W^{\pm}, Z$ and γ are a mixture of the gauge field B^{μ} corresponding to the hypercharge interaction and the three vector fields $W_{\mu}^{1,2,3}$, related to the weak isospin interaction. The mixing is fixed by the Weinberg angle θ_W:

$$W_{\mu}^{\pm} = \frac{1}{\sqrt{2}}\left(W_{\mu}^{1} \mp iW_{\mu}^{2}\right), \qquad I_3 = \pm 1,$$
$$\begin{pmatrix} A_{\mu} \\ Z_{\mu} \end{pmatrix} = \begin{pmatrix} \cos\theta_W & \sin\theta_W \\ -\sin\theta_W & \cos\theta_W \end{pmatrix} \begin{pmatrix} B_{\mu} \\ W_{\mu}^{3} \end{pmatrix}, \qquad I_3 = 0.$$

In the SM, the electroweak interactions are combined with the strong interactions, the QCD [2]. Both forces are associated with spin–1 fields, the gauge bosons, while gravity is, according to general relativity, mediated by a spin–2 field, the graviton. The latter cannot yet be interpreted as a proper quantum phenomenon and is not included in the SM.

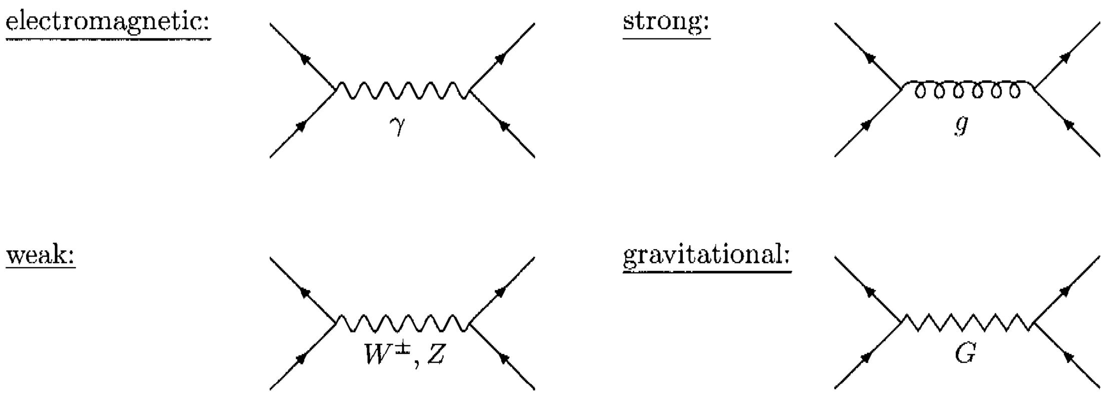

Figure 1.1: *Forces acting between the fermionic particles of the SM.*

The theories of electroweak and strong interactions can be formulated as quantum gauge field theories [8]: the fields are attributed to representations of the symmetry group, while the interactions of the gauge fields with fermionic matter and their self-interactions are determined by the gauge symmetry. The SM is based on the gauge group product $SU(3)_c \times SU(2)_L \times U(1)_Y$. The $SU(3)_c$ is the symmetry group of the non-abelian strong interactions, while $SU(2)_L \times U(1)_Y$ represents the electroweak interactions. The Lagrangian describing the SM is invariant under any local gauge transformation corresponding to this product of groups.

Pure gauge field theories include only massless gauge bosons. The introduction of explicit mass terms in the Lagrangian destroys the gauge invariance and thereby the renormalisability of the theory. However, experimental evidences require the electroweak gauge bosons $W^{\pm}$ and Z to be massive [9], thus the gauge group $SU(2)_L \times U(1)_Y$ is not visible in the physical states. How the electroweak symmetry is hidden is one of the fundamental questions of particle physics. The most attractive way suggested so far is to introduce a

Higgs sector [10], which hides the gauge symmetry, but leaves the theory renormalisable[3]. The gluons and photons are massless, so that the $SU(3)_c \times U(1)_{\text{elm}}$ symmetries remain visible in the physical states and interactions.

3. Higgs mechanism: If the fundamental particles are requested to be weakly interacting up to high energies, the electroweak symmetry has to be spontaneously broken by the implementation of one or more fundamental scalar Higgs bosons (for a review of electroweak symmetry breaking and Higgs physics see e.g. [12]). An alternative to spontaneous symmetry breaking[4] would be dynamical breaking by a new strong force at the interaction scale $\Lambda \sim 1$ TeV [13] leading to non-perturbative physics in analogy to chiral symmetry breaking in QCD.

In the SM, a complex $SU(2)_L$ Higgs doublet

$$\phi \equiv \frac{1}{\sqrt{2}} \begin{pmatrix} \phi_1 + i\phi_2 \\ \phi_3 + i\phi_4 \end{pmatrix}$$

with the four real fields $\phi_{1,\dots,4}$ is introduced. The Higgs Lagrangian

$$\mathcal{L}_{\mathrm{H}} = (\partial_\mu\phi)^\dagger(\partial^\mu\phi) - \mu^2\phi^\dagger\phi - \lambda/2(\phi^\dagger\phi)^2 = (\partial_\mu\phi)^\dagger(\partial^\mu\phi) - V(\phi) \tag{1.1}$$

is invariant under *global* $SU(2)_L \times U(1)_Y$ phase transformations[5]

$$\phi \longrightarrow \phi' = e^{i\alpha_a\sigma_a/2 + i\beta Y/2}\phi,$$

with $a = 1,2,3$. The partial derivatives are defined by $\partial_\mu \equiv (\frac{\partial}{\partial t}, \nabla)$ and $\partial^\mu \equiv (\frac{\partial}{\partial t}, -\nabla)$, respectively. λ is the quartic Higgs coupling constant and for $\mu^2 > 0$ the Lagrangian $\mathcal{L}_H$ in equation (1.1) describes a scalar field with mass μ. To implement *local* $SU(2)_L \times U(1)_Y$ invariance $[\alpha_a,\ \beta \longrightarrow \alpha_a(x),\ \beta(x)]$ the covariant derivatives

$$D_\mu = \partial_\mu + i\,g\,\frac{\sigma_a}{2}\,\mathbf{W}^a_\mu + i\,g'\,\frac{Y}{2}\,B_\mu$$

have to be introduced to replace the partial derivatives.

The Higgs potential $V(\phi)$ in equation (1.1) possesses, if $\lambda > 0$ and $\mu^2 < 0$, an infinite number of non-trivial minima $|\phi|^2 \equiv v^2/2 = -\mu^2/\lambda$. The fluctuation $H(x)$ around any of these ground states defines the physical *Higgs field.* Thus, the Higgs doublet ϕ is parameterised by the four real fields[6] $\theta_1, \theta_2, \theta_3$ and H:

$$\phi(x) \equiv e^{-i\sigma_a\,\theta_a(x)/v}\,\frac{1}{\sqrt{2}} \begin{pmatrix} 0 \\ v + H(x) \end{pmatrix}.$$

[3]The renormalisability of the SM has been proven by 't Hooft and Veltman [11].

[4]For global symmetries *spontaneous symmetry breaking* means that the symmetry is broken: $\langle\phi\rangle \neq 0$ and a goldstone boson appears in the spectrum, whereas for local symmetry it means that the symmetry is hidden: $\langle\phi\rangle = 0$, but $\langle|\phi|^2\rangle \neq 0$ and a would-be goldstone boson appears.

[5]α_a, β are gauge parameters of the groups $SU(2)_L$ and $U(1)_Y$, respectively. The Pauli matrices $\sigma_a/2$ are the generators of $SU(2)_L$ and the hypercharge Y is the generator of $U(1)_Y$.

[6]With an expansion for small field strength and the explicit form of the Pauli matrices the correlation between the four component $\phi_{1,\dots,4}$ of the Higgs doublet and the four fields $\theta_{1,2,3}$ and H are given by: $\phi_1 \propto -\theta_2$, $\phi_2 \propto -\theta_1, \phi_3 \propto H$, $\phi_4 \propto \theta_3$.

The coefficient $e^{-i\sigma_a\theta_a(x)/v}$ can be absorbed by a gauge transformation. By fixing the gauge, one special minimum is selected, the $SU(2)_L$ symmetry is hidden and the preservation of gauge symmetry renders the theory renormalisable. The $SU(2)_L$ gauge bosons acquire their masses by absorption of the three fields θ_a, the massless would-be goldstone bosons. The scalar degrees of freedom appear as the longitudinal polarisation of the massive gauge bosons. The masses of the fermions are generated by Yukawa interactions with the Higgs field. The photon is the only massless gauge boson of the electroweak sector: the gauge group $U(1)_{\text{elm}}$ is the only visible symmetry of the electroweak interaction[7].

1.1.1 SM Lagrangian

The Lagrangian of the SM including the Higgs sector can be written as:

$$\begin{aligned}\mathcal{L}_{\text{SM}} = & - \frac{1}{4}\mathbf{W}_{\mu\nu}\mathbf{W}^{\mu\nu} - \frac{1}{4}B_{\mu\nu}B^{\mu\nu} - \frac{1}{4}\mathbf{G}_{\mu\nu}\mathbf{G}^{\mu\nu} \\ & + \sum_f \left[\bar{f}(i\not{D})\,f - g_f\,\bar{f}_L\,(\phi+\phi_c)\,f_R + h.c.\right] \\ & + |D_\mu\,\phi|^2 - \frac{\lambda}{2}\left(|\phi|^2 - \frac{v^2}{2}\right)^2 . \end{aligned} \tag{1.2}$$

with the charge conjugated Higgs doublet $\phi_c \equiv i\sigma_2\phi^*$. The covariant derivatives including all three gauge interactions are defined by[8]:

$$D_\mu = \partial_\mu + i\,g\,\frac{\sigma_a}{2}\,\mathbf{W}^a_\mu + i\,g'\,\frac{Y}{2}\,B_\mu + g_s\,\frac{\lambda_b}{2}\,\mathbf{G}^b_\mu,$$

The first row of equation (1.2) contains the kinetic energies and self-interactions of the gauge bosons[9] $\mathbf{W}_\mu$, B_μ and $\mathbf{G}_\mu$. The second line covers the fermionic sector with the kinetic energies of the fermions, their interactions with the gauge bosons and the Yukawa couplings of the fermions to the Higgs boson with $g_f = \sqrt{2}m_f/v$. Note that the left and right-handed fermions carry different isospin and hypercharge quantum numbers and thus interact differently with the gauge bosons. The masses of the gauge and Higgs bosons as well as the Higgs self-couplings are determined by the terms in the third line with $\lambda = m_H^2/v^2$.

1.1.2 SM Higgs Mass

The only unknown parameter in the Higgs sector of the SM is the mass of the Higgs boson m_H. Although this is not predicted by the theory, an upper and a lower bound can be found (Figure 1.2) [14, 15].

Quantum fluctuations affect the self-interaction of the Higgs boson, leading, for the coupling constant λ, to a dependence on the energy scale μ at which λ is measured. The

[7] This is what is meant by the statement that $SU(2)_L \times U(1)_Y$ is broken down to $U(1)_{\text{elm}}$.

[8] The $\mathbf{G}^b_\mu$ refers to the gluon fields and the Gell-Mann matrices λ_b are the generators of $SU(3)_c$.

[9] The field strength tensors are given by $V_{\mu\nu} = \partial_\nu V_\mu - \partial_\mu V_\nu - ig\,[V_\mu, V_\nu]$ with the vector potentials V_μ and the gauge couplings g_V.

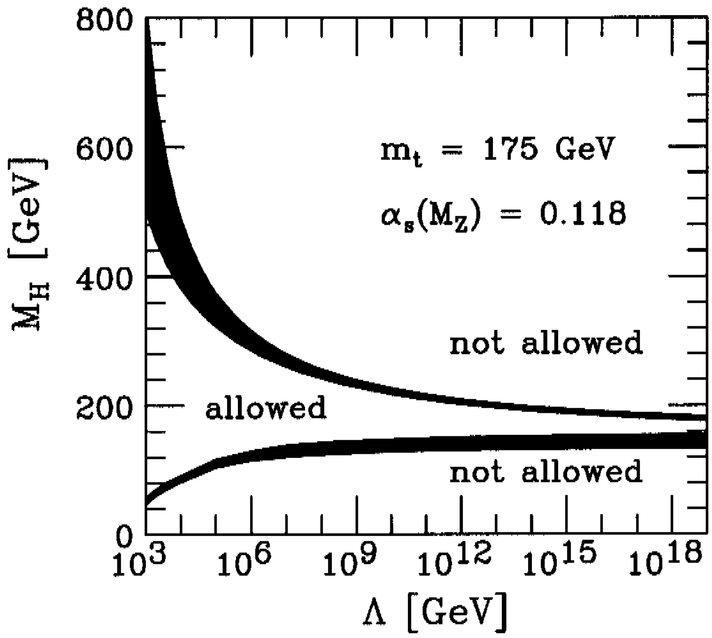

Figure 1.2: *Bounds of the SM Higgs boson mass as functions of the cutoff scale Λ. Above the cutoff the Higgs boson starts to interacting strongly. The lower bound comes from the condition of vacuum stability [14]. The width of the bands shows the uncertainties entering by the strong coupling constant and the top quark mass.*

variation of this effective quartic Higgs coupling $\lambda(\mu)$ is described by the approximate renormalisation group equation (RGE):

$$\frac{d\lambda(\mu)}{d\log(\mu^2/v^2)} \approx \frac{3}{8\pi^2}\left[\lambda^2(\mu) + \lambda(\mu)\, g_t^2(\mu) - g_t^4(\mu)\right],$$
$$\text{with} \quad \lambda(v) = m_H^2/v^2 \quad \text{and} \quad g_t(v) = \sqrt{2}m_t/v\,,$$

where m_t is the mass of the top quark, which is known with an uncertainty of $\pm$ 2 GeV [16]. For large Higgs masses the quartic coupling rises with increasing scale μ, as the β function of the RGE is positive: $d\lambda/d\log(\mu^2/v^2) \propto +\lambda^2$ and becomes divergent at a certain scale $\mu = \Lambda$. This is the cutoff up to which the theory is consistent. The condition $\lambda(E) < \infty$ for any energy $E < \Lambda$ leads to the upper bound on m_H. For small Higgs masses λ decreases with increasing scale μ, due to a negative β function $d\lambda/d\log(\mu^2/v^2) \propto -g_t^4$ and becomes negative at a certain scale $\mu = \Lambda$, so that the electroweak ground state is no longer stable. Thus, to prevent vacuum instability, the Higgs mass has to be larger than a minimal value. A minimal cutoff $\Lambda = 1$ TeV and a cutoff at the GUT scale, respectively, leads to the following allowed mass ranges for the SM Higgs boson [14]:

$$\Lambda = 1 \text{ TeV}: \qquad 55 \text{ GeV} \lesssim m_H \lesssim 700 \text{ GeV},$$
$$= 10^{13} \text{ TeV}: \qquad 130 \text{ GeV} \lesssim m_H \lesssim 190 \text{ GeV}.$$

The direct search for the Higgs boson at the LEP2 collider[10] in the Higgs-strahlung process $e^+e^- \to HZ$ and the vector-boson fusion processes[11] $e^+e^- \to H\nu\bar{\nu}$ and He^+e^-, respectively, resulted in a lower limit of 114.4 GeV at 95% CL [17].

The precision electroweak data, from LEP, SLC[12] and Tevatron strongly support the SM with a weakly coupling Higgs boson as inferred in Figure 1.3a. The "blue-band plot" in Figure 1.3b shows the $\Delta\chi^2$ curve derived from the high energy precision electroweak measurements, as a function of the Higgs mass, assuming the SM to be the correct theory. This global fit predicts a SM Higgs mass of $m_H = 89^{+42}_{-30}$ GeV, at 68% CL without taking the theoretical uncertainties into account [18]. Including experimental and theoretical uncertainties, shown as the blue band, leads to a Higgs mass below 166 GeV at 95% CL. This limit increases to about 200 GeV by including the direct limit of 114.4 GeV. The χ^2 probability is around 18% and it is only little affected by the low energy results such as the NuTeV measurement.

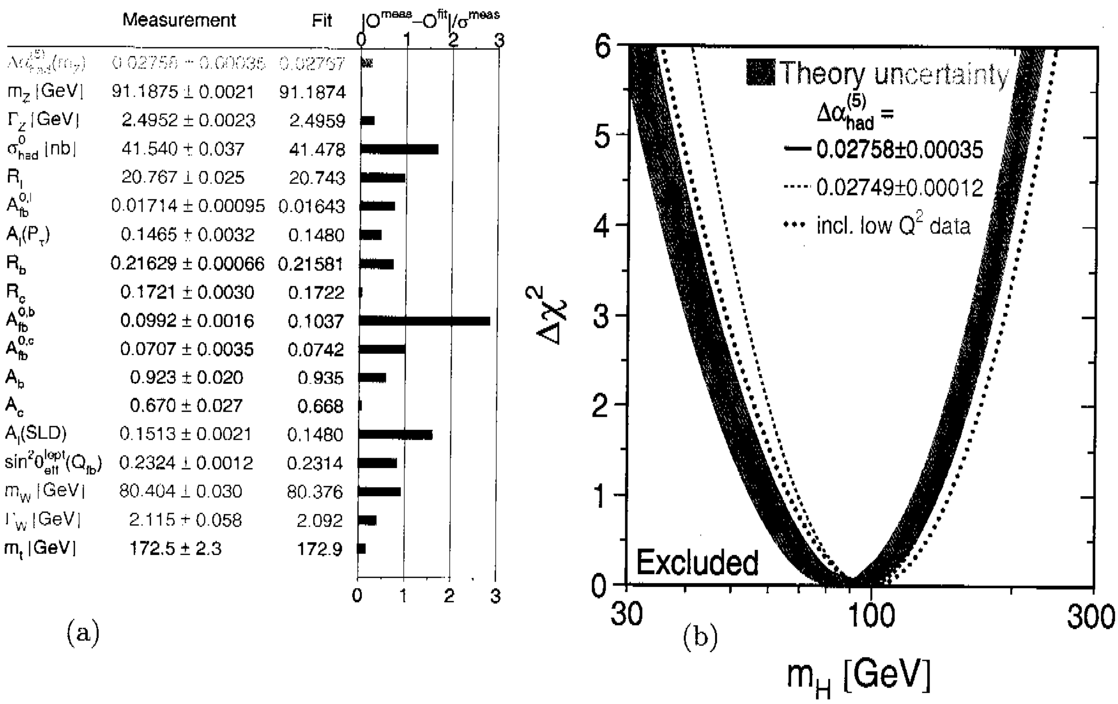

Figure 1.3: *(a) Used data (summer 2006) in the electroweak fit and their agreement with the SM prediction. (b) $\Delta\chi^2$ as a function of the Higgs mass for the electroweak precision data, assuming the SM to be the correct theory [18]. The blue band shows the theoretical uncertainties and the yellow shaded area is excluded by direct searches at LEP2.*

The Tevatron continues the Higgs search up to a mass of $\sim$180 GeV [19] and the LHC can discover a SM Higgs boson up to its theoretical upper limit.

[10] From 1989 to 2000 the Large Electron Positron (LEP) collider at CERN provided e^+e^- collisions at center of mass energies from 90 GeV (LEP1) up to a maximum of 209 GeV (LEP2).

[11] The vector-boson fusion gives small contributions only at the highest LEP2 energies.

[12] The Stanford Linear Collider (SLC) was a two mile linear e^+e^- accelerator running at 90 GeV. The Tevatron and the LHC are discussed in Chapter 2.

1.2 Supersymmetry

Supersymmetry [3] connects fermionic $|F\rangle$ and bosonic states $|B\rangle$:

$$Q|B\rangle = |F\rangle \qquad \text{and} \qquad Q|F\rangle = |B\rangle.$$

The supersymmetric operator Q must carry spin $= 1/2$. The possible forms for such symmetries in interacting quantum field theories (QFTs) are highly restricted by the Haag-Lopuszanski-Sohnius extension [20] of the Coleman-Mandula theorem[13] [21]: SUSY is a nontrivial extension of the Poincaré group. For theories containing chiral fermions this theorem implies that the generator Q and its hermitian conjugate $Q^\dagger$ must satisfy the graded Lie algebra[14] [22]:

$$\begin{aligned} \{Q, Q^\dagger\} &= P^\mu, \\ \{Q, Q\} &= \{Q^\dagger, Q^\dagger\} = 0, \\ [P^\mu, Q] &= [P^\mu, Q^\dagger] = 0. \end{aligned} \tag{1.3}$$

P^μ is the spacetime translation operator and transforms under Lorentz transformation as a spin–1 object. The irreducible representations of the SUSY algebra (1.3) are called *supermultiplets*. The properties $[-P^2, Q] = [-P^2, Q^\dagger] = 0$ imply that members of one supermultiplet must have the same eigenvalues of $-P^2$ and, therefore, the same masses[15]. The SUSY operators also commute with the generators of all gauge transformations, hence the particles and their superpartners have the same gauge quantum numbers: electric charge, weak isospin, hypercharge and colour. Each supermultiplet contains an equal number of fermionic and bosonic degrees of freedom.

1.2.1 SUSY Assessment

Supersymmetric extensions have to include the SM as a low energy limit. They constitute a class of theories with attractive aspects:

- SUSY is the only fundamental new continuous symmetry in addition to the gauge and Poincaré symmetries. The S-Matrix contains the maximal number of different kinds of symmetries [20].
- Provided that fermionic and bosonic interactions, which are related by SUSY have the same coupling strength, the quadratic divergences cancel by Supersymmetry and thus the hierarchy problem is solved, if $M_{\text{SUSY}} \lesssim \mathcal{O}(\text{TeV})$ [5].
- The minimal supersymmetric extension of the SM, the MSSM, predicts, for a sufficiently heavy supersymmetric spectrum, the electroweak observables as well as the SM. The heavier the supersymmetric spectrum the smaller the differences to the SM [23].

[13] No-go theorem: the only conserved bosonic quantities except for generators of the Poincaré group in four dimensional QFTs must be Lorentz scalars. In other words, an interplay between spacetime symmetries and internal symmetries is forbidden for bosonic symmetry operators.

[14] This is the only graded Lie algebra of the S-matrix consistent with relativistic QFT.

[15] SUSY has to be broken, because e.g. no scalar partner of the electron with the same mass and quantum numbers has been found.

- SUSY theories can be embedded in grand unified theories (GUT) [24] in a natural way: the coupling constants which are evolved up to high energies meet at the GUT scale at one point. The MSSM included in a GUT results in a theoretical prediction of the electroweak mixing angle $\sin^2\theta_W^{\text{th}} = 0.2336 \pm 0.0017$ in striking agreement with the experimental value $\sin^2\theta_W^{\text{exp}} = 0.2317 \pm 0.0003$ [25].

- In SUSY GUTs the electroweak symmetry breaking can be of dynamical origin if the mass of the top quark ranges between 100 GeV $\lesssim m_t \lesssim$ 200 GeV [26], which has been experimentally confirmed [16]. Radiative corrections lead, for a positive squared Higgs mass at the GUT scale, to a negative squared Higgs mass at the electroweak scale, by means of RGE evolution, and thus to a non-vanishing vacuum expectation value for the Higgs field.

- Local SUSY automatically includes gravity [27].

- If the lightest SUSY particle (LSP) is stable, it provides a potential candidate for cold dark matter [28].

- Supersymmetric theories contain additional CP-violating sources [29] and has, therefore, the potential to explain the asymmetry between matter and antimatter in the universe [30].

SUSY cannot solve all of the open SM questions:

- Why are there three generations of quarks and leptons? What is the origin of their masses and mixing angles?

- The fine-tuning problem of the cosmological constant [31] is not solved.

And it even creates new problems:

- E.g. no scalar electron with a mass of 511 keV has been found, so that SUSY has to be broken. The mechanism of this breaking is not yet understood. Different breaking mechanisms are discussed in Chapter 1.2.2. Without the introduction of any breaking mechanism all the soft SUSY breaking terms must be introduced by hand leading to a huge number of more than 100 new parameters, which are independent of each other.

- SUSY CP-problem [32]: additional CP phases must be strongly suppressed so that e.g the dipole moment of the neutron does not become too large.

- In general the mass of the gravitino is of the order of the generic SUSY masses and it lives longer than the lifetime of the universe. In many cosmological models this leads to an over critical mass density and to a closed short living universe [34].

1.2.2 SUSY Breaking

If the minimum of the Higgs potential happens to be supersymmetric, the superpartners would have the same mass as their ordinary partners. This is clearly ruled out by experiments. To break SUSY the vacuum can be shifted to a non-supersymmetric state and

SUSY is spontaneously broken or it can be broken explicitly by introducing soft breaking terms. The Girardello-Palumbo mass-sum-rule [35] states that in spontaneous broken SUSY at least one boson mass must be lighter than the mass of the associated fermion. Since this is in contradiction with the experiments SUSY has to be broken explicitely. The mechanism behind this explicit breaking is not yet known. It is usually assumed that the SUSY breaking occurs at a high energy scale, in a so called hidden sector. The effects are then communicated by messenger particles down to the visible sector at the electroweak scale. The different breaking models contain different messenger particles:

- Gravitons: in minimal supergravity (mSUGRA) [36] this communication is mediated by gravitational interactions. All scalar masses, gaugino masses and trilinear scalar couplings are unified at the GUT scale ($M_{\rm GUT} \sim 10^{16}$ GeV) to m_0, $m_{1/2}$ and A_0, respectively. The physics in the visible sector is determined by five parameters: m_0, $m_{1/2}$, A_0, tanβ and sign(μ). This breaking mechanism, as well as these parameters are discussed in more details in Chapter 1.4.

- Gauge bosons: in gauge-mediated SUSY breaking (GMSB) [37] the breaking effects are transmitted by the known SM gauge interactions. The direct coupling of N_{mess} messenger particles, with mass M_{mess} and $SU(3)_c \times SU(2)_L \times U(1)_Y$ quantum numbers, to the hidden sector generates a SUSY breaking spectrum. The breaking scale $\langle F \rangle$ ranges between 10^5 and 10^9 GeV. The SUSY breaking is transmitted to the visible sector by the virtual exchange of messenger particles. The MSSM spectrum is specified by only five parameters: N_{mess}, M_{mess}, $\langle F \rangle$, tanβ and sign(μ). In these models the gravitino $\tilde{G}$ is the lightest SUSY particle (LSP) with a mass $m_{\tilde{G}} \simeq (\sqrt{F}/100\,\mathrm{TeV})^2 \cdot 2.37$ eV.

- No messenger particles: in anomaly-mediated SUSY breaking (AMSB) [38] the SUSY breaking happens on a separate brane in extra dimensions and is communicated to the visible world via the super-Weyl anomaly. The masses of gauginos and squarks are generated through one and two loop effects, respectively. The low energy models are described by only four parameters: m_{aux}, m_0, tanβ and sign(μ). The SUSY particle mass scale is set by m_{aux}, which is the vacuum expectation value of the auxiliary field in the supergravity multiplet. The m_0 is introduced to avoid negative squared slepton masses, and the lightest wino, the superpartner of the W bosons, is the LSP.

As a consequence of this "communication", effective soft breaking terms arise in the visible sector, giving mass to sparticles and generating non-vanishing trilinear couplings among scalar fields. A remarkable aspect of SUSY breaking in a hidden sector is the fact, that the generated masses do not involve terms of the size of the high energy scale that is, the breaking is soft. Thus, no new quadratic divergences are introduced.

1.3 The Minimal Supersymmetric Extension of the SM

The minimal supersymmetric extension of the SM [5], the MSSM, contains the minimal possible particle content including two complex Higgs doublets. This is a necessary condition for an analytical superpotential, if SUSY is conserved, and for the theory to remain free of anomalies:

- The up-type quarks receive their masses from H_u^0, while the down-type quarks obtain them from H_d^0.[16]
- The gauge anomalies cancel if $Tr[I_3^2 Y] = 0$ and $Tr[Y^3] = 0$, where the traces run over all left-handed fermionic degrees of freedom of the chiral supermultiplets. The superpartner of one isospin Higgs doublet has hypercharge $+1$ or -1 leading to a non-vanishing contribution to the above mentioned traces. Anomaly cancellation requires the introduction of two Higgs doublets with opposite hypercharges, so that the total contribution to the traces vanishes and the theory remains free of gauge anomalies.

Supersymmetric theories can be constructed in the *superfield formalism* [39]. A *superfield* contains the field quanta of the SM and their supersymmetric partners as the supermultiplets contain the particles of the SM and their superpartners. There exists two classes of superfields:

- The massless *vector superfield* includes a massless gauge field and a gaugino, a two component fermion field[17].
- The *chiral superfield* contains a two component Weyl spinor and a complex scalar.

The SM gauge bosons and their superpartners, the gauginos, are arranged in the massless *vector superfield* in Table 1.2. The higgsinos and the gauginos are not mass eigenstates. After electroweak symmetry breaking the two charged winos and the two charged higgsinos mix to four charginos $\chi_{1,2}^{\pm}$ with electric charge $+1$ and -1, respectively. The neutral wino, the bino and the two neutral higgsinos mix resulting in four neutralinos $\chi_{1,\ldots,4}^0$.

superfield	$SU(3)_c$	$SU(2)_L$	Y	boson (V)	fermion ($\widetilde{V}$)	notation
$\widehat{\mathbf{G}}^b$	8	1	0	$\mathbf{G}^b$	$\widetilde{\mathbf{G}}^b$	gluon, gluino
$\widehat{\mathbf{W}}^a$	1	3	0	$\mathbf{W}^a$	$\widetilde{\mathbf{W}}^a$	W boson, wino
$\widehat{B}$	1	1	0	B	$\widetilde{B}$	B boson, bino

Table 1.2: *The vector superfields of the MSSM with their quantum numbers. The superpartner of the gauge fields are called gauginos.*

The *chiral superfields* in Table 1.3 contain the fermionic quarks and leptons and their superpartners, the bosonic squarks and sleptons, as well as the Higgs bosons and their superpartners, the higgsinos. Although the left-handed lepton supermultiplet $\widehat{L}$ has exactly the same $SU(3)_c \times SU(2)_L \times U(1)_Y$ quantum numbers as the "down-type" Higgs superfield $\widehat{H}_d$ they cannot be described by a single superfield. It would generate problems with gauge anomalies (analogous to the argument why two Higgs doublets are needed), lepton-number conservation and the mass of at least one neutrino would be in conflict with experimental bounds [40].

[16] In the SM the masses of the down- and up-type quarks are generated by ϕ and $\phi^c = i\sigma_2\phi^*$, respectively.
[17] The neutral gauginos are Majorana particles.

superfield	$SU(3)_c$	$SU(2)_L$	Y	fermion ($f_{L,R}$)	boson ($\tilde{f}_{L,R}$)	notation
$\widehat{Q}$	3	2	$\frac{1}{3}$	(u_L, d_L)	$(\tilde{u}_L, \tilde{d}_L)$	quark, squark
$\widehat{U}^c$	$\bar{3}$	1	$-\frac{4}{3}$	$u_R^\dagger$	$\tilde{u}_R^*$	"
$\widehat{D}^c$	$\bar{3}$	1	$\frac{2}{3}$	$d_R^\dagger$	$\tilde{d}_R^*$	"
$\widehat{L}$	1	2	-1	(ν_L, e_L)	$(\tilde{\nu}_L, \tilde{e}_L)$	lepton, slepton
$\widehat{E}^c$	1	1	2	$e_R^\dagger$	$\tilde{e}_R^*$	"
				fermion ($\widetilde{H}_{u,d}$)	boson ($H_{u,d}$)	
$\widehat{H}_u$	1	2	1	$\widetilde{H}_u = \begin{pmatrix} \widetilde{H}_u^+ \\ \widetilde{H}_u^0 \end{pmatrix}$	$H_u = \begin{pmatrix} H_u^+ \\ H_u^0 \end{pmatrix}$	Higgs, higgsino
$\widehat{H}_d$	1	2	-1	$\widetilde{H}_d = \begin{pmatrix} \widetilde{H}_d^0 \\ \widetilde{H}_d^- \end{pmatrix}$	$H_d = \begin{pmatrix} H_d^0 \\ H_d^- \end{pmatrix}$	"

Table 1.3: *The chiral superfields of the MSSM and their quantum numbers. A standard convention is to define all the chiral supermultiplets in terms of left-handed Weyl spinors, hence the charge conjugated right-handed fermions ($u_R^\dagger, d_R^\dagger, e_R^\dagger$) appear in this Table.*

1.3.1 MSSM Lagrangian

The Lagrangian of the MSSM contains the Lagrangian of the SM, $\mathcal{L}_{\rm SM}$ of equation (1.2) without the Higgs sector, $\mathcal{L}_{\rm H}$ of equation (1.1), and additionally all allowed terms which leave the Lagrangian invariant under supersymmetric transformations as well as renormalisable:

$$\begin{aligned}
\mathcal{L}_{\rm MSSM} = & - \frac{1}{4}\mathbf{W}_{\mu\nu}\mathbf{W}^{\mu\nu} - \frac{1}{4}B_{\mu\nu}B^{\mu\nu} - \frac{1}{4}\mathbf{G}_{\mu\nu}\mathbf{G}^{\mu\nu} \\
& + Tr\left[\overline{\widetilde{\mathbf{W}}}\, i\not{D}\, \widetilde{\mathbf{W}}\right] + \frac{1}{2}\overline{\widetilde{B}}\, i\not{\partial}\, \widetilde{B} + Tr\left[\overline{\widetilde{\mathbf{G}}}\, i\not{D}\, \widetilde{\mathbf{G}}\right] \\
& + \sum_{\psi} \overline{\psi}\,(i\not{D})\,\psi + \sum_{\phi} |D_\mu\,\phi|^2 \\
& + i \sum_{\psi,\phi,V} \frac{g_V}{\sqrt{2}} \left[\overline{\psi_L}\, T^a \widetilde{V}^a\, \phi - \overline{\widetilde{V}^a}\, T^a\, \psi_L\, \phi^*\right] - \frac{1}{2}\sum_{a,V} |g_V\, \phi_i^* T_{ij}^a\, \phi_j|^2 \\
& - \sum_{\phi} \left|\frac{\partial W}{\partial \phi}\right|^2 - \frac{1}{2}\sum_{i,j} \overline{(\psi_{iL})^c}\, \frac{\partial^2 W}{\partial\phi_i \partial\phi_j}\, \psi_{jL} + h.c. \\
& + \mathcal{L}_{\rm soft}.
\end{aligned} \tag{1.4}$$

The bosonic parts of the chiral multiplets are called $\phi = H_{u,d},\ \tilde{f}_{L,R}$ and the fermionic ones $\psi = \widetilde{H}_{u,d},\ f_{L,R}$. The gauginos are denoted as $\widetilde{V}^a$, and T^a are the generators of the different gauge groups[18].

The kinetic energy and the self interactions of the gauge bosons are given in the first

[18] $U(1)_Y:\ T^a = Y/2$, $SU(2)_L:\ T^a = \sigma^a/2$ and $SU(3)_c:\ T^a = \lambda^a/2$.

line of equation (1.4). The fermionic kinetic energy terms for the gauginos and interactions with the SM gauge bosons can be read off from the second line. E.g. the coupling strength of the supersymmetric $\tilde{g}\tilde{g}g$ interaction is exactly the same as for ggg, which is known from QCD. The winos only interact with weak gauge bosons, and the bino, a colour and weak isospin singlet with $Y = 0$, does not interact with any SM gauge boson at all. The higgsinos carry kinetic energy and interact with SM gauge bosons in exactly the same way as the left-handed leptons as inferred in the first term of the third line. The sfermions are bosons, as the Higgs doublets, so that the kinetic energy for both, the masses of the gauge bosons and the interaction of gauge bosons with sfermions arise from the second term in the third line in the Lagrangian. Corresponding to the interaction of two fermions with one gauge boson, interactions of gauginos with fermion-sfermion pairs emerge in the fourth line. The second term in this line is the D-term which generates four sfermion and quartic Higgs boson interactions with the gauge couplings as coupling strengths.

The terms originating from the superpotential W contribute to the Higgs and the higgsino mass terms. They generate the Higgs couplings to sfermions, four sfermion interactions and Yukawa couplings for the SM fermions. There are R-parity conserving as well as violating contributions to the superpotential:

$$\begin{aligned} W &= W_R + W_{\not R}, \qquad (1.5) \\ W_R &= -\varepsilon_{ij}\left[\mu H_u^i H_d^j + \lambda_l H_d^i \widetilde{L}_j \widetilde{E}^c + \lambda_d H_d^i \widetilde{Q}_j \widetilde{D}^c + \lambda_u H_u^i \widetilde{Q}_j \widetilde{U}^c\right], \\ W_{\not R} &= \lambda \widetilde{L}_i \widetilde{L}_j \widetilde{E}_k^c + \lambda' \widetilde{L}_i \widetilde{Q}_j \widetilde{D}_k^c + \lambda'' \widetilde{U}_i^c \widetilde{D}_j^c \widetilde{D}_k^c, \end{aligned}$$

with $\varepsilon_{11} = \varepsilon_{22} = 0$ and $\varepsilon_{12} = -\varepsilon_{21} = -1$. The R-parity, defined as $R = (-1)^{3B+2S+L}$, with $B =$ baryon number, $S =$ spin and $L =$ lepton number is a new discrete symmetry, which distinguishes SM particles ($R = 1$) from their SUSY partners ($R = -1$) [41]. In R-parity conserving models the sparticles can only be produced/annihilated in pairs, so that the lightest SUSY particle, the LSP is stable. The dimensionless Yukawa couplings $\lambda_{l,d,u}$ are 3×3 matrices. However, since the τ leptons, the bottom and top quarks are the heaviest fermions in the SM it is useful to approximate the Yukawa coupling matrices by

$$\lambda_{l,d,u} \approx \begin{pmatrix} 0 & 0 & 0 \\ 0 & 0 & 0 \\ 0 & 0 & \lambda_{\tau,b,t} \end{pmatrix}.$$

This parameterisation also avoids generation mixing through the Yukawa couplings.

The R-parity violating terms do not conserve lepton number nor baryon number in general. From the experimental limits on the proton decay and the decay $\tau^- \to e^-\nu_\tau\bar{\nu}_e$, for example, it is known that at least some of the couplings λ, λ', λ'' must be very small. However, there exist no deeper theoretical reason for them to vanish. Nevertheless, R-parity is often assumed to be conserved, since it provides the LSP as a candidate for cold dark matter. In addition R-parity prevents the proton to decay too rapid.

The soft breaking Lagrangian $\mathcal{L}_{\text{soft}}$ only contains mass terms and interaction terms with coefficients of positive mass dimensions[19], in order to maintain the hierarchy between the

[19]Renormalisability requires the energy dimension of the operators in the Lagrangian to be always ≤ 4.

electroweak and the GUT scale Q_{GUT}:

$$\begin{aligned}\mathcal{L}_{\rm soft} = &- \frac{1}{2} \sum_{a=1,2,3} M_i \,\overline{\widetilde{V}_i^a}\, \widetilde{V}_i^a - m_{H_u}^2 \,|H_u|^2 - m_{H_d}^2 \,|H_d|^2 + B\mu\varepsilon_{ij}(H_u^i\, H_d^j \,+\, H_d^i\, H_u^j) \\ &- \mathbf{m}_{\tilde{l}}^2\, \widetilde{l}_L^*\, \widetilde{l}_L - \mathbf{m}_{\tilde{e}}^2\, \widetilde{e}_R^*\, \widetilde{e}_R - \mathbf{m}_{\tilde{q}}^2\, \widetilde{q}_L^*\, \widetilde{q}_L - \mathbf{m}_{\tilde{u}}^2\, \widetilde{u}_R^*\, \widetilde{u}_R - \mathbf{m}_{\tilde{d}}^2\, \widetilde{d}_R^*\, \widetilde{d}_R \\ &+ \frac{g\,\varepsilon_{ij}}{\sqrt{2} m_W} \left[\frac{m_l}{\cos\beta} \mathbf{A}_l H_d^i\, \widetilde{l}_L^j\, \widetilde{e}_R^* + \frac{m_d}{\cos\beta} \mathbf{A}_d H_d^i\, \widetilde{q}_L^j\, \widetilde{d}_R^* + \frac{m_u}{\sin\beta} \mathbf{A}_u H_u^i\, \widetilde{q}_L^j\, \widetilde{u}_R^* \right].\end{aligned} \tag{1.6}$$

$M_{1,2,3}$ are the bino, wino and gluino mass terms and the $m_{H_{u,d}}$ the Higgs masses. The last term in the first line in equation (1.6) contributes to the Higgs mass matrix, too. The sfermions acquire their large masses from the second row, where the $\mathbf{m}$'s are $3{\times}3$ matrices in the family space. The entries can be complex, but the matrices must be hermitian so that the Lagrangian is real. These mass matrices are sources of potentially dangerous flavour-changing (FC) and CP-violating effects. To avoid these experimentally strongly limited phenomena one can assume that SUSY breaking is universal in the sense that $\mathbf{m} \propto m \cdot \mathbb{1}$ and that no new complex phases are introduced. In addition to the mass terms soft SUSY breaking generates new trilinear scalar couplings. Since they are proportional to the ordinary fermion masses $m_{l,d,u}$ they are only relevant for the third generation $\mathbf{A}_{l,d,u} \to A_{\tau,b,t}$. These terms introduce additional contributions to the Higgs–sfermion–sfermion coupling.

1.3.2 MSSM Sfermion Sector

For every fermion f, with two fermionic degrees of freedom L and R, two scalar bosons $\tilde{f}_{L,R}$, each with one bosonic degree of freedom, are introduced. The index L and R for these bosons are related to the chirality of the fermions. The physical mass eigenstates $\tilde{f}_{1,2}$ are connected to the current eigenstates $\tilde{f}_{L,R}$ by the mixing angles θ_f:

$$\begin{pmatrix} \tilde{f}_1 \\ \tilde{f}_2 \end{pmatrix} = \begin{pmatrix} \cos\theta_f & \sin\theta_f \\ -\sin\theta_f & \cos\theta_f \end{pmatrix} \begin{pmatrix} \tilde{f}_L \\ \tilde{f}_R \end{pmatrix}.$$

The masses and the mixing angles are given by:

$$m_{\tilde{f}_{1,2}}^2 = m_f^2 + \frac{1}{2}\left[m_{\tilde{f}_L}^2 + m_{\tilde{f}_R}^2 \mp \sqrt{\left(m_{\tilde{f}_L}^2 - m_{\tilde{f}_R}^2\right)^2 + 4 m_f^2 \,(A_f - \mu r_f)^2}\,\right],$$

$$\sin(2\theta_f) = \frac{2 m_f\,(A_f - \mu r_f)}{m_{\tilde{f}_1}^2 - m_{\tilde{f}_2}^2}, \qquad \cos(2\theta_f) = \frac{m_{\tilde{f}_L}^2 - m_{\tilde{f}_R}^2}{m_{\tilde{f}_1}^2 - m_{\tilde{f}_2}^2},$$

with $r_f = \cot\beta$ for up-type and $r_f = \tan\beta$ for down-type sfermions. The parameters A_f originate from the soft SUSY breaking and μ is the Higgsino mass parameter. Since the mixing angles are proportional to the masses of the ordinary fermions, mixing effects are only important for the third-generation sfermions.

1.3.3 MSSM Higgs Sector

Contrary to the SM the MSSM contains two complex Higgs doublets H_u and H_d. The masses and the self-couplings of the Higgs fields are given by the Higgs potential:

$$\begin{aligned} V = &+ \left(m_{H_u}^2 + \mu^2\right)|H_u|^2 + \left(m_{H_d}^2 + \mu^2\right)|H_d|^2 + B\mu\left(H_u^+ H_d^- - H_u^0 H_d^0 + h.c\right) \\ &+ \frac{g^2 + g'^2}{8}\left(|H_u|^2 - |H_d|^2\right)^2 + \frac{g^2}{2}\left|H_u^\dagger H_d\right|^2 . \end{aligned}$$

The $m_{H_{u,d}}^2$ and the $B\mu$ terms in the first line are SUSY breaking terms from the soft breaking Lagrangian in equation (1.6). The quartic Higgs couplings are fixed by the gauge couplings g of $SU(2)_L$ and g' of $U(1)_Y$ thus resulting in an upper mass limit for the lightest Higgs boson. This is in strong contrast to the SM, where the quartic Higgs coupling λ is not fixed at all. The electroweak symmetry is hidden if the neutral components of both Higgs doublets acquire vacuum expectation values (VEVs) v_u and v_d, respectively[20]. Due to spontaneous symmetry breaking, five of the original eight degrees of freedom of the two complex $SU(2)_L$ Higgs doublets remain as physical particles in the spectrum:

- *two CP-even, neutral (scalar) Higgs bosons h and H,*
- *one CP-odd, neutral (pseudoscalar) Higgs boson A,*
- *two charged Higgs bosons $H^\pm$.*

The three would-be Goldstone bosons are absorbed by the gauge bosons as in the SM. The two scalar Higgs bosons emerge from mixing of the two neutral CP-even components of the Higgs doublets by the mixing angle α:

$$\begin{pmatrix} h \\ H \end{pmatrix} = \begin{pmatrix} -\sin\alpha & \cos\alpha \\ \cos\alpha & \sin\alpha \end{pmatrix} \begin{pmatrix} \sqrt{2}\,\mathfrak{Re}(H_u^0) - v_u \\ \sqrt{2}\,\mathfrak{Re}(H_d^0) - v_d \end{pmatrix}. \tag{1.7}$$

Due to electroweak symmetry breaking, the Higgs sector of the MSSM can, in leading order, be described by just two free parameters. In general, the ratio of the VEVs $v_u/v_d \equiv \tan\beta$ and the mass of the pseudoscalar Higgs boson m_A are chosen. The other six parameters of the Higgs sector are completely defined by these two variables:

$$\begin{aligned} v_u &= v\cdot\sin\beta \qquad \text{and} \qquad v_d = v\cdot\cos\beta, \\ B\mu &= m_A^2 \sin\beta\cos\beta, \\ m_{H_{\left[\begin{smallmatrix} u \\ d \end{smallmatrix}\right]}}^2 + \mu^2 &= -\frac{m_Z^2}{2} + \left(m_A^2 + m_Z^2\right)\begin{bmatrix}\cos^2\beta \\ \sin^2\beta\end{bmatrix}, \\ \tan 2\alpha &= \tan 2\beta \frac{m_A^2 + m_Z^2}{m_A^2 - m_Z^2} \qquad \text{with } -\pi/2 < \alpha < 0. \end{aligned}$$

The 2×2 mixing matrix in equation (1.7) determines the masses of the scalar Higgs bosons as functions of these two free parameters. At tree level, the light scalar is lighter than the Z boson and should have been observed at LEP2. Considering radiative corrections, whose

[20] $v = \sqrt{v_u^2 + v_d^2} \simeq 246\,\text{GeV}$.

leading universal part[21] grows with the fourth power of the top mass and the logarithm of the stop masses

$$\varepsilon \equiv \frac{3G_F}{\sqrt{2}\pi^2}\frac{m_t^4}{\sin^2\beta}\left\{\log\left(\frac{m_{\tilde{t}_1}m_{\tilde{t}_2}}{m_t^2}\right)+\frac{X_t^2}{M_{\rm SUSY}^2}\left(1-\frac{X_t^2}{12\,M_{\rm SUSY}^2}\right)\right\},$$

with $X_t = A_t - \mu\cot\beta$, the mass of the light scalar is given by

$$m_h^2 = \frac{1}{2}\left\{m_A^2+m_Z^2+\varepsilon-\left[(m_A^2+m_Z^2+\varepsilon)^2 -4m_A^2m_Z^2\cos^2(2\beta)-4\varepsilon\left(m_A^2\sin^2\beta+m_Z^2\cos^2\beta\right)\right]^{1/2}\right\}.$$

The correction ε is positive, as long as $m_{\tilde{t}_1}m_{\tilde{t}_2} \geq m_t^2$ and thus the mass of the light scalar increases with growing top mass and lies beyond the reach of LEP2. Nevertheless, for given values of $\tan\beta$, $m_{\tilde{t}_{1,2}}$, X_t and $M_{\rm SUSY}$ an upper bound for m_h, strongly depending on the top quark mass, can be found:

$$\tan\beta \text{ large and } M_{SUSY} \lesssim 2 \text{ TeV} \implies m_h \lesssim 140 \text{ GeV},$$

where M_{SUSY} means a generic mass of SUSY particles.

These radiative corrections affect also the mass of the heavy scalar but not the masses of the charged Higgs bosons:

$$m_H^2 = m_A^2+m_Z^2-m_h^2+\varepsilon,$$
$$m_{H^\pm}^2 = m_A^2+m_W^2.$$

For small (large) pseudoscalar masses the mass of the heavy (light) scalar Higgs boson is independent of m_A as indicated in Figure 1.4.

Lower limits for the MSSM Higgs boson masses result from the negative direct searches for the processes $e^+e^- \to hZ,\ HZ,\ hA,\ HA,\ h\nu_e\bar{\nu}_e,\ H\nu_e\bar{\nu}_e,\ H^+H^-$ at LEP2 (95% CL) [44]:

$$m_{h/H} \gtrsim 91.0 \text{ GeV}, \qquad m_A \gtrsim 91.9 \text{ GeV} \qquad \text{and} \qquad m_{H^\pm} \gtrsim 78.6 \text{ GeV}.$$

In Figure 1.5 the theoretical upper bound of 130–140 GeV for the light scalar Higgs boson mass is shown. LEP excluded the $\tan\beta$ region between 0.5 and 1.5 as well as a pseudoscalar mass below 92 GeV for a top mass of 174.3 GeV. For a larger top mass the bounds are weakened. The lower bounds of about 92 GeV for $\tan\beta > 10$ and about 114 GeV for small $\tan\beta$ can be read off from Figure 1.5, too.

Since the allowed mass range of the light scalar Higgs boson will be covered by the LHC without any problems, a negative result in SUSY Higgs searches would be a strong indication for the theory to be incomplete or even wrong.

1.3.4 MSSM Couplings

The Yukawa couplings of the neutral Higgs bosons in the MSSM (Table 1.4) are in general defined relative to the Yukawa couplings in the SM[22]: $g_f^{SM} = \sqrt{2}m_f/v$ and $g_V^{SM} = 2m_V^2/v$.

[21] The mixing parameters A_b from soft SUSY breaking (Chapter 1.3.1) is neglected in this approximation.

[22] The pseudoscalar Higgs coupling to fermions receives an additional $-i\gamma_5$ factor.

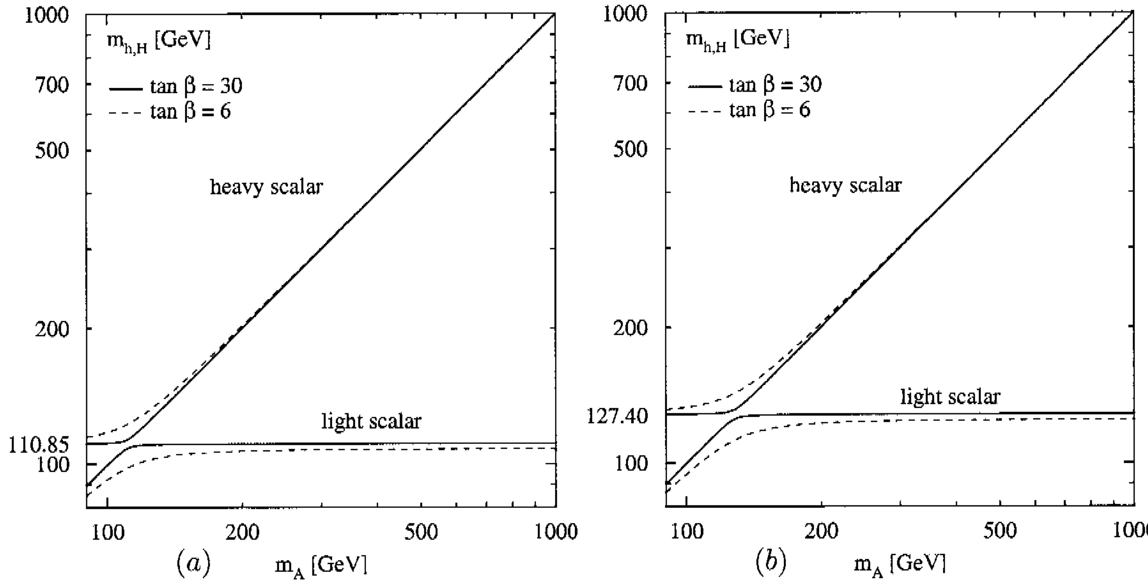

Figure 1.4: *The masses of the scalar Higgs bosons h and H as functions of the pseudoscalar mass m_A for* tanβ = *6 and 30, respectively. The top mass is set to m_t = 174.3 GeV. The other SUSY parameters are chosen in (a) according to the "small α_{eff} scenario" [42] and in (b) to the "maximal mixing scenario" [43]. The different scenarios are described in Chapter 2.3.*

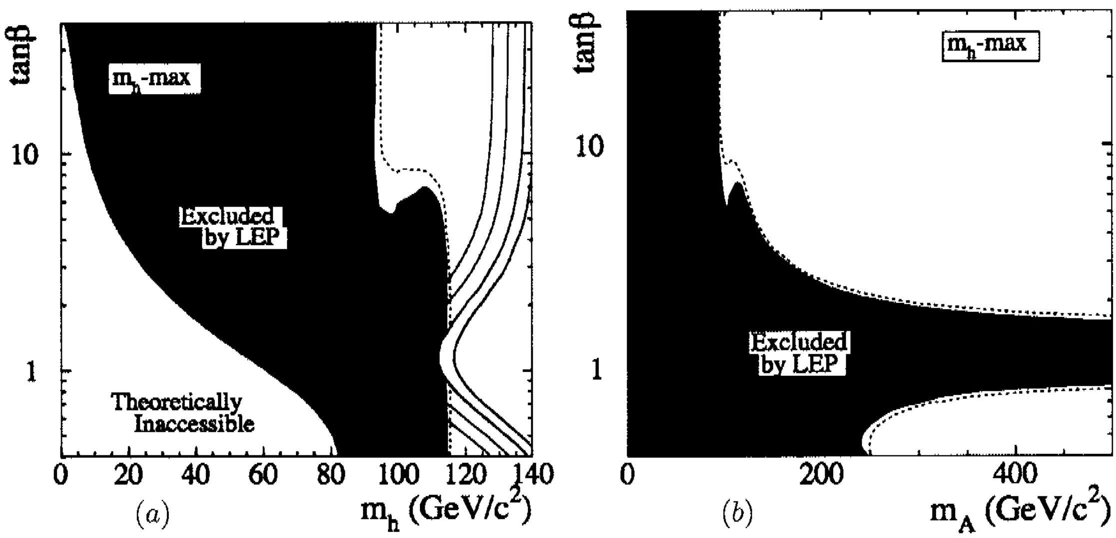

Figure 1.5: *The LEP2 contours for the 95% CL excluding limit for (a) m_h and (b) m_A depending on tanβ for a top mass of 174.3 GeV [19]. The parameters were chosen according to the "maximal mixing scenario" [43] as described in Chapter 2.3.*

model	Higgs boson (ϕ)	g_u^ϕ	g_d^ϕ	g_V^ϕ
SM	H	1	1	1
MSSM	h	$\cos\alpha/\sin\beta$	$-\sin\alpha/\cos\beta$	$\sin(\beta-\alpha)$
	H	$\sin\alpha/\sin\beta$	$\cos\alpha/\cos\beta$	$\cos(\beta-\alpha)$
	A	$1/\tan\beta$	$\tan\beta$	0

Table 1.4: *The couplings of the MSSM Higgs bosons to fermions (u = up-type and d = down-type) and gauge bosons (V = W,Z) relative to the SM couplings.*

With the approximation

$$\tan 2\alpha \;=\; \tan 2\beta\,\frac{m_A^2+m_Z^2}{m_A^2-m_Z^2+\varepsilon/\cos 2\beta}, \qquad \text{with} \quad -\pi/2 < \alpha < 0,$$

the couplings of the scalar Higgs bosons can be estimated in the limits of large and small m_A:

$$\begin{aligned} m_A \gg m_Z: &\quad \alpha \to \beta - \pi/2, \\ m_A \ll m_Z: &\quad \alpha \to -\beta. \end{aligned}$$

For large tanβ the couplings in the MSSM to down-type fermions are strongly increased compared to the SM, while the couplings to the up-type fermions and to the gauge bosons are strongly suppressed (Table 1.5). The behaviour of the different couplings of the scalar Higgs bosons are shown in Figure 1.6 for two different values of tanβ.

limes	Higgs boson (ϕ)	g_u^ϕ	g_d^ϕ	g_V^ϕ
$m_A \to \infty$	h	1	1	1
	H	$-1/\tan\beta$	$\tan\beta$	0
	A	$1/\tan\beta$	$\tan\beta$	0
$m_A \to 0$	h	$1/\tan\beta$	$\tan\beta$	$\sin(2\beta)$
	H	-1	1	$\cos(2\beta)$
	A	$1/\tan\beta$	$\tan\beta$	0

Table 1.5: *The couplings of the MSSM Higgs bosons to fermions and gauge bosons relative to the SM couplings for the limits $m_A \to \infty$ and $m_A \to 0$.*

The couplings of the neutral MSSM Higgs bosons to the up-type and down-type sfermions depend on I_{3f}, the third component of the weak isospin, the fermion charge e_f, the Wein-

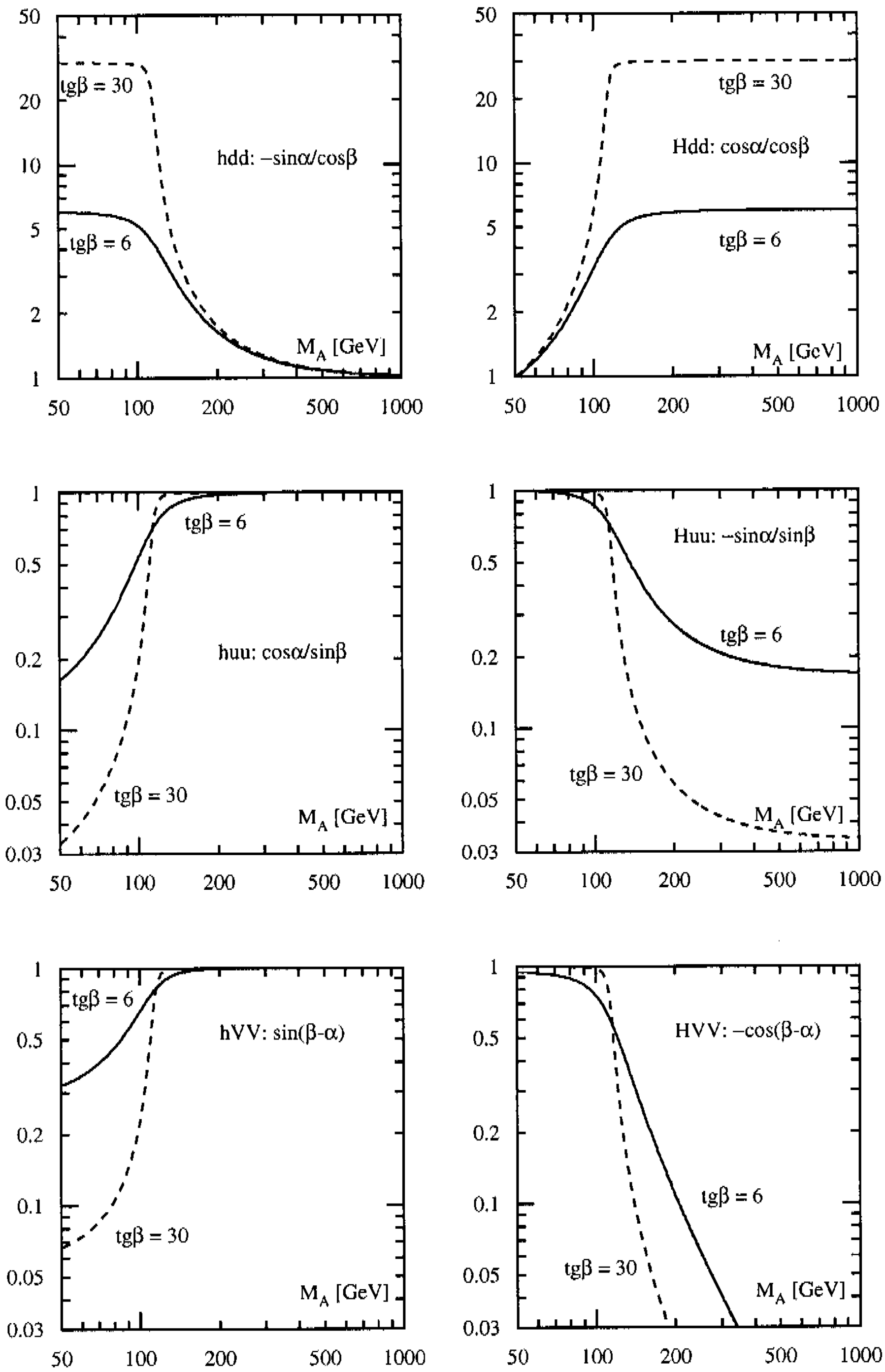

Figure 1.6: *The couplings of the neutral MSSM Higgs bosons as functions of the pseudoscalar mass m_A for two different values of $tan\beta$ = 6 (full lines) and 30 (dashed lines), respectively, and vanishing mixing [12]. The couplings are defined in the Table 1.4.*

berg angle θ_W and the Z boson mass m_Z:

$$\begin{aligned}
g^{\phi}_{\tilde{f}_L \tilde{f}_L} &= m_f^2 g_1^{\phi} + m_Z^2 \left(I_{3f} - e_f \sin^2\theta_W\right) g_2^{\phi}, \\
g^{\phi}_{\tilde{f}_R \tilde{f}_R} &= m_f^2 g_1^{\phi} + m_Z^2\, e_f \sin^2\theta_W\, g_2^{\phi}, \\
g^{\phi}_{\tilde{f}_L \tilde{f}_R} &= -\frac{m_f}{2}\left(\mu g_3^{\phi} - A_f\, g_4^{\phi}\right).
\end{aligned}$$

The coefficients $g^{\phi}_{1,\ldots,4}$ are defined in Table 1.6. The fermion mass dependent part of these couplings originates from the superpotential defined in equation (1.5) while the contributions proportional to the vectorial fraction of the $Zf\bar{f}$ coupling result from the D-terms in the Lagrangian (1.4) after electroweak symmetry breaking.

$\tilde{f}$	Higgs boson (ϕ)	g_1^{ϕ}	g_2^{ϕ}	g_3^{ϕ}	g_4^{ϕ}
up-type	h	$\cos\alpha/\sin\beta$	$-\sin(\alpha+\beta)$	$-\sin\alpha/\sin\beta$	$\cos\alpha/\sin\beta$
	H	$\sin\alpha/\sin\beta$	$\cos(\alpha+\beta)$	$\cos\alpha/\sin\beta$	$\sin\alpha/\sin\beta$
	A	0	0	-1	$1/\tan\beta$
down-type	h	$-\sin\alpha/\cos\beta$	$-\sin(\alpha+\beta)$	$\cos\alpha/\cos\beta$	$-\sin\alpha/\cos\beta$
	H	$\cos\alpha/\cos\beta$	$\cos(\alpha+\beta)$	$\sin\alpha/\cos\beta$	$\cos\alpha/\cos\beta$
	A	0	0	-1	$\tan\beta$

Table 1.6: *Coefficients of the neutral MSSM Higgs boson couplings to sfermions.*

The couplings of a Z boson to a scalar and pseudoscalar Higgs boson pair are given by:

$$g_{ZAh} = \frac{m_Z}{v}\cos(\beta-\alpha) \qquad \text{and} \qquad g_{ZAH} = -\frac{m_Z}{v}\sin(\beta-\alpha).$$

The couplings of sfermions to the neutral SM gauge bosons are defined according to the corresponding couplings of fermions to gauge bosons in the SM with the strong (α_s) and the electromagnetic (α_{elm}) coupling constant:

$$\begin{aligned}
g_{G^a \tilde{f}_i \tilde{f}_j} &= \sqrt{4\pi\alpha_s}\, T^a\, \delta_{ij}, \\
g_{\gamma \tilde{f}_i \tilde{f}_j} &= \sqrt{4\pi\alpha_{\text{elm}}}\, e_f\, \delta_{ij}, \\
g_{Z \tilde{f}_L \tilde{f}_L} &= \frac{\sqrt{4\pi\alpha_{\text{elm}}}}{\sin\theta_W \cos\theta_W}\left(I_{3f} - e_f \sin^2\theta_W\right), \\
g_{Z \tilde{f}_R \tilde{f}_R} &= -\frac{\sqrt{4\pi\alpha_{\text{elm}}}}{\sin\theta_W \cos\theta_W} e_f \sin^2\theta_W, \\
g_{Z \tilde{f}_L \tilde{f}_R} &= 0.
\end{aligned}$$

1.4 Minimal Supergravity Models

The mSUGRA models are based on local Supersymmetry[23]. From the graded Lie algebra in equation (1.3) it can be inferred that invariance under local SUSY transformations implies invariance under local coordinate change, which is the underlying principle of general relativity. Thus, local SUSY naturally includes gravity.

At the GUT scale the masses of the gauginos are unified to a common gaugino mass $m_{1/2}$, the scalar boson masses to a common scalar mass m_0 and the couplings $A_{\tau,b,t}$ to the common trilinear scalar coupling A_0 (Figure 1.7). The absolute value of μ is fixed by the Z boson mass through radiative electroweak symmetry breaking. The Higgs sector depends on tanβ and sign(μ)[24]. Finally, we are left with only five additional input parameters to the SM ones:

$$\boxed{m_0,\ m_{1/2},\ A_0,\ \text{sign}(\mu),\ \tan\beta},$$

in contrast to 105 free parameters in the MSSM without assuming any breaking models.

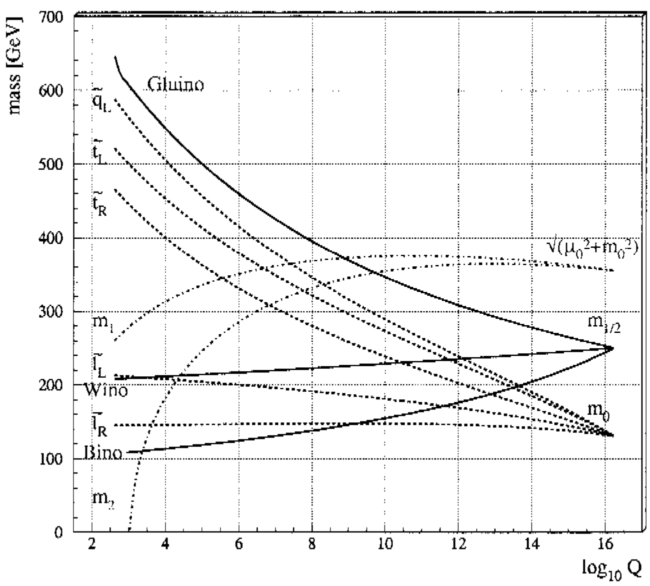

Figure 1.7: *Unification of the sparticle masses at the GUT scale $Q = 10^{16}$ GeV [45]. The common gaugino mass $m_{1/2}$ and the common scalar mass m_0 are input parameters of mSUGRA. One of the squared Higgs masses ($m_1 \hat{=} m_{H_u}$, $m_2 \hat{=} m_{H_d}$) turns out to be negative at the electroweak scale ($Q \sim 100$ GeV), so that the electroweak symmetry is radiatively broken.*

The masses and couplings at the electroweak scale can be derived from the input parameters at the GUT scale by applying the RGEs. The latter also sum possible large

[23] Global SUSY can only be broken spontaneously if there is a positive vacuum energy, leading to a potentially large cosmological constant.

[24] The value of the pseudoscalar Higgs boson mass is fixed by m_0 and $m_{1/2}$ together with tanβ.

logarithms of the type $\log(Q_{\mathrm{GUT}}/m_W)$. This evolution does neither introduce new CP-violating phases nor new FC sources, thus - if universality at the input scale is assumed - SUSY contributions to the FC and CP-violating observables do not violate the present experimental limits.

For the sparticles masses at the electroweak scale there exist some approximate dependencies on the input parameters as shown in Figure 1.8:

- For the squark and slepton masses: $m^2 \sim a_1 \cdot m_0^2 + a_2 \cdot m_{1/2}^2 + a_3 \cdot m_z^2 \cos 2\beta$ approximately holds, where $a_{1,2,3} \in \mathbb{R}$. The left-handed superpartners are generally heavier than the right-handed ones and squarks are often heavier than sleptons. Due to large mixing effects the $\tilde{t}_1$ and the $\tilde{\tau}_1$ are most probably the lightest sfermions.
- Gluino masses are roughly $m_{\tilde{g}} \sim 2.7\, m_{1/2}$, chargino masses $m_{\chi_1^\pm} \sim 0.8\, m_{1/2}$, the lightest neutralino mass $m_{\tilde{\chi}_1^0} \sim 0.4\, m_{1/2}$ and $m_{\tilde{\chi}_2^0} \sim 2\, m_{\tilde{\chi}_1^0} \sim m_{\chi_1^\pm}$.

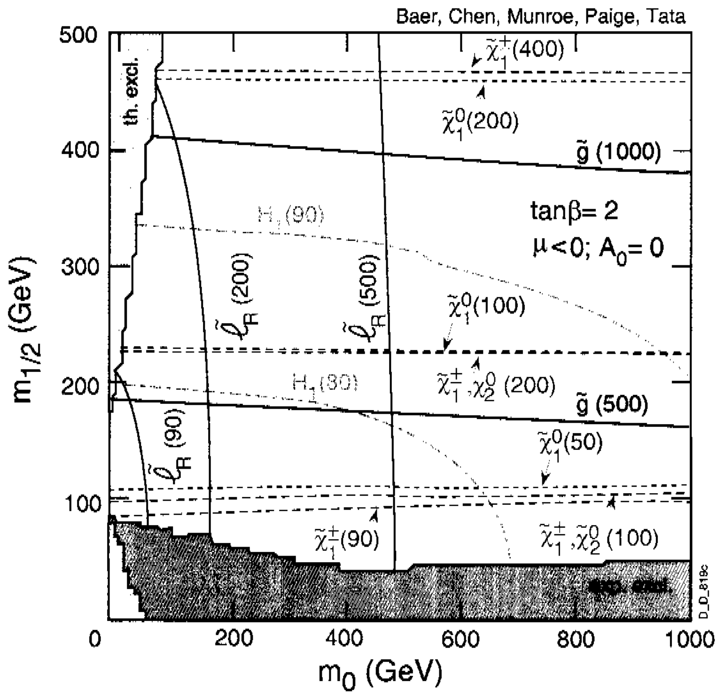

Figure 1.8: *Dependence of the sparticles masses on the input parameters m_0 and $m_{1/2}$ for $\tan\beta$ = 2, sign(μ) < 0 and vanishing A_0 [46]. In parentheses the masses of the sparticles are given.*

Chapter 2

Higgs Phenomenology at Colliders

The different production processes and decay channels of SM and neutral MSSM Higgs bosons at the LHC and the Tevatron as well as at a planned linear e^+e^- collider are discussed. Since associated Higgs production with heavy quarks is the dominant production channel in several scenarios, it is a very important process. The associated Higgs production with top quarks provides one of the most promising channels to measure the top Yukawa couplings for Higgs masses below the top threshold. For large $\tan\beta$ values the associated Higgs production with bottom quarks allows to determine the bottom Yukawa couplings and thereby $\tan\beta$.

2.1 The Colliders

The Large Hadron Collider (LHC), which should start operation end of 2007, is a proton–proton collider with a center of mass collision energy of 14 TeV [47]. One year of running in the low (high) luminosity phase with $\mathcal{L} = 10^{33}\text{cm}^{-2}\text{s}^{-1}$ ($\mathcal{L} = 10^{34}\text{cm}^{-2}\text{s}^{-1}$) delivers an integrated luminosity of 10 fb^{-1} (100 fb^{-1}).

In the year 1983 the Tevatron, a proton–antiproton machine with an energy of ~ 2 TeV, started to take data [48]. The goal is to reach an integrated luminosity of 4–8 fb^{-1} per experiment until shutdown in 2009.

The International Linear Collider (ILC) is a proposed linear electron–positron collider, operating at center of mass energy $\sqrt{s} \lesssim 1$ TeV [49, 50]. The luminosity will be of $\mathcal{O}(10^3)$ times higher than the luminosity at LEP for $\sqrt{s} = 200$ GeV, where it was roughly 30 pb^{-1} per year. The ILC has a rich research potential for deeper investigations of the SM as well as possible extensions. It will allow to explore the properties of the Higgs bosons very precisely if they will be discovered at the LHC.

An overview of the Higgs phenomenology can be found in [51, 52] for the SM and the MSSM Higgs bosons, respectively. A summary of QCD corrections in Higgs physics is given in [53]. The Higgs searches at the LHC are well described in the CMS and ATLAS TDR [47] and at the Tevatron in [54]. Details about Higgs searches at the ILC are collected in [55].

2.2 Production and Decay of the SM Higgs Boson

2.2.1 Production Processes at the LHC

In the whole Higgs mass range below 1 TeV *gluon fusion* $gg \to H$ (Figure 2.1a) [56] represents the dominant production process as shown in Figure 2.2a. Since gluons do not interact with the Higgs boson at tree-level this is a pure loop induces process. The NLO QCD [57] corrections to the top and bottom quark loops increase the total cross section by $50-100\%$ and the NNLO terms [58], only known in the heavy quark approximation[1], contribute further 20%, while the electroweak [59] corrections are small. The theoretical uncertainties of the total cross section are estimated to be $\sim 20\%$ at NNLO, originating in the residual scale dependence, the uncertainties of the parton densities and the neglected quark mass effects.

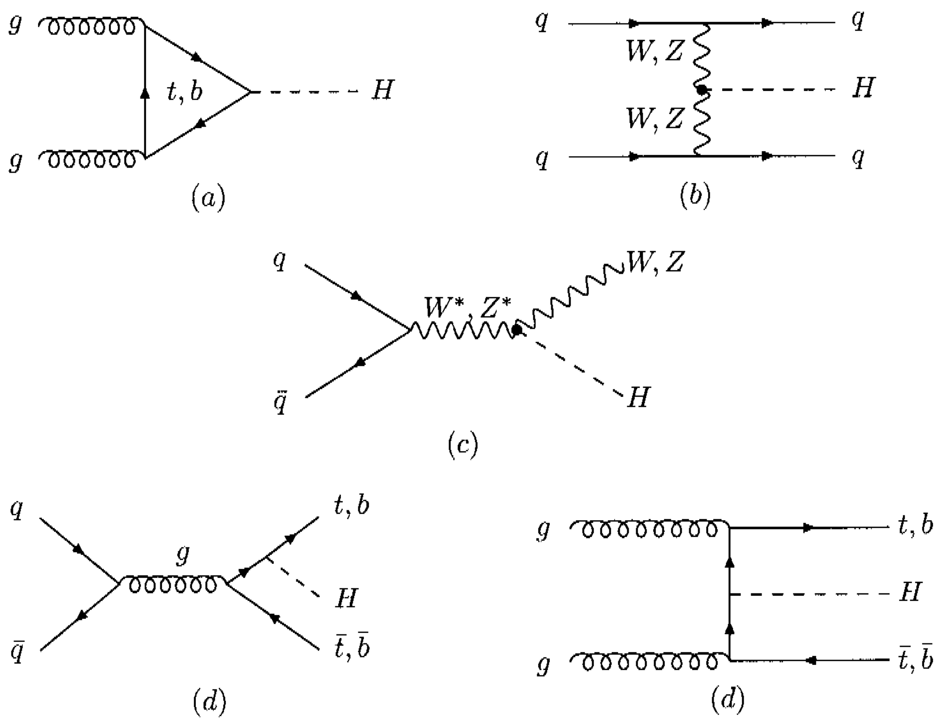

Figure 2.1: *Leading order Feynman diagrams of (a) gluon fusion $gg \to H$, (b) vector-boson fusion $qq \to Hqq$, (c) Higgs-strahlung $q\bar{q} \to HV$ and (d) associated Higgs production with top and bottom quarks $q\bar{q}, gg \to Ht\bar{t}$ and $Hb\bar{b}$, respectively.*

The cross section of *vector-boson fusion* $qq \to Hqq$ (Figure 2.1b) [60] ranges one order below the *gluon fusion* cross section in the intermediate mass range (Figure 2.2a). However, the two additional quarks in the final state offer the opportunity to reduce the background significantly [61]. For $m_H \gtrsim 800$ GeV the two cross sections are of the same

[1] In this approximation an expansion in the inverse quark mass is performed and only the leading term is taken into account. A full NNLO result is not available, thus the NNLO result cannot be trusted in the large Higgs mass range.

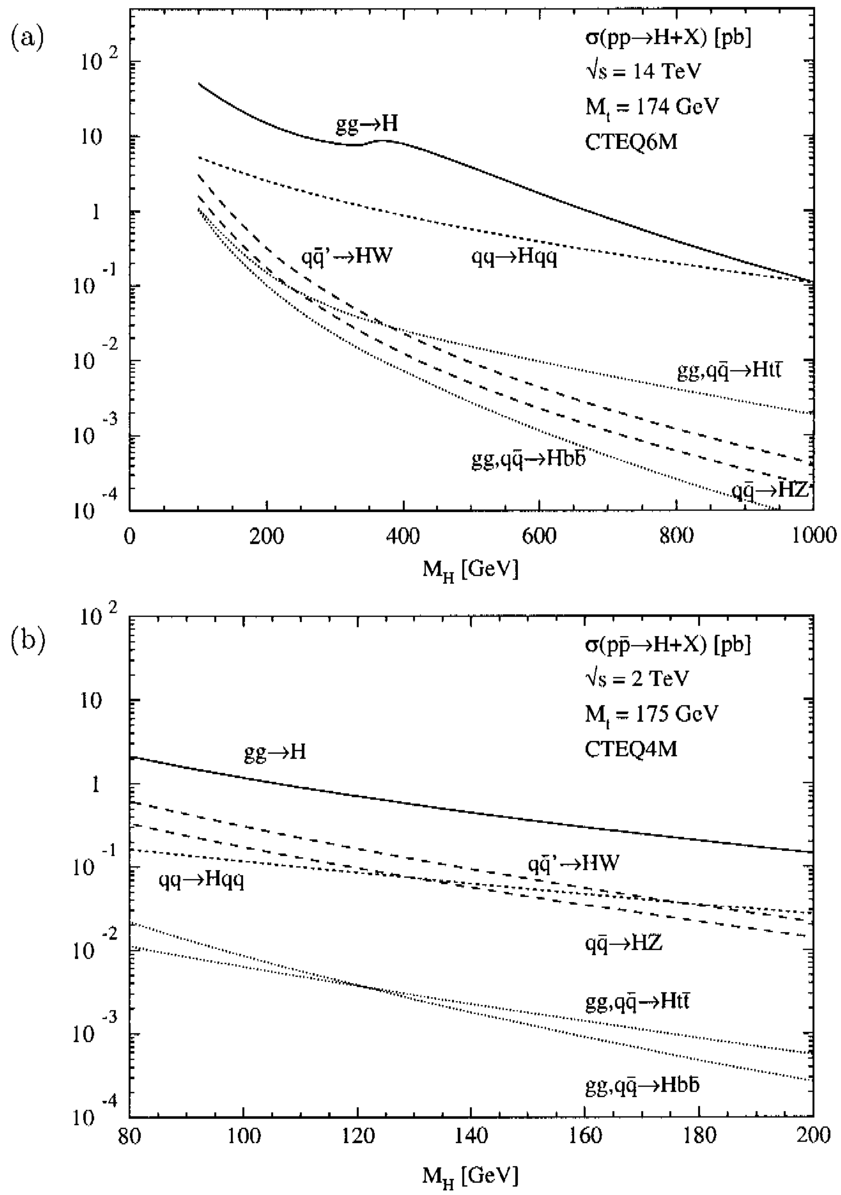

Figure 2.2: *Cross sections of several SM Higgs production channels at (a) the LHC [47] and (b) the Tevatron [54] as a function of the Higgs mass. For the LHC the full QCD-corrected results are shown, while in the plot for the Tevatron the QCD corrections are included only for gluon fusion $gg \to H$, vector-boson fusion $qq \to Hqq$ and Higgs-strahlung $q\bar{q} \to HV$.*

order. The NLO QCD [62] corrections for the total cross section are of $\mathcal{O}(10\%)$ and for the differential cross section of $\mathcal{O}(20\%)$ [63]. The theoretical uncertainties are about 5%.

The *associated Higgs production with top quarks* $q\bar{q}, gg \to Ht\bar{t}$ (Figure 2.1d) [64] is an important production channel for Higgs bosons with a mass below ~ 150 GeV. NLO QCD [65] corrections increase the total cross section by $\sim 20\%$. The predicted signal observability[2] is in excess of $\sim 3\sigma$ for Higgs masses up to 130 GeV. The associated jets help to discriminate signal against QCD background. The *associated Higgs production with bottom quarks* is overwhelmed by the background and thus irrelevant for the SM Higgs boson.

The *Higgs-strahlung* process $q\bar{q} \to HV$ (Figure 2.1c) [66] provides alternative signatures in the intermediate mass range. The NLO QCD [67] corrections are of $\mathcal{O}(30\%)$ and at NNLO [68] they are small. The full electroweak [69] corrections result in a decrease of the total cross section by 5−10%. The total theoretical uncertainties are of $\mathcal{O}(5\%)$.

Figure 2.2 summarises the Higgs production cross sections for (a) the LHC and (b) the Tevatron. For the LHC the full QCD-corrected results are shown, while the plot for the Tevatron contains the full QCD-corrected results up to the LO result of associated Higgs production with heavy quarks. The relevant SM Higgs production cross sections are, at the Tevatron energy, of the order of 0.1−1 pb, while at the LHC they can reach $\mathcal{O}(10)$ pb.

2.2.2 Decay Channels at the LHC

In the SM, the Higgs boson branching ratios are completely determined, once the Higgs boson mass is fixed. The search can be divided into three mass ranges (Figure 2.3a):

(i) The dominant decay of the Higgs boson with a mass $m_H \lesssim 140$ GeV is $H \to b\bar{b}$ with a branching ratio of up to 80%. The QCD corrections to Higgs decays into two quarks are known up to three-loop [71] and the electroweak up to NLO [72]. However, it is very difficult to extract a signal, since the QCD background is about eight orders larger and it cannot be suppressed by adequate cuts [73]. The only possible production processes to observe a signal from $H \to b\bar{b}$ are the associated production with gauge bosons and with $t\bar{t}$ pairs, respectively. The decays into $\tau^+\tau^-$, gg and $c\bar{c}$ pairs cannot be detected due to the large backgrounds. The most promising channel to detect a light SM Higgs boson is the rare decay $H \to \gamma\gamma$ with a branching ration of $\mathcal{O}(10^{-3})$ [74]. The NLO QCD [74] and electroweak [75] corrections are known to be small in the relevant Higgs mass range for the LHC. With an integrated luminosity of $\int\mathcal{L} = 100$ fb^{-1}, of the order of 10^4 $pp \to H(\to \gamma\gamma) + X$ events in the mass range 80 GeV $\lesssim m_H \lesssim 150$ GeV can be expected. However, very good energy and angular resolutions are needed to be able to separate this process from the backgrounds.

(ii) The gold-plated decays $H \to ZZ^{(*)} \to 4l^\pm$ produce very clear signals with small SM backgrounds for 140 GeV $\lesssim m_H \lesssim 800$ GeV [76]. Below the ZZ threshold one of the gauge bosons is off-shell. In the range 170 GeV $\lesssim m_H \lesssim 200$ GeV the $ZZ-$branching ratio drops down to $\sim 2\%$ due to the opening of the decay channels $H \to WW^{(*)} \to l^+l^-\nu\bar{\nu}$. Those are characterised by strong spin correlations between the charged leptons, which provides an important tool for background reduction. These channels play crucial roles for the Higgs search in the range 135 GeV $\lesssim m_H \lesssim 200$ GeV [77]. The electroweak [78] corrections to WW and ZZ decays are of moderate size.

[2] Including full simulation and reconstruction and an integrated luminosity of 100 fb^{-1}.

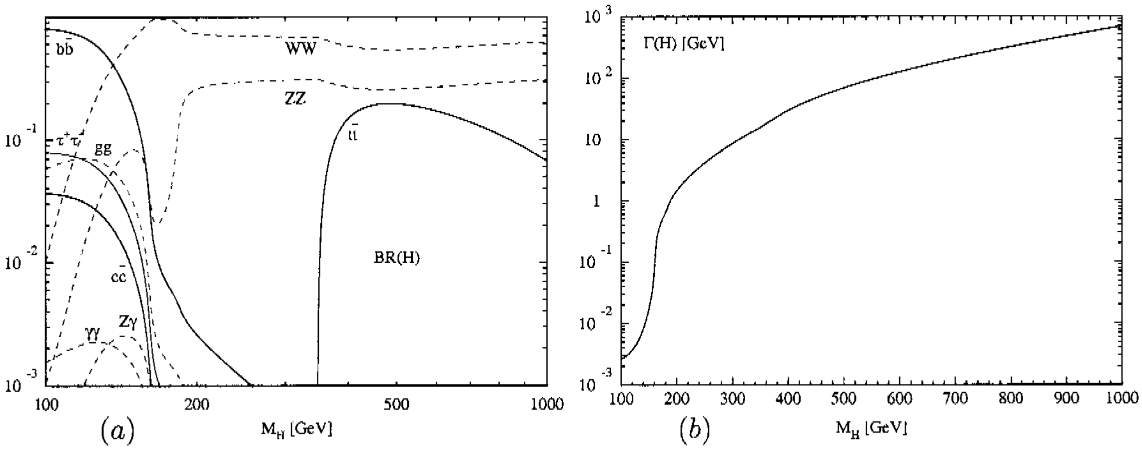

Figure 2.3: *(a) Branching ratios of different decay channels and (b) total decay width of the SM Higgs boson as functions of the Higgs mass. The results have been generated with the program HDECAY [70] and contain higher order corrections.*

(iii) In the mass range $m_H \gtrsim 800$ GeV the best experimental signatures are from $H \rightarrow VV \rightarrow l^+l^-\nu\bar{\nu}$ [47]. From the decay $H \rightarrow t\bar{t}$ no signal can be extracted in spite of a branching ratio of $\sim 10\%$ due to the large backgrounds.

By adding up all possible decay channels the total Higgs boson decay width is obtained (Figure 2.3b). Up to Higgs masses of 140 GeV it is smaller than 10 MeV. However, with the opening of the gauge boson channels, the Higgs state becomes rapidly wider: 1 GeV at the ZZ threshold and it broadens further with increasing mass up to the order of the Higgs mass itself at the TeV mass scale, leading to a questionable interpretation of the Higgs boson as a resonance.

2.2.3 Production Processes and Decay Channels at the Tevatron

For $m_H \lesssim 140$ GeV *gluon fusion* (Figure 2.1a) does not play any role, since both dominant decays $H \rightarrow b\bar{b}$, $\tau^+\tau^-$ of a directly produced light Higgs boson do not lead to detectable signals. For a Higgs mass larger than roughly 140 GeV the decays $H \rightarrow WW^{(*)} \rightarrow l^+l^-\nu\bar{\nu}, l\nu + 2jets$ become dominant and give the direct Higgs production more relevance.

The most important production mechanism at the Tevatron for a Higgs boson below 140 GeV is the *Higgs-strahlung* process (Figure 2.1c) with a cross section of 0.1−1 pb in this mass range (Figure 2.2b).

Although the cross section of *Vector-boson fusion* is of the same order as the *Higgs-strahlung* process (Figure 2.2b) no signal can be extracted from this channel since it can not be discriminated against background.

The *associated Higgs production with top quarks* is strongly limited by kinematics and leads to a less than 2σ effect, and the *associated Higgs production with bottom quarks* is overwhelmed by background.

Figure 2.4 shows the needed integrated luminosity per experiment to either exclude a SM Higgs boson at 95% CL or to discover it at the 3σ and 5σ level, respectively, as a function of the Higgs mass. In the low Higgs mass region the curves are obtained by combining the $l\nu b\bar{b}$, $\nu\bar{\nu}b\bar{b}$ and $l^+l^-b\bar{b}$ channels, while in the high-mass region the $l^\pm l^\pm jj$ and $l^+l^-\nu\bar{\nu}+X$ final states are used. To exclude the SM up to a mass of 180 GeV a combined integrated luminosity of 10 fb^{-1} is needed. With 20 fb^{-1} a 3σ evidence in the combined sensitivity of the two Tevatron experiments can be achieved. To discover a SM Higgs boson with a mass below 130 GeV the integrated luminosity must be $\sim$30 fb^{-1}.

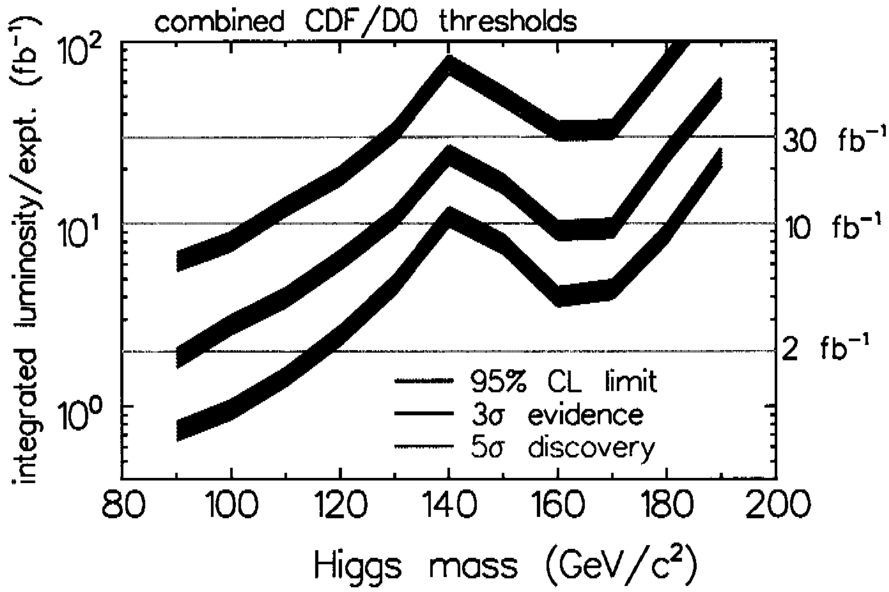

Figure 2.4: *The integrated luminosity required per experiment at the Tevatron, to either exclude a SM Higgs boson at 95% CL or discover it at the 3σ and 5σ level, respectively, as a function of the Higgs mass [48].*

2.2.4 Production Processes at the ILC

The main production mechanisms of the SM Higgs boson in e^+e^- collision are the *Higgs-strahlung* (Figure 2.5a) and the *WW fusion* (Figure 2.5b) [55] processes. The cross section for the *Higgs-strahlung* scales as $1/s$ and dominates at low energies, while the cross section for the *WW fusion* grows logarithmically in s and starts to dominate at higher energies. In Figure 2.6 the cross sections as functions of the Higgs mass for three different center of mass energies $\sqrt{s} = 350, 500$ and 800 GeV show this behaviour. The SM Higgs boson can be discovered up to a mass of about 70% of the $\sqrt{s}$.

The cross section of the *ZZ fusion* process (Figure 2.5b) is suppressed by one order of magnitude compared to the *WW fusion*, due to the ratio of charged to neutral current couplings.

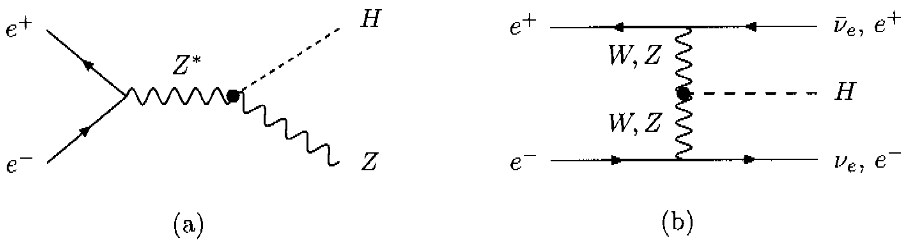

Figure 2.5: *LO Feynman diagrams of (a) the Higgs-strahlung process $e^+e^- \to HZ$, (b) WW fusion $e^+e^- \to H\nu_e\bar{\nu}_e$ and ZZ fusion $e^+e^- \to He^+e^-$.*

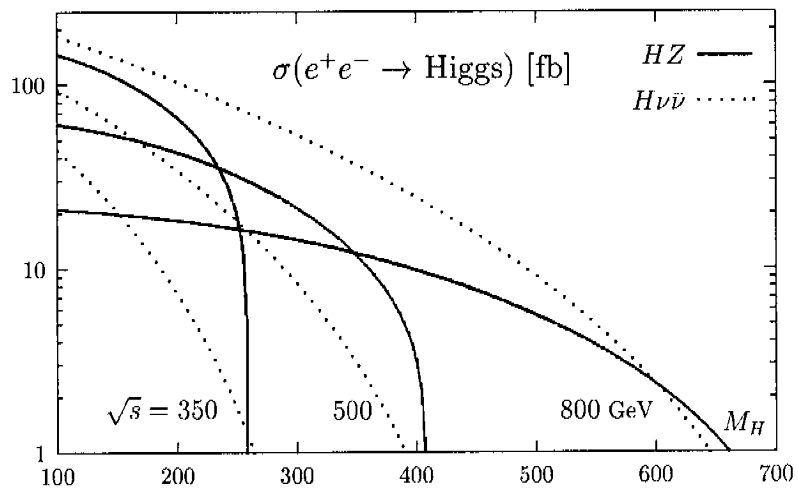

Figure 2.6: *The Higgs-strahlung and WW fusion production cross section vs. the Higgs mass m_H for center of mass energies $\sqrt{s}$ = 350, 500 and 800 GeV [50].*

2.2.5 Decay Channels at the ILC

For a Higgs boson lighter than about 140 GeV the decay into $b\bar{b}$ pairs dominates (Figure 2.3a). The decays into $\tau^+\tau^-$, $c\bar{c}$ and two gluons are suppressed but important to test the scaling of the Higgs couplings with the fermion masses. The running of the quark masses and the QCD corrections to hadronic decays introduce uncertainties.

Between the $VV^{(*)}$ and the $t\bar{t}$ threshold, the Higgs boson decays almost exclusively into $WW^{(*)}$ or $ZZ^{(*)}$ pairs[3]. The top quark and W boson mediated loop decays into $\gamma\gamma$ and $Z\gamma$ final states have small branching ratios of $\mathcal{O}(10^{-3})$. However, they lead to clear signals and are interesting because they are sensitive to new heavy particles.

[3]The factor 2 between the BR of Higgs decay into W^+W^- and ZZ originates in the indistinguishability of the two Z bosons.

2.3 Production and Decay of the Neutral MSSM Higgs Bosons

In this section the supersymmetric spectrum is considered to be heavy, so that the decays into SUSY particles are kinematically forbidden. The neutral MSSM Higgs bosons h, H and A are denoted by ϕ, while $\mathcal{H}$ stays for the scalar Higgs bosons only. The discovery potential of the different production and decay channels strongly depend on the MSSM scenario [52]. Typical constrained models with seven free parameters $M_{\text{SUSY}}, \mu, M_2, m_{\tilde{g}}, A_t$, $\tan\beta$ and m_A are chosen. The top mass is fixed at 174.3 GeV and M_{SUSY} defines a generic SUSY mass. Two typical scenarios are characterised by the stop mixing: $X_t = A_t - \mu \cot\beta$, where A_t is the trilinear scalar stop-Higgs coupling in $\mathcal{L}_{\text{soft}}$ (1.6) and a third one by the mixing angle α of the scalar Higgs sector:

- In the *minimal (stop) mixing* or *no-mixing* scenario it is assumed that there is no mixing between the left and right-handed sfermions. The upper limit for the light scalar Higgs mass is roughly 115 GeV in this scenario. The seven parameters are given by:

  $$\begin{array}{llll} M_{\text{SUSY}} = 1 \text{ TeV}, & \mu = 200 \text{ MeV}, & M_2 = 200 \text{ GeV}, & m_{\tilde{g}} = 0.8\, M_{\text{SUSY}}, \\ X_t^{\text{OS}} = X_t^{\overline{\text{MS}}} = 0, & 0.4 < \tan\beta < 40, & 4 \text{ GeV} < m_A < 1 \text{ TeV}, & \end{array}$$

  with the on-shell and $\overline{\text{MS}}$ renormalised X_t^{OS} and $X_t^{\overline{\text{MS}}}$, respectively.

- The upper limit of the light Higgs mass increased to a maximum of ~ 140 GeV in the *maximal (stop) mixing* scenario, where the parameters are defined as in the previous scenario except of X_t and $\tan\beta$,

  $$X_t^{\text{OS}} = 2\, M_{\text{SUSY}}, \quad X_t^{\overline{\text{MS}}} = \sqrt{6}\, M_{\text{SUSY}}, \quad 4 < \tan\beta < 30.$$

  This scenario provides the largest parameter space and therefore the most conservative exclusion limit among all the CP-conserving scenarios.

- In the *small* α_{eff} scenario the light Higgs boson decays into $b\bar{b}$ and $\tau^+\tau^-$ are suppressed, due to $\tilde{b} - \tilde{g}$ loops. The upper limit of the the light Higgs mass is in this scenario about 110 GeV:

  $$\begin{array}{lll} M_{\text{SUSY}} = 800 \text{ GeV}, & \mu = 2.0 \text{ MeV}, & M_2 = 500 \text{ GeV}, \\ m_{\tilde{g}} = 500 \text{ GeV}, & X_t^{\text{OS}} = -1.1 \text{ TeV}, & X_t^{\overline{\text{MS}}} = -1.2 \text{ TeV}, \\ 0.4 < \tan\beta < 40, & 4 \text{ GeV} < m_A < 1 \text{ TeV}. & \end{array}$$

The expected production rates and decay channels vary rapidly with m_A and $\tan\beta$. However, some features hold in the whole MSSM range:

- $\mathcal{H}VV$ couplings are suppressed compared to the SM and AVV couplings are absent at all (Table 1.4). Thus, the other branching ratios such as $\phi \to \tau\tau$ and $\phi \to t\bar{t}$ are in general enhanced.

- For large $\tan\beta$ the bottom and the τ Yukawa couplings are enhanced (Table 1.4) leading to a dominance of the processes generated by theses couplings.

- Decay modes with more than one Higgs boson involved exist: e.g. $H \to hh$ and $A \to Zh$.

2.3.1 Production Processes at the LHC

The dominant production mechanism for all three neutral MSSM Higgs bosons in the low and moderate $\tan\beta$ range is *gluon fusion* $gg \to \phi$ (Figure 2.7a) [56]. In addition to top and bottom quark loops, stop and sbottom loops contribute for the scalar Higgs bosons[4], as long as the squark masses range below about 400 GeV. The NLO QCD [79] corrections to the quark loops increase the cross section by up to 100% for small $\tan\beta$ and up to about 60% for very large $\tan\beta$. The NNLO QCD [80] corrections for these loops are only known in the heavy quark limit and are thus not valid for large $\tan\beta$. The QCD [81] corrections to the squark loops are only known in the heavy squark approximation and are of about the same size as those to the quark loops. The SUSY-QCD [82] corrections in the limit of heavy squarks and gluinos are small.

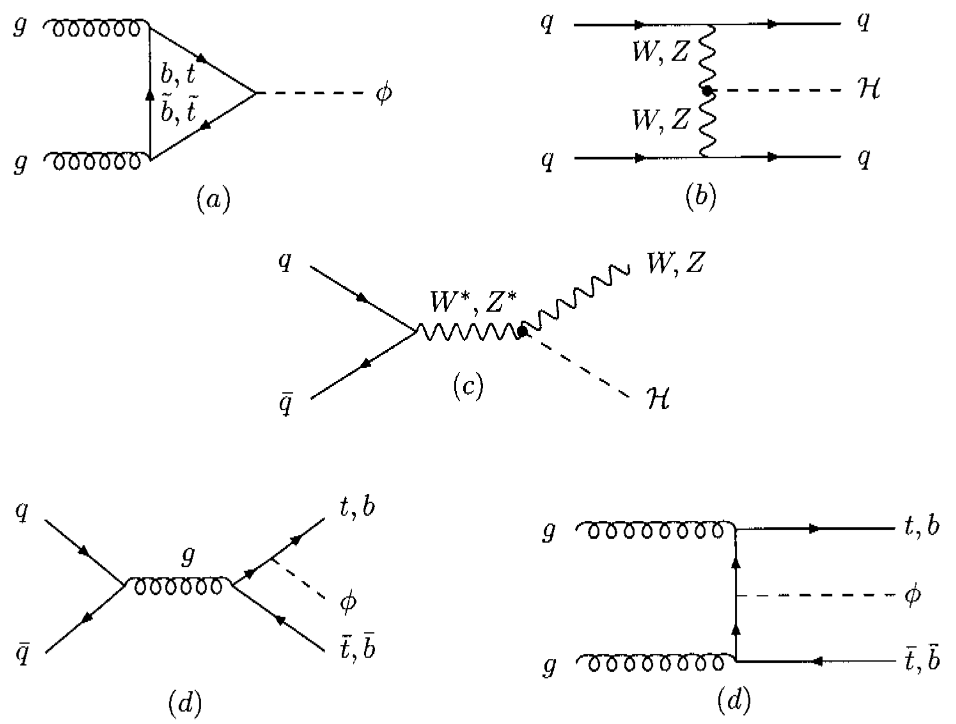

Figure 2.7: *LO Feynman diagrams of (a) gluon fusion $gg \to \phi$, (b) vector-boson fusion $qq \to \mathcal{H}qq$, (c) Higgs-strahlung $q\bar{q} \to \mathcal{H}V$ and (d) associated Higgs production with top and bottom quarks $q\bar{q}, gg \to \phi t\bar{t}$ and $\phi b\bar{b}$, respectively.*

The *vector-boson fusion* processes $qq \to \mathcal{H}qq$ (Figure 2.7b) [83] play an important role only for a light scalar Higgs boson closed to its upper bound, where it becomes SM-like, and for the heavy Higgs bosons at its lower bound as can be read off from Figure 2.8a. In the other regions they are suppressed by the SUSY factors (Table 1.4). The NLO QCD [62]

[4]The pseudoscalar Higgs bosons only couple to a combination of left- and right-handed squarks, while the gluons only couple to two squarks with the same "chirality".

corrections can be inferred from the SM Higgs case and are of the same size: of $\mathcal{O}(10\%)$ for the total cross section and $\sim 20\%$ for the differential one. The SUSY-QCD [84] corrections mediated by virtual gluino and squark exchange at the vertices are small.

In contrast to the SM, the *Higgs-strahlung* processes $q\bar{q} \to \mathcal{H}V$ (Figure 2.7c) [66] do not play a major role for the neutral MSSM Higgs bosons at the LHC. The NLO [67] and NNLO QCD [68] corrections are the same as in the SM and the SUSY-QCD [84] corrections are small, while the SUSY electroweak corrections are unknown.

The *associated Higgs production with top quarks* $q\bar{q}, gg \to \phi t\bar{t}$ (Figure 2.7d) [64] is an important production process[5] only for the light scalar Higgs boson. The NLO QCD [65] corrections are the same as for the SM Higgs boson with modified top and bottom Yukawa couplings and of moderate size. The full NLO SUSY-QCD [85] corrections to the light scalar are of moderate size, too.

For large values of tanβ, the *associated Higgs productions with bottom quarks* $q\bar{q}, gg \to \phi b\bar{b}$ (Figure 2.7d) [64] provide the dominant production processes for all three neutral Higgs bosons (Figure 2.8). The NLO QCD corrections can be taken from the analogous calculations involving top quarks. However, they turn out to be very large [86]. The NLO SUSY-QCD corrections are not yet known and are the subject of this thesis. In Figure 2.9 the 5σ discovery regions for the neutral Higgs bosons produced in association with bottom quarks are shown for an integrated luminosity of 30 fb^{-1} for the CMS detector.

2.3.2 Decay Channels at the LHC

The searches for MSSM Higgs bosons at the LHC are more involved than for the SM Higgs boson (Figures 2.9, 2.10 and 2.11).

(i) In the whole MSSM parameter region with $m_A \gtrsim 100$ GeV the light scalar Higgs boson can be detected by the associated $ht\bar{t}$ production in the $h \to b\bar{b}$ decay. More recent realistic studies show that this channel has not the potential of a discovery channel. However, it is still a very important process to measure the top Yukawa coupling.

(ii) The neutral MSSM Higgs bosons can be discovered for tan$\beta \gtrsim 20$ and $m_A > 100$ GeV in the associated Higgs production with bottom quarks followed by leptonic Higgs decays.

(iii) The light scalar Higgs boson, from direct or associated hW and $ht\bar{t}$ production, can only be discovered in the photonic decay $h \to \gamma\gamma$, if $m_A \gtrsim 200$ GeV.

(iv) For tan$\beta \lesssim 7$ and 100 GeV $\lesssim m_A \lesssim$ 350 GeV the decay channels $H \to ZZ^{(*)} \to 4l^{\pm}$ play a role [87].

[5]The top Yukawa couplings to heavy scalar as well as the pseudoscalar Higgs bosons are suppressed for not too small values of m_A. In addition, there are kinematical limits to produce three particles with masses above ~ 150 GeV.

(a)

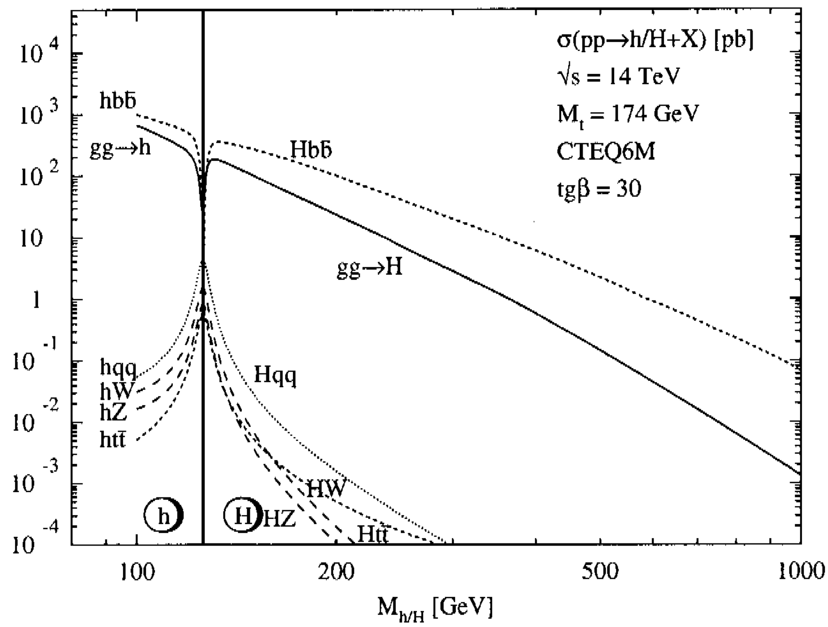

(b)

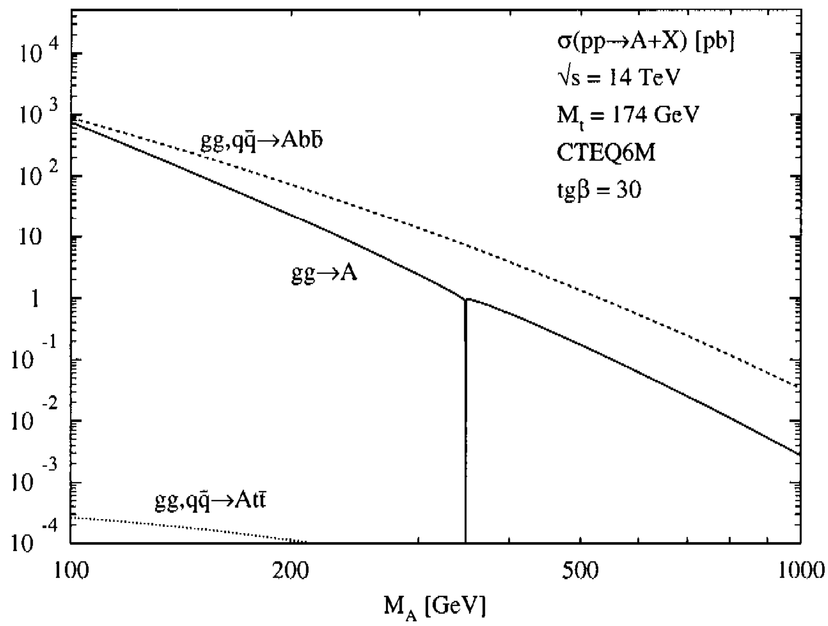

Figure 2.8: *Cross sections of different production channels for (a) the scalar and (b) the pseudoscalar Higgs bosons at the LHC as a function of the Higgs mass for* $\tan\beta = 30$*. For all of these processes the complete QCD corrections at NLO are known and included in the cross sections. For the associated Higgs production with top quarks the NLO SUSY-QCD corrections are only known for the light scalar Higgs boson and for bottom quarks not at all [47]. They are the subject of this thesis.*

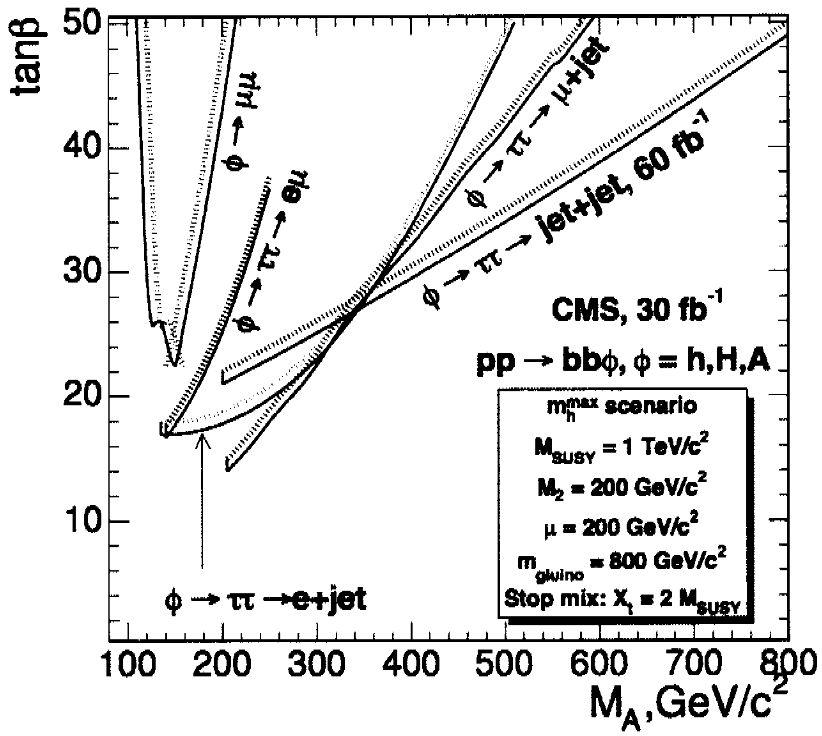

Figure 2.9: *The 5σ discovery regions for the neutral Higgs bosons produced in the associated Higgs production with bottom quarks are shown in the "maximal mixing scenario". An integrated luminosity of 30 fb^{-1} was assumed [47].*

(v) For $\tan\beta \lesssim 3$ and $200 \text{ GeV} \lesssim m_A \lesssim 350 \text{ GeV}$ the pseudoscalar Higgs boson can be found in the decay channels $A \to hZ \to b\bar{b}l^+l^-$ and the heavy scalar one in $H \to hh \to b\bar{b}\gamma\gamma$.

(vi) For large $\tan\beta \gtrsim 6$ and $m_A \gtrsim 100$ GeV the decay channels $H, A \to \tau^+\tau^-$ and $\mu^+\mu^-$ become visible. Unlike in the SM, in the MSSM these processes play a crucial role, since the decays $H \to VV$ are suppressed and $A \to VV$ forbidden, while the down-type Yukawa couplings are enhanced.

(vii) In the region $m_A \gtrsim 200$ GeV and $3 \lesssim \tan\beta \lesssim 7{-}10$ it is very difficult to detect a MSSM Higgs boson except the light one. The other Higgs bosons are too heavy or the signal processes are not separable from the backgrounds. The light scalar can, even including SUSY-QCD corrections, not be distinguished from the SM Higgs boson, if the SUSY particles decouple.

The decay widths of the three neutral Higgs bosons (Figure 2.10c) differ a lot from the width of the SM Higgs boson: for masses below 140 GeV they are much bigger than for the SM Higgs boson and for heavier H and A they are much smaller, strongly depending on the value of $\tan\beta$. However, in contrast to the SM, the decay widths never exceeds about $\mathcal{O}(10 \text{ GeV})$.

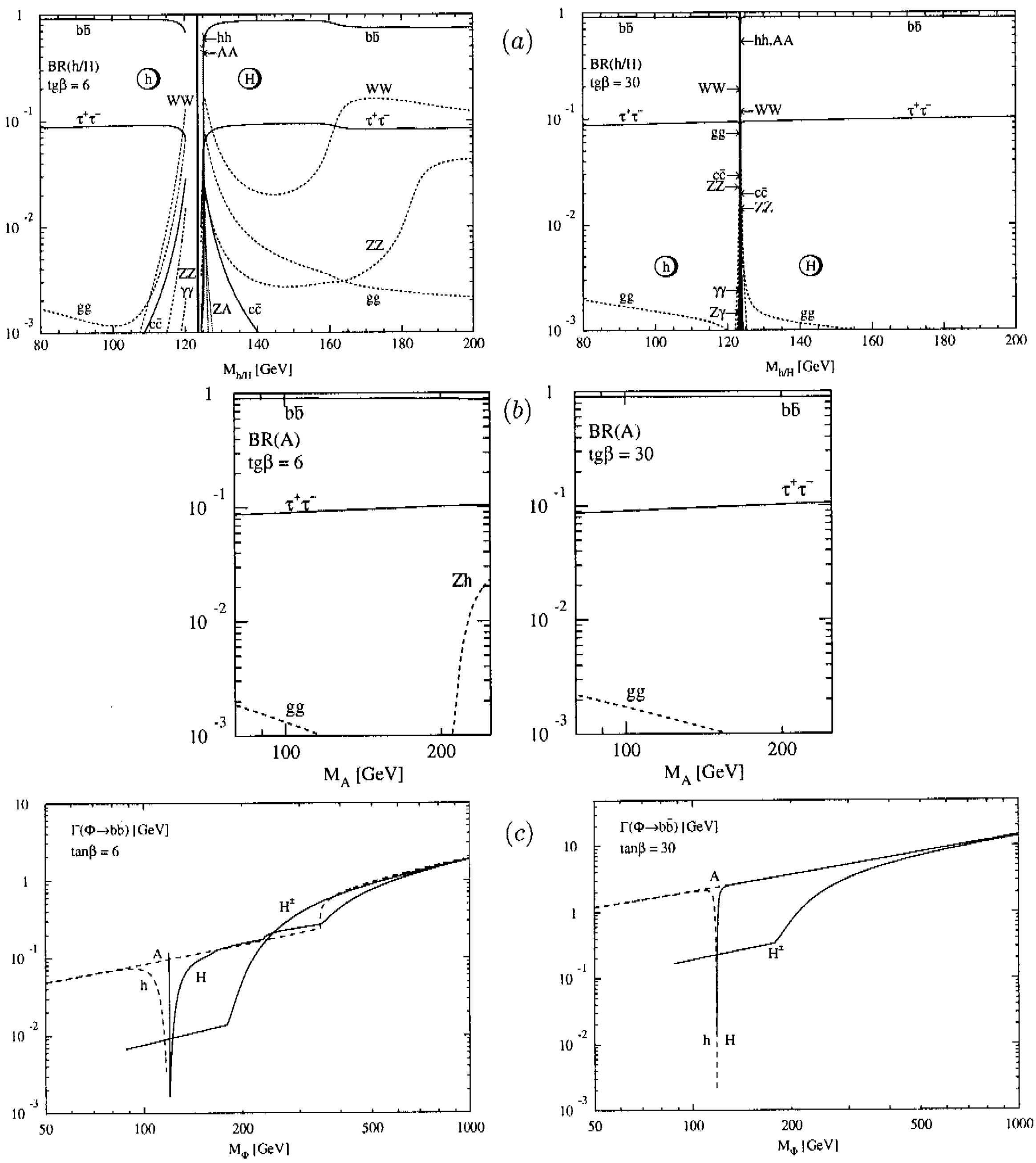

Figure 2.10: *Branching ratios of (a) the scalar and (b) the pseudoscalar MSSM Higgs bosons and (c) total decay widths of all MSSM Higgs bosons for the non-SUSY decays are shown for* $\tan\beta = 6$ *and 30, respectively, as functions of their masses. The Higgs masses and the branching ratios are, due to the radiative corrections, sensitive to the third generation of the squark spectrum. The plots were made with an average SUSY mass of 1 TeV and the other parameters chosen according to the "minimal mixing scenario" [48].*

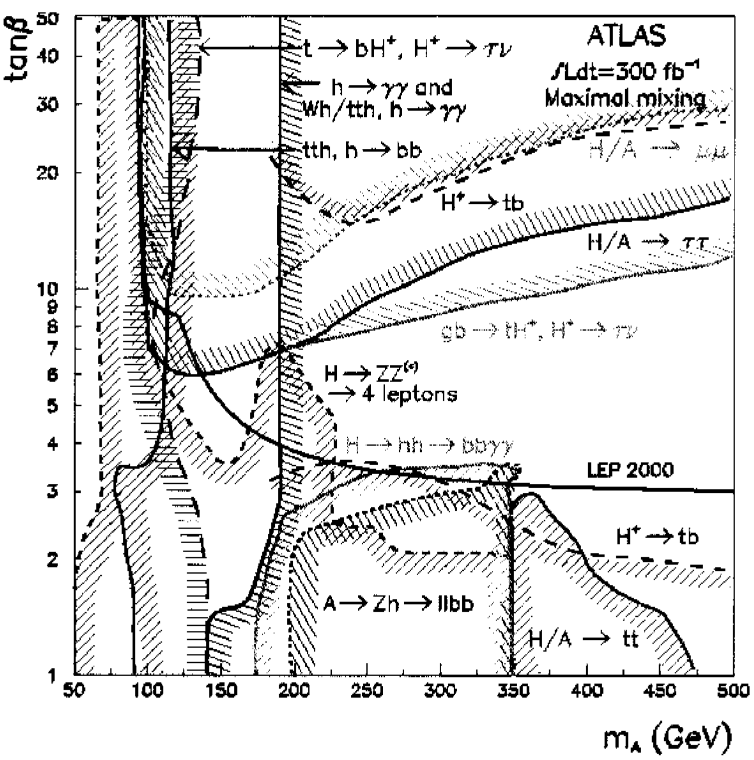

Figure 2.11: *The 5σ discovery contour curves are shown in the $m_A - \tan\beta$ plane for individual channels and for an integrated luminosity of 300 fb^{-1}. The LEP2 limits are included, too [47].*

2.3.3 Production Processes and Decay Channels at the Tevatron

The dominant production process of the neutral MSSM Higgs bosons at the Tevatron is *gluon fusion* (Figure 2.7a). Like at the LHC, the decays to $b\bar{b}$ pairs are plagued by large backgrounds and make detections in these channels $gg \to \phi \to b\bar{b}$ difficult. On the other hand the decay channels into $WW^{(*)}$ become important in a large mass region. For small $\tan\beta$ the decay $H \to hh$ is dominant in the mass region $m_H \lesssim 350$ GeV of the heavy scalar Higgs boson.

For large $\tan\beta$ the *associated Higgs production with bottom quarks* (Figure 2.7d) is important for the light scalar as well as for the pseudoscalar Higgs boson, strongly depending on the MSSM scenario. The *associated Higgs production with top quarks* is suppressed by the SUSY coupling factors and kinematically limited.

In the decoupling region of the light scalar as well as for large $\tan\beta$ and small pseudoscalar mass the *Higgs-strahlung* is an important process. For Higgs masses above 135 GeV the cross section of this production mechanism is too small, compared to the background, to produce visible events.

To test nearly the whole MSSM parameter space at the 95% exclusion level an integrated luminosity of 5 fb^{-1} per experiment would be enough (Figure 2.12a green shaded area). For the discovery of a CP-even MSSM Higgs boson at the 5σ level over the full MSSM parameter space 20 fb^{-1} are needed (Figure 2.12b light blue plus green shaded area). The Tevatron with an integrated luminosity of ~ 1 fb^{-1} per experiment until 2005 cannot significantly improve the MSSM Higgs limit obtained from LEP. However, if the integrated luminosity can be increased to about 10 fb^{-1} before shutdown, substantial improvements are achievable.

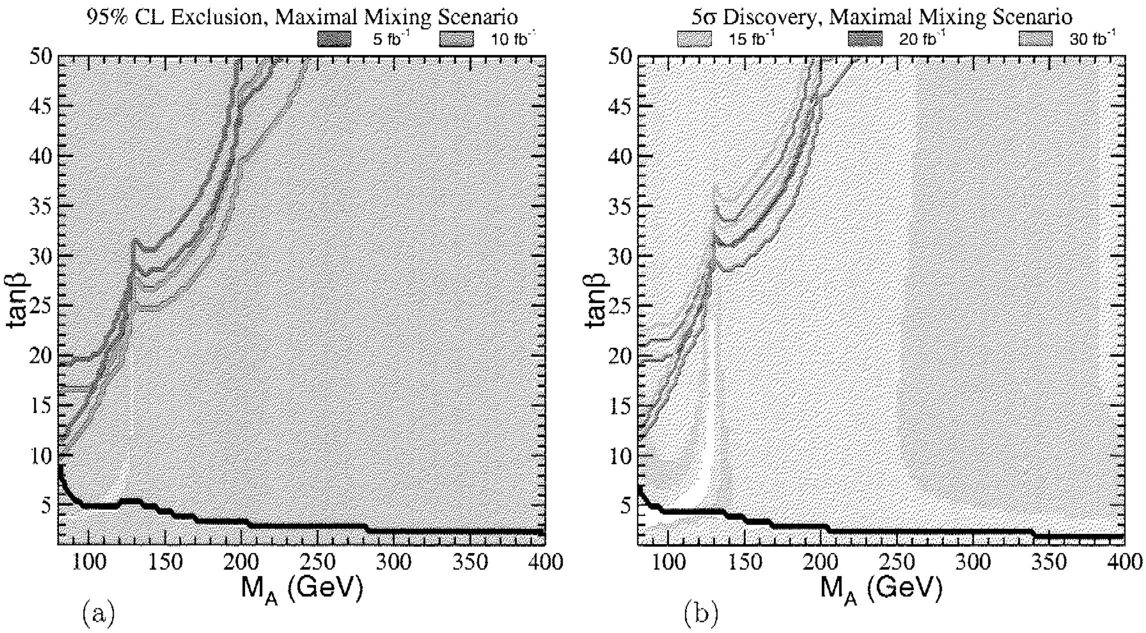

Figure 2.12: *(a) 95% CL exclusion region and (b) 5σ discovery region in the $m_A - \tan\beta$ plane, for the maximal mixing scenario and two different search channels: $q\bar{q} \to \mathcal{H}V$, $\mathcal{H} \to b\bar{b}$ (shaded regions) and $gg, q\bar{q} \to \phi b\bar{b}$, $\phi \to b\bar{b}$ (region in the upper left-hand corner bounded by the solid lines). Different integrated luminosities are explicitly shown by the colour coding. The two sets of lines (for a given colour) correspond to the CDF and DØ simulations, respectively. The region below the solid black line near the bottom of the plot is excluded by direct searches at LEP2 [48].*

2.3.4 Production Processes at the ILC

The two scalar Higgs bosons can be produced in the *vector-boson fusion*, in the *Higgs-strahlung* process or in *pair production* (Figure 2.13) [88]. The pseudoscalar Higgs boson does not couple to gauge bosons, therefore it can, in leading order, only be produced in *pair production*.

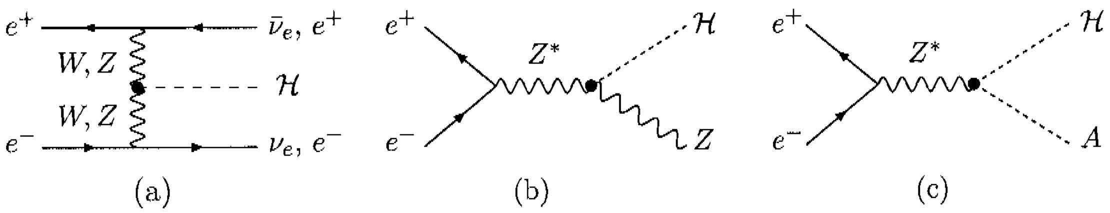

Figure 2.13: *Leading order Feynman diagrams of (a) vector-boson fusions $e^+e^- \to \mathcal{H}\nu_e\bar{\nu}_e$ and $e^+e^- \to \mathcal{H}e^+e^-$, (b) Higgs-strahlung process $e^+e^- \to \mathcal{H}Z$ and (c) pair production $e^+e^- \to \mathcal{H}A$.*

The cross sections are related to the SM cross section by the SUSY coupling factors (defined in Chapter 1.3.4):

$$\begin{aligned}
\sigma_{\text{MSSM}}(\mathcal{H}\nu_e\bar{\nu}_e) &= \left(g_W^{\mathcal{H}}\right)^2 \cdot \sigma_{\text{SM}}(H\nu_e\bar{\nu}_e), \\
\sigma_{\text{MSSM}}(\mathcal{H}e^+e^-) &= \left(g_Z^{\mathcal{H}}\right)^2 \cdot \sigma_{\text{SM}}(He^+e^-), \\
\sigma_{\text{MSSM}}(\mathcal{H}Z) &= \left(g_V^{\mathcal{H}}\right)^2 \cdot \sigma_{\text{SM}}(HZ), \\
\sigma_{\text{MSSM}}(\mathcal{H}A) &= (g_{ZA\mathcal{H}})^2 \cdot \bar{\lambda} \cdot \sigma_{\text{SM}}(HZ).
\end{aligned}$$

$\bar{\lambda}$ accounts for the P-wave suppression of $\mathcal{H}A$ near threshold.

Figure 2.14 shows the production cross sections at a linear e^+e^- collider with 350 GeV center of mass energy for the *Higgs-strahlung* and *pair production*. The solid lines are related to $\tan\beta = 3$ and the dotted to $\tan\beta = 30$. The complementarity of the two classes of processes ($\mathcal{H}Z$ vs. $\mathcal{H}A$) is clearly visible: e.g. as soon as the production of hA closes around 120 GeV the hZ channel opens for $\tan\beta = 30$.

At the ILC the cross sections of the *associated Higgs production with top quarks* range about two orders of magnitude below the corresponding values for the *Higgs-strahlung* process. However, as these cross sections can be measured with an accuracy of about 5% the Yukawa couplings can be extracted with a similar accuracy. Therefore, the *associated Higgs production with $t\bar{t}$* will be one of the most promising channels to measure the top Yukawa couplings for Higgs masses below the top threshold [89]. The SUSY-QCD correction for the light scalar Higgs production can be of measurable size [90]. For $m_\phi > 2m_t$ they can be measured in the decays of the neutral Higgs bosons into $t\bar{t}$ pairs.

In the MSSM the Yukawa coupling to down-type fermions can be strongly enhanced by $\tan\beta$. Thus, *associated Higgs production with bottom quarks* is important to extract $\tan\beta$ through the Yukawa couplings. As the experimental uncertainties will be small, NLO calculations are needed, first to reduce the theoretical uncertainties and secondly, because the NLO corrections yield sizeable contributions.

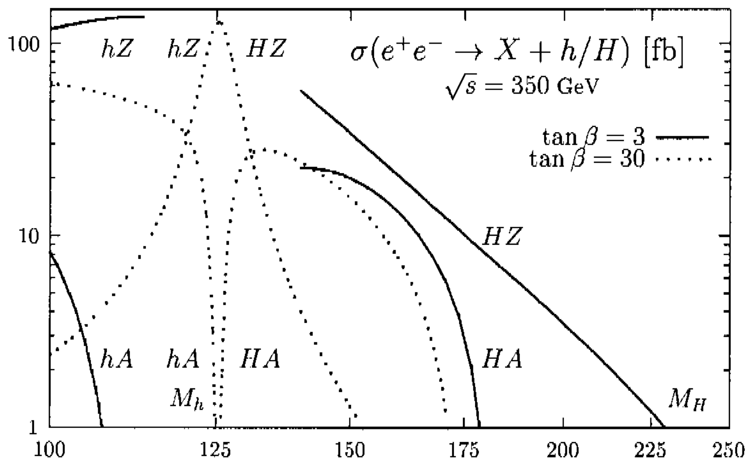

Figure 2.14: *Production cross sections of the neutral MSSM Higgs bosons at a linear e^+e^- collider with 350 GeV center of mass energy for the Higgs-strahlung and pair production for* tanβ = *3 and 30 as functions of the Higgs boson masses [50].*

2.3.5 Decay Channels at the ILC

The decay pattern of the Higgs bosons in the MSSM is more complicated than in the SM and depends strongly on the value of tanβ (Figures 2.10a and b). The light scalar Higgs bosons will decay mainly into fermion pairs, $b\bar{b}$ and $\tau^+\tau^-$, since its mass is smaller than $\sim$140 GeV. This is, in general, also the dominant decay mode of the heavy scalar Higgs boson. However, depending on tanβ the picture becomes somewhat more complicated: the decay rate into two light scalar or two pseudoscalar Higgs bosons may reach relatively large values. The pseudoscalar Higgs boson almost exclusively decays into $b\bar{b}$ and $\tau^+\tau^-$ pairs.

2.4 Summary

The ratio R for the quantitative analysis of the experimental results is defined as:

$$R \equiv \frac{\sigma(\text{production process in the MSSM})}{\sigma(\text{production process in the SM})} \times \frac{BR(\text{decay channel in the MSSM})}{BR(\text{decay channel in the SM})}.$$

Therewith, the results of SM can be approximately rescaled to the MSSM. Basically, the ratio of the production cross sections depends only on the ratio of the Yukawa couplings (listed in Table 1.4) of the two theories, except for gluon fusion. This assumption is valid as long as the radiative corrections in the MSSM and the SM are the same, but it breaks down as soon as e.g. SUSY-QCD corrections become important. For the branching ratios the possible radiative corrections have to be considered. This rescaling cannot be applied to the pseudoscalar MSSM Higgs boson, since its Yukawa coupling contains an additional γ_5 matrix.

Vector-boson fusion is about one order of magnitude smaller in the MSSM than in the SM, due to the suppression $\propto \left(g_V^{\mathcal{H}}\right)^2$. Nevertheless, it is a very important production channel for the scalar MSSM Higgs bosons in the intermediate mass region. The two additional quarks in the final state offer the opportunity to reduce the backround significantly. The *Higgs-strahlung* process is suppressed by the same factor and thus in the MSSM far less important than in the SM. The cross section of *associated Higgs production with bottom quarks* scales with $\left(g_b^{\phi}\right)^2$ up to non-leading contributions from the top quark loops. This channel can be strongly enhanced for large tanβ values. After *gluon fusion*, which is in the SM and in the MSSM for small and moderate tanβ the dominant production process of neutral Higgs bosons in hadronic collisions, *associated Higgs production with bottom quarks* is in the MSSM much more important than in the SM. Together with the *Higgs-strahlung* process and *vector-boson fusion*, the *pair production* can play a significant role for the scalar MSSM Higgs production in e^+e^- collisions. The latter is the only relevant production process for a pseudoscalar Higgs boson at leading order.

If the mass of a light Higgs boson ranges below the gauge boson threshold, the decays into $b\bar{b}$ and $\tau^+\tau^-$ pairs dominate in both theories. The running mass of the bottom quark is almost twice the mass of the τ lepton and quarks appear in three colours. Thus, the branching ratio of $\phi \to b\bar{b}$ with up to 90% is about one order of magnitude larger than the roughly 10% of $\phi \to \tau^+\tau^-$ (Figures 2.10a and b). The MSSM Yukawa coupling is increased by a factor g_d^{ϕ} compared to the SM. The decay width of a light MSSM Higgs boson can be much larger than for a SM Higgs boson of comparable mass, especially for large tanβ values [91]. For large Higgs masses the total SM Higgs decay width is proportional to m_H^3 (Figure 2.3b). This behaviour arises from the Higgs coupling $\lambda \propto m_H^2$ to the longitudinal components of the W and Z gauge bosons. In the MSSM, on the other hand, $\lambda \propto m_Z^2$ and thus the decay width grows linearly in m_{ϕ} (Figure 2.10c). Therefore, a heavy SM Higgs boson is much broader than a MSSM Higgs boson of the same mass. The decay widths of the MSSM Higgs bosons are predominantly defined by the hadronic width. These effects are important to distinguish between a SM Higgs boson and a neutral supersymmetric candidate, if a Higgs boson is discovered.

Chapter 3

Technical Details

The unrenormalised Lagrangian suffers from divergencies, which can be treated in a systematic way by applying *regularisation* as well as *renormalisation* techniques. One difficulty in performing calculations for hadronic initial states is the non-fundamental nature of hadrons: they are bound states of quarks and gluons. Thus, one has to calculate the partonic cross sections which are convolved with the *parton distribution functions* to obtain the hadronic cross sections. Leptons, on the other hand, are elementary particles and the cross sections can be calculated directly. For associated Higgs production with heavy quarks a *massive three-particle phase space integration* has to be performed. By taking advantage of kinematics and symmetries the nine-dimensional integration can be reduced to a four-dimensional one. The NLO SUSY-QCD corrections to associated Higgs production for e^+e^- collisions are derived by applying the *standard matrix element method* by hand, while for the partonic initial states, the calculation is fully automised based on `QGRAF`, `FORM` and `MAPLE`. These two methods are described in details.

3.1 Regularisation

Calculating higher order effects leads to ultraviolet (UV) and infrared (IR) divergences. This can be seen, e.g, in the one loop vertex correction:

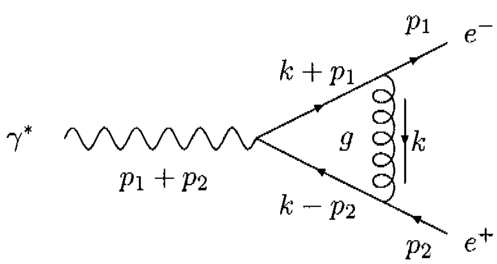

$$\longrightarrow \quad I = \int \frac{d^4k}{(2\pi)^4} \frac{f(k^2)}{k^2(k+p_1)^2(k-p_2)^2} \, .$$

Two types of divergences can appear in such an integral:

- UV divergences, which are associated with singularities occurring at large loop momenta: $k \to \infty \quad \Longrightarrow \quad I \to \infty,$
- IR divergences, which are generated, if one of the propagators in the loop vanishes:
$$\left.\begin{array}{l} k \to 0,\ -p_1,\ +p_2 \ \text{(soft) or} \\ \cos\vartheta \to 1 \ \text{(collinear)} \end{array}\right\} \quad \Longrightarrow \quad I \to \infty, \text{ for } p_1^2 = p_2^2 = 0$$

The loop integrals are well behaved, if regularisation techniques are applied. The *dimensional regularisation* (DR) [92] by 't Hooft and Veltman preserves gauge and Lorentz invariance[1]. The integration in the 4-dimensional Minkowski space is replaced by a D-dimensional integration, where $D = 4 - 2\varepsilon$ and ε is a small parameter. The analytically continued integrals in D dimensions are well defined and the divergences can be quantified as poles in ε: $1/\varepsilon^n$ and $n \in \mathbb{N}$. For the action

$$S = \int d^D x\, \mathcal{L}$$

to remain dimensionless a new scale μ, the *'t Hooft scale*, has to be introduced and the coupling constants g are replaced by $\bar{g} \equiv g\mu^{\varepsilon}$. The physical observables are independent of this artificial scale. However, by performing higher-order calculations the perturbative series is truncated at a certain order n, destroying the μ–independence of the theoretical result. The remaining scale dependence quantifies part of the theoretical uncertainties caused by unknown higher-order corrections.

Some freedom concerning the dimensionality of the external momenta and the number of polarisations for internal and external particles is left. Throughout this thesis the *conventional* DR is used, in which no distinction is made between real and virtual particles, massless quarks have two helicity states and gluons have $D - 2$.

3.2 Renormalisation

In renormalisable theories the UV divergences are[2] absorbed in physical (renormalised) quantities by redefinitions of the bare (unphysical) masses, fields and coupling constants by multiplicative Z-factors[3] with $Z \equiv 1 + \delta Z$:

$$\begin{array}{llcl} \text{fermion field:} & \psi_f^0 & = & Z_\psi^{1/2}\, \psi_f^R, \\ \text{gluon field:} & G_\mu^{a,0} & = & Z_G^{1/2}\, G_\mu^{a,R}, \\ \text{fermion mass:} & m_f^0 & = & Z_m\, m_f^R, \\ \text{strong coupling constant:} & g_s^0 & = & Z_{g_s}\, g_s^R. \end{array}$$

[1]The γ_5, defined by t'Hooft and Veltman, explicitely breaks Lorentz invariance. However, it can be recovered by the proper counterterm.

[2]The IR divergences cancel out for physical meaningful quantities by adding up real and virtual corrections contributing to the same order of the perturbation series. The remaining initial state collinear singularities are absorbed in the renormalised parton distribution functions (Chapter 3.3).

[3]$Z_m \equiv 1 - \delta m_f/m_f$ and $Z_{g_s} \equiv 1 + \delta g_s/g_s$ to be multiplicative factors, too.

The Lagrangian as a function of the bare quantities can be reexpressed as a function of the renormalised quantities and counterterms by expanding in the δZ's:

$$\begin{aligned}\mathcal{L}\left(\psi_f^0, G_\mu^{a,0}, m_f^0, g_s^0\right) &= \mathcal{L}\left(Z_\psi^{1/2}\,\psi_f^R,\, Z_G^{1/2}\,G_\mu^{a,R},\, Z_m\,m_f^R,\, Z_{g_s}\,g_s^R\right)\\ &= \mathcal{L}\left(\psi_f^R, G_\mu^{a,R}, m_f^R, g_s^R\right) + \mathcal{L}_{CT}.\end{aligned}$$

Renormalisability means that all UV divergences are cancelled by counterterms corresponding to a finite number of interactions with mass dimension ≤ 4. In non-renormalisable theories new counterterms must be added at each new order in perturbation theory.

Gauge invariance leads to a number of relations among the Z-factors; the Slavnov-Taylor identities in QCD [93] and Ward-Takahashi identities in QED [94]. E.g., the strong coupling constant appears in several terms in the Lagrangian:

- gluon–quark–antiquark vertex:

$$\begin{aligned}-g_s^0\,T_{jk}^a\,\bar\psi_j^0\;\not{G}^{a,0}\psi_k^0 \quad &\rightarrow \quad -Z_{g_s}Z_G^{1/2}Z_\psi\;\bar g_s^R\,T_{jk}^a\,\bar\psi_j^R\;\not{G}^{a,R}\psi_k^R\\ &\equiv \quad -Z_{G\psi\bar\psi}^{1/2}\quad \bar g_s^R\,T_{jk}^a\,\bar\psi_j^R\;\not{G}^{a,R}\psi_k^R,\end{aligned}$$

- triple gluon vertex:

$$\begin{aligned}g_s^0\,f_{abc}\left(\partial_\mu G_\nu^{a,0}\right)G_\mu^{b,0}G_\nu^{c,0} \quad &\rightarrow \quad Z_{g_s}Z_G^{3/2}\;\bar g_s^R\,f_{abc}\left(\partial_\mu G_\nu^{a,R}\right)G_\mu^{b,R}G_\nu^{c,R}\\ &\equiv\; Z_{G^3}^{1/2}\;\;\bar g_s^R\,f_{abc}\left(\partial_\mu G_\nu^{a,R}\right)G_\mu^{b,R}G_\nu^{c,R}.\end{aligned}$$

Uniqueness of the strong coupling constant leads to:

$$Z_{g_s} = \frac{Z_{G\psi\bar\psi}^{1/2}}{Z_G^{1/2}Z_\psi} \stackrel{!}{=} \frac{Z_{G^3}^{1/2}}{Z_G^{3/2}}.$$

There exists some freedom in shifting parts of the finite contribution into the $Z-$factors which defines the different *renormalisation schemes.* Physical observables have to be independent of this choice. The most commonly used schemes are:

- *On-shell* scheme [95]: the renormalised masses are chosen at the poles of the propagators, the renormalisation constants of fields are adjusted such that all the external self-energies vanish and that the residue of the renormalised fermion propagator is one. The fermion self-energy contains scalar, vectorial and axialvectorial[4] contributions:

$$\begin{aligned}\Sigma(\not{p}) &= m_\psi\Sigma_\psi^S\left(p^2\right) + \not{p}\Sigma_\psi^V\left(p^2\right) + \not{p}\gamma_5\Sigma_\psi^A\left(p^2\right)\\ &= \delta m_\psi + \left(\not{p} - m_\psi\right)\delta Z_V + \not{p}\gamma_5\,\delta Z_A + \Sigma^R(\not{p}).\end{aligned} \tag{3.1}$$

[4]The axialvectorial contribution vanishes for QCD but not for SUSY-QCD.

The fermionic renormalisation constants are defined as:

$$\begin{aligned}
\delta m_\psi^{\mathrm{OS}} &\equiv m_\psi \left[\Sigma_\psi^S\left(m_\psi^2\right) + \Sigma_\psi^V\left(m_\psi^2\right)\right], \\
\delta Z_V^{\mathrm{OS}} &\equiv \frac{\partial}{\partial \not{p}} \left[m_\psi \Sigma_\psi^S\left(p^2\right) + \not{p}\,\Sigma_\psi^V\left(p^2\right)\right]_{p^2=m_\psi^2} \\
&= \Sigma_\psi^V\left(m_\psi^2\right) + 2m_\psi^2 \frac{\partial}{\partial p^2}\left[\Sigma_\psi^V\left(p^2\right) + \Sigma_\psi^S\left(p^2\right)\right]_{p^2=m_\psi^2}, \\
\delta Z_A^{\mathrm{OS}} &\equiv \Sigma_\psi^A\left(m_\psi^2\right).
\end{aligned}$$

The left- and right-handed states contain vectorial as well as axialvectorial contributions, which have to be renormalised separately:

$$\delta Z_{\psi,R}^{\mathrm{OS}} = \delta Z_V^{\mathrm{OS}} + \delta Z_A^{\mathrm{OS}} \qquad \text{and} \qquad \delta Z_{\psi,L}^{\mathrm{OS}} = \delta Z_V^{\mathrm{OS}} - \delta Z_A^{\mathrm{OS}}.$$

The gluon vacuum polarisation is given by:

$$\begin{aligned}
\Pi^{\mu\nu}(q) &= \left(g^{\mu\nu} - \frac{q^\mu q^\nu}{q^2}\right)\Pi(q) \\
&= \left(g^{\mu\nu} - \frac{q^\mu q^\nu}{q^2}\right)\delta Z_G + \Pi^{\mu\nu,R}(q),
\end{aligned}$$

leading for the gluon renormalisation constant to:

$$\delta Z_G^{\mathrm{OS}} = \Pi(q)\Big|_{q^2=0}.$$

- *Modified minimal subtraction* scheme ($\overline{\mathrm{MS}}$) [96]: in one-loop corrections the UV poles always occur in the combination:

$$\Delta_{\mathrm{UV}} = \frac{\Gamma(1+\varepsilon)}{\varepsilon}(4\pi)^\varepsilon = \frac{1}{\varepsilon} - \gamma_E + \log(4\pi) + \mathcal{O}(\varepsilon) \equiv \frac{1}{\bar{\varepsilon}},$$

with the Gamma function $\Gamma(x)$ and the Euler constant $\gamma_E \simeq 0.5772$. In the $\overline{\mathrm{MS}}$ scheme the whole Δ_{UV} is absorbed, while in the MS scheme only the poles are absorbed. Thus, the renormalisation constants are defined as:

$$\begin{aligned}
\delta m_\psi^{\overline{\mathrm{MS}}} &\equiv m_\psi \left[\Sigma_\psi^S\left(p^2\right) + \Sigma_\psi^V\left(p^2\right)\right]\Big|_{\mathrm{div}}, \\
\delta Z_V^{\overline{\mathrm{MS}}} &\equiv \frac{\partial}{\partial \not{p}}\left[m_\psi \Sigma_\psi^S\left(p^2\right) + \not{p}\,\Sigma_\psi^V\left(p^2\right)\right]_{\mathrm{div}}, \\
\delta Z_A^{\overline{\mathrm{MS}}} &\equiv \Sigma_\psi^A\left(p^2\right)\Big|_{\mathrm{div}}, \\
\delta Z_G^{\overline{\mathrm{MS}}} &\equiv \Pi\left(p^2\right)\Big|_{\mathrm{div}}.
\end{aligned}$$

Through quantum fluctuations, as shown in Figure 3.1, large logarithms emerge, which can be absorbed by the running of the strong coupling constant $\alpha_s(\mu)$. The corresponding QCD and SUSY-QCD renormalisation constants in the $\overline{\mathrm{MS}}$ scheme are given by:

$$\begin{aligned}
\delta Z_{g_s}^{\overline{\mathrm{MS}}} &= \delta Z_{g_s}^{\mathrm{QCD}} + \delta Z_{g_s}^{\mathrm{SQCD}}, \\
\delta Z_{g_s}^{\mathrm{QCD}} &= \frac{\alpha_s(\mu_R)}{4\pi}\left[\left(-\frac{1}{\bar{\varepsilon}} + \log\frac{\mu_R^2}{\mu^2}\right)\frac{\beta_0^{\mathrm{QCD}}}{2} - \frac{1}{3}\log\frac{m_t^2}{\mu_R^2}\right], \qquad (3.2) \\
\delta Z_{g_s}^{\mathrm{SQCD}} &= \frac{\alpha_s(\mu_R)}{4\pi}\left[\left(-\frac{1}{\bar{\varepsilon}} + \log\frac{\mu_R^2}{\mu^2}\right)\frac{\beta_0^{\mathrm{SQCD}}}{2} - \frac{N_c}{3}\log\frac{m_{\tilde{g}}^2}{\mu_R^2}\right. \\
&\qquad\left. - \frac{n_f+1}{6}\sum_{\tilde{q}_j}\log\frac{m_{\tilde{q}_j}^2}{\mu_R^2}\right]. \qquad (3.3)
\end{aligned}$$

The top quark, the gluinos and the squarks are decoupled from the running by subtracting the corresponding logarithms. Therefore, the running of $\alpha_s(\mu)$ is specified solely by the gluons and the light SM quarks and

$$\beta_0^{\mathrm{QCD}} = \frac{11}{3}N_c - \frac{2}{3}n_f - \frac{2}{3} \qquad \& \qquad \beta_0^{\mathrm{SQCD}} = -\frac{2}{3}N_c - \frac{1}{3}(n_f+1),$$

where $N_c = 3$ counts the number of colours and $n_f = 5$ the number of active flavours.

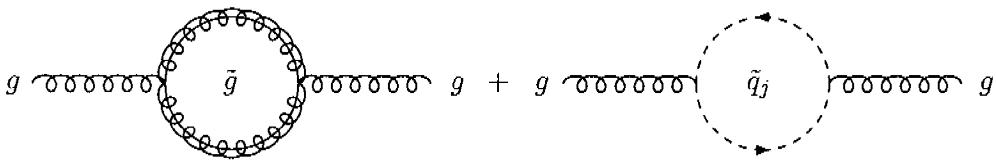

Figure 3.1: *SUSY-QCD quantum fluctuations of the gluon propagator.*

3.3 Hadronic Initial States

One of the main complications of performing calculations for hadron colliders are the hadronic initial states, which are bound states of partons rather than elementary particles. The confinement of these partons originates from the growing of the strong coupling constant with decreasing energy and rising distance, respectively. These bound partons are not accessible by perturbation theory, since this requires small coupling constants. On the other hand, the initial particles of the perturbative calculations are partons rather than hadrons. The cross sections of these partonic processes can be calculated in perturbation theory as the coupling constants of these short distance (hard) scatterings are small enough for a perturbative expansion: the calculations are performed in the *parton model.* This model is based on several assumptions:

(i) Hadrons are made up of constituents called partons, which are identified as the strongly interacting quarks and gluons.

(ii) Every parton carries a longitudinal momentum $p_i^\mu = x_i P^\mu$ equal to a fraction x_i of the hadron momentum P^μ, with $0 \leq x_i \leq 1$, and negligible transverse momentum.

(iii) In hard scattering processes the parton masses are neglected[5].

(iv) The typical time-scale of hard scattering processes are much shorter than the interaction time-scale of partons among each other. Thus, the asymptotically free partons can be treated as quasi-free particles which scatter incoherently at large energies.

The cross section of the hadronic process $h_1 h_2 \to X$ can be written as a convolution of the perturbatively computable partonic cross sections $p_i p_j \to X$ with the *parton distribution functions* (PDFs) $f_{p_i|h_k}(x_i)$ and $f_{p_j|h_k}(x_j)$, summed over all partons $p_{i,j} = g, u, \bar{u}, \ldots$ contained in the hadrons h_k, where $k = 1, 2$:

$$\sigma_{h_1 h_2}(s) = \sum_{i,j} \int_0^1 dx_i \int_0^1 dx_j \, f_{p_i|h_1}(x_i) \, f_{p_j|h_2}(x_j) \, \sigma_{p_i p_j}(\hat{s} = x_i x_j s).$$

The universal (process independent) PDFs parametrise the low-energetic parton binding within the hadrons. They can be interpreted as probability distributions of finding the parton p_i in the hadron h_k with a fraction x_i of the longitudinal hadron momentum and are not calculable by perturbation theory. Therefore, they must be determined experimentally, e.g. from deep inelastic scattering (DIS) in electron-proton collisions at HERA[6] [98]. The factorisation theorems of QCD [99] ensure that the collinear singularities, originating from the massless partons in the initial state, factorise universally from the hard scattering process and can thus be absorbed by renormalisation of the bare PDFs. The measured PDFs contain two ambiguities, which have to be taken into account in perturbative calculations:

- The PDFs involve the DIS momentum transfer, which may differ from the energy scale of the calculated process. The DGLAP equations [100] evolve the PDFs from the experimental values to the required factorisation scales μ_F.
- Apart from singularities one is free to absorb any universal non-singular terms, appearing in the partonic cross section, in the PDFs. The terms included in the renormalised PDFs fix the *factorisation scheme*. The two most common ones are:
  - the *DIS* scheme, where universal non-singular terms are absorbed in the PDFs such that the DIS structure function F_2 is free of radiative corrections,
  - the $\overline{MS}$ scheme, which includes only the singular terms with some trivial constants in the PDFs in analogy to the $\overline{\mathrm{MS}}$ scheme in the UV-renormalisation.

The partonic cross section at NLO can be separated into the leading order cross section $\sigma^{\mathrm{LO}}_{p_1 p_2}(\hat{s})$ and the NLO virtual and real corrections $\sigma^{\mathrm{virt}}_{p_1 p_2}(\hat{s})$ and $\sigma^{\mathrm{real}}_{p_1 p_2}(\hat{s})$, respectively:

$$\sigma^{\mathrm{NLO}}_{p_1 p_2}(\hat{s}) = \sigma^{\mathrm{LO}}_{p_1 p_2}(\hat{s}) + \sigma^{\mathrm{virt}}_{p_1 p_2}(\hat{s}) + \sigma^{\mathrm{real}}_{p_1 p_2}(\hat{s}).$$

[5] There are no heavy quarks allowed in the initial state [97].

[6] The Hadron-Elektron Ring Anlage (HERA) is a particle accelerator at DESY in Hamburg. The electrons or positrons are collided with protons at a center of mass energy of 318 GeV.

The real corrections have to be included because detectors are not sensitive to particles produced with too low energies (IR singularities) or too small angles relative to the emitting particle (collinear singularities). However, only light particles can have too small energies to be identified or can be radiated so closed to the emitter so that their track cannot be separated from the emitter track. Due to the coupling of these extra particles in the final state the real corrections are of the same order in the coupling constants as the virtual corrections and thus both contribute to the same order of the perturbation series. In this work SUSY-QCD corrections with heavy squarks and gluinos are calculated, therefore, no real corrections have to be taken into account.

3.4 Massive Three-Particle Phase Space

The integral over the massive three-particle phase space (PS_3) in four dimensions is given by:

$$\begin{aligned}\int d\mathrm{PS}_3 &= \int\left(\prod_{i=3}^{5}\frac{d^3\mathbf{p_i}}{(2\pi)^3 2p_i^0}\right)(2\pi)^4\delta^{(4)}(p_1+p_2-p_3-p_4-p_5)\\ &= \frac{s}{512\pi^4}\int dx_3\,dx_4\,d\cos\theta\,d\chi\end{aligned}$$

with $p_i = (p_i^0, \mathbf{p}_i) = (\frac{\sqrt{s}}{2}x_i, \mathbf{p}_i)$ and $|\mathbf{p}_i| = \sqrt{(p_i^0)^2 - m_i^2} \equiv \beta_i\, p_i^0$. In the center of mass system of the initial particles the total three-momentum vanishes:

$$p_1 + p_2 = \sqrt{s}(1, \mathbf{0}) = \left(p_3^0 + p_4^0 + p_5^0,\ \mathbf{p_3} + \mathbf{p_4} + \mathbf{p_5}\right).$$

The process is symmetric under rotations around the beam axis, thus, the integration over the angle φ leads to a factor 2π. The angles θ and χ defined in Figure 3.2 range within:

$$0 \le \theta \le \pi, \qquad \text{and} \qquad 0 \le \chi \le 2\pi.$$

The polar angle of $\mathbf{p_4}$ relative to $\mathbf{p_3}$ is given by:

$$\cos\theta_{34} = \frac{\mathbf{p_3}\cdot\mathbf{p_4}}{|\mathbf{p_3}||\mathbf{p_4}|}.$$

The boundaries of x_3 and x_4 emerge from the condition $|\cos\theta_{34}| \le 1$:

$$(x_3)_{\mathrm{min,max}} = \frac{(2-x_4)(A_4+m_3^2-m_5^2) \pm \sqrt{x_4^2 - \left(\frac{2m_4}{\sqrt{s}}\right)^2}\,\kappa(A_4, m_3^2, m_5^2)}{2A_4},$$

with the abbreviation $A_4 \equiv s\,(1-x_4) + m_4^2$ and the Källén function

$$\kappa^2(x,y,z) \equiv x^2 + y^2 + z^2 - 2(xy + yz + zx).$$

The limits for x_4 are reached when the integration interval for x_3 vanishes:

$$\begin{aligned}(x_4)_{\mathrm{min}} &= \frac{2m_4}{\sqrt{s}},\\ (x_4)_{\mathrm{max}} &= \frac{s+m_3^2-(m_4+m_5)^2}{s}.\end{aligned}$$

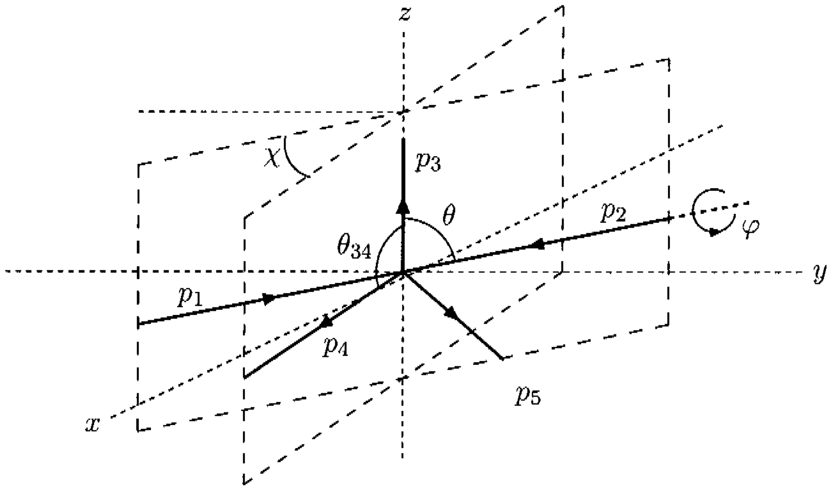

Figure 3.2: *Kinematics of a 2→3 process with the momenta* $p_{1,2}$ *for the initial and* $p_{3,4,5}$ *for the final states.*

3.5 Standard Matrix Element Method

The SUSY-QCD corrections to the associated Higgs production with heavy quarks in e^+e^- collisions have been calculated using the *standard matrix element* (SME) method. The amplitude $\mathcal{M}$ of any process, which depends on the momenta p_j, colour indices c_j and spins s_j of the external particles $j = 1, \ldots, n$ can be decomposed into Lorentz-invariant formfactors $F(p_j)$, colour structures $C(c_j)$ and SMEs $\mathcal{M}_i(p_j;\, s_j)$:

$$\mathcal{M} = \mathcal{M}(c_j;\, p_j;\, s_j) = \sum_{i,k} C_k(c_j)\, F_{ki}(p_j)\, \mathcal{M}_i(p_j;\, s_j).$$

All LO and NLO SUSY-QCD diagrams of $e^+e^- \to \phi Q\bar{Q}$ have the identical initial-state $e^+e^- \to V$, with $V = \gamma, Z$, structure. Thus, the SMEs needed to describe this process simplify to:

$$\mathcal{M}_i^V \;\; \equiv \;\; \Gamma_i^{Q\bar{Q}} \left[v_V^e\, \Gamma_\mu^{ee} + a_V^e\, \Gamma_{5\mu}^{ee} \right], \qquad i = 1, \ldots, 16,$$

depending on the involved gauge boson V. The tensors $\Gamma^{ee}_{\mu,5\mu}$ characterise the leptonic initial state and $\Gamma^{Q\bar{Q}}_{1,\ldots,16}$ the strongly interacting final state:

$$\begin{aligned}
\Gamma^{ee}_{\mu,\,5\mu} &= \bar{v}_{e^+}(p_2)\,\{\gamma_\mu,\, \gamma_5\gamma_\mu\}\, u_{e^-}(p_1), \\
\Gamma^{Q\bar{Q}}_{1,\ldots,6} &= \bar{u}_Q(p_3)\,\{p_{3\mu},\, p_{4\mu},\, p_{5\mu},\, p_{3\mu}\gamma_5,\, p_{4\mu}\gamma_5,\, p_{5\mu}\gamma_5\}\, v_{\bar{Q}}(p_4), \\
\Gamma^{Q\bar{Q}}_{7,8} &= \bar{u}_Q(p_3)\,\{\gamma_\mu,\, \gamma_5\gamma_\mu\}\, v_{\bar{Q}}(p_4), \\
\Gamma^{Q\bar{Q}}_{9,\ldots,14} &= \bar{u}_Q(p_3)\,\{p_{3\mu}\,\not{p}_5,\, p_{4\mu}\,\not{p}_5,\, p_{5\mu}\,\not{p}_5,\, p_{3\mu}\gamma_5\,\not{p}_5,\, p_{4\mu}\gamma_5\,\not{p}_5,\, p_{5\mu}\gamma_5\,\not{p}_5\}\, v_{\bar{Q}}(p_4), \\
\Gamma^{Q\bar{Q}}_{15,16} &= \bar{u}_Q(p_3)\,\{\gamma_\mu\,\not{p}_5,\, \gamma_5\gamma_\mu\,\not{p}_5\}\, v_{\bar{Q}}(p_4).
\end{aligned}$$

The amplitudes factorise as

$$\mathcal{M}(e^+e^- \to \phi Q_k \bar{Q}_l) = \delta_{kl} \sum_{V=\gamma,Z} \sum_{i=1}^{16} F_i^V(p_j)\, \mathcal{M}_i^V(p_j;\, s_j).$$

Trivial colour structures δ_{kl} appear in this decomposition since the underlying process $e^+e^- \to \phi Q_k \bar{Q}_l$ proceeds trough electroweak interactions.

This method has the advantage that the time consuming evaluations of traces of Dirac matrices in the squared amplitudes need to be calculated only once. The contraction of amplitudes is reduced to multiplications of formfactors. The analytical results can be cast into a readable form and the numerical evaluation is reduced significantly.

3.6 Qgraf Method

For the calculation of the NLO SUSY-QCD corrections to associated Higgs production with heavy quarks at hadron colliders the `QGRAF 3.0` program [101] has been used to generate Feynman diagrams. Most of the algebraic evaluations have been performed with `FORM 3.1` [102], while the expressions have been simplified with `MAPLE 9.5`. In Figure 3.3 the schematic succession from the choice of the process to be calculated to a numerically evaluable Fortran code is shown.

The *model*-file defines the physical model: the possible propagators and vertices with their coupling strengths, while the *style.sty* defines the appearance of the output of *qgraf*. Those two files are needed by *qgraf.dat*, the input file for the `QGRAF` program:

```
output= 'diagram.dat';
style= 'style.sty';
model= 'MSSM';
in= quark[p1], qbar[p2];
out= Quark[p3], Qbar[p4], higgs[p5];
loops= 1;
loop_momentum= k;
options= onshell, notadpole;
true= iprop[higgs,0,0];
true= vsum[gpow,4,4];
```

The output file here is called *diagram.dat*, it is written in the *style.sty* style and contains all possible MSSM NLO diagrams for $q(p_1)\,\bar{q}(p_2) \to Q(p_3)\,\bar{Q}(p_4)\,H(p_5)$. The options chosen here avoid external self-energy and tadpole diagrams. The "true" statements specify to have no Higgs propagators in the diagrams and only diagrams which are proportional to g_s^4.

The *diagram.dat* is read in by the `MAPLE` program *translate.map*, where the abstract Feynman diagrams are translated to external/internal particles and vertices with the proper colour, spin, squark and Lorentz indices.

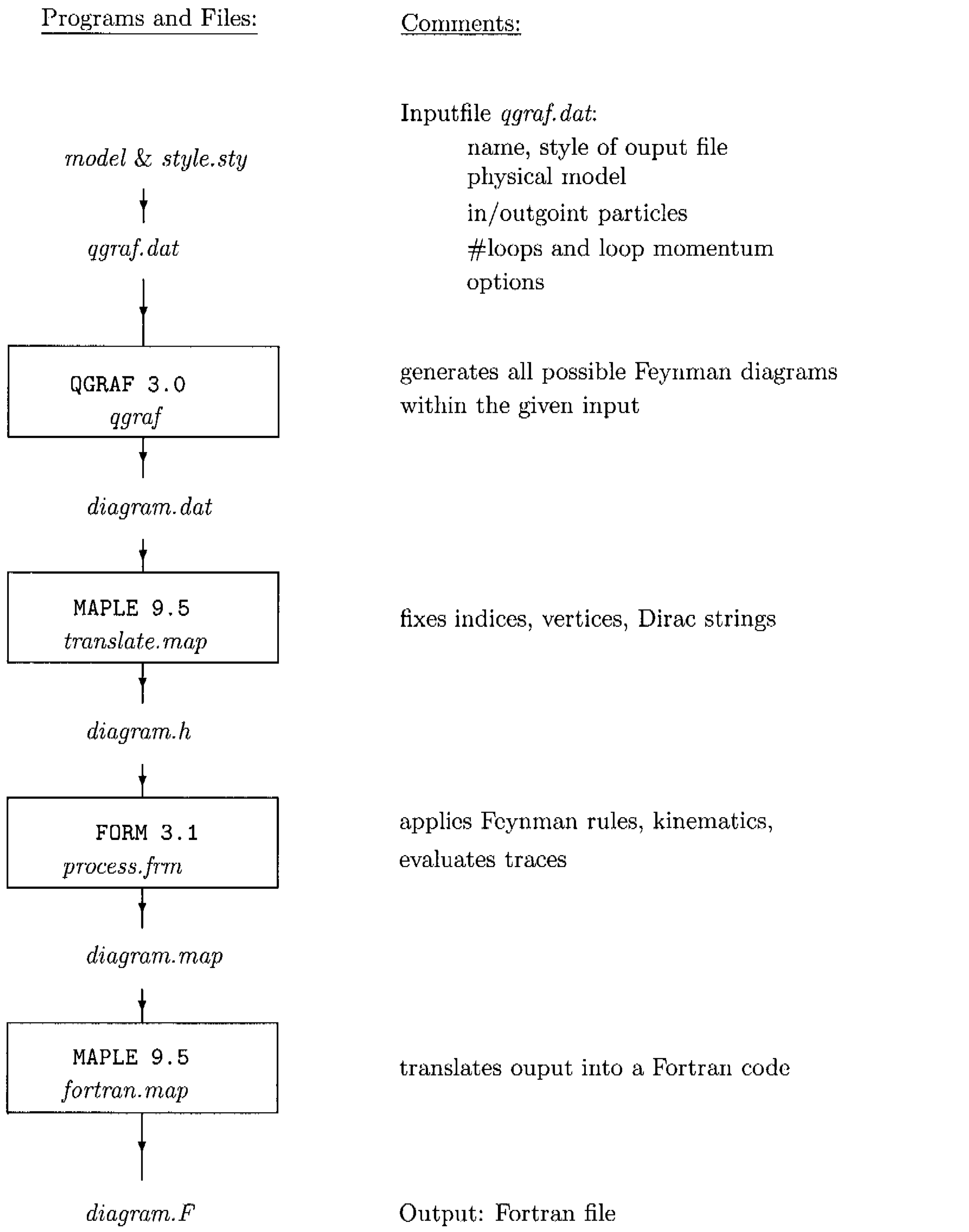

Figure 3.3: *Schematic depiction of the way to perform loop calculations using* `QGRAF`, `MAPLE` *and* `FORM`.

In the FORM program *process.frm* the particles and vertices of *diagram.h* are transformed, using the Feynman rules, into coefficients, colour factors, Lorentz structures and spinors. The matrix element is contracted with the proper LO matrix element. The traces of the spinor strings are evaluated in four dimensions. Tensor reduction is applied and the scalar one-loop integrals are introduced. At the end the Lorentz indices are contracted and the output is saved in the file *diagram.map*.

The *fortran.map* converts the analytical FORM output into the numerically evaluable Fortran code *diagram.F*.

The advantage of this method is the fully automated way to calculate virtual corrections once a program chain like the one in Figure 3.3 is build up. By modifying the *model* and the *qgraf.dat* files calculations of other processes in other theories can be performed, too. The MAPLE produced Fortran codes *diagram.F* are optimised. The external self-energy diagrams and the counterterms are not included, they have to be calculated separately.

Chapter 4

$e^+e^- \to \phi Q\bar{Q}$

The necessity of including NLO SUSY-QCD corrections to associated Higgs production with heavy quarks is discussed. The calculations are performed by the SME method (Chapter 3.5) and the LO results are given analytically. The existing QCD corrections are shortly reviewed. The NLO SUSY-QCD corrections are discussed with focus on the external self-energies and the counterterms. For large tanβ values the bottom Yukawa couplings are strongly enhanced. The leading corrections to associated Higgs production with bottom quarks can be absorbed into the bottom Yukawa couplings in a universal way. This resummation can also be applied to the associated Higgs production with top quarks, but since the top Yukawa coupling is not enhanced by tanβ rather than suppressed, these contributions are non-leading and there is no need for resummation. Finally, numerical results for two benchmark points for a linear e^+e^- collider with a center of mass energy of 1 TeV are discussed.

4.1 Motivation

Although the cross sections of associated Higgs production with heavy quarks range at the ILC about two orders of magnitude below the dominant Higgs-strahlung process, it is a very important channel to measure the top Yukawa couplings for Higgs masses below the $t\bar{t}$ threshold. For $m_\phi > 2m_t$ these couplings are directly accessible in the Higgs decay $\phi \to t\bar{t}$. Given the cross section at $\sqrt{s} = 800$ GeV and assuming an integrated luminosity of 1000 fb^{-1} the SM Higgs boson can be measured with an uncertainty of $\sim 5.5\%$ (stat.+syst.), leading to about the same accuracy for the top Yukawa coupling (Figure 4.1a). The main sources of uncertainties are failures of the jet-clustering and of the b-tagging due to hard gluon radiation and too large multiplicities. NLO corrections are needed first to reduce the theoretical uncertainties originating from scale and scheme dependencies and secondly, because they can give sizeable contributions.

The ratio of the VEVs, tanβ, is one of the most difficult MSSM parameters to determine. The associated Higgs production with bottom quarks $e^+e^- \to \phi b\bar{b}$ followed by $\phi \to b\bar{b}$ provides excellent channels to measure tanβ for moderate m_A and tanβ values. The experimental challenges are the expected low production rate and the large irreducible

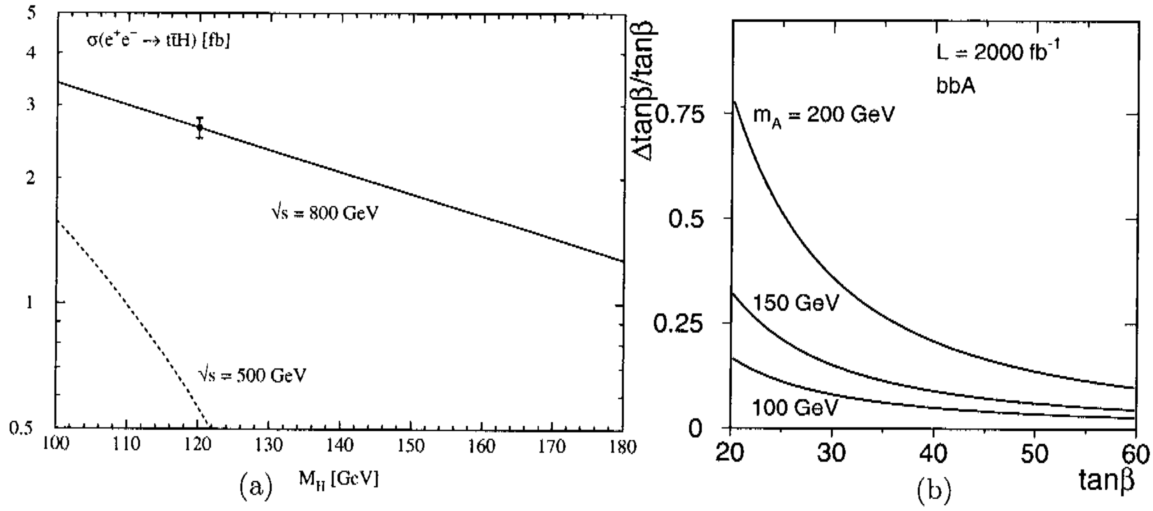

Figure 4.1: *(a) SM cross sections of associated Higgs production with top quarks as functions of the Higgs mass at a linear* e^+e^- *collider. The dashed/full line corresponds to a center of mass energy of* $\sqrt{s}$ *= 500 and 800 GeV. The error bar is shown for an integrated luminosity of 1000* fb^{-1} *and includes systematical and statistical uncertainties [50]. (b) The statistical error of* tanβ *as a function of* tanβ *assuming an integrated luminosity of 2000* fb^{-1} *and pseudoscalar Higgs masses* m_A *= 100, 150 and 200 GeV at a linear* e^+e^- *collider with* $\sqrt{s}$ *= 500 GeV [103].*

backgrounds for four-jet final states. In Figure 4.1b the statistical errors of tanβ for an integrated luminosity of 2000 fb^{-1} and pseudoscalar Higgs masses m_A =100, 150 and 200 GeV at a linear e^+e^- collider with $\sqrt{s}$ = 500 GeV are shown [103].

4.2 Leading Order Cross Sections

At leading order (LO) associated Higgs production with heavy quarks in e^+e^- collision

$$e^- (p_1) + e^+ (p_2) \to Q (p_3) + \bar{Q} (p_4) + \phi (p_5)$$

is described by the Feynman diagrams in Figure 4.2. The four dimensional vectors p_i denote the momenta of the massless incoming leptons ($i = 1, 2$), the massive outgoing quarks ($i = 3, 4$) and the Higgs boson ($i = 5$) with masses $m_i = \sqrt{p_i^2}$.

These diagrams split into three different classes of contributions: (1) *Higgs radiation off the heavy (anti)quark*, (2) *scalar Higgs radiation off the Z boson* and (3) *Z boson splitting into scalar-pseudoscalar Higgs pairs with one of them dissociating into a heavy quark pair.* Depending on the masses of the corresponding particles, resonant contributions arise, which require the inclusion of finite decay widths of the Z and Higgs bosons in the corresponding propagators. Conventional Breit-Wigner propagators have been used for the resonant $Z \to b\bar{b}$ and $\phi \to t\bar{t}/b\bar{b}$ decays.

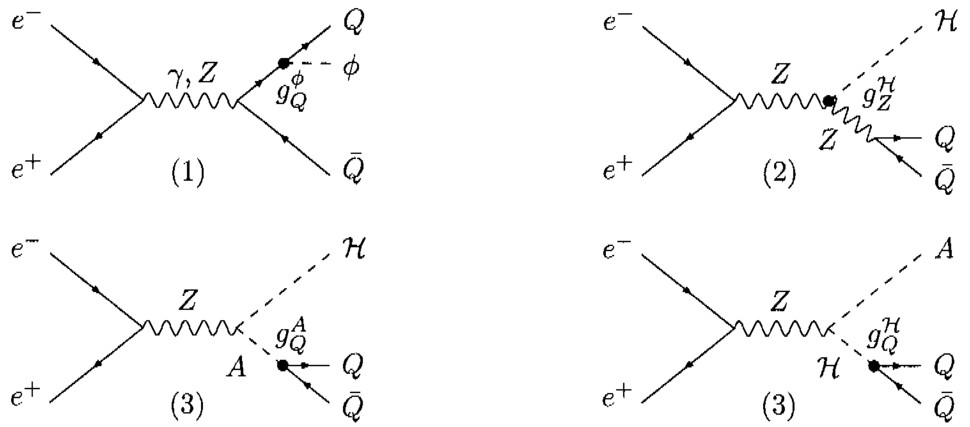

Figure 4.2: *Individual channels of scalar and pseudoscalar associated Higgs production with heavy quarks $Q = t, b$ in e^+e^- collisions:* (1) *Higgs radiation off the heavy (anti)quark,* (2) *scalar Higgs radiation off the Z boson and* (3) *Z boson splitting into scalar-pseudoscalar Higgs pairs with one of them dissociating into a heavy $Q\bar{Q}$ pair. ϕ denotes all three neutral MSSM Higgs bosons, while $\mathcal{H}$ stays for the scalar ones only.*

The LO matrix elements can be decomposed according to the different Higgs couplings:

$$\mathcal{M}_{\rm LO}^{\mathcal{H}} = g_Q^{\mathcal{H}}\, \mathcal{C}_1^{\rm LO} + g_Z^{\mathcal{H}}\, \mathcal{C}_2^{\rm LO} + g_Q^{A}\, \mathcal{C}_3^{\rm LO},$$
$$\mathcal{M}_{\rm LO}^{A} = g_Q^{A}\, \mathcal{D}_1^{\rm LO} + g_Q^{h}\, \mathcal{D}_{3h}^{\rm LO} + g_Q^{H}\mathcal{D}_{3H}^{\rm LO}\,.$$

The $\mathcal{C}$'s for scalar Higgs production can be factorised pursuant to the SME method (Chapter 3.5):

$$\begin{aligned}
\mathcal{C}_1^{\rm LO} &= \sum_{V=\gamma,Z} c_1^V \cdot \Big\{ F_3^{1V}\, \mathcal{M}_3^V + F_6^{1V}\, \mathcal{M}_6^V + F_7^{1V}\, \mathcal{M}_7^V + \\
&\qquad\qquad F_8^{1V}\, \mathcal{M}_8^V + F_{15}^{1V}\, \mathcal{M}_{15}^V + F_{16}^{1V}\, \mathcal{M}_{16}^V \Big\}, \\
\mathcal{C}_2^{\rm LO} &= c_2 \cdot \Big\{ F_4^{2Z}\, \mathcal{M}_4^Z + F_5^{2Z}\, \mathcal{M}_5^Z \Big\}, \\
\mathcal{C}_3^{\rm LO} &= c_3 \cdot \Big\{ F_4^{3Z}\, \mathcal{M}_4^Z + F_5^{3Z}\, \mathcal{M}_5^Z + F_6^{3Z}\, \mathcal{M}_6^Z \Big\}.
\end{aligned}$$

The coefficients c_i depend only on the coupling constants and the gauge and Higgs boson propagators:

$$\begin{aligned}
c_1^V &= i\, g_Q^{\rm SM}\, \frac{4\pi\alpha_{\rm elm}}{s - m_V^2}, \\
c_2 &= i\, g_Z^{\rm SM}\, \frac{4\pi\alpha_{\rm elm}}{s - m_Z^2}\, \frac{1}{s_{34} - m_Z^2}, \\
c_3 &= i\, g_Q^{\rm SM}\, g_{ZA\mathcal{H}}\, \frac{\sqrt{4\pi\alpha_{\rm elm}}}{s - m_Z^2}\, \frac{1}{s_{34} - m_A^2},
\end{aligned}$$

where $s_{ij} \equiv (p_i + p_j)^2$. The formfactors $F_i^{jV/Z}$ with the shortcuts $f_3 \equiv (s_{35} - m_Q^2)^{-1/2}$, $f_4 \equiv (s_{45} - m_Q^2)^{-1/2}$ and $f_{34}^{\pm} \equiv f_3 \pm f_4$ are listed in Table 4.1.

j	F_3^{jV}	$F_4^{jZ} = F_5^{jZ}$	F_6^{jV}	$F_7^{jV/Z}$	$F_8^{jV/Z}$	F_{15}^{jV}	F_{16}^{jV}
1	$2v_V^Q f_3$	–	$-2a_V^Q f_3$	$2m_Q v_V^Q f_{34}^+$	$2m_Q a_V^Q f_{34}^+$	$-v_V^Q f_{34}^+$	$a_V^Q f_{34}^-$
2	–	$-2m_Q/m_Z^2 a_Z^Q$	–	–	–	–	–
3	–	1	-1	–	–	–	–

Table 4.1: *Formfactors of the LO diagrams for $e^+e^- \to \mathcal{H}Q\bar{Q}$.*

The axialvectorial and vectorial coupling coefficients a_V^Q and v_V^Q are defined in Appendix A.

The $\mathcal{D}$'s for the pseudoscalar Higgs production can be decomposed as:

$$\begin{aligned}
\mathcal{D}_1^{\mathrm{LO}} &= \sum_{V=\gamma,Z} d_1^V \cdot \left\{ F_3^{1V}\,\mathcal{M}_3^V + F_6^{1V}\,\mathcal{M}_6^V + F_{15}^{1V}\,\mathcal{M}_{15}^V + F_{16}^{1V}\,\mathcal{M}_{16}^V \right\}, \\
\mathcal{D}_{3\mathcal{H}}^{\mathrm{LO}} &= d_{3\mathcal{H}} \cdot \left\{ F_1^{3Z}\,\mathcal{M}_1^Z + F_2^{3Z}\,\mathcal{M}_2^Z + F_3^{3Z}\,\mathcal{M}_3^Z \right\},
\end{aligned}$$

with the coefficients:

$$\begin{aligned}
d_1^V &= g_Q^{\mathrm{SM}} \frac{4\pi\alpha_{\mathrm{elm}}}{s - m_V^2}, \\
d_{3\mathcal{H}} &= g_Q^{\mathrm{SM}} \frac{\sqrt{4\pi\alpha_{\mathrm{elm}}}}{s - m_Z^2} \frac{1}{s_{34} - m_{\mathcal{H}}^2} g_{ZA\mathcal{H}},
\end{aligned}$$

and the formfactors $F_i^{jV/Z}$ listed in Table 4.2.

j	$F_1^{jZ} = F_2^{jZ}$	$F_3^{jV/Z}$	F_6^{jV}	F_{15}^{jV}	F_{16}^{jV}
1	–	$-2\,a_V^Q\,f_3$	$2\,v_V^Q\,f_3$	$2\,a_V^Q\,f_{34}^-$	$-2\,v_V^Q\,f_{34}^+$
3	1	-1	–	–	–

Table 4.2: *Formfactors of the LO diagrams for $e^+e^- \to AQ\bar{Q}$.*

The unpolarised LO cross sections are defined by:

$$\boxed{\sigma_{\mathrm{LO}}^{\phi} \equiv \frac{1}{2s} \int d\mathrm{PS}_3 \sum_{\mathrm{spin}} \overline{|\mathcal{M}_{\mathrm{LO}}^{\phi}|^2},}$$

with $d\mathrm{PS}_3$ denoting the three-particle phase space element (Chapter 3.4). The sum has to be performed over the spins of the initial and final state particles, supplemented by an averaging over the spins of the initial particles indicated by the overline.

4.3 QCD Corrections

The QCD corrections were calculated some years ago [104]. The strong coupling α_s is evaluated at NLO with five active flavours at the renormalisation scale $\mu_R = \sqrt{s}$ and is normalised to $\alpha_s(m_Z) = 0.119$. The ultraviolet divergences are removed by the renormalisation of the quark masses and Yukawa couplings, which are connected to the quark masses. They are renormalised on-shell, because they define the allowed phase space. Since the top mass is of the same order as the Higgs masses no large logarithms arise for the top Yukawa couplings, thus, the latter are renormalised on-shell, too. In the bottom quark case large logarithms appear, which are mapped into the running $\overline{\mathrm{MS}}$ bottom mass:

$$\begin{aligned} m_b^0 &= \overline{m}_b(\mu)\,[1+\delta_{QCD}] \quad \text{with} \quad \delta_{QCD} = -\frac{\alpha_s}{\pi}\Gamma(\varepsilon)(4\pi)^{\varepsilon}, \\ \overline{m}_b(\mu) &= m_b\left[1 + C_F\frac{\alpha_s(\mu)}{\pi}\left(-\frac{3}{4}\log\frac{\mu^2}{m_b^2} - 1\right) + \mathcal{O}\left(\alpha_s^2(\mu)\right)\right], \end{aligned} \tag{4.1}$$

where m_b^0 denotes the bare bottom mass, m_b the bottom pole mass, $\overline{m}_b(\mu)$ the $\overline{\mathrm{MS}}$ mass at the scale μ and δ_{QCD} the corresponding QCD counterterm. Thus, renormalisation of the bottom Yukawa couplings introduces the $\overline{\mathrm{MS}}$ Yukawa couplings of QCD evaluated at the scale μ given by the squared momentum flow through the corresponding Higgs boson line.

The value of the electromagnetic coupling is taken to be $\alpha_{\mathrm{elm}} = 1/128$ and the Weinberg angle to be $\sin^2\theta_W = 0.23$. The mass of the Z boson is set to $m_Z = 91.187$ GeV, and the pole masses of the top and bottom quarks to $m_t = 175$ GeV[1] and $m_b = 4.62$ GeV, respectively. This value for the perturbative pole mass of the bottom quark corresponds in NLO to an $\overline{\mathrm{MS}}$ mass $\overline{m}_b(\overline{m}_b) = 4.28$ GeV. The masses of the MSSM Higgs bosons and their couplings are related to tanβ and the pseudoscalar Higgs boson mass m_A. Higher-order corrections up to two loops in the effective-potential approach are included in the used relations [106]. The Z boson width is chosen as $\Gamma_Z = 2.49$ GeV, and the Higgs boson widths are computed with the program HDECAY [70].

At a linear e^+e^- collider with a center of mass energy of 500 GeV, the QCD corrections to associated scalar Higgs production with top quarks decrease the cross section by about 3–5%. They are slightly positive for the pseudoscalar Higgs production with top quarks for $\sqrt{s} = 1$ TeV. For the $b\bar{b}$ final state, the QCD corrections increase the cross section by some 5–25% due to the resonant contributions from the on-shell $Z \to b\bar{b}$ and $\phi \to b\bar{b}$ decays.

4.4 SUSY-QCD Corrections

The NLO SUSY-QCD corrections emerge from virtual gluino and squark exchanges as depicted in Figure 4.3. They consist of (i) internal self-energies, (ii) vertex, (iii) box contributions, (iv) external self-energies (Chapter 4.4.1) and (v) counterterms (Chapter 4.4.2).

[1] The top mass has been chosen in accordance with the definitions of the Snowmass benchmark points of the MSSM [105].

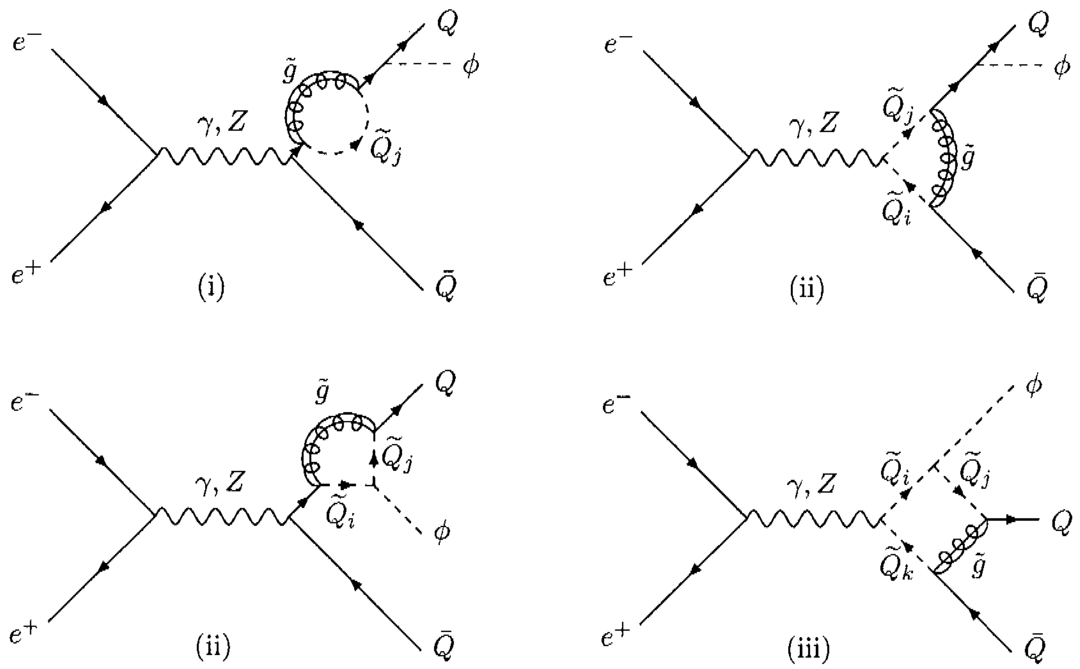

Figure 4.3: *Typical diagrams of the NLO SUSY-QCD corrections to* $e^+e^- \to \phi Q\bar{Q}$ *[*$Q = t, b$*] mediated by gluino* $\tilde{g}$ *and squark* $\tilde{Q} = \tilde{t}, \tilde{b}$ *exchanges:* (i) *internal self-energy,* (ii) *vertex corrections to gauge and Yukawa coupling and* (iii) *box diagram.*

The virtual corrections

$$\boxed{\mathcal{M}^{\phi}_{\text{virt}} = \mathcal{M}^{\phi}_{\text{ise}} + \mathcal{M}^{\phi}_{\text{vertex}} + \mathcal{M}^{\phi}_{\text{box}}}$$

are calculated within dimensional regularisation in the standard way. Since all virtual particles are massive, no infrared nor collinear singularities arise. The loop integral are evaluated with `LoopTools` [107]. The quark masses and the top Yukawa coupling are renormalised on-shell as in the pure QCD calculation. The gluino and the sbottom contributions are decoupled from the running of the bottom Yukawa couplings. Thus, the pure $\overline{\text{MS}}$ Yukawa couplings of QCD are used for the SUSY-QCD corrections, too.

4.4.1 External Self-Energies

In SUSY-QCD no external self-energies exist at the initial leptonic legs. The shaded ovals $\widehat{\mathcal{M}}^{\phi}_{\text{LO}}$ in Figure 4.4 symbolise the amplitude of all LO diagrams of Figure 4.2 with amputated quark and antiquark spinors: $\mathcal{M}^{\phi}_{\text{LO}} \equiv \bar{u}_3\, \widehat{\mathcal{M}}^{\phi}_{\text{LO}}\, v_4$.

The SUSY-QCD self-energy of quarks from equation (3.1) leads to the external self-energy contributions:

$$\Sigma_{\text{ese}}\,(\not{p}) \;\;=\;\; \frac{1}{2}\,(\not{p} - m_{\psi})\;\delta Z_V + \not{p}\,\gamma_5\,\delta Z_A + \Sigma^R\,(\not{p})\;.$$

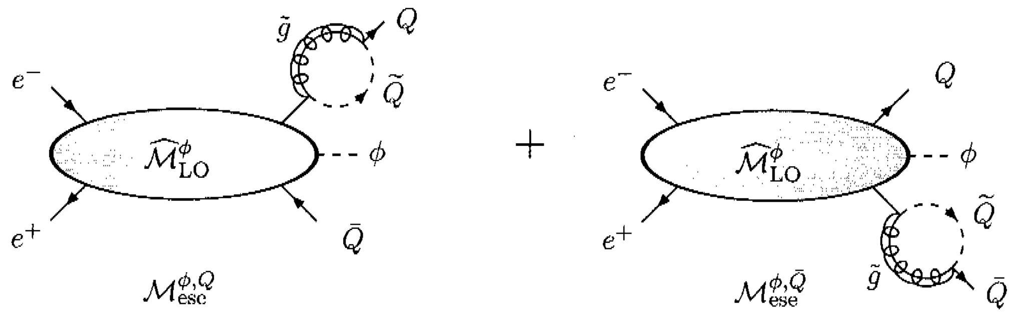

Figure 4.4: *Schematic external self-energy diagrams: the shaded oval* $\widehat{\mathcal{M}}^{\phi}_{LO}$ *represents all LO diagrams of Figure 4.2 with amputated quark and antiquark spinors.*

The factor 1/2 originates from the proper transition from the Green's functions to the S-matrix. The renormalised Σ^R does not contribute, since it is of order $(\not{p} - m)^2$.

The on-shell renormalised external self-energy at the quark leg is thus given by:

$$\begin{aligned}
\mathcal{M}^{\phi,Q}_{\rm ese} &= \bar{u}_3 \Big(-i\,\Sigma^{\rm OS}_{\rm ese}(\not{p}_3)\Big) \frac{i}{\not{p}_3 - m_Q} \widehat{\mathcal{M}}^{\phi}_{\rm LO}\, v_4 \Big|_{\not{p}_3 = m_Q} \\
&= \bar{u}_3 \left[\frac{1}{2}(\not{p}_3 - m_Q)\,\delta Z_V^{\rm OS} + \not{p}_3\,\gamma_5\,\delta Z_A\right] \frac{1}{\not{p}_3 - m_Q} \widehat{\mathcal{M}}^{\phi}_{\rm LO}\, v_4 \Big|_{\not{p}_3 = m_Q} \\
&= \frac{1}{2}\,\delta Z_V^{\rm OS}\,\bar{u}_3\,\widehat{\mathcal{M}}^{\phi}_{\rm LO}\, v_4 + m_Q\,\delta Z_A\,\bar{u}_3 \frac{1}{-\not{p}_3 - m_Q}\gamma_5\,\widehat{\mathcal{M}}^{\phi}_{\rm LO}\, v_4 \Big|_{\not{p}_3 = m_Q} \\
&= \frac{1}{2}\,\delta Z_V^{\rm OS}\,\mathcal{M}^{\phi}_{\rm LO} - \frac{1}{2}\,\delta Z_A^{\rm OS}\,\bar{u}_3\,\gamma_5\,\widehat{\mathcal{M}}^{\phi}_{\rm LO}\, v_4\,,
\end{aligned}$$

and analogously the external self-energy at the antiquark leg:

$$\begin{aligned}
\mathcal{M}^{\phi,\bar{Q}}_{\rm ese} &= \bar{u}_3\,\widehat{\mathcal{M}}^{\phi}_{\rm LO} \frac{i}{-\not{p}_4 - m_Q}\Big(-i\,\Sigma^{\rm OS}_{\rm ese}(-\not{p}_4)\Big) v_4 \Big|_{-\not{p}_4 = m_Q} \\
&= \frac{1}{2}\,\delta Z_V^{\rm OS}\,\mathcal{M}^{\phi}_{\rm LO} + \frac{1}{2}\,\delta Z_A^{\rm OS}\,\bar{u}_3\,\widehat{\mathcal{M}}^{\phi}_{\rm LO}\,\gamma_5\, v_4.
\end{aligned}$$

The external self-energies finally contribute to the NLO SUSY-QCD corrections as:

$$\boxed{\mathcal{M}^{\phi}_{\rm ese} = \delta Z_V^{\rm OS}\,\mathcal{M}^{\phi}_{\rm LO} + \frac{1}{2}\,\delta Z_A^{\rm OS}\,\bar{u}_3\left[\widehat{\mathcal{M}}^{\phi}_{\rm LO}, \gamma_5\right] v_4.}$$

With the SUSY-QCD self-energy of the quark propagator in Figure 4.5:

$$\begin{aligned}
-i\Sigma(\not{p}) &= \frac{\bar{g}_s^2}{2}\,(T^a T^a)_{lk} \sum_j \int \frac{d^D k}{(2\pi)^D} \frac{(v_j + a_j\gamma_5)(\not{k} + m_{\tilde{g}})(v_j - a_j\gamma_5)}{\left(k^2 - m_{\tilde{g}}^2\right)\left((k-p)^2 - m_{\tilde{Q}_j}^2\right)} \\
&= \frac{\bar{g}_s^2}{2}\,C_F\delta_{kl} \sum_j \Big[\left(v_j^2 - a_j^2\right) m_{\tilde{g}}\, B_0\left(p^2; m_{\tilde{g}}^2, m_{\tilde{Q}_j}^2\right) \\
&\qquad + \left(v_j^2 + a_j^2 + 2a_j v_j \gamma_5\right) \not{p}\, B_1\left(p^2; m_{\tilde{g}}^2, m_{\tilde{Q}_j}^2\right)\Big],
\end{aligned}$$

the renormalisation constants are given by:

$$\begin{aligned}
\delta m_Q^{\rm OS} &= 2i\,\bar{g}_s^2 \sum_j \Big[m_{\tilde{g}} \left(v_j^2 - a_j^2\right) B_0 + m_Q \left(v_j^2 + a_j^2\right) B_1 \Big], \\
\delta Z_V^{\rm OS} &= 2i\,\bar{g}_s^2 \sum_j \Big[2 m_{\tilde{g}} m_Q \left(v_j^2 - a_j^2\right) B_0' + \left(v_j^2 + a_j^2\right) \left(B_1 + 2 m_Q^2 B_1'\right) \Big], \\
\delta Z_A^{\rm OS} &= -2i\,\bar{g}_s^2 \sum_j \Big[2 a_j v_j B_1 \Big].
\end{aligned}$$

B_i abbreviates the scalar integrals $B_i\left(p^2; m_{\tilde{g}}^2, m_{\tilde{Q}_j}^2\right)$ evaluated at $p^2 = m_Q^2$ (Appendix B). The B_i' are the partial derivatives with respect to p^2 and $\bar{g}_s = g_s \mu_R^{\varepsilon}$. The coupling coefficients of the heavy squarks are $a_{1/2} = \cos\theta \pm \sin\theta$ and $v_{1/2} = \pm\cos\theta - \sin\theta$, where θ is the mixing angle in the squark sector (Chapter 1.3.2).

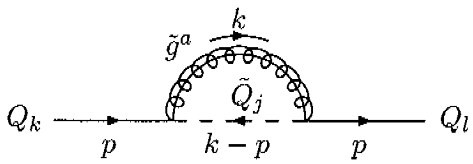

Figure 4.5: *Feynman diagram of the SUSY-QCD quark self-energy.*

4.4.2 Counterterms

The leptonic initial state does not have any SUSY-QCD corrections and thus no counterterms. In the final state the wave function, the quark mass, the Yukawa and the strong gauge coupling couplings have to be renormalised (Figure 4.6). Neither the electroweak coupling constant nor the Higgs field are renormalised in SUSY-QCD.

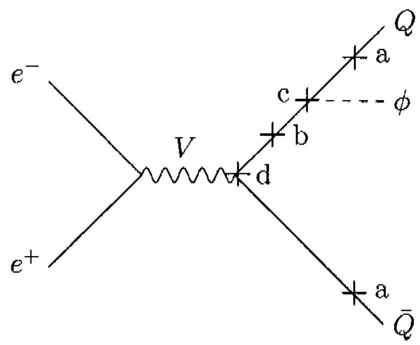

Renormalisation constants:

a = quark field $\dfrac{1}{\sqrt{Z_{Q_{L/R}}}}$

b = quark propagator $\dfrac{1}{\sqrt{Z_{Q_L}}\sqrt{Z_{Q_R}}}\left(1 - \dfrac{\delta m_Q}{\not{p} - m_Q}\right)$

c = $Q\bar{Q}\phi$−vertex $\sqrt{Z_{Q_L}}\sqrt{Z_{Q_R}}Z_m$

d = $Q\bar{Q}V$−vertex $\sqrt{Z_{Q_L}}\sqrt{Z_{Q_R}}$

Figure 4.6: *Multiplicative renormalisation constants of the wave function, the quark mass, the Yukawa and the strong gauge couplings.*

The counterterms to the NLO SUSY-QCD corrections can be derived from Figure 4.6:

$$
\begin{aligned}
\Big\{\mathrm{a}\times\mathrm{c}\times\mathrm{b}\times\mathrm{d}\times\mathrm{a}\Big\} &= \Bigg\{\frac{1}{\sqrt{Z_{Q_{L/R}}}}\times\sqrt{Z_{Q_L}}\sqrt{Z_{Q_R}}\,Z_m\times\frac{1}{\sqrt{Z_{Q_L}}\sqrt{Z_{Q_R}}}\left(1-\frac{\delta m_Q}{\not p-m_Q}\right)\\
&\quad\times\sqrt{Z_{Q_L}}\sqrt{Z_{Q_R}}\times\frac{1}{\sqrt{Z_{Q_{R/L}}}}\Bigg\}\\
&= Z_m\times\left(1-\frac{\delta m_Q}{\not p-m_Q}\right).
\end{aligned}
$$

Hence, the only parameters which need to be renormalised are the Yukawa couplings

$$
\begin{aligned}
\mathcal{M}^{\mathcal{H}}_{\mathrm{Yuk}} &= -\frac{\delta m_Q}{m_Q}\cdot\Big[g^{\mathcal{H}}_Q\mathcal{C}^{\mathrm{LO}}_1+g^A_Q\mathcal{C}^{\mathrm{LO}}_3\Big],\\
\mathcal{M}^{A}_{\mathrm{Yuk}} &= -\frac{\delta m_Q}{m_Q}\cdot\Big[g^A_Q\,\mathcal{D}^{\mathrm{LO}}_1+g^h_Q\mathcal{D}^{\mathrm{LO}}_{3h}+g^H_Q\mathcal{D}^{\mathrm{LO}}_{3H}\Big],
\end{aligned}
$$

and the quark mass for Higgs boson radiation off the quark and off the antiquark leg:

$$
\begin{aligned}
\mathcal{M}^{\mathcal{H}}_{\mathrm{mass}} &= -i\,g^{\mathcal{H}}_Q g^{\mathrm{SM}}_Q\,\delta m_Q\sum_V\frac{4\pi\alpha}{s-m_V^2}\\
&\quad\bar u_3\Bigg\{\frac{(\not p_3+\not p_5+m_Q)(\not p_3+\not p_5+m_Q)\gamma_\mu(v^Q_V-a^Q_V\gamma_5)}{(s_{35}-m_Q^2)^2}\\
&\quad+\frac{\gamma_\mu(v^Q_V-a^Q_V\gamma_5)(-\not p_4-\not p_5+m_Q)(-\not p_4-\not p_5+m_Q)}{(s_{45}-m_Q^2)^2}\Bigg\}v_4\\
&\quad\bar v_2\gamma^\mu(v^e_V-a^e_V\gamma_5)u_1\\
&= -i\,g^{\mathcal{H}}_Q g^{\mathrm{SM}}_Q\,\delta m_Q\sum_V\frac{4\pi\alpha}{s-m_V^2}\Bigg\{\Big[4\,m_Q\,v^Q_V\,f_3^2\Big]\,\mathcal{M}^V_3+\Big[-4\,m_Q\,a^Q_V\,f_3^2\Big]\,\mathcal{M}^V_6\\
&\quad+\Big[\Big(f_3+f_4+4m_Q^2\,(f_3^2+f_4^2)\Big)v^Q_V\Big]\mathcal{M}^V_7\\
&\quad+\Big[\Big(f_3+f_4+4m_Q^2\,(f_3^2+f_4^2)\Big)a^Q_V\Big]\mathcal{M}^V_8\\
&\quad+\Big[-2m_Q\,v^Q_V\,(f_3^2+f_4^2)\Big]\,\mathcal{M}^V_{15}+\Big[2m_Q\,a^Q_V\,(f_3^2-f_4^2)\Big]\,\mathcal{M}^V_{16}\Bigg\}.
\end{aligned}
$$

The quark mass renormalisation for the radiation off the pseudoscalar Higgs boson is computed accordingly, with the scalar Yukawa coupling replaced by the pseudoscalar one:

$$
\begin{aligned}
\mathcal{M}^{A}_{\mathrm{mass}} &= -i\,g^{A}_Q g^{\mathrm{SM}}_Q\,\delta m_Q\sum_V\frac{4\pi\alpha}{s-m_V^2}\\
&\quad\bar u_3\Bigg\{[-i\gamma_5]\,\frac{(\not p_3+\not p_5+m_Q)(\not p_3+\not p_5+m_Q)\gamma_\mu(v^Q_V-a^Q_V\gamma_5)}{(s_{35}-m_Q^2)^2}\\
&\quad+\frac{\gamma_\mu(v^Q_V-a^Q_V\gamma_5)(-\not p_4-\not p_5+m_Q)(-\not p_4-\not p_5+m_Q)}{(s_{45}-m_Q^2)^2}[-i\gamma_5]\Bigg\}v_4\\
&\quad\bar v_2\gamma^\mu(v^e_V-a^e_V\gamma_5)u_1
\end{aligned}
$$

$$
\begin{aligned}
= & -g_Q^A g_Q^{\rm SM}\, \delta m_Q \sum_V \frac{4\pi\alpha}{s-m_V^2} \Big\{ \left[-4m_Q\, a_V^Q\, f_3^2\right] \mathcal{M}_3^V + \left[4\, m_Q\, v_V^Q\, f_3^2\right] \mathcal{M}_6^V \\
& + \left[(f_3 - f_4)\, a_V^Q \right] \mathcal{M}_7^V + \left[(f_3 - f_4)\, v_V^Q \right] \mathcal{M}_8^V \\
& + \left[2m_Q\, a_V^Q\, (f_3^2 - f_4^2) \right] \mathcal{M}_{15}^V + \left[-2m_Q\, v_V^Q\, (f_3^2 + f_4^2) \right] \mathcal{M}_{16}^V \Big\}.
\end{aligned}
$$

The counterterms finally contribute to the NLO SUSY-QCD corrections with:

$$
\boxed{\mathcal{M}_{\rm CT}^\phi = \mathcal{M}_{\rm Yuk}^\phi + \mathcal{M}_{\rm mass}^\phi\,.}
$$

4.4.3 Bottom Quark Final State

The renormalised bottom Yukawa coupling is defined in terms of the $\overline{\rm MS}$ running bottom mass of equation (4.1) as described in Chapter 4.3. This $\overline{\rm MS}$ Yukawa coupling is used whenever the bottom Yukawa coupling appears.

For large values of tanβ significant "non-decoupling" corrections to $\phi b\bar{b}$ production arise at higher order, which can be absorbed into the bottom Yukawa couplings in a universal way[2] [109]. These contributions of $\mathcal{O}(A_b)$ and $\mathcal{O}(\mu\tan\beta)$ to the NLO SUSY-QCD corrections can be of $\mathcal{O}(1)$. For this reason one has to worry about higher order contributions. In references [110, 111] it has been shown that they can be resummed to improve the reliability of the perturbative result.

There exist three basic contributions (Figure 4.7) to the bottom Yukawa coupling in the Lagrangian (1.4):

(i) LO: the bottom Yukawa coupling is proportional to the bottom pole mass.

(ii) Superpotential: the couplings of the neutral component of H_u to sbottoms are proportional to the higgsino mass parameter μ. By reexpressing H_u^0 through v_d this coupling becomes proportional to tanβ. Analogously there exists a coupling of the neutral component of the down-type Higgs doublet to stops, but this becomes tanβ–suppressed compared to the LO coupling.

(iii) Soft breaking terms: the couplings of the neutral component of H_d to sbottoms are proportional to the scalar trilinear coupling A_b. The analogous coupling exists for the stops, but as the non-decoupling contributions are small, there is no need for resummation in the case of the top Yukawa coupling.

These three contributions can be cast into the form [110]:

$$
\mathcal{L}_{\rm Yuk}^{\rm LO+NLO} = -g_b^0\, \bar{b}^0 \left\{ (1+\Delta_1)\, H_d^0 + \frac{\Delta m_b}{\tan\beta} H_u^0 \right\} b^0 + h.c.
$$

[2] It should be noted that these contributions vanish for large sbottom and gluino masses while keeping the μ parameter fixed [108]. Non-decoupling effects only arise, if the μ parameter is increased together with the SUSY particle masses.

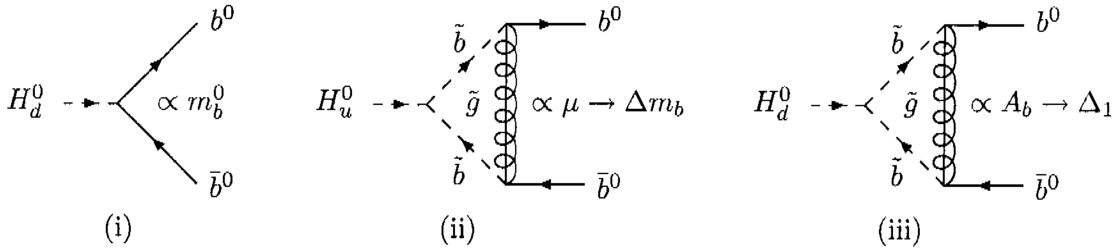

Figure 4.7: *LO and NLO SUSY-QCD contributions to the bottom Yukawa coupling. The $H^0_{d,u}$ are the neutral components of the two Higgs doublets, while the b^0, $\bar{b}^0$ and m_b^0 are the unrenormalised bottom wave functions and bottom pole mass, respectively.*

with

$$\begin{aligned}
\Delta m_b &= \frac{2}{3}\frac{\alpha_s}{\pi} m_{\tilde{g}}\, \mu\, \tan\beta\, I(m^2_{\tilde{b}_1}, m^2_{\tilde{b}_2}, m^2_{\tilde{g}}), \\
\Delta_1 &= -\frac{2}{3}\frac{\alpha_s}{\pi} m_{\tilde{g}}\, A_b\, I(m^2_{\tilde{b}_1}, m^2_{\tilde{b}_2}, m^2_{\tilde{g}}), \\
I(a,b,c) &= -\frac{ab\log\dfrac{a}{b} + bc\log\dfrac{b}{c} + ca\log\dfrac{c}{a}}{(a-b)(b-c)(c-a)}\,.
\end{aligned}$$

Renormalisation of the Yukawa coupling leads to:

$$\mathcal{L}^{\text{LO+NLO}}_{\text{Yuk}} = -g_b\, \bar{b}\left\{H_d^0 + \frac{\Delta_b}{\tan\beta} H_u^0\right\} b + h.c.$$

with $g_b = g_b^0\,(1+\Delta_1)$ and $\Delta_b = \dfrac{\Delta m_b}{1+\Delta_1}$. These leading higher order contributions result in a shift in the relation between the bottom Yukawa coupling and the bottom pole mass:

$$m_b = g_b^0\, v_d \longrightarrow g_b^0\, v_d\ (1+\Delta_1+\Delta m_b) \longrightarrow g_b\, v_d\ (1+\Delta_b)\,.$$

The effective Yukawa interaction Lagrangian can be reexpressed in the physical MSSM Higgs boson fields:

$$\begin{aligned}
\mathcal{L}^{\text{LO+NLO}}_{\text{Yuk}} &= -\frac{m_b}{v\,(1+\Delta_b)}\,\bar{b}\left\{g_b^h\left(1-\frac{\Delta_b}{\tan\alpha\tan\beta}\right)h\right. \\
&\qquad \left. + g_b^H\left(1+\Delta_b\frac{\tan\alpha}{\tan\beta}\right)H - i\gamma_5\, g_b^A\left(1-\frac{\Delta_b}{\tan^2\beta}\right)A\right\} b \\
&\equiv -\frac{m_b}{v}\,\bar{b}\left\{\tilde{g}_b^h\, h + \tilde{g}_b^H\, H - i\gamma_5\, \tilde{g}_b^A\, A\right\} b,
\end{aligned}$$

defining the resummed bottom Yukawa couplings to[3]:

$$
\begin{aligned}
\tilde{g}_b^h &= \frac{g_b^h}{1+\Delta_b}\left(1 - \frac{\Delta_b}{\tan\alpha\ \tan\beta}\right), \\
\tilde{g}_b^H &= \frac{g_b^H}{1+\Delta_b}\left(1 + \Delta_b\frac{\tan\alpha}{\tan\beta}\right), \\
\tilde{g}_b^A &= \frac{g_b^A}{1+\Delta_b}\left(1 - \frac{\Delta_b}{\tan^2\beta}\right).
\end{aligned} \tag{4.2}
$$

If the LO cross sections are expressed in terms of these resummed bottom Yukawa couplings, the corresponding NLO pieces have to be subtracted from the higher order contributions to avoid double counting. This is equivalent to an additional (finite) renormalisation, given explicitly by:

$$
\begin{aligned}
g_b^\phi &= \tilde{g}_b^\phi\left[1 + \Delta_b^\phi\right] + \mathcal{O}(\alpha_s^2), \\
\Delta_b^\phi &= \kappa_\phi\,\Delta m_b, \\
\kappa_h &= 1 + \frac{1}{\tan\alpha\ \tan\beta}, \\
\kappa_H &= 1 - \frac{\tan\alpha}{\tan\beta}, \\
\kappa_A &= 1 + \frac{1}{\tan^2\beta}.
\end{aligned} \tag{4.3}
$$

Thus, supplementary finite counterterms have to be added to the NLO SUSY-QCD corrections[4] for $b\bar{b}$ final states:

$$
\begin{aligned}
\Delta\mathcal{M}^{\mathcal{H}} &= g_b^{\mathcal{H}}\Delta_b^{\mathcal{H}}\mathcal{C}_1^{\rm LO} + g_b^A\Delta_b^A\mathcal{C}_3^{\rm LO}, \\
\Delta\mathcal{M}^A &= g_b^A\Delta_b^A\mathcal{D}_1^{\rm LO} + g_b^h\Delta_b^h\mathcal{D}_{3h}^{\rm LO} + g_b^H\Delta_b^H\mathcal{D}_{3H}^{\rm LO}.
\end{aligned} \tag{4.4}
$$

In the LO matrix elements the resummed Yukawa couplings are used:

$$
\begin{aligned}
\widetilde{\mathcal{M}}_{\rm LO}^{\mathcal{H}} &= \tilde{g}_b^{\mathcal{H}}\mathcal{C}_1^{\rm LO} + g_Z^{\mathcal{H}}\mathcal{C}_2^{\rm LO} + \tilde{g}_b^A\mathcal{C}_3^{\rm LO} \\
\widetilde{\mathcal{M}}_{\rm LO}^A &= \tilde{g}_b^A\mathcal{D}_1^{\rm LO} + \tilde{g}_b^h\mathcal{D}_{3h}^{\rm LO} + \tilde{g}_b^H\mathcal{D}_{3H}^{\rm LO},
\end{aligned} \tag{4.5}
$$

so that the SUSY-QCD corrections to the cross sections are given by:

$$
\boxed{\Delta\sigma_{\rm SQCD}^{\phi b\bar{b}} = \frac{1}{2s}\int d{\rm PS}_3\ 2\Re\mathfrak{e}\sum_{\rm spin}\overline{\widetilde{\mathcal{M}}_{\rm LO}^{\phi\dagger}\mathcal{M}_{\rm SQCD}^{\phi b\bar{b}}},} \tag{4.6}
$$

with

$$
\boxed{\mathcal{M}_{\rm SQCD}^{\phi b\bar{b}} = \mathcal{M}_{\rm virt}^\phi + \mathcal{M}_{\rm ese}^\phi + \mathcal{M}_{\rm CT}^\phi + \Delta\mathcal{M}^\phi.}
$$

[3]Analogous effective couplings can be defined for top quarks, too, but in this case the non-decoupling contributions are small and thus do not require resummation.

[4]Note that in the residual matrix elements of the SUSY-QCD corrections the unresummed bottom Yukawa couplings are kept in order to avoid artificial singularities for vanishing mixing angle α [111].

In the QCD corrections the resummed bottom Yukawa couplings are also inserted everywhere, since the non-decoupling terms Δ_b^ϕ factorise from the pure QCD corrections initiated by light particle interactions.

4.4.4 Top Quark Final State

The top Yukawa couplings are suppressed by $1/\tan\beta$. Thus, there is no need for resummation. The NLO SUSY-QCD matrix elements for $e^+e^- \to \phi t\bar{t}$ are given by:

$$\boxed{\mathcal{M}_{\rm SQCD}^{\phi t\bar{t}} = \mathcal{M}_{\rm virt}^{\phi} + \mathcal{M}_{\rm ese}^{\phi} + \mathcal{M}_{\rm CT}^{\phi}\,.}$$

Therewith the SUSY-QCD corrections to the cross sections result in:

$$\boxed{\Delta\sigma_{\rm SQCD}^{\phi t\bar{t}} = \frac{1}{2s}\int d{\rm PS}_3\; 2\Re e \sum_{\rm spin} \overline{\mathcal{M}_{\rm LO}^{\phi\dagger}\mathcal{M}_{\rm SQCD}^{\phi t\bar{t}}}\,,}$$

with the conventional Yukawa coupling in the LO matrix elements.

4.5 Numerical Results

The numerical results are presented for a linear e^+e^- collider with a center of mass energy of 1 TeV. The Snowmass point SPS5 has been chosen for associated Higgs production with top quarks and SPS1b for the bottom quark case [105]. The MSSM parameters of these two benchmark scenarios are given by[5]:

$$\begin{array}{llll}
\underline{\text{SPS5}:} & & \underline{\text{SPS1b}:} & \\
\tan\beta = 5 & & \tan\beta = 30 & \\
\mu = 639.8\text{GeV} & & \mu = 495.6\text{GeV} & \\
A_t = -905.6\text{GeV} & & A_t = -729.3\text{GeV} & \\
A_b = -1671.4\text{GeV} & & A_b = -987.4\text{GeV} & \\
m_{\tilde{g}} = 710.3\text{GeV} & & m_{\tilde{g}} = 916.1\text{GeV} & \\
m_{\tilde{q}_L} = 535.2\text{GeV} & & m_{\tilde{q}_L} = 762.5\text{GeV} & \\
m_{\tilde{b}_R} = 620.5\text{GeV} & & m_{\tilde{b}_R} = 780.3\text{GeV} & \\
m_{\tilde{t}_R} = 360.5\text{GeV}, & & m_{\tilde{t}_R} = 670.7\text{GeV}\,. &
\end{array}$$

The pseudoscalar Higgs mass is left free in both scenarios in order to scan the corresponding Higgs mass ranges.

The total cross section for associated pseudoscalar Higgs production with top quarks is displayed at LO and NLO in Figure 4.8a. The cross section is small for pseudoscalar

[5] We have neglected the corresponding translations of $\overline{\rm DR}$ masses into $\overline{\rm MS}$ masses, since they are not relevant for the characterisation of the results.

Higgs masses below about 350 GeV, while above it rapidly increases to a level of 1 fb due to the intermediate on-shell $H \to t\bar{t}$ decay. The total size of the corrections amounts to $\mathcal{O}(10\%)$ apart from the threshold of the resonant contribution, where the Coulomb singularity raises the QCD corrections to more than 100% [112]. The Coulomb singularity is an artefact of the narrow-width approximation[6]. A proper treatment of the threshold region requires the inclusion of finite-width effects and QCD-potential contributions. Thus, the result obtained in this work is not valid in a small margin around the $t\bar{t}$ threshold of the resonant part. The individual relative corrections, defined as

$$\sigma_{\rm NLO} = \sigma_{\rm LO}(1 + \delta_{\rm QCD} + \delta_{\rm SQCD}),$$

can be inferred from Figure 4.8b. Except for the threshold region of the resonant part, the QCD corrections are of moderate size [104]. The SUSY-QCD corrections [113] are of similar magnitude as the pure QCD corrections but with opposite sign. Thus, large cancellation of the QCD corrections against the SUSY-QCD part are observable in this scenario. This signalises the importance of including both types of corrections in future analyses.

An analogous picture emerges for the light and heavy scalar Higgs bosons as shown in Figures 4.9. The cross section for the light scalar Higgs boson is always of the order of 1 fb with small corrections due to the partial cancellation of QCD and SUSY-QCD corrections (Figure 4.9b). The QCD Coulomb singularity for $m_A \sim 350$ GeV is much more pronounced than in the pseudoscalar case, since for the heavy scalar Higgs boson the S-wave pseudoscalar Higgs decay $A \to t\bar{t}$ constitutes the resonant part[7]. The relative threshold corrections remain finite in both cases due to the remaining continuum contributions.

The results for $Ab\bar{b}$ production are presented in Figure 4.10. The total cross section, shown in Figure 4.10a, reaches a size of $\mathcal{O}(10 \text{ fb})$ for smaller pseudoscalar masses. The relative corrections are depicted in Figure 4.10b. The pure SUSY-QCD and total corrections are shown without and with resummation of the Δ_b terms according to equations (4.2) – (4.6). It is clearly visible that the resummed bottom Yukawa couplings absorb the bulk of the SUSY-QCD corrections, so that the terms of equation (4.4) provide a reasonable approximation of the final result. After resummation the SUSY-QCD corrections are of similar magnitude as the pure QCD corrections. Thus, as in the top quark case the inclusion of both corrections is of vital importance. A comparison of the total resummed and unresummed NLO cross sections in Figure 4.10a implies good agreement within 10% and thus a significant improvement of the perturbative stability from LO to NLO. An analogous picture emerges for the light and heavy scalar Higgs bosons as can be inferred from Figure 4.11. Again the resummed Yukawa couplings absorb the bulk of the SUSY-QCD corrections. A significant cancellation of the QCD and SUSY-QCD corrections is observed after resummation in the SPS1b scenario, too. The drops of the relative corrections towards $m_A \sim 500$ GeV in Figures 4.10 and 4.11 are caused by the kinematical closure of the intermediate on-shell HA pair production.

[6] In this approximation the width of the top quark is neglected.

[7] Since the pseudoscalar Higgs boson A carries the same quantum numbers as the 0^{-+} ground state of the $t\bar{t}$ pair, the decay $A \to t\bar{t}$ is dominated by an S-wave contribution at threshold. In contrast the scalar Higgs decay $H \to t\bar{t}$ suffers from a P-wave suppression at threshold.

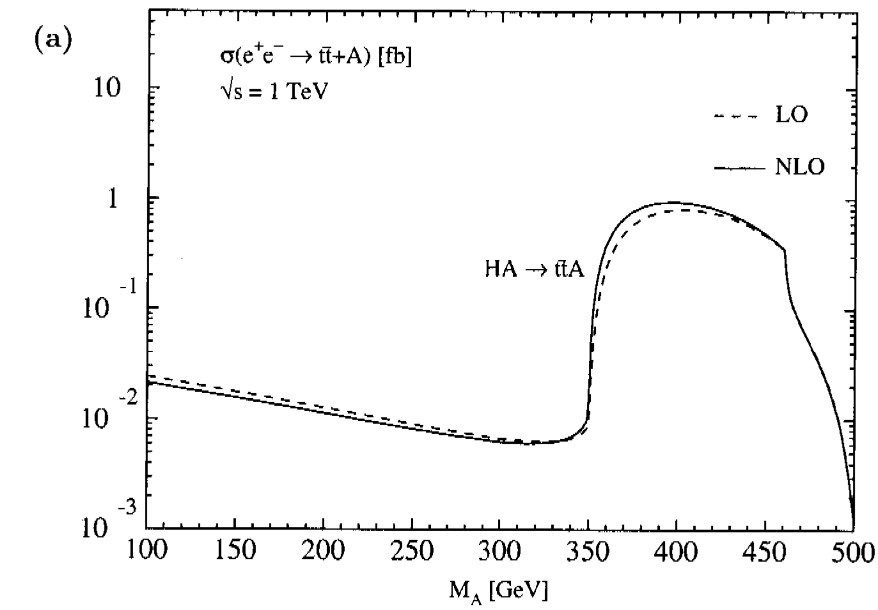

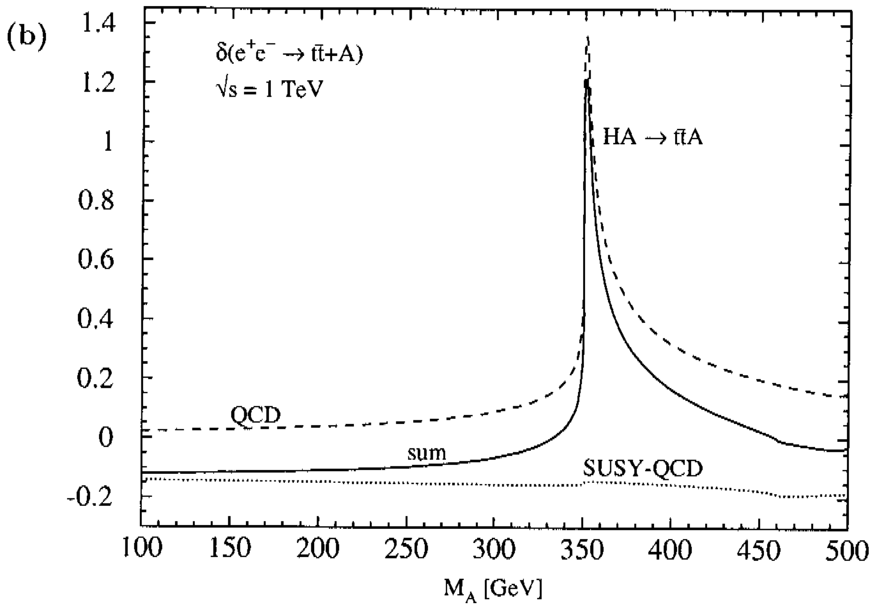

Figure 4.8: *(a) The LO (dashed line) cross section of associated pseudoscalar Higgs production with top quarks in e^+e^- collisions is plotted as a function of the pseudoscalar Higgs boson mass for the SPS5 benchmark point [105]. The QCD- and SUSY-QCD corrected NLO cross section is depicted by the full line. (b) The relative QCD, SUSY-QCD and total corrections to associated pseudoscalar Higgs production with top quarks are displayed as functions of the pseudoscalar Higgs boson mass. The sharp (finite) peak around $m_A = 350$ GeV originates from the Coulomb singularity in the QCD corrections to the resonant $H \to t\bar{t}$ decay.*

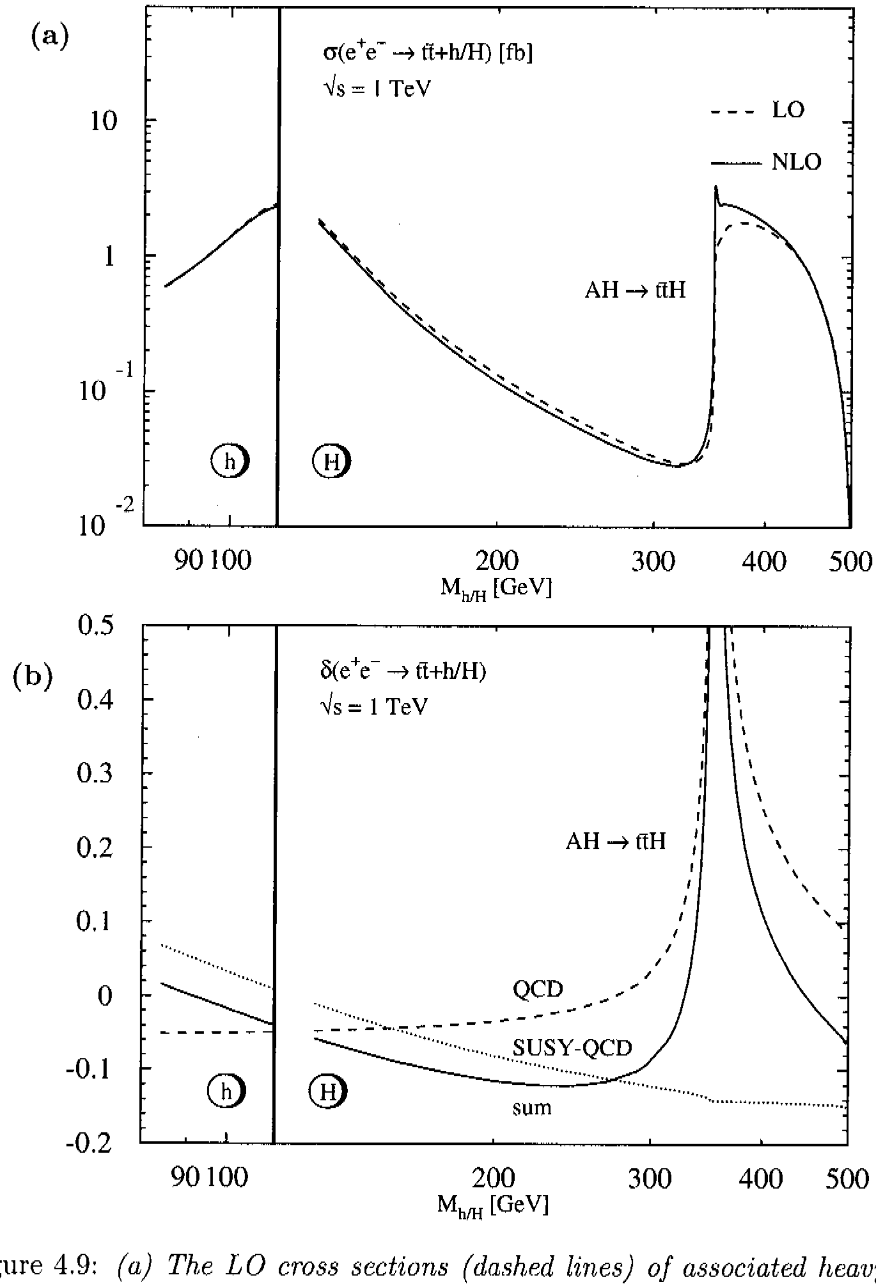

Figure 4.9: *(a) The LO cross sections (dashed lines) of associated heavy and light scalar Higgs production with top quarks in* e^+e^- *collisions are plotted as functions of the scalar Higgs boson masses for the SPS5 benchmark point [105]. The QCD- and SUSY-QCD corrected NLO cross sections are depicted by the full lines. (b) The relative QCD, SUSY-QCD and total corrections to associated scalar Higgs production with top quarks are displayed as functions of the scalar Higgs boson masses. The sharp (finite) peak around* $m_H = 350$ *GeV originates from the Coulomb singularity in the QCD corrections to the resonant* $A \to t\bar{t}$ *decay.*

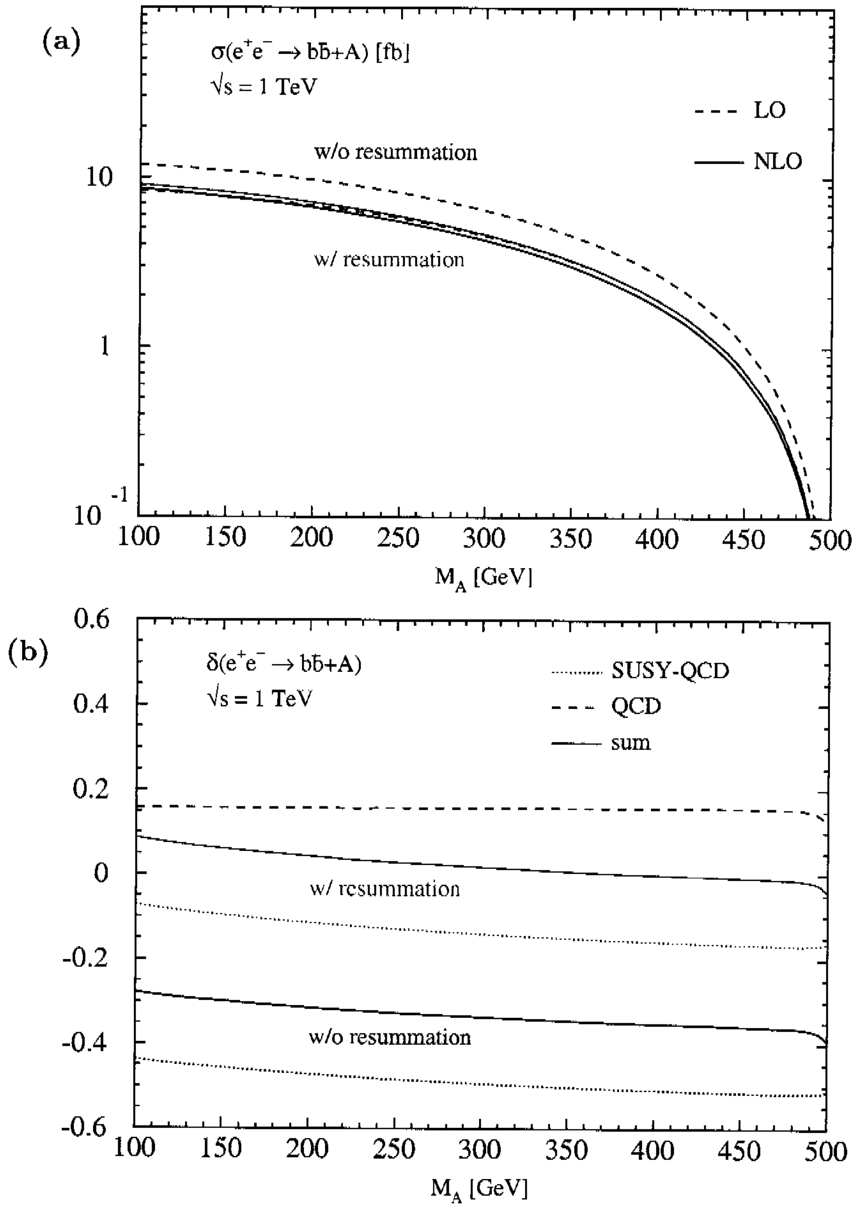

Figure 4.10: *(a) The LO cross sections (dashed lines) of associated pseudoscalar Higgs production with bottom quarks in* e^+e^- *collisions with (red curves) and without (black curves) resummation of the* Δ_b *terms are plotted as functions of the pseudoscalar Higgs boson mass for the SPS1b benchmark point [105]. The QCD- and SUSY-QCD corrected NLO cross sections are depicted by the full lines, with (red) and without (black) resummation. (b) The relative QCD, SUSY-QCD and total corrections to associated pseudoscalar Higgs production with bottom quarks are displayed with (red lines) and without (black lines) resummation as functions of the pseudoscalar Higgs boson mass. The pure QCD corrections are indistinguishable in both cases.*

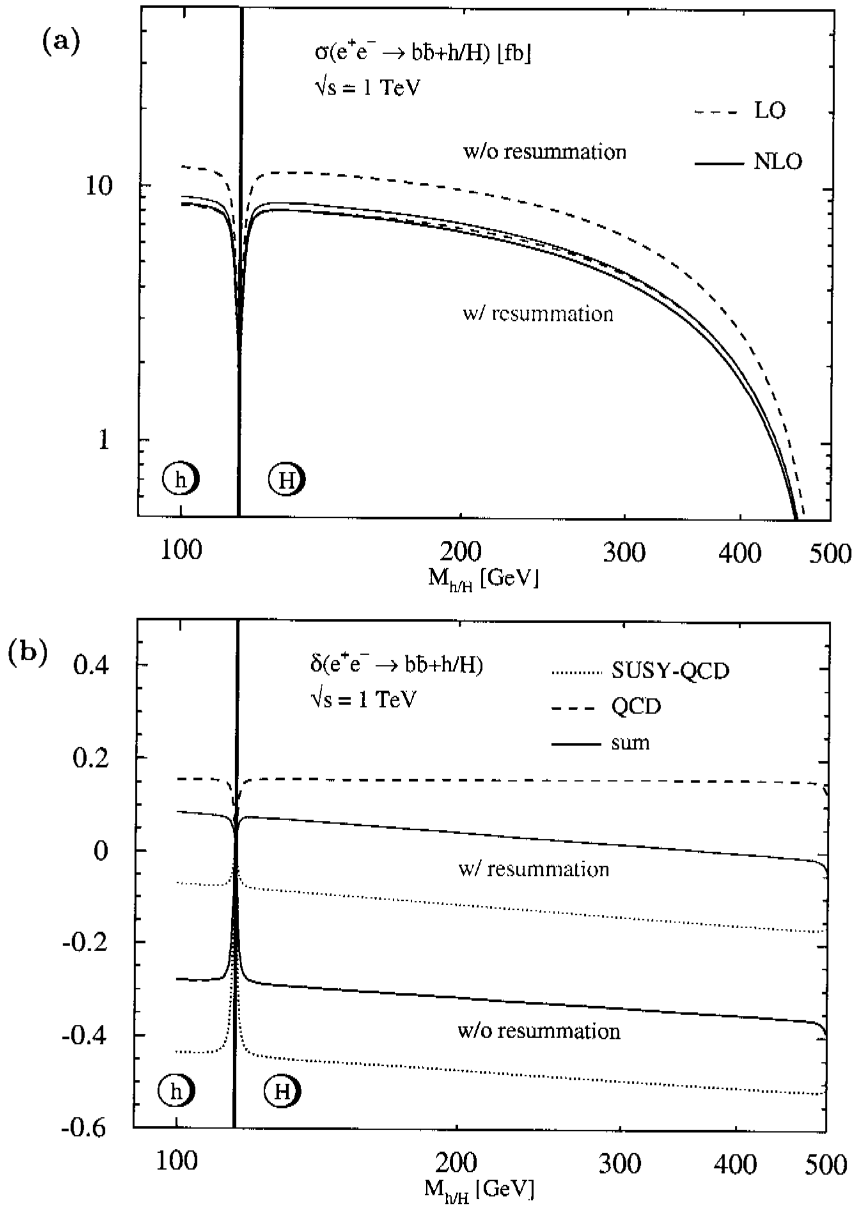

Figure 4.11: *(a) The LO cross sections (dashed lines) of associated heavy and light scalar Higgs production with bottom quarks in* e^+e^- *collisions with (red curves) and without (black curves) resummation of the* Δ_b *terms are plotted as functions of the scalar Higgs boson masses for the SPS1b benchmark point [105]. The QCD- and SUSY-QCD corrected NLO cross sections are depicted by the full lines, with (red) and without (black) resummation. (b) The relative QCD, SUSY-QCD and total corrections to associated scalar Higgs production with bottom quarks are displayed with (red lines) and without (black lines) resummation as functions of the scalar Higgs boson masses. The pure QCD corrections are indistinguishable in both cases.*

The associated Higgs production with bottom quarks is, however, dominated by the resonant $h, H \to b\bar{b}$ decays in the pseudoscalar case and the resonant $Z, A \to b\bar{b}$ decays in the scalar case. Thus, the absorption of the bulk of the SUSY-QCD part by the resummed Yukawa couplings could be expected from the analogous findings for the corresponding Higgs decays [111]. In order to investigate, if this also holds for continuum $\phi b\bar{b}$ production, the Higgs energy distribution in Figure 4.12 for associated pseudoscalar Higgs production with bottom quarks for a pseudoscalar Higgs mass $m_A = 200$ GeV has been analysed. The dimensionless parameters x_ϕ are defined as $x_\phi = 2E_\phi/\sqrt{s}$. Figure 4.12a displays the x_A distribution at LO and NLO, while Figure 4.12b exhibits the individual relative corrections. The sharp peak at $x_A \sim 1$ originates from the resonant $h, H \to b\bar{b}$ decays, while the regions apart from the peak represent continuum $Ab\bar{b}$ production. The resulting picture indeed turns out to be analogous to the total cross sections. The bulk of the SUSY-QCD corrections can be absorbed by the resummed bottom Yukawa couplings leaving moderate residual corrections. These cancel the pure QCD corrections to a large extent in the resonant as well as the continuum regions.

The light scalar Higgs energy distribution for associated Higgs production with top quarks is shown in Figure 4.13 for a light scalar Higgs mass $m_h = 100$ GeV. For $x_h \lesssim 0.8$ both the QCD and SUSY-QCD corrections are of moderate size. The sharp rise of the QCD corrections towards $x_h \sim 0.9$ is induced by the Coulomb singularity at the subthreshold of the $t\bar{t}$ pair [104]. It leads to a finite cross section at the upper bound of the x_h range. Since the total corrections are not constant, the shape of the Higgs energy distribution is slightly modified from LO to NLO, as can be inferred from Figure 4.13a.

4.6 Summary

The cross sections and relative corrections for LO and NLO QCD and SUSY-QCD are exemplary shown for a linear e^+e^- colliders with a center of mass energy of 1 TeV.

The NLO SUSY-QCD corrections to the associated neutral MSSM Higgs production with top quarks amount to 10–20%. The previously obtained pure NLO QCD corrections are of similar magnitude [104]. Strongly depending on the scenario cancellation or constructive interference effects between the QCD and SUSY-QCD corrections occurs. Therefore, it is important to include both corrections in future analyses of these processes at linear e^+e^- colliders.

At large values of tanβ, associated Higgs production with bottom quarks provides a possibility to measure tanβ. It has been demonstrated that the bulk of the pure QCD corrections can be absorbed in the running bottom Yukawa couplings, defined at the scale of the corresponding Higgs momentum flows [104]. The SUSY-QCD corrections are dominated by the non-decoupling Δm_b terms, which can be absorbed and resummed in the corresponding bottom Yukawa couplings. This absorption reduces the SUSY-QCD corrections to a moderate size. Both remaining corrections contribute with about 10–20%.

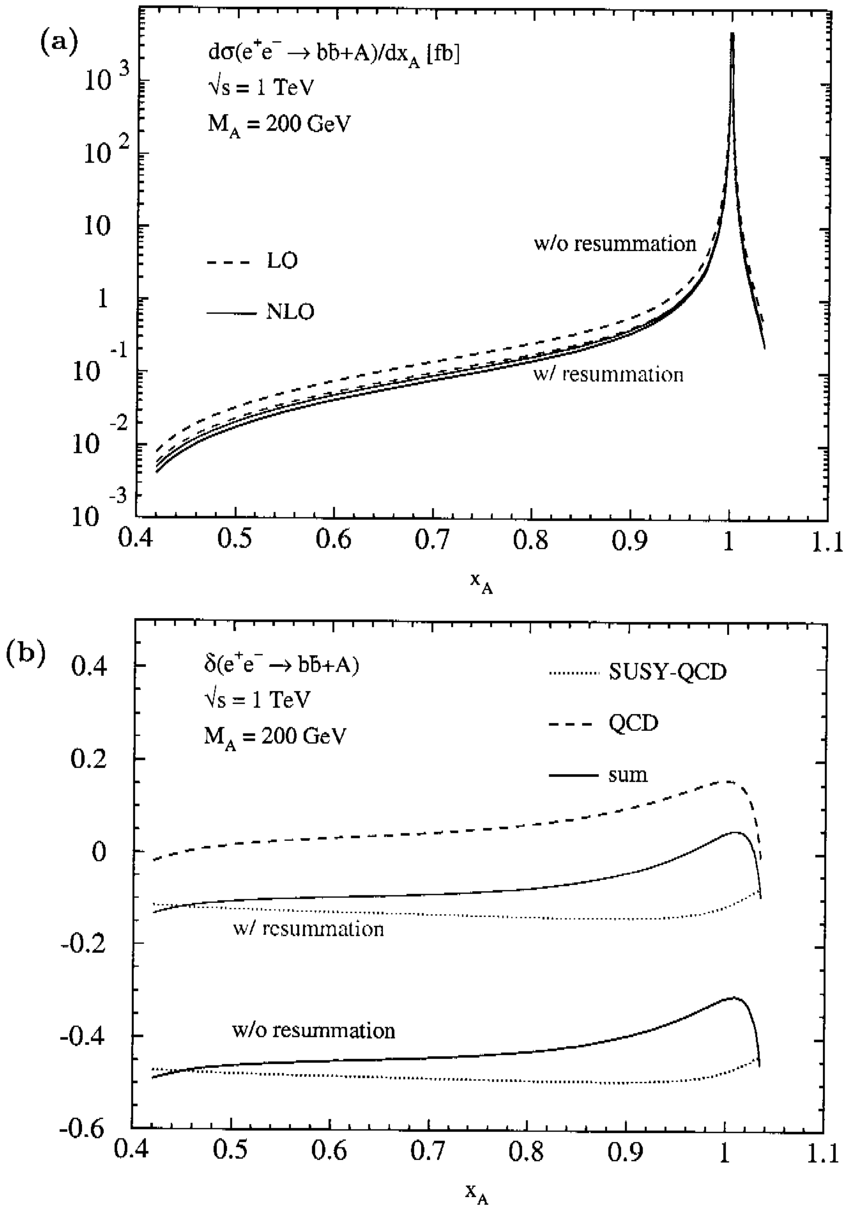

Figure 4.12: *(a) The Higgs energy distributions of associated pseudoscalar Higgs production with bottom quarks in e^+e^- collisions with (red curves) and without (black curves) resummation of the Δ_b terms are plotted as functions of x_A for the SPS1b benchmark point [105]. The LO cross sections are depicted by the dashed lines and the QCD- and SUSY-QCD corrected NLO cross sections by the full lines. The peak at $x_A \sim 1$ originates from the resonant $h, H \to b\bar{b}$ decays. (b) The relative QCD, SUSY-QCD and total corrections to associated pseudoscalar Higgs production with bottom quarks are displayed with (red lines) and without (black lines) resummation. The pure QCD corrections are indistinguishable in both cases.*

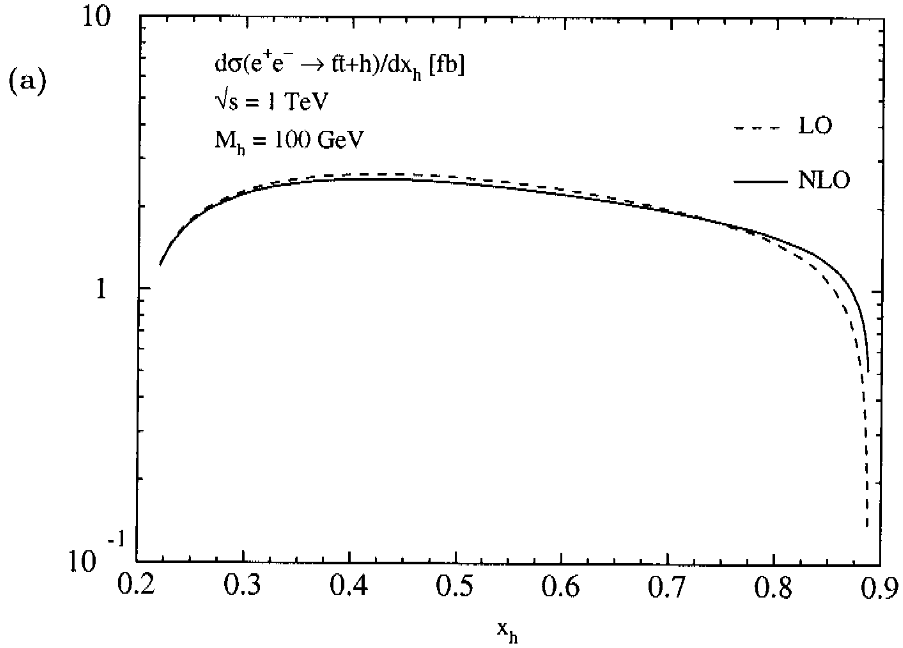

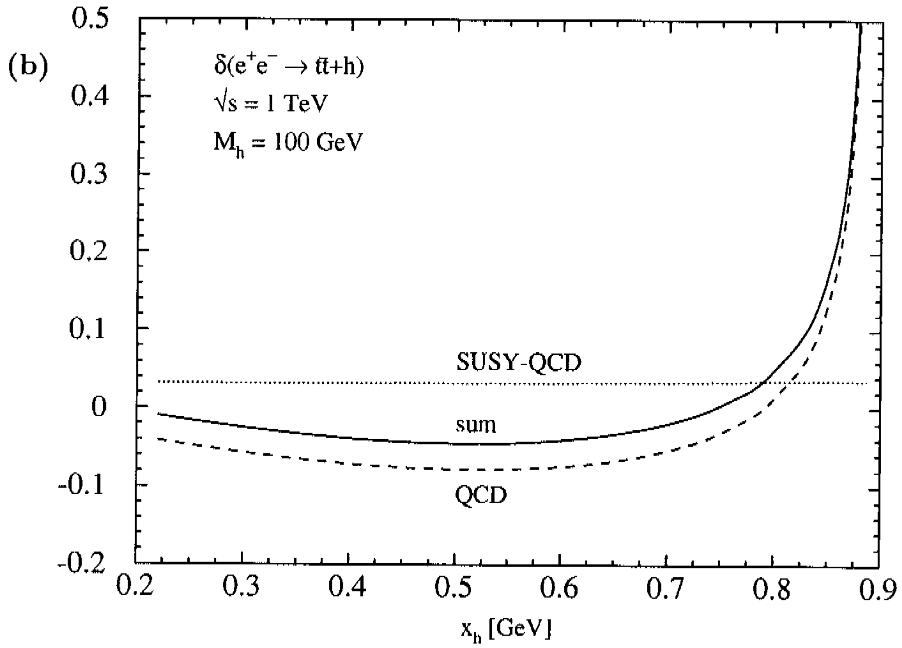

Figure 4.13: *(a) The Higgs energy distributions of associated light scalar Higgs production with top quarks in* e^+e^- *collisions are plotted as functions of* x_h *for the SPS5 benchmark point [105]. The LO cross section is depicted by the dashed line and the QCD- and SUSY-QCD corrected NLO cross section by the full line. (b) The relative QCD, SUSY-QCD and total corrections to associated light scalar Higgs production with top quarks are displayed. The sharp rise of the QCD corrections towards* $x_h \sim 0.9$ *is induced by the Coulomb singularity.*

Seite Leer /
Blank leaf

Chapter 5

$q\bar{q}/gg \to \phi Q\bar{Q}$

The importance of including the NLO SUSY-QCD corrections to associated Higgs production with heavy quarks in hadron collisions is briefly discussed. For the calculation of the LO and the large number of NLO SUSY-QCD diagrams a program chain based on `QGRAF`, `FORM` and `MAPLE` is set up as described in Chapter 3.6. The pure NLO QCD results are shortly reviewed. The partonic initial state can be split in $q\bar{q}$ and gluonic contributions. For the $q\bar{q}$ initial state one has to take care of fermion number violating diagrams originating from the Majorana nature of the gluinos. The external self-energies and counterterm diagrams are calculated explicitely. The leading terms of the NLO SUSY-QCD corrections for the bottom quark final state can be absorbed in the resummed bottom Yukawa coupling. For the top quark final state these contributions are non-leading due to the suppression of the top Yukawa coupling by the SUSY factors and thus there is no need for resummation. Finally, numerical results are discussed for the Tevatron and the LHC.

5.1 Motivation

At the LHC, associated Higgs production with top quarks is only important for the light scalar Higgs boson production. The top Yukawa couplings of heavy scalar and pseudoscalar Higgs bosons are, in the preferred large m_A region, suppressed by tanβ compared to the light scalar one (Table 1.5). For large tanβ values, on the other hand, the associated Higgs production with bottom quarks becomes the dominant production channel for all three neutral MSSM Higgs bosons due to the tanβ enhancement of the bottom Yukawa couplings.

The potential of the associated Higgs production with bottom quarks at the Tevatron depends strongly on the MSSM scenario, while the associated Higgs production with top quarks does not play any role at the Tevatron, due to kinematical reasons.

The LO predictions for the cross sections are plagued by large uncertainties due to the strong dependence on the renormalisation and factorisation scales, originating from the parton densities and the strong coupling constant. The running bottom mass provides for $b\bar{b}$ in the final state an additional source of scale dependence. The NLO QCD and SUSY-QCD corrections should reduce the scale dependencies and thus stabilise the theoretical predictions.

5.2 Leading Order Cross Sections

The associated Higgs production with heavy quarks at hadron colliders can be split into $q\bar{q}$ and gg initial states at LO and at NLO SUSY-QCD[1]. Two and eight diagrams contribute to the $q\bar{q}$ (Figure 5.1) and the gluonic (Figure 5.2) initial states, respectively:

$$\begin{aligned} q_i(p_1) + \bar{q}_j(p_2) &\to Q_k(p_3) + \bar{Q}_l(p_4) + \phi(p_5), \\ g^a_{\mu,\varepsilon_1}(p_1) + g^b_{\nu,\varepsilon_2}(p_2) &\to Q_k(p_3) + \bar{Q}_l(p_4) + \phi(p_5). \end{aligned}$$

The initial state quarks[2] u, d, s, c, b are taken to be massless, such that $p_1^2 = p_2^2 = 0$ holds for all initial states. The final states are defined on-shell with $p_3^2 = p_4^2 = m_Q^2$ and $p_5^2 = m_\phi^2$. The gluon polarisation vectors $\varepsilon_{1,2}$ satisfy the transversality condition $\varepsilon_i\, p_i = 0$ and the axial gauge $\varepsilon_1\, p_2 = \varepsilon_2\, p_1 = 0$.

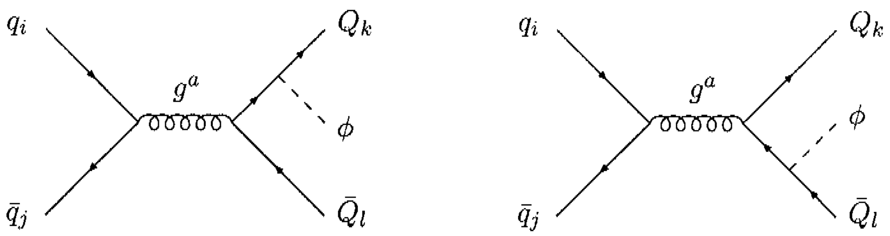

Figure 5.1: *The LO diagrams of associated Higgs production with heavy quarks $Q = t, b$ in $q\bar{q}$ collisions. The indices i, j and k, l denote the colour indices of the external quarks.*

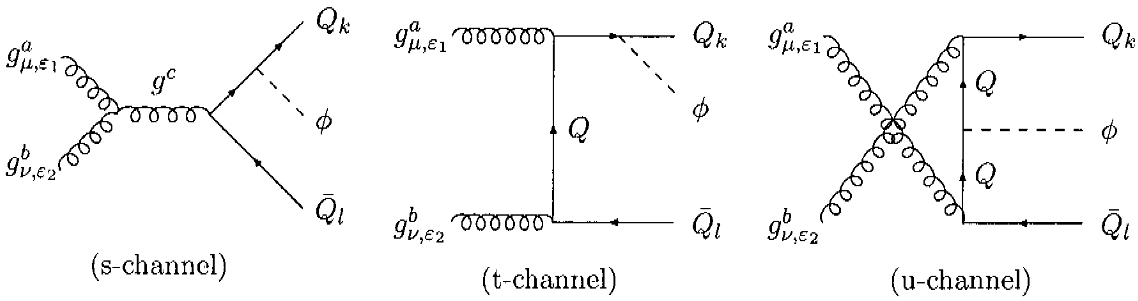

Figure 5.2: *Typical LO diagrams of associated Higgs production with heavy quarks $Q = t, b$ for gluonic initial states. The external gluons carry colour indices a, b, Lorentz indices μ, ν and the polarisation vectors $\varepsilon_{1,2}$.*

[1] The virtual NLO QCD corrections also split in this two initial states, but, there exist real NLO QCD corrections to gq and to $g\bar{q}$ initial states which contribute to the total NLO QCD corrections.

[2] Bottom quarks are not allowed in the initial state for associated Higgs production with bottom quarks, since it would lead to inconsistencies to treat them massless in the initial state and massive in the final state.

The colour factor of the two LO $q\bar{q}$ diagrams is given by $C^{q\bar{q}} \equiv T^a_{ij} T^a_{kl}$, leading to a factor of two for the squared LO matrix element. For the gluonic initial state diagrams it is convenient to define three different colour factors:

$$C_1^{gg} \equiv \delta^{ab}\, \mathbb{1}_{kl}, \qquad C_2^{gg} \equiv i f^{abc}\, \lambda^c_{kl}, \qquad C_3^{gg} \equiv d^{abc}\, \lambda^c_{kl}, \tag{5.1}$$

with the colour indices k, l for the final state quarks and the matrices $T^a \equiv \frac{1}{2}\lambda^a$. The C_1^{gg} corresponds to a colour-singlet state, while the latter two describe colour-octet states of the final quarks. The totally symmetric and antisymmetric $SU(3)_c$ structure constants f^{abc} and d^{abc}, respectively, are defined by:

$$\begin{aligned} [T^a, T^b] &\equiv i\, f^{abc}\, T^c, \\ \{T^a, T^b\} &\equiv \frac{1}{3}\delta^{ab}\,\mathbb{1} + d^{abc}\, T^c. \end{aligned}$$

The LO $gg \to \phi Q\bar{Q}$ colour factors are given in terms of $C_{1,2,3}^{gg}$ by:

$$\begin{aligned} C_s^{gg} &= \frac{1}{2} C_2^{gg} && \text{for the s-channel,} \\ C_t^{gg} &= \frac{1}{6} C_1^{gg} + \frac{1}{4} C_2^{gg} + \frac{1}{4} C_3^{gg} && \text{for the t-channel,} \\ C_u^{gg} &= \frac{1}{6} C_1^{gg} - \frac{1}{4} C_2^{gg} + \frac{1}{4} C_3^{gg} && \text{for the u-channel.} \end{aligned} \tag{5.2}$$

The different $C_{1,2,3}^{gg}$ do not interfere, thus the matrix elements squared can be decomposed according to the three colour factors squared:

$$c_1^{gg} = (C_1^{gg})^2 = 24, \qquad c_2^{gg} = |C_2^{gg}|^2 = 48, \qquad c_3^{gg} = (C_3^{gg})^2 = \frac{80}{3}.$$

The LO as well as the NLO SUSY-QCD matrix elements are calculated by a program chain based on `QGRAF`, `FORM` and `MAPLE`. Thus, no analytical results, except for external self-energies and counterterms, are written down.

5.3 QCD Corrections

The NLO QCD corrections to associated SM Higgs production with top quarks were calculated some years ago by two groups [65]. The transition to scalar MSSM Higgs bosons can be performed by rescaling the cross section with the squared Yukawa coupling factors defined in Table 1.4: $(g_u^h)^2$ for the light scalar and $(g_u^H)^2$ for the heavy scalar Higgs boson[3].

The NLO QCD corrections to associated SM Higgs production with bottom quarks were also calculated by two groups [86]. In LO, the transition to scalar MSSM Higgs bosons can be performed analogously to the top quark final state, but with the down-type SUSY factors $(g_d^{\mathcal{H}})^2$. At NLO diagrams exist, in which the Higgs boson couples to closed top quark loops (Figure 5.3). These contributions are not proportional to the bottom Yukawa coupling and spoil the relation between the SM and the MSSM results. However, in the

[3] As long as all quark masses, except the top mass, are neglected this scaling is exact.

SM it has been shown [86] that the contributions of these diagrams are 5−10%, i.e. small enough to be ignored. Thus, scaling the NLO QCD result with the squared Yukawa coupling factors leads to good approximations for the total cross sections.

The pseudoscalar Yukawa couplings contain, normalised to the SM couplings, not only Yukawa coupling factors (Table 1.4) but also an additional $[-i\gamma_5]$. Therefore, the NLO QCD corrections to associated pseudoscalar Higgs production with heavy quarks cannot be derived by just scaling the SM results with the modified Yukawa coupling constant $\left(g^A_{u,d}\right)^2$.

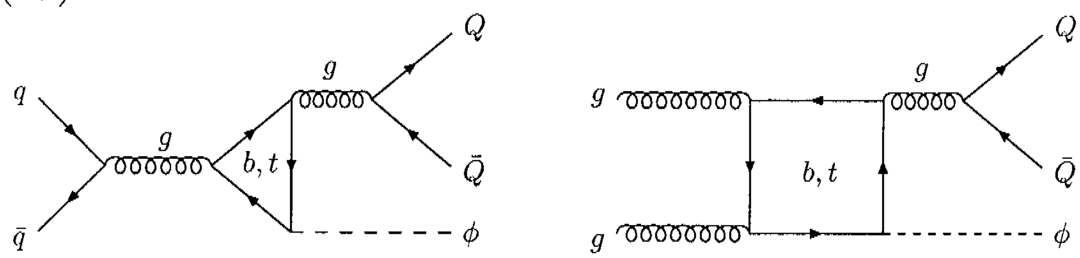

Figure 5.3: *Typical virtual QCD corrections to associated Higgs production with heavy quarks $Q = t, b$ with closed quark loops.*

The UV, IR and collinear singularities are isolated using dimensional regularisation (Chapter 3.1). Renormalisation and factorisation are performed in the $\overline{\text{MS}}$ scheme with the top mass defined on-shell. The running of the strong coupling constant $\alpha_s(\mu)$ is generated solely by logarithmic contributions of the light quarks and the gluon loops. The top quark contributions are decoupled by the renormalisation condition, thus, they to not contribute to the running of $\alpha_s(\mu)$ as shown in equation (3.2). For the convolution to the hadronic $p\bar{p}$ and pp cross section the CTEQ6L and CTEQ6M PDFs [114] at LO and NLO, corresponding to the QCD parameters with five active flavours $\Lambda_5^{\text{LO}} = 165$ MeV and $\Lambda_5^{\overline{\text{MS}}} = 226$ MeV, are used. The SM top Yukawa coupling is defined by $g_t^{\text{SM}} = \sqrt{2}m_t/v$ with $v = 246$ GeV and a top mass of 174 GeV. The bottom Yukawa coupling is evaluated with the running bottom quark mass $\overline{m}_b(\mu)$ of equation (4.1) defined in the $\overline{\text{MS}}$ scheme in order to sum large logarithmic corrections $\log(m_b/m_H)$. The bottom pole mass is set to $m_b = 4.60$ GeV corresponding to a $\overline{\text{MS}}$ mass to $\overline{m}_b(\overline{m}_b) = 4.26$ GeV. This leads to a SM bottom Yukawa coupling of $g_b^{\text{SM}}(\mu) = \sqrt{2}\,\overline{m}_b(\mu)/v$ with μ evaluated at the corresponding Higgs mass.

The exact calculations of the NLO QCD corrections to associated neutral MSSM Higgs production will be published soon [115]. At the LHC they turn out to range within 20−50% for the top quark final state [65], while they can be even larger for $\phi b\bar{b}$ production. The NLO QCD corrections to associated Higgs production with bottom quarks at the Tevatron enhance the cross secion by 60−130% [86].

5.4 SUSY-QCD Corrections

5.4.1 $q\bar{q} \to \phi Q\bar{Q}$

The NLO SUSY-QCD corrections can be classified by the number of squark indices and closed squark loops. In Figure 5.4 typical diagrams with zero squark indices (0SI), one squark index (1SI), one closed squark loop (1SL), two squark indices (2SI) and three squark indices (3SI) are depicted. The virtual SUSY-QCD corrections are given by:

$$\boxed{\mathcal{M}^{q\bar{q},\phi}_{\rm virt} = \mathcal{M}^{q\bar{q},\phi}_{\rm 0SI} + \mathcal{M}^{q\bar{q},\phi}_{\rm 1SI} + \mathcal{M}^{q\bar{q},\phi}_{\rm 1SL} + \mathcal{M}^{q\bar{q},\phi}_{\rm 2SI} + \mathcal{M}^{q\bar{q},\phi}_{\rm 3SI}\,.} \tag{5.3}$$

The diagrams involving three squark indices are "pentagon" diagrams with five-point functions. Since all the particles involved in the loops are massive no problems with IR divergences exist. The numerical evaluations of all the scalar integrals are performed with the `LoopTools` program [107].

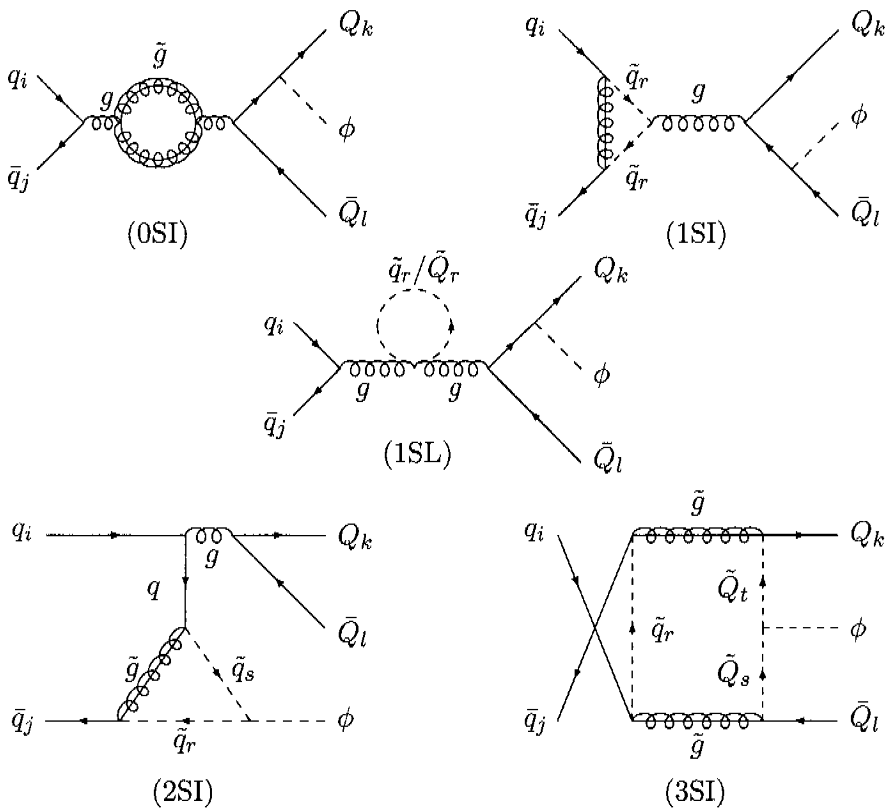

Figure 5.4: *Typical diagrams of NLO SUSY-QCD corrections to associated Higgs production with heavy quarks $Q = t, b$ in $q\bar{q}$ collisions. The individual channels can be classified by the number of squark indices and closed squark loops:* (0SI) *zero squark indices,* (1SI) *one squark index,* (1SL) *one closed squark loop,* (2SI) *two squark indices and* (3SI) *three squark indices.*

The colour factors of all NLO SUSY-QCD diagrams can be reduced to multiples of the LO colour structure $C^{q\bar{q}}$ and multiples of $\delta_{ij}\delta_{kl}$. The interference of $C^{q\bar{q}}$ with the latter vanishes, since they are orthogonal to each other. Thus, $C^{q\bar{q}}$ is the only relevant colour structure in LO as well as NLO and the produced $Q\bar{Q}$ pairs are in a pure colour-octet state.

Some of the box diagrams, e.g. diagram (3SI) in Figure 5.4, contain fermion number violating (FNV) interactions due to the Majorana nature of the gluinos. Feynman rules for Majorana particles are known for a long time [116]. The only Majorana particles appearing in this calculation are the gluinos. To handle FNV diagrams the fermion number flow is supplemented by a chosen fermion flow for each complete fermion string. Every vertex involving Majorana particles is assigned to two analytical expressions: one for the fermion flow parallel to the flow of the fermion number, the *"usual"* vertex, and one for the two flows antiparallel, the *"reversed"* FNV vertex. Exemplary this is presented for the squark-quark-gluino vertices in Figure 5.5. The *"usual"* squark-quark-gluino interactions are given by:

$$\Gamma_+ \;=\; \frac{g_s}{\sqrt{2}} T^a \left(v_j + a_j \gamma_5\right) \qquad \text{and} \qquad \Gamma_- = \frac{g_s}{\sqrt{2}} T^a \left(v_j - a_j \gamma_5\right).$$

The FNV interactions are flagged with a prime ($'$), which is defined to be:

$$\Gamma' \;\equiv\; C\,\Gamma^T C^{-1} \quad \text{with} \quad C \equiv -i\gamma^2\gamma^0 \quad \text{and} \quad C^{-1} = C^\dagger = C^T = -C.$$

For the Dirac matrices this leads to $\gamma'_\mu = -\gamma_\mu$ and $\gamma'_5 = \gamma_5$, and thereby to $\Gamma'_\pm = \Gamma_\pm$.

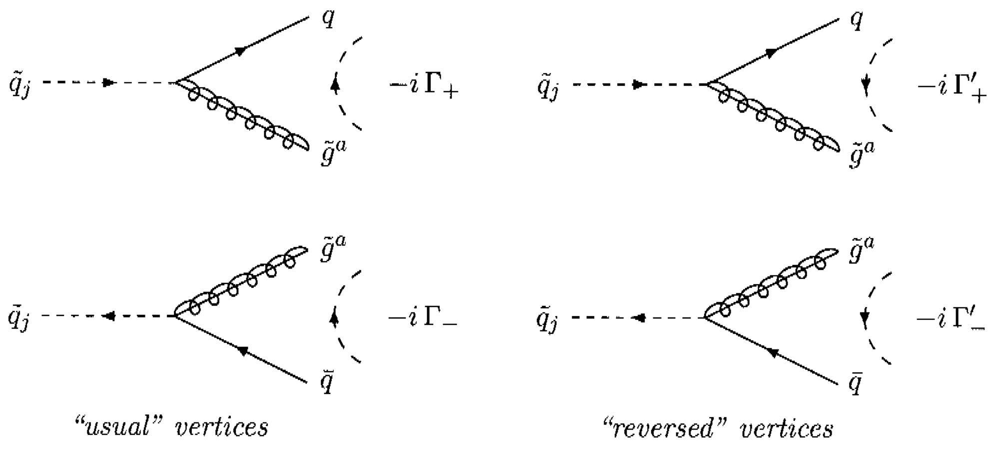

Figure 5.5: *The left column shows the "usual" Feynman diagrams for squark-quark-gluino interactions, whereas in the right column the FNV "reversed" vertices are shown. The fermion number flows are indicated by the fermions lines q and $\bar{q}$, while the dashed curved arrows show the chosen fermion flows.*

For Dirac fermions two propagators are defined in Figure 5.6: the *"usual"* Dirac propagator $iS^q(p)$ with parallel fermion and fermion number flow and the antiparallel *"reversed"* propagator $iS^q(-p)$, which violates fermion number conservation. The *"reversed"* propagator has nothing to do with an antiparticle propagator, since the fermion number flow and the momentum flow have still the same orientation. For Majorana particles there exist also two propagators $iS^{\tilde{g}}(p)$ and $iS^{\tilde{g}}(-p)$. Since the Majorana fermions do not have a defined fermion number flows, they are not separated into *"usual"* and *"reversed"* propagators, respectively.

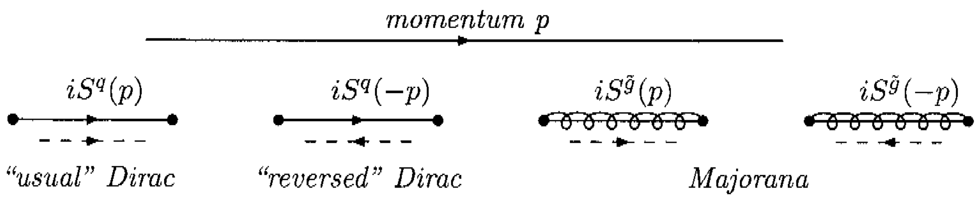

Figure 5.6: *Dirac propagators S^q with the orientation of the chosen fermion flow (dashed arrows) relative to the fermion number flows (solid arrows between vertices) are depicted. The "usual" Dirac propagator has the two flows parallel, while they are antiparallel for the "reversed" FNV one. Majorana particles, like gluinos, do not have a defined fermion number flow direction, thus no arrow is drawn on the gluino line. The momentum p flows from the left to the right side.*

Incoming and outgoing Dirac fermions and antifermions are described by four spinors (Figure 5.7):

$\bar{u}$ $\hat{=}$ outgoing *"usual"* Dirac particle $\hat{=}$ outgoing *"reversed"* Dirac antiparticle,
v $\hat{=}$ outgoing *"usual"* Dirac antiparticle $\hat{=}$ outgoing *"reversed"* Dirac particle,
u $\hat{=}$ incoming *"usual"* Dirac particle $\hat{=}$ incoming *"reversed"* Dirac antiparticle,
$\bar{v}$ $\hat{=}$ incoming *"usual"* Dirac antiparticle $\hat{=}$ incoming *"reversed"* Dirac particle,

while only two spinors $\bar{u}$ and u are needed for the Majorana fermions:

$\bar{u}$ $\hat{=}$ outgoing Majorana particle, with fermion flow and momentum parallel
$\hat{=}$ incoming Majorana particle, with fermion flow and momentum antiparallel,
u $\hat{=}$ outgoing Majorana particle, with fermion flow and momentum antiparallel
$\hat{=}$ incoming Majorana particle, with fermion flow and momentum parallel.

The amplitude of the FNV diagram in Figure 5.8, e.g., can be calculated with these expanded Feynman rules:

$$\begin{aligned}
\mathcal{M}_{\rm FNV}^{q\bar{q},\phi} &= i^{10}(-1)^5\, g_Q^\phi\, g_Q^{\rm SM}\bar{u}(p_3)\int\frac{d^Dk}{(2\pi)^D}\Big[S^q(p_3+p_5)\,\Gamma_+\,S^{\tilde{g}}(k+p_3+p_5)\,\Gamma'_+\,u(p_2)\\
&\qquad S^{\tilde{q}}(k+p_1-p_4)\,\bar{v}(p_1)\,\Gamma'_-\,S^{\tilde{g}}(k-p_4)\,\Gamma_-\,S^{\tilde{q}}(k)\Big]\,v(p_4)\\
&\propto\ \bar{u}(p_3)\,[\ldots]\,u(p_2)\,\bar{v}(p_1)\,[\ldots]\,v(p_4).
\end{aligned}$$

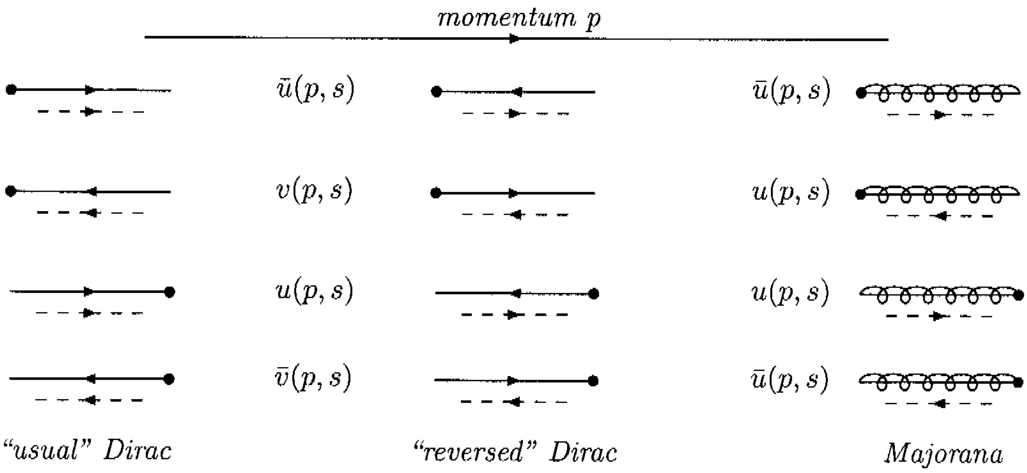

Figure 5.7: *In the first two columns Dirac spinors with their fermion number flow and in the third column Majorana spinors are shown. The dashed arrows indicate the chosen fermion flow direction. The vertex (black dots) on the left/right end of the arrows symbolise outgoing/incoming particles. "usual" indicates that the chosen fermion flow is parallel to the fermion number flow, while "reversed" indicates that the chosen fermion flow is antiparallel to the fermion number flow and therefore fermion number conservation is violated.*

The incoming light quarks are, with the chosen fermion flow defined in Figure 5.8, described by *"reversed"* spinors. Thus the light quark currents of the charge conjugated LO diagrams have to be adapted to match with such a FNV diagram. The spinor structure of the complex conjugated FNV LO diagram of Figure 5.9 is given by:

$$\left(\mathcal{M}^{q\bar{q},\phi}_{\mathrm{LO,FNV}}\right)^{\dagger} \;\propto\; \bar{u}(p_2)\,[\ldots]\,v(p_1)\,\bar{v}(p_4)\,[\ldots]\,u(p_3).$$

The interference of the FNV box diagram with this FNV LO diagram leads to:

$$\begin{aligned}\left(\mathcal{M}^{q\bar{q},\phi}_{\mathrm{LO,FNV}}\right)^{\dagger}\mathcal{M}^{q\bar{q},\phi}_{\mathrm{FNV}} &\propto \Big\{\bar{u}(p_2)\,[\ldots]\,v(p_1)\,\bar{v}(p_4)\,[\ldots]\,u(p_3)\Big\}\\ &\quad\Big\{\bar{u}(p_3)\,[\ldots]\,u(p_2)\,\bar{v}(p_1)\,[\ldots]\,v(p_4)\Big\}\\ &\propto \bar{u}(p_2)\,[\ldots]\,v(p_1)\,\bar{v}(p_1)\,[\ldots]\,v(p_4)\,\bar{v}(p_4)\,[\ldots]\,u(p_3)\,\bar{u}(p_3)\,[\ldots]\,u(p_2).\end{aligned}$$

Therefore, the FNV diagrams can be treated as the non-FNV diagrams, by applying the proper Feynman rules. But, they interfere with the FNV LO diagrams, leading to the conventional spinor structure known from $|\mathcal{M}^{q\bar{q},\phi}_{\mathrm{LO}}|^2$ and the non-FNV NLO interferences with the original LO, $(\mathcal{M}^{q\bar{q},\phi}_{\mathrm{LO}})^{\dagger}\mathcal{M}^{q\bar{q},\phi}_{\mathrm{NLO}}$.

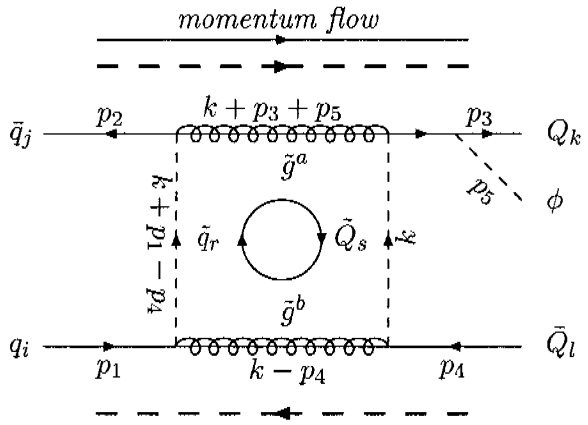

Figure 5.8: *Representative FNV box diagram. The dashed lines above and below the diagram indicate the directions of the chosen fermion flows, while the fermion lines show the directions fermion number flows. The momentum of the external particles flows from left to right and in the loop according to the circle in the middle.*

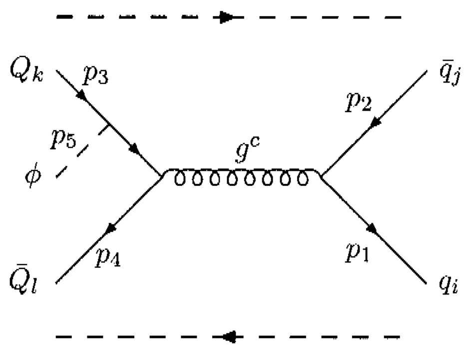

Figure 5.9: *Complex conjugated FNV LO diagram* $\left(\mathcal{M}^{q\bar{q},\phi}_{LO,FNV}\right)^\dagger$ *with chosen fermion flow (dashed lines with arrow) according to the FNV box diagram in Figure 5.8.*

5.4.2 $gg \to \phi Q\bar{Q}$

The NLO SUSY-QCD corrections to the gluonic initial state (Figure 5.10) can be classified according to the number of squark indices and closed squark loops analogous to the $q\bar{q}$ initial state (Chapter 5.4.1):

$$\boxed{\mathcal{M}^{gg,\phi}_{\text{virt}} = \mathcal{M}^{gg,\phi}_{\text{0SI}} + \mathcal{M}^{gg,\phi}_{\text{1SI}} + \mathcal{M}^{gg,\phi}_{\text{1SL}} + \mathcal{M}^{gg,\phi}_{\text{2SI}}} \tag{5.4}$$

All colour factors of the NLO SUSY-QCD corrections can be expressed in terms of the LO colour factors $C^{gg}_{1,2,3}$ defined in (5.1).

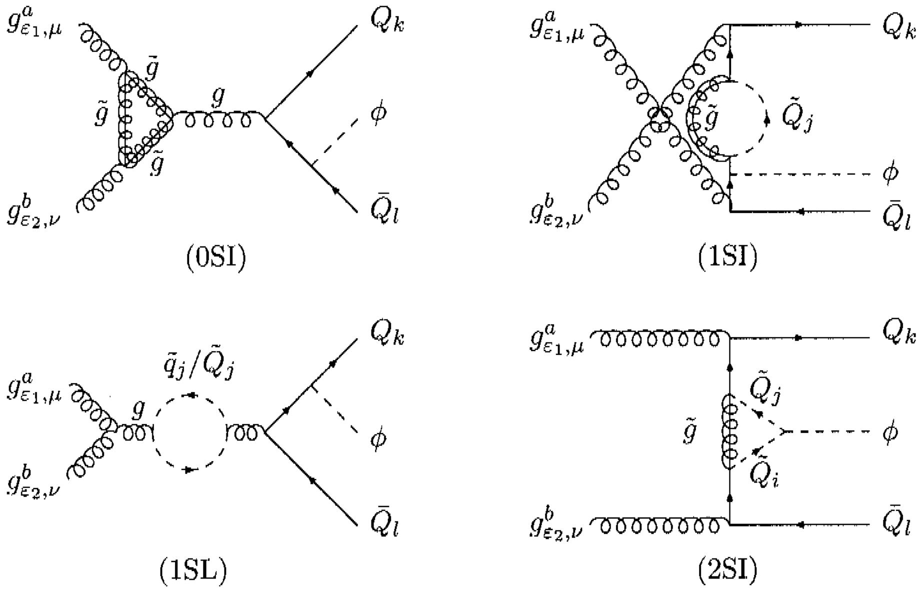

Figure 5.10: *Typical diagrams of the NLO SUSY-QCD corrections to associated Higgs production with heavy quarks $Q = t, b$ in gluon fusion. The individual diagrams can be classified by the number of squark indices and closed squark loops:* (0SI) *zero squark indices,* (1SI) *one squark index,* (1SL) *one closed squark loop and* (2SI) *two squark indices.*

There exist two classes of diagrams which vanish:

- Diagrams with closed squark loops, where the pseudoscalar Higgs boson is radiated by the squarks in the loop, vanish. Because of the specific form the squark-squark-pseudoscalar Higgs couplings, $g^A_{\tilde{Q}_1\tilde{Q}_1} = g^A_{\tilde{Q}_2\tilde{Q}_2} = 0$ and $g^A_{\tilde{Q}_1\tilde{Q}_2} = -g^A_{\tilde{Q}_2\tilde{Q}_1}$, the contributions from opposite squark momentum directions in the loop exactly cancel.

- Diagrams with a gluon-gluon-squark-squark vertex together with a gluon-squark-squark vertex at one squark loop (Figure 5.11) vanish due to the Furry theorem [117]. The loop-integral of such a diagram is given by:

$$
\begin{aligned}
I &= \int \frac{d^D k}{(2\pi)^D} \frac{(2k + p_1 + p_2)_\rho}{(k^2 - m^2_{\tilde{q}_j})((k + p_1 + p_2)^2 - m^2_{\tilde{q}_j})} \\
&= 2B_\rho(p_1 + p_2, m_{\tilde{q}_j}, m_{\tilde{q}_j}) + (p_1 + p_2)_\rho B_0(p_1 + p_2, m_{\tilde{q}_j}, m_{\tilde{q}_j}) \\
&= (p_1 + p_2)_\rho \underbrace{\left(2B_1(p_1 + p_2, m_{\tilde{q}_j}, m_{\tilde{q}_j}) + B_0(p_1 + p_2, m_{\tilde{q}_j}, m_{\tilde{q}_j})\right)}_{= 0 \text{ due to } B_1(p,m,m) = -\frac{1}{2} B_0(p,m,m)} \\
&= 0 \,.
\end{aligned}
$$

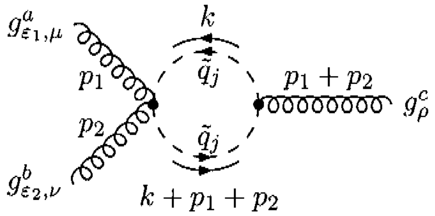

Figure 5.11: *Typical NLO SUSY-QCD diagram with gluon-gluon-squark-squark and gluon-squark-squark vertex at one squark loop.*

5.4.3 External Self-Energies

The final state external self-energies for associated Higgs production at hadron colliders are calculated exactly in the same way as for the leptonic initial state in Chapter 4.4.1. The $\widehat{\mathcal{M}}^{q\bar{q},\phi}_{\mathrm{LO}}$ and $\widehat{\mathcal{M}}^{gg,\phi}_{\mathrm{LO}}$ symbolise the amplitudes of all LO diagrams of Figure 5.1 and Figure 5.2, respectively, with amputated final quark and antiquark spinors:

$$\boxed{\mathcal{M}^{xx,\phi}_{\mathrm{ese,final}} = \delta Z^{\mathrm{OS}}_V\, \mathcal{M}^{xx,\phi}_{\mathrm{LO}} + \frac{1}{2}\,\delta Z^{\mathrm{OS}}_A\, \bar{u}_3 \left[\widehat{\mathcal{M}}^{xx,\phi}_{\mathrm{LO}}, \gamma_5\right] v_4.}$$

Whenever the matrix elements for the two different initial states have the same structure xx stays representative for $q\bar{q}$ and gg.

Since the initial state particles are strongly interacting they receive external self-energies, too. The calculation for the $q\bar{q}$ initial state is performed analogous to the final state, but with $\widehat{\mathcal{M}}^{q\bar{q},\phi}_{\mathrm{LO},q}$ having amputated initial quark and antiquark spinors:

$$\boxed{\mathcal{M}^{q\bar{q},\phi}_{\mathrm{ese,initial}} = \delta Z^{\mathrm{OS},q}_V\, \mathcal{M}^{q\bar{q},\phi}_{\mathrm{LO}} + \frac{1}{2}\,\delta Z^{\mathrm{OS},q}_A\, \bar{v}_2 \left[\widehat{\mathcal{M}}^{q\bar{q},\phi}_{\mathrm{LO},q}, \gamma_5\right] u_1.}$$

The on-shell renormalisation constants depend on the light squark masses:

$$\begin{aligned}
\delta Z^{\mathrm{OS},q}_V &= 2i\,\bar{g}_s^2 \sum_{\tilde{q}_j} \left[(v^q_j)^2 + (a^q_j)^2\right] B_1(0; m^2_{\tilde{g}}, m^2_{\tilde{q}_j}) = 4i\,\bar{g}_s^2 \sum_{\tilde{q}_j} B_1(0; m^2_{\tilde{g}}, m^2_{\tilde{q}_j}),\\
\delta Z^{\mathrm{OS},q}_A &= -2i\,\bar{g}_s^2 \sum_{\tilde{q}_j} \left[2\,a^q_j v^q_j\, B_1(0; m^2_{\tilde{g}}, m^2_{\tilde{q}_j})\right] = -4i\,\bar{g}_s^2 \sum_{\tilde{q}_j} (-1)^{j+1} B_1(0; m^2_{\tilde{g}}, m^2_{\tilde{q}_j}),
\end{aligned}$$

with the coupling coefficients of the light quarks[4]: $a^q_j = 1$ and $v^q_j = \pm 1$ for $j = L, R$.

The gluonic initial state develops three types of initial external self-energies (Figure 5.12). The gluon propagator at NLO SUSY-QCD is given by:

$$\begin{aligned}
D^{(1)}_{\mu\nu} &= D^{(0)}_{\mu\rho}\,\left[I^{\tilde{g}}_{\rho\sigma} + I^{\tilde{q},1}_{\rho\sigma} + I^{\tilde{q},2}_{\rho\sigma}\right]\, D^{(0)}_{\rho\sigma} \;\equiv\; D^{(0)}_{\mu\nu}\,\left[\Pi^{\tilde{g}}(0) + \Pi^{\tilde{q}}(0)\right],\\
D^{(0)}_{\mu\nu} &\equiv -i\frac{g_{\mu\nu} - \frac{p_\mu p_\nu}{p^2}}{p^2},
\end{aligned}$$

[4] For the squarks of the first two generations the mixing is neglected.

with the gluino loop, the squark[5] loops and the squark tadpoles contributing with:

$$
\begin{aligned}
I^{\tilde g}_{\rho\sigma} &\equiv (-1/2)\,\bar g_s^2\, f_{axy} f_{byx} \int \frac{d^Dk}{(2\pi)^D}\,\frac{Tr[\gamma_\rho\,(\not k + m_{\tilde g})\,\gamma_\sigma\,(\not k + \not p + m_{\tilde g})]}{(k^2-m_{\tilde g}^2)((k+p)^2-m_{\tilde g}^2)}, \\
I^{\tilde q,1}_{\rho\sigma} &\equiv \bar g_s^2\, Tr[T^a T^b] \sum_{\tilde q_j} \int \frac{d^Dk}{(2\pi)^D}\,\frac{(2k+p)_\rho(2k+p)_\sigma}{\left(k^2-m_{\tilde q_j}^2\right)\left((k+p)^2-m_{\tilde q_j}^2\right)}, \\
I^{\tilde q,2}_{\rho\sigma} &\equiv -\bar g_s^2\, Tr[\{T^a,T^b\}]\, g_{\rho\sigma} \sum_{\tilde q_j} \int \frac{d^Dk}{(2\pi)^D}\,\frac{1}{\left(k^2-m_{\tilde q_j}^2\right)}.
\end{aligned}
$$

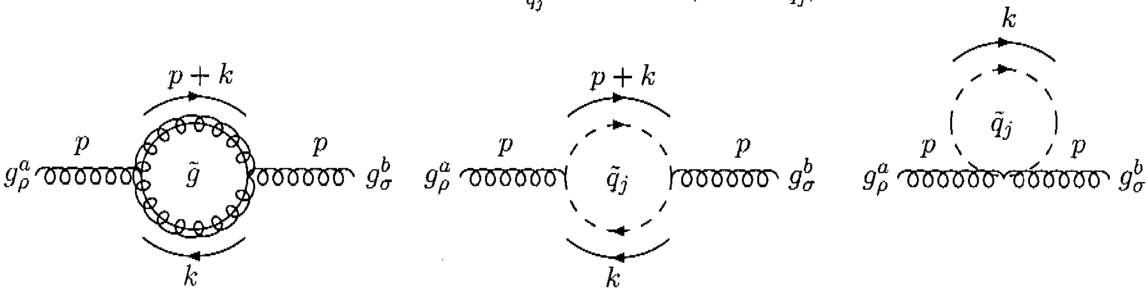

Figure 5.12: *The three one-loop SUSY-QCD contributions to the gluon vacuum polarisation.*

Evaluating the traces, applying tensor reduction and introducing the scalar integrals

$$
\begin{aligned}
A_0^{\tilde g} &\equiv A_0(m_{\tilde g}^2), & A_0^{\tilde q_j} &\equiv A_0(m_{\tilde q_j}^2) \\
B_i^{\tilde g} &\equiv B_i(p^2, m_{\tilde g}^2, m_{\tilde g}^2), & B_i^{\tilde q_j} &\equiv B_i(p^2, m_{\tilde q_j}^2, m_{\tilde q_j}^2)
\end{aligned}
$$

leads to:

$$
\begin{aligned}
I^{\tilde g}_{\rho\sigma} &= -(-1/2)\,\bar g_s^2\, N_c\, \delta_{ab}\, 4\left[2B^{\tilde g}_{\rho\sigma} + p_\rho B^{\tilde g}_\sigma + p_\sigma B^{\tilde g}_\rho - g_{\rho\sigma}(A_0^{\tilde g} + p_\kappa B^{\tilde g}_\kappa)\right] \\
&= 6\,\bar g_s^2\,\delta_{ab}\left[g_{\rho\sigma}(2B^{\tilde g}_{00} - A_0^{\tilde g} - p^2 B_1^{\tilde g}) + p_\rho p_\sigma(2B^{\tilde g}_{11} + 2B^{\tilde g}_1)\right] \\
&= 2\,\bar g_s^2\,\delta_{ab}\left(-g_{\rho\sigma} + \frac{p_\rho p_\sigma}{p^2}\right)\left[2\left(A_0^{\tilde g} - m_{\tilde g}^2 B_0^{\tilde g} - m_{\tilde g}^2\right) + p^2\left(-B_0^{\tilde g} + \frac{1}{3}\right)\right], \\
I^{\tilde q,1}_{\rho\sigma} &= \bar g_s^2\,\frac{1}{2}\,\delta_{ab}\sum_{\tilde q_j}\left[4B^{\tilde q_j}_{\rho\sigma} + 2p_\rho B^{\tilde q_j}_\sigma + 2p_\sigma B^{\tilde q_j}_\rho + p_\rho p_\sigma B_0^{\tilde q_j}\right] \\
&= \frac{\bar g_s^2}{2}\,\delta_{ab}\sum_{\tilde q_j}\left[g_{\rho\sigma}4B^{\tilde q_j}_{00} + p_\rho p_\sigma\left(4B^{\tilde q_j}_{11} + 4B^{\tilde q_j}_1 + B_0^{\tilde q_j}\right)\right] \\
&= \frac{\bar g_s^2}{6}\,\delta_{ab}\sum_{\tilde q_j}\left\{\left(-g_{\rho\sigma} + \frac{p_\rho p_\sigma}{p^2}\right)\left[4\left(A_0^{\tilde q_j} - m_{\tilde q_j}^2 B_0^{\tilde q_j} - m_{\tilde q_j}^2\right) + p^2\left(B_0^{\tilde q_j} + \frac{2}{3}\right)\right]\right. \\
&\qquad\qquad \left. + g_{\rho\sigma}\left[6A_0^{\tilde q_j}\right]\right\}, \\
I^{\tilde q_j,2}_{\rho\sigma} &= -\bar g_s^2\,\delta_{ab}\, g_{\rho\sigma}\sum_{\tilde q_j} A_0^{\tilde q_j}.
\end{aligned}
$$

[5] All six squark flavours contribute to the vacuum polarisation of the gluon.

The last term of $I^{\tilde{q},1}_{\rho\sigma}$, proportional to $g_{\rho\sigma}$, exactly cancels against $I^{\tilde{q},2}_{\rho\sigma}$.

With the explicit form of A_0 and B_0 for vanishing momenta and equal masses:

$$\begin{aligned} A_0(m) &= i\,C_\varepsilon\, m^2 \left[\frac{1}{\varepsilon} + 1 + \mathcal{O}(\varepsilon)\right] \\ B_0(0,m,m) &= i\,C_\varepsilon \left[\frac{1}{\varepsilon} + \mathcal{O}(\varepsilon)\right], \end{aligned}$$

it can be shown that $(A_0 - m^2(B_0+1)) \to 0$ in the limes $p \to 0$. The remaining two contributions for an on-shell gluon become:

$$\begin{aligned} D^{(1)}_{\mu\nu}(\tilde{g}) &= 2\,\bar{g}_s^2\,\delta_{ab}\left[p^2\left(-B_0^{\tilde{g}} + \frac{1}{3}\right)\right] \frac{g_{\mu\rho} - \frac{p_\mu p_\rho}{p^2}}{p^2}\left(-g_{\rho\sigma} + \frac{p_\rho p_\sigma}{p^2}\right)\frac{g_{\sigma\nu} - \frac{p_\sigma p_\nu}{p^2}}{p^2} \\ D^{(1)}_{\mu\nu}(\tilde{q}) &= \frac{\bar{g}_s^2}{6}\,\delta_{ab}\sum_{\tilde{q}_j}\left[p^2\left(B_0^{\tilde{q}_j} + \frac{2}{3}\right)\right] \underbrace{\frac{g_{\mu\rho} - \frac{p_\mu p_\rho}{p^2}}{p^2}\left(-g_{\rho\sigma} + \frac{p_\rho p_\sigma}{p^2}\right)\frac{g_{\sigma\nu} - \frac{p_\sigma p_\nu}{p^2}}{p^2}}_{-\frac{1}{p^4}\left(g_{\mu\nu} - \frac{p_\mu p_\nu}{p^2}\right)}. \end{aligned}$$

Thus, the gluino and the squark contribution to the one loop SUSY-QCD gluon vacuum polarisation in the on-shell scheme are given by:

$$\begin{aligned} \Pi^{\tilde{g}}(0) &= -2i\,\bar{g}_s^2\,\delta_{ab}\left[-B_0\left(0, m_{\tilde{g}}^2, m_{\tilde{g}}^2\right) + \frac{1}{3}\right], \\ \Pi^{\tilde{q}}(0) &= -\frac{i}{6}\,\bar{g}_s^2\,\delta_{ab}\sum_{\tilde{q}_j}\left[B_0\left(0, m_{\tilde{q}_j}^2, m_{\tilde{q}_j}^2\right) + \frac{2}{3}\right], \end{aligned}$$

where the sum runs over all squark flavours, each with two degrees of freedom. The external self-energies of the initial gluons are given by:

$$\boxed{\mathcal{M}^{gg,\phi}_{\text{ese,initial}} = \left(\Pi^{\tilde{g}}(0) + \Pi^{\tilde{q}}(0)\right)\,\mathcal{M}^{gg,\phi}_{\text{LO}}.}$$

Therefore, the external self-energies contribute to the NLO SUSY-QCD corrections with:

$$\boxed{\mathcal{M}^{xx,\phi}_{\text{ese}} = \mathcal{M}^{xx,\phi}_{\text{ese,initial}} + \mathcal{M}^{xx,\phi}_{\text{ese,final}}.} \qquad (5.5)$$

5.4.4 Counterterms

The wave functions, the gluon and quark propagators, the strong couplings and the Yukawa couplings have to be renormalised (Figure 5.13).

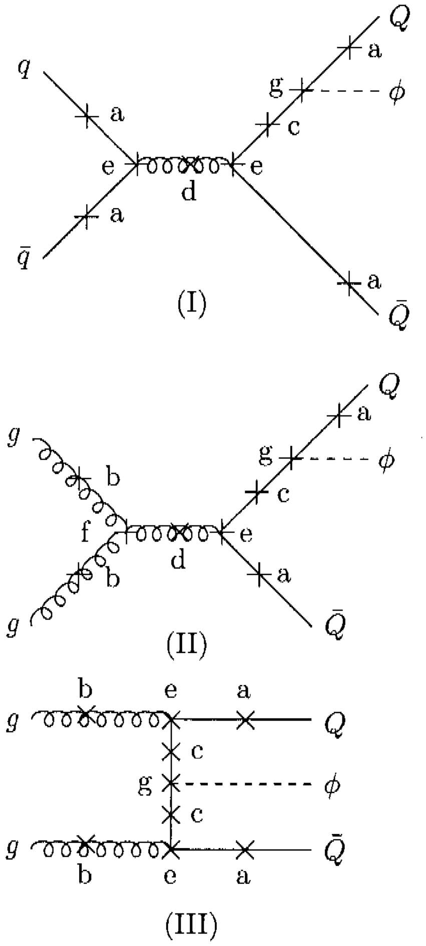

Renormalisation constants:

a = quark field $\dfrac{1}{\sqrt{Z_{q_{L/R}}}}$, $\dfrac{1}{\sqrt{Z_{Q_{L/R}}}}$

b = gluon field $\dfrac{1}{\sqrt{Z_G}}$

c = quark propagator
$$\frac{1}{\sqrt{Z_{Q_L}}\sqrt{Z_{Q_R}}}\left(1-\frac{\delta m_Q}{\not{p}-m_Q}\right)$$

d = gluon propagator $\dfrac{1}{Z_G}$

e = $gq\bar{q}/Q\bar{Q}$–vertex
$$\frac{1}{Z_{g_s}}\sqrt{Z_{q_L/Q_L}}\sqrt{Z_{q_R/Q_R}}\sqrt{Z_G}$$

f = ggg–vertex $\dfrac{1}{Z_{g_s}}Z_G^{3/2}$

g = $\phi Q\bar{Q}$–vertex $\sqrt{Z_{Q_L}}\sqrt{Z_{Q_R}}Z_m$

Figure 5.13: *Multiplicative renormalisation constants of the wave functions, the gluon and quark propagators, the strong gauge and the Yukawa couplings.*

The counterterms for the $q\bar{q}$ initial state can be derived from Figure 5.13(I):

$$\begin{aligned}
&\Big\{\mathrm{a}\times\mathrm{e}\times\mathrm{a}\Big\}\times\mathrm{d}\times\Big\{\mathrm{a}\times\mathrm{g}\times\mathrm{c}\times\mathrm{e}\times\mathrm{a}\Big\} \\
&\quad=\left\{\frac{1}{\sqrt{Z_{q_{L/R}}}}\times\frac{1}{Z_{g_s}}\sqrt{Z_{q_L}}\sqrt{Z_{q_R}}\sqrt{Z_G}\times\frac{1}{\sqrt{Z_{q_{R/L}}}}\right\}\times\frac{1}{Z_G}\times \\
&\qquad\left\{\frac{1}{\sqrt{Z_{Q_{L/R}}}}\times\sqrt{Z_{Q_L}}\sqrt{Z_{Q_R}}Z_m\times\frac{1}{\sqrt{Z_{Q_L}}\sqrt{Z_{Q_R}}}\left(1-\frac{\delta m_Q}{\not{p}-m_Q}\right)\times\right. \\
&\qquad\left.\frac{1}{Z_{g_s}}\sqrt{Z_{Q_L}}\sqrt{Z_{Q_R}}\sqrt{Z_G}\times\frac{1}{\sqrt{Z_{Q_{R/L}}}}\right\} \;=\; \frac{1}{Z_{g_s}}\times Z_m\times\left(1-\frac{\delta m_Q}{\not{p}-m_Q}\right).
\end{aligned}$$

For the gluonic s-channel the multiplicative renormalisation shown in Figure 5.13(II) leads to:

$$
\begin{aligned}
\Big\{\mathrm{b}\times\mathrm{f}\times\mathrm{b}\Big\} &\times \mathrm{d} \times \Big\{\mathrm{a}\times\mathrm{g}\times\mathrm{c}\times\mathrm{e}\times\mathrm{a}\Big\} \\
&= \left\{\frac{1}{\sqrt{Z_G}} \times \frac{1}{Z_{g_s}} Z_G^{3/2} \times \frac{1}{\sqrt{Z_G}}\right\} \times \frac{1}{Z_G} \times \\
&\quad \left\{\frac{1}{\sqrt{Z_{Q_{L/R}}}} \times \sqrt{Z_{Q_L}}\sqrt{Z_{Q_R}} Z_m \times \frac{1}{\sqrt{Z_{Q_L}}\sqrt{Z_{Q_R}}}\left(1 - \frac{\delta m_Q}{\not p - m_Q}\right) \times \right. \\
&\quad \left. \frac{1}{Z_{g_s}} \sqrt{Z_{Q_L}}\sqrt{Z_{Q_R}}\sqrt{Z_G} \times \frac{1}{\sqrt{Z_{Q_{R/L}}}}\right\} \\
&= \frac{1}{Z_{g_s}} \times Z_m \times \left(1 - \frac{\delta m_Q}{\not p - m_Q}\right),
\end{aligned}
$$

and for the gluonic t- and u-channels follows from Figure 5.13(III):

$$
\mathrm{b}\times\mathrm{e}\times\mathrm{a}\times\mathrm{c}\times\mathrm{g}\times\mathrm{c}\times\mathrm{a}\times\mathrm{e}\times\mathrm{b} = \frac{1}{Z_{g_s}} \times Z_m \times \left(1 - \frac{\delta m_Q}{\not p - m_Q}\right) \times \left(1 - \frac{\delta m_Q}{\not p' - m_Q}\right),
$$

with p and p' are the momenta of the two quark propagators.

Thus, three kinds of counterterms contribute for the partonic initial states:

- the strong coupling counterterms,
- the Yukawa coupling counterterms,
- the mass counterterms.

The strong coupling renormalisation for the SUSY-QCD corrections is given by equation (3.3) leading to:

$$
\boxed{
\begin{aligned}
\mathcal{M}_{\alpha_s}^{xx,\phi} = \mathcal{M}_{\mathrm{LO}}^{xx,\phi}\left(g_s^2(\mu_R)\right)\, 2\,\frac{g_s^2(\mu_R)}{16\pi^2}\Bigg[&-2\left(-\frac{1}{\bar\varepsilon} + \log\frac{\mu_R^2}{\mu^2}\right) \\
&- \log\frac{m_{\tilde g}^2}{\mu_R^2} - \frac{1}{12}\sum_{\tilde Q_j}\log\frac{m_{\tilde Q_j}^2}{\mu_R^2}\Bigg].
\end{aligned}
}
$$

$\mathcal{M}_{\mathrm{LO}}^{xx,\phi}\left(g_s^2(\mu_R^2)\right)$ symbolises the LO amplitude for both initial states evaluated at the renormalisation scale μ_R. The sum runs over all squark flavours, each with two degrees of freedom.

The Yukawa coupling counterterms for the neutral MSSM Higgs bosons production are given by:

$$
\boxed{\mathcal{M}_{\mathrm{Yuk}}^{xx,\phi} = -\frac{\delta m_Q}{m_Q} \cdot \mathcal{M}_{\mathrm{LO}}^{xx,\phi},}
$$

with the SUSY-QCD mass renormalisation

$$\delta m_Q^{\rm OS} = 2i\,\bar{g}_s^2 \sum_{\tilde{Q}_j} \Big[m_{\tilde{g}} (v_j^2 - a_j^2) B_0\left(m_Q^2; m_{\tilde{g}}^2, m_{\tilde{Q}_j}^2\right) + m_Q \left(v_j^2 + a_j^2\right) B_1 \left(m_Q^2; m_{\tilde{g}}^2, m_{\tilde{Q}_j}^2\right)\Big].$$

The mass counterterms for the $q\bar{q}$ initial state results in:

$$\boxed{\begin{aligned}\mathcal{M}_{\rm mass}^{q\bar{q},\phi} = -\,i\,g_Q^\phi\,g_Q^{\rm SM}\frac{\bar{g}_s^2}{s}\,C^{q\bar{q}}\,\delta m_Q\,\bar{u}_3 \Bigg\{ [-i\gamma_5]\,\frac{(\not p_3 + \not p_5 + m_Q)(\not p_3 + \not p_5 + m_Q)\gamma_\mu}{(s_{35} - m_Q^2)^2} \\ + \frac{\gamma_\mu(-\not p_4 - \not p_5 + m_Q)(-\not p_4 - \not p_5 + m_Q)}{(s_{45} - m_Q^2)^2}\,[-i\gamma_5]\Bigg\} v_4\,\bar{v}_2 \gamma^\mu u_1,\end{aligned}}$$

where the factors $[-i\gamma_5]$ are only inserted for the pseudoscalar Higgs boson and the invariants $s_{ij} \equiv (p_i + p_j)^2$.

For the eight gluonic LO diagrams 14 mass counterterms exist, one for both s-channel and two for every t- and u-channel LO diagram. With the LO colour factors defined in (5.2) and $t_{ij} \equiv (p_i - p_j)^2$ the mass counterterm for the gluonic initial state are analytically given by:

$$\begin{aligned}
\mathcal{M}_{{\rm mass},1+2}^{gg,\phi} &= i\,g_Q^\phi\,g_Q^{\rm SM}\frac{\bar{g}_s^2}{s}\,C_{\rm s}^{gg}\,\delta m_Q\,\bar{u}_3 \Bigg\{ [-i\gamma_5]\,\frac{(\not p_3 + \not p_5 + m_Q)\,(\not p_3 + \not p_5 + m_Q)\,\gamma_\rho}{(s_{35} - m_Q^2)^2} \\
&\quad + \frac{\gamma_\rho\,(-\not p_4 - \not p_5 + m_Q)\,(-\not p_4 - \not p_5 + m_Q)}{(s_{45} - m_Q^2)^2}\,[-i\gamma_5]\Bigg\}\, v_4 \\
&\quad \varepsilon_{1,\mu}^{\lambda_1}\left[g^{\mu\nu}(p_1 - p_2)^\rho + g^{\nu\rho}(p_1 + 2p_2)^\mu + g^{\rho\mu}(-2p_1 - p_2)^\nu\right]\varepsilon_{2,\nu}^{\lambda_2}, \\
\mathcal{M}_{{\rm mass},3}^{gg,\phi} &= i\,g_Q^\phi\,g_Q^{\rm SM}\,\frac{\bar{g}_s^2}{s}\,\frac{1}{(t_{24} - m_Q^2)(s_{35} - m_Q^2)}\,C_{\rm t}^{gg}\,\delta m_Q \\
&\quad \varepsilon_{1,\mu}^{\lambda_1}\,\varepsilon_{2,\nu}^{\lambda_2}\,\bar{u}_3\,[-i\gamma_5]\,(\not p_3 + \not p_5 + m_Q) \\
&\quad \left\{\gamma^\mu\,\frac{\not p_2 - \not p_4 + m_Q}{t_{24} - m_Q^2} + \frac{\not p_3 + \not p_5 + m_Q}{s_{35} - m_Q^2}\,\gamma^\mu\right\}(\not p_2 - \not p_4 + m_Q)\,\gamma^\nu\,v_4, \\
\mathcal{M}_{{\rm mass},4}^{gg,\phi} &= i\,g_Q^\phi\,g_Q^{\rm SM}\,\frac{\bar{g}_s^2}{s}\,\frac{1}{(t_{13} - m_Q^2)(t_{24} - m_Q^2)}\,C_{\rm t}^{gg}\,\delta m_Q \\
&\quad \varepsilon_{1,\mu}^{\lambda_1}\,\varepsilon_{2,\nu}^{\lambda_2}\,\bar{u}_3\,\gamma^\mu\,(\not p_3 - \not p_1 + m_Q) \\
&\quad \left\{\frac{\not p_3 - \not p_1 + m_Q}{t_{13} - m_Q^2}\,[-i\gamma_5] + [-i\gamma_5]\,\frac{\not p_2 - \not p_4 + m_Q}{t_{24} - m_Q^2}\right\}(\not p_2 - \not p_4 + m_Q)\,\gamma^\nu\,v_4,
\end{aligned}$$

$$
\begin{aligned}
\mathcal{M}^{gg,\phi}_{\text{mass},5} &= i\, g^{\phi}_{Q}\, g^{\text{SM}}_{Q}\, \frac{\bar{g}_s^2}{s}\, \frac{1}{(t_{13}-m_Q^2)(s_{45}-m_Q^2)}\, C^{gg}_{\text{t}}\, \delta m_Q \\
&\quad \varepsilon^{\lambda_1}_{1,\mu}\, \varepsilon^{\lambda_2}_{2,\nu}\, \bar{u}_3\, \gamma^{\mu}\, (\not{p}_3 - \not{p}_1 + m_Q) \\
&\quad \left\{ \frac{\not{p}_3 - \not{p}_1 + m_Q}{t_{13}-m_Q^2}\, \gamma^{\nu} + \gamma^{\nu}\, \frac{-\not{p}_4 - \not{p}_5 + m_Q}{s_{45}-m_Q^2} \right\} (-\not{p}_4 - \not{p}_5 + m_Q)\, [-i\gamma_5]\, v_4, \\
\mathcal{M}^{gg,\phi}_{\text{mass},6} &= i\, g^{\phi}_{Q}\, g^{\text{SM}}_{Q}\, \frac{\bar{g}_s^2}{s}\, \frac{1}{(t_{14}-m_Q^2)(s_{35}-m_Q^2)}\, C^{gg}_{\text{u}}\, \delta m_Q \\
&\quad \varepsilon^{\lambda_1}_{1,\mu}\, \varepsilon^{\lambda_2}_{2,\nu}\, \bar{u}_3\, [-i\gamma_5]\, (\not{p}_3 + \not{p}_5 + m_Q) \\
&\quad \left\{ \gamma^{\nu}\, \frac{\not{p}_1 - \not{p}_4 + m_Q}{t_{14}-m_Q^2} + \frac{\not{p}_3 + \not{p}_5 + m_Q}{s_{35}-m_Q^2}\, \gamma^{\nu} \right\} (\not{p}_1 - \not{p}_4 + m_Q)\, \gamma^{\mu}\, v_4, \\
\mathcal{M}^{gg,\phi}_{\text{mass},7} &= i\, g^{\phi}_{Q}\, g^{\text{SM}}_{Q}\, \frac{\bar{g}_s^2}{s}\, \frac{1}{(t_{14}-m_Q^2)(t_{23}-m_Q^2)}\, C^{gg}_{\text{u}}\, \delta m_Q \\
&\quad \varepsilon^{\lambda_1}_{1,\mu}\, \varepsilon^{\lambda_2}_{2,\nu}\, \bar{u}_3\, \gamma^{\nu}\, (\not{p}_3 - \not{p}_2 + m_Q) \\
&\quad \left\{ [-i\gamma_5] \frac{\not{p}_1 - \not{p}_4 + m_Q}{t_{14}-m_Q^2} + \frac{\not{p}_3 - \not{p}_2 + m_Q}{t_{23}-m_Q^2} [-i\gamma_5] \right\} (\not{p}_1 - \not{p}_4 + m_Q)\, \gamma^{\mu}\, v_4, \\
\mathcal{M}^{gg,\phi}_{\text{mass},8} &= i\, g^{\phi}_{Q}\, g^{\text{SM}}_{Q}\, \frac{\bar{g}_s^2}{s}\, \frac{1}{(t_{23}-m_Q^2)(s_{45}-m_Q^2)}\, C^{gg}_{\text{u}}\, \delta m_Q \\
&\quad \varepsilon^{\lambda_1}_{1,\mu}\, \varepsilon^{\lambda_2}_{2,\nu}\, \bar{u}_3\, \gamma^{\nu}\, (\not{p}_3 - \not{p}_2 + m_Q) \\
&\quad \left\{ \frac{\not{p}_3 - \not{p}_2 + m_Q}{t_{23}-m_Q^2}\, \gamma^{\mu} + \gamma^{\mu}\, \frac{-\not{p}_4 - \not{p}_5 + m_Q}{s_{45}-m_Q^2} \right\} (-\not{p}_4 - \not{p}_5 + m_Q)\, [-i\gamma_5]\, v_4,
\end{aligned}
$$

Thus, the counterterms contribute to the NLO SUSY-QCD corrections as:

$$
\boxed{
\begin{aligned}
\mathcal{M}^{q\bar{q},\phi}_{\text{CT}} &= \mathcal{M}^{q\bar{q},\phi}_{\alpha_s} + \mathcal{M}^{q\bar{q},\phi}_{\text{Yuk}} + \mathcal{M}^{q\bar{q},\phi}_{\text{mass}}, \\
\mathcal{M}^{gg,\phi}_{\text{CT}} &= \mathcal{M}^{gg,\phi}_{\alpha_s} + \mathcal{M}^{gg,\phi}_{\text{Yuk}} + \sum_{j=1}^{8} \mathcal{M}^{gg,\phi}_{\text{mass},j}\,.
\end{aligned}
}
\tag{5.6}
$$

The total NLO SUSY-QCD corrections for the associated Higgs production with heavy quarks for $q\bar{q}$ and gluonic initial states finally contain the virtual corrections (5.3) and (5.4), the external self-energies (5.5) and the counterterms (5.6):

$$
\boxed{\mathcal{M}^{xx,\phi}_{\text{SQCD}} = \mathcal{M}^{xx,\phi}_{\text{virt}} + \mathcal{M}^{xx,\phi}_{\text{ese}} + \mathcal{M}^{xx,\phi}_{\text{CT}}.}
$$

5.4.5 Bottom Quark Final State

The renormalised bottom Yukawa coupling is defined in terms of the $\overline{\text{MS}}$ running bottom mass. Since not all diagrams contain bottom Yukawa couplings the following recipe is applied for consistency:

- in diagrams with the bottom Yukawa couplings the running $\overline{\text{MS}}$ bottom Yukawa couplings are used,
- diagrams with vertex corrections to the Yukawa couplings are rescaled by $\overline{m}_b(\mu)/m_b$, with μ evaluated at the corresponding Higgs momentum flow,
- diagrams with one closed squark loop and the Higgs boson coupled to this loop are not rescaled.

For large $\tan\beta$ the same technique of absorbing the leading contributions in the bottom Yukawa couplings as in $e^+e^- \to \phi Q\bar{Q}$ is applied (Chapter 4.4.3). In the LO matrix elements the resummed Yukawa couplings are used:

$$\widetilde{\mathcal{M}}_{\text{LO}}^{xx,\phi} = \frac{\tilde{g}_b^\phi}{g_b^\phi}\,\mathcal{M}_{\text{LO}}^{xx,\phi}.$$

Supplementary finite counterterms,

$$\Delta\mathcal{M}^{xx,\phi} = \Delta_b^\phi\,\mathcal{M}_{\text{LO}}^{xx,\phi},$$

have to be added to the NLO SUSY-QCD corrections, so that the SUSY-QCD corrections to the cross section are given by:

$$\boxed{\Delta\sigma_{\text{SQCD}}^{xx,\phi b\bar{b}} = \frac{1}{2s}\int d\text{PS}_3\; 2\mathfrak{Re}\sum_{\text{spin,colour}} \overline{\widetilde{\mathcal{M}}_{\text{LO}}^{xx,\phi\dagger}\mathcal{M}_{\text{SQCD}}^{xx,\phi b\bar{b}}}\,,}$$

with

$$\boxed{\mathcal{M}_{\text{SQCD}}^{xx,\phi b\bar{b}} = \mathcal{M}_{\text{virt}}^{xx,\phi} + \mathcal{M}_{\text{ese}}^{xx,\phi} + \mathcal{M}_{\text{CT}}^{xx,\phi} + \Delta\mathcal{M}^{xx,\phi}\,.}$$

In the QCD corrections the resummed bottom Yukawa coupling are inserted everywhere, too, since the non-decoupling terms Δ_b^ϕ factorise from the pure QCD corrections involving light particle interactions only.

5.4.6 Top Quark Final State

In the top quark final states the Yukawa couplings are renormalised on-shell. They are suppressed by $1/\tan\beta$ and therefore there is no need for resummation. The NLO SUSY-QCD matrix elements are given by:

$$\boxed{\mathcal{M}_{\text{SQCD}}^{xx,\phi t\bar{t}} = \mathcal{M}_{\text{virt}}^{xx,\phi} + \mathcal{M}_{\text{ese}}^{xx,\phi} + \mathcal{M}_{\text{CT}}^{xx,\phi}\,.}$$

Thereby, the SUSY-QCD corrections to the cross sections for the $q\bar{q}$ and the gluonic initial state result in:

$$\boxed{\Delta\sigma_{\text{SQCD}}^{xx,\phi t\bar{t}} = \frac{1}{2s}\int d\text{PS}_3\; 2\mathfrak{Re}\sum_{\text{spin,colour}} \overline{\mathcal{M}_{\text{LO}}^{xx,\phi\dagger}\mathcal{M}_{\text{SQCD}}^{xx,\phi t\bar{t}}}\,,}$$

with the conventional Yukawa coupling in the LO matrix elements.

5.5 Numerical Results

The numerical results are evaluated for associated Higgs production with top quarks at the LHC with the MSSM parameters fixed according to the Snowmass scenario SPS5 [105]. For the bottom quark final state the SPS1b benchmark scenario has been chosen for the LHC and the Tevatron. The MSSM parameters of these two scenarios are listed in Chapter 4.5. The pseudoscalar Higgs mass is left free in both scenarios in order to scan the corresponding Higgs mass ranges.

In Figure 5.14a the LO and NLO SUSY-QCD cross sections for associated pseudoscalar Higgs production with top quarks at the LHC are depicted for $q\bar{q}$ (blue curves) and gluonic (red curves) initial states. The black curves indicate the sum of the two partonic contributions. The total cross section decreases from a level of 10 fb at low m_A by roughly one order of magnitude for $\Delta m_A \approx 300$ GeV. The relative SUSY-QCD corrections $\delta \equiv \sigma_{\rm NLO}/\sigma_{\rm LO}$ contribute with about 10% to the quark initial state and with some 20% to the gluonic initial state (Figure 5.14b). Since the gluonic initial state dominates the total cross section, the relative NLO SUSY-QCD corrections are of $\mathcal{O}(20\%)$. The previously obtained NLO QCD correction range between 35% and 50% [65]. The relative sign between the QCD and the SUSY-QCD corrections depends on the sign of the μ parameter.

The cross sections of $t\bar{t}H$ production at the LHC exhibit a much steeper decline than the pseudoscalar Higgs boson production, starting at significantly higher values of $\mathcal{O}(10^2\,\text{fb})$ at $m_A \approx 100$ GeV as indicated in Figure 5.15a. The relative corrections, shown in Figure 5.15b, are moderate for the $q\bar{q}$ initial state and reach a level of 30% for the gluonic contributions at higher Higgs masses. In the SPS5 scenario these corrections are negative. The kink in the relative corrections lies exactly at a Higgs mass of $m_H = 2\,m_{\tilde{t}_1}$ and appears in both initial states. At this $\tilde{t}_1\bar{\tilde{t}}_1$ threshold the diagrams with $H\tilde{t}_1\bar{\tilde{t}}_1$ couplings (Figure 5.16) develop a resonant behaviour. These type of diagrams do not contribute to the $At\bar{t}$ final state since the coupling $A\tilde{t}_1\bar{\tilde{t}}_1$ vanishes. The light scalar Higgs production cross sections amount to about 10^3 fb and the relative SUSY-QCD corrections are small. The pure QCD corrections contribute to scalar Higgs production with 20–30% [86].

The cross sections for associated pseudoscalar Higgs production with bottom quarks at the LHC are shown in Figure 5.17a. The dominant gg cross section decreases from $\mathcal{O}(10^5\,\text{fb})$ at $m_A \approx 100$ GeV down to $\mathcal{O}(10^2\,\text{fb})$ at $m_A \approx 500$ GeV. The NLO SUSY-QCD corrections are dominated by the Δ_b terms. By resumming these dominant contributions and including them in the bottom Yukawa couplings the leading contributions of the NLO SUSY-QCD corrections are absorbed. This behaviour is clearly visible e.g. in the $q\bar{q}$ initial state in Figure 5.17a, where the LO cross section after resummation lies very close to the NLO cross section of the naive calculation. Thus, the relative SUSY-QCD corrections after resummation (Figure 5.17b) are small compared to the relative corrections without resummation, which are roughly 50%.

A similar picture emerges for the cross sections and relative corrections of light and heavy scalar Higgs production in association with bottom quarks, apart from scalar Higgs masses near the mass bounds (Figure 5.18). At the upper/lower mass bound of the light/heavy

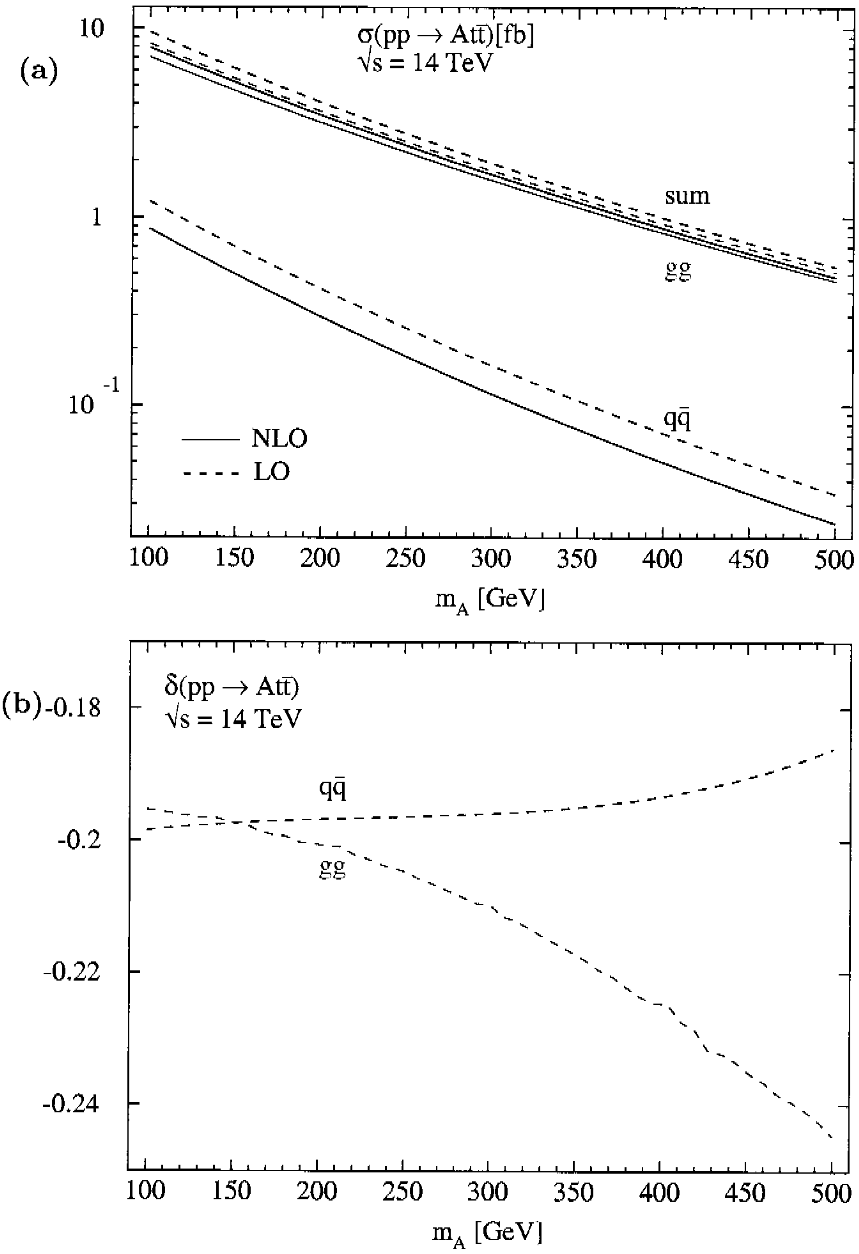

Figure 5.14: *(a) The LO (dashed lines) cross sections of associated pseudoscalar Higgs production with top quarks at the LHC are plotted as functions of the pseudoscalar Higgs boson mass for the SPS5 benchmark point [105]. The SUSY-QCD corrected cross sections are depicted by the full lines. The hadron initial state splits into $q\bar{q}$ (blue) and gluonic (red) initial state. The total cross sections are shown in black. (b) The relative SUSY-QCD corrections to associated pseudoscalar Higgs production with top quarks are depicted for the two partonic contributions separately as functions of the pseudoscalar Higgs boson mass.*

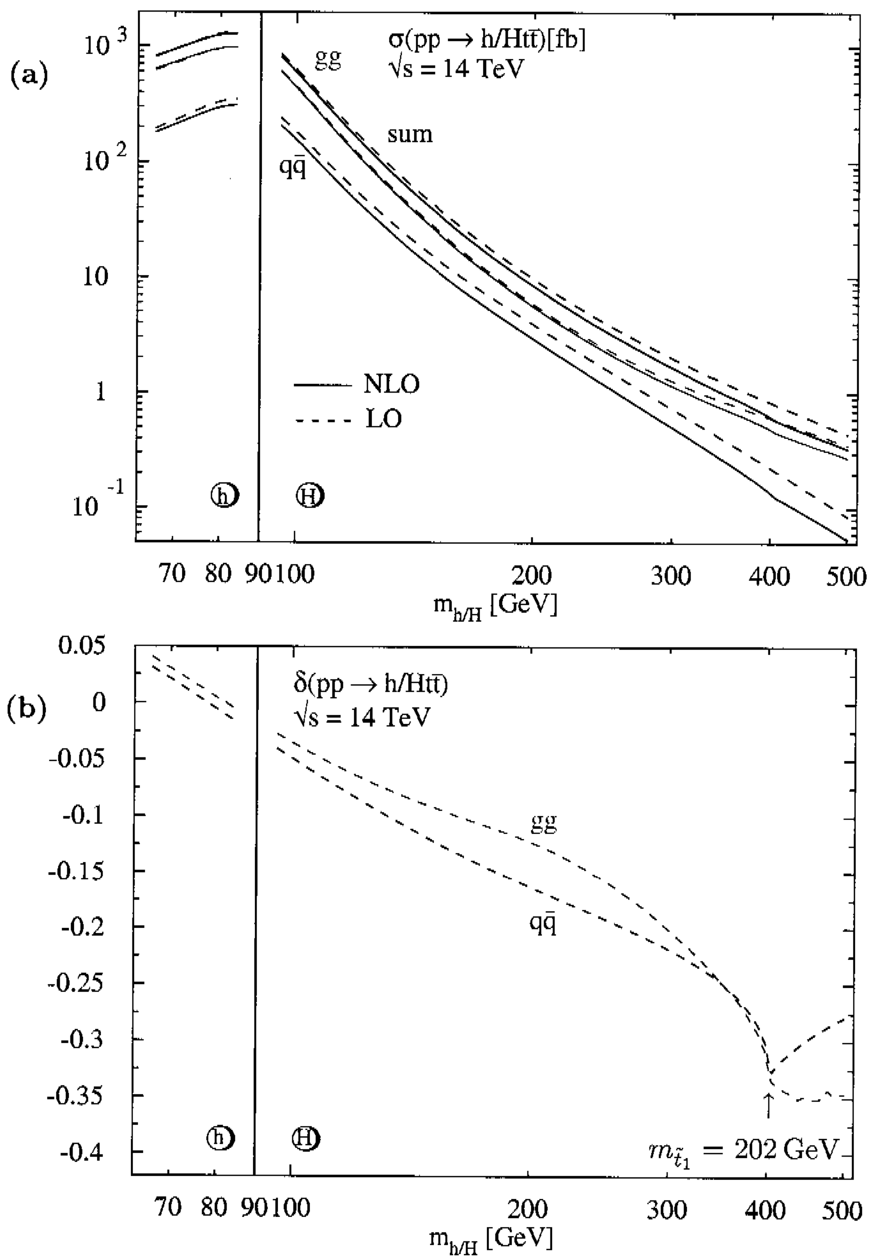

Figure 5.15: *(a) The LO (dashed lines) cross sections of associated heavy and light scalar Higgs production with top quarks at the LHC are plotted as functions of the scalar Higgs boson masses for the SPS5 benchmark point [105]. The SUSY-QCD corrected cross sections are depicted by the full lines. The hadron initial state splits into $q\bar{q}$ (blue) and gluonic (red) initial state. The total cross sections are shown in black. (b) The relative SUSY-QCD corrections to associated scalar Higgs production with top quarks are depicted for the two partonic contributions separately as functions of the scalar Higgs boson masses. At $m_H \approx 2\, m_{\tilde{t}_1}$ resonant contributions arise.*

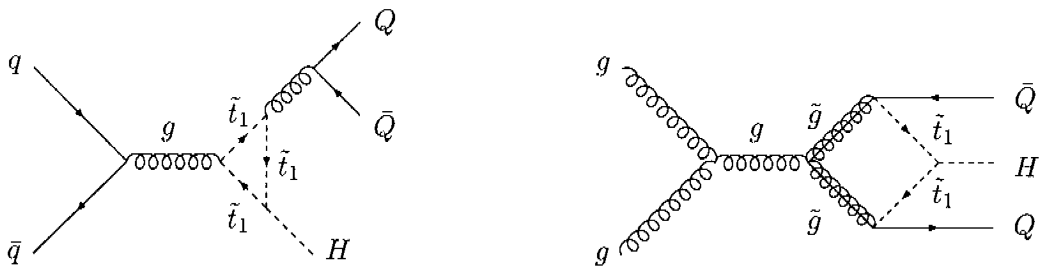

Figure 5.16: *Typical diagrams which contribute to the kink at the $\tilde{t}_1\bar{\tilde{t}}_1$ threshold.*

scalar Higgs boson the cross sections rapidly decrease due to the SUSY factors of the bottom Yukawa couplings. Far off the mass bounds the bottom Yukawa coupling for light and heavy scalar Higgs bosons are enhanced by tanβ (Table 1.5). In the limit of large pseudoscalar masses the SUSY factor approaches the SM value ($g_b^h \to 1$). For vanishing m_A the heavy scalar Higgs boson and thereby g_b^H becomes SM-like. The unresummed NLO SUSY-QCD corrections are large but they can be absorbed in the resummed bottom Yukawa coupling to a large extent.

The cross sections for associated Higgs production with bottom quarks at the Tevatron (Figures 5.19 and 5.20) range about two orders of magnitude below the corresponding LHC values and show a similar behaviour. The relative NLO SUSY-QCD corrections are of $\mathcal{O}(50\%)$ for the dominant gg channel. One may naively expect the $q\bar{q}$ initial state to dominate at the Tevatron, since the q and $\bar{q}$ are valence quarks in the proton and the antiproton, respectively. However, at these energies the gluonic parton density are much larger than the quark and antiquark densities, respectively. Thus, for the Tevatron the gluonic initial states dominate, too. The different slopes of the LO and NLO cross section (e.g. in the gluonic initial state in Figure 5.19a) originate from the PDFs evaluated at LO and NLO, respectively.

5.6 Summary

The LO and NLO SUSY-QCD cross sections have been evaluated for the bottom quark final state at the LHC and the Tevatron. The top quark final state is only depicted for the LHC, since this process is irrelevant for the Tevatron.

For the top quark final state at the LHC the LO cross sections range within 10^{-1}–10 fb for the pseudoscalar and within $10^{-1} - 10^2$ fb for the heavy scalar Higgs boson, for m_A up to 500 GeV in the SPS5 benchmark scenario. The NLO SUSY-QCD corrections reduce the cross section by 20–30%. The cross section of light scalar Higgs boson production is of $\mathcal{O}(10^2\,\text{fb})$ and the NLO SUSY-QCD corrections are small. The QCD corrections are of the same order of magnitude [65]. Thus, it is important to include both contributions in further analyses of these process.

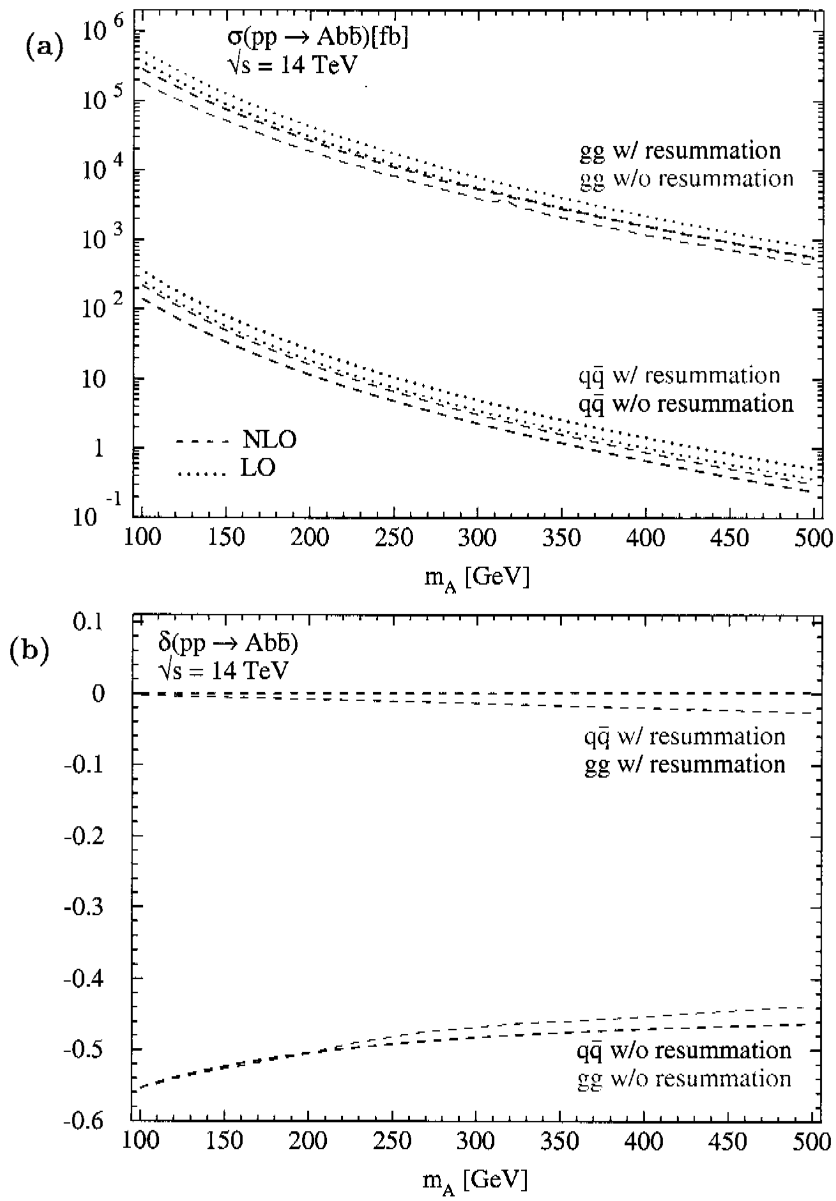

Figure 5.17: *(a) The LO (dotted lines) cross sections of associated pseudoscalar Higgs production with bottom quarks at the LHC are plotted with (red/blue) and without (black/magenta) resummation of the Δ_b terms as functions of the pseudoscalar Higgs boson mass for the SPS1b benchmark point [105]. The SUSY-QCD corrected cross sections are depicted by the dashed lines. The hadron initial state splits into $q\bar{q}$ (red/black) and gluonic (blue/magenta) initial state. (b) The relative SUSY-QCD corrections to associated pseudoscalar Higgs production with bottom quarks are displayed with and without resummation for the two partonic contributions separately as functions of the pseudoscalar Higgs boson mass.*

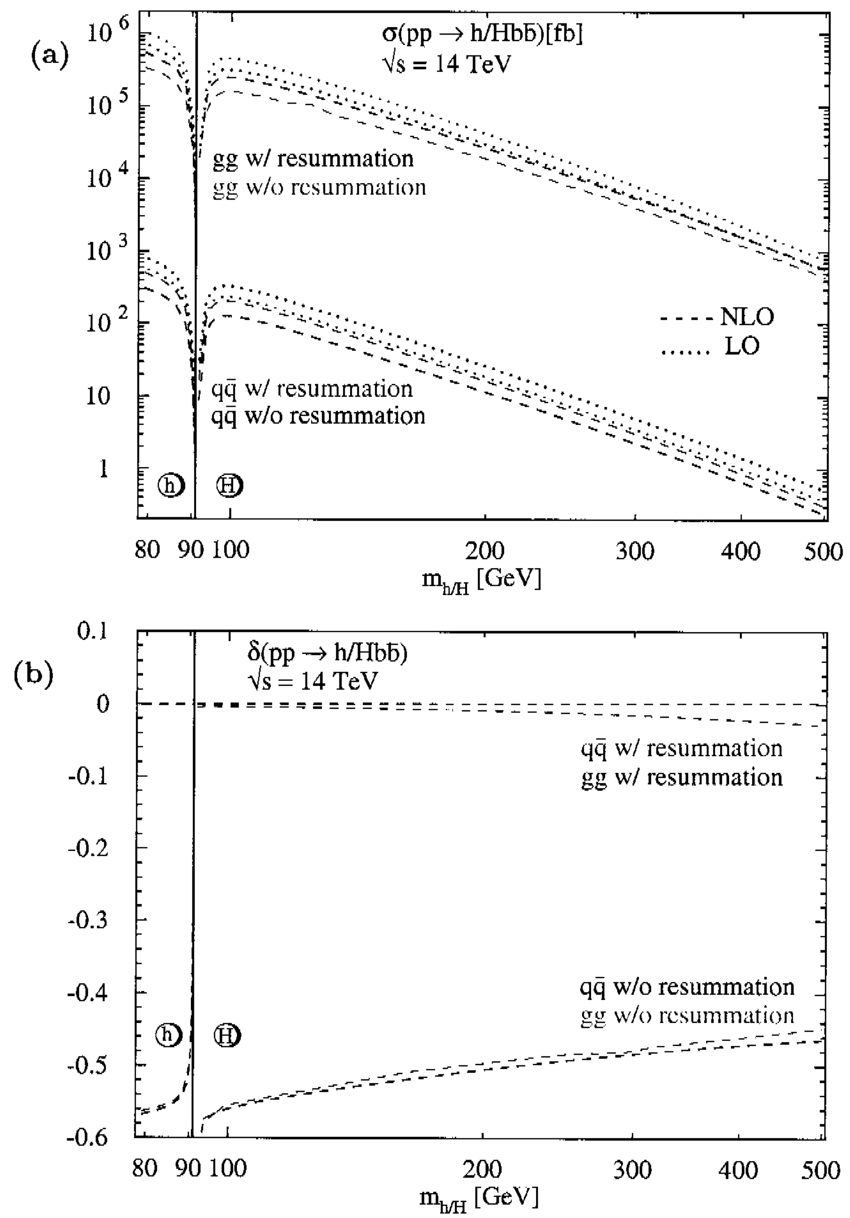

Figure 5.18: *(a) The LO (dotted lines) cross sections of associated light and heavy scalar Higgs production with bottom quarks at the LHC are plotted with (red/blue) and without (black/magenta) resummation of the Δ_b terms as functions of the scalar Higgs boson masses for the SPS1b benchmark point [105]. The SUSY-QCD NLO corrected cross sections are depicted by the dashed lines. The hadron initial state splits into $q\bar{q}$ (red/black) and gluonic (blue/magenta) initial state. (b) The relative SUSY-QCD corrections to associated scalar Higgs production with bottom quarks are displayed with and without resummation for the two partonic contributions separately as functions of the scalar Higgs boson masses.*

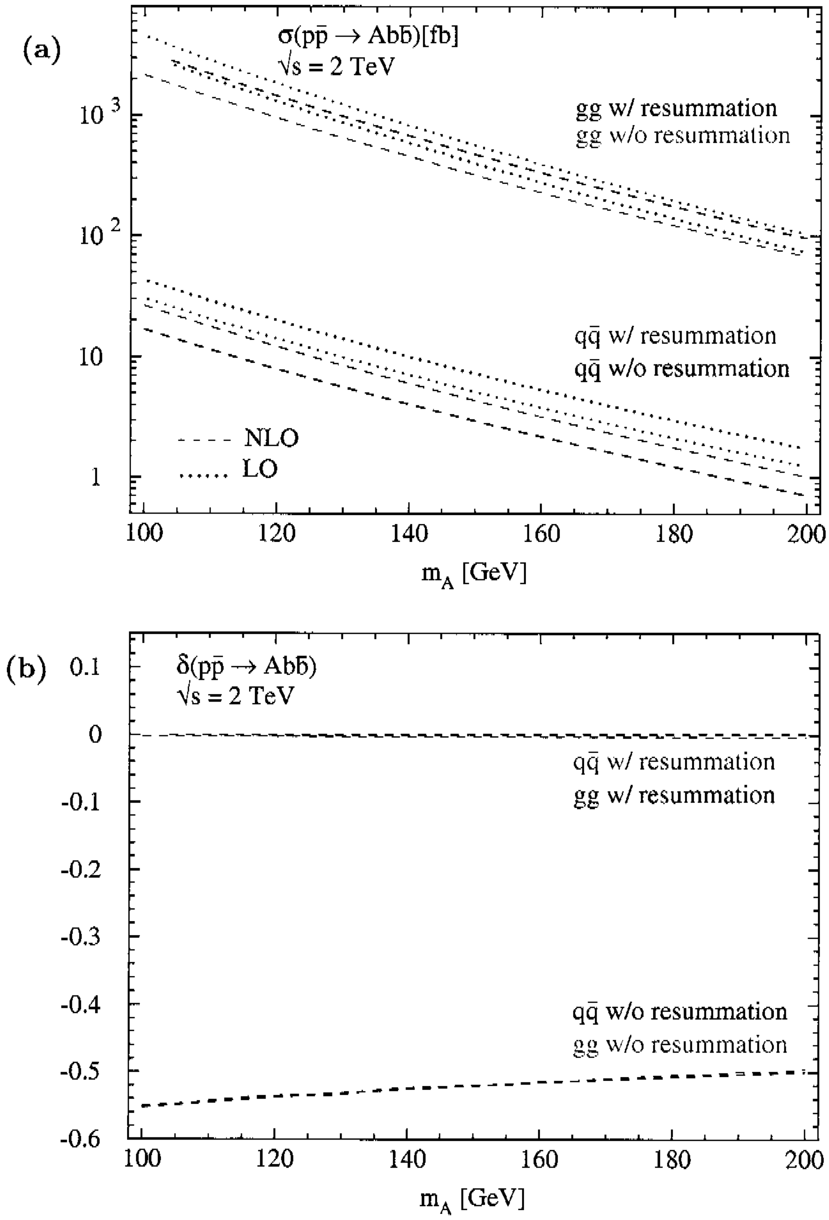

Figure 5.19: *(a) The LO (dotted lines) cross sections of associated pseudoscalar Higgs production with bottom quarks at the Tevatron are plotted with (red/blue) and without (black/magenta) resummation of the Δ_b terms as functions of the pseudoscalar Higgs boson mass for the SPS1b benchmark point [105]. The SUSY-QCD NLO corrected cross sections are depicted by the dashed lines. The hadron initial state splits into $q\bar{q}$ (red/black) and gluonic (blue/magenta) initial state. (b) The relative SUSY-QCD corrections to associated pseudoscalar Higgs production with bottom quarks are displayed with and without resummation for the two partonic contributions separately as functions of the pseudoscalar Higgs boson mass.*

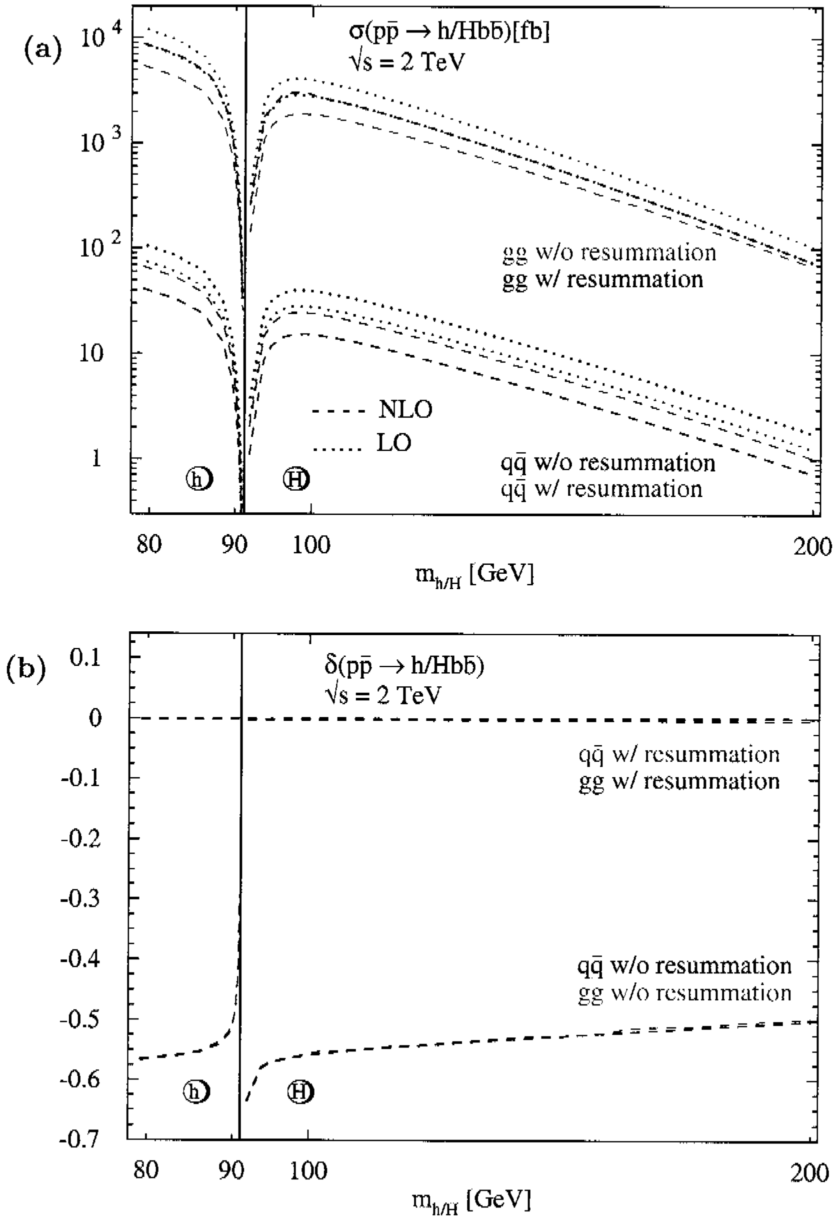

Figure 5.20: *(a) The LO (dotted lines) cross sections of associated light and heavy scalar Higgs production with bottom quarks at the Tevatron are plotted with (red/blue) and without (black/magenta) resummation of the Δ_b terms as functions of the scalar Higgs boson masses for the SPS1b benchmark point [105]. The SUSY-QCD NLO corrected cross sections are depicted by the dashed lines. The hadron initial state splits into $q\bar{q}$ (red/black) and gluonic (blue/magenta) initial state. (b) The relative SUSY-QCD corrections to associated scalar Higgs production with bottom quarks are displayed with and without resummation for the two partonic contributions separately as functions of the scalar Higgs boson masses.*

The bottom quark final state has been analysed for the SPS1b benchmark scenario. The cross sections at the LHC decrease from $\mathcal{O}(10^5\,\text{fb})$ at small Higgs masses down to $\mathcal{O}(10^3\,\text{fb})$ at $m_A \approx 500$ GeV. At the Tevatron the values are roughly a factor 100 smaller. The NLO SUSY-QCD corrections are about 50% for both collider, completely dominated by the gluonic contribution. The leading contributions of these corrections can be absorbed by resummation of the bottom Yukawa couplings. The remaining corrections are small in the whole mass range. The NLO QCD corrections range within 10−80% at the LHC and within 60−130% at the Tevatron [86].

Seite Leer /
Blank leaf

Chapter 6

Impact of A_0 on the mSUGRA Parameter Space

Since several years it is known that the measured amount of baryonic matter in the universe did not suffice to generate the universe in its present form. Dark energy contributes with $\sim 74\%$ and *dark matter* (DM) with $\sim 22\%$ to the total amount of energy stored in the universe. However, the question concerning the nature of these two contributions remains unanswered. The relic density of *cold dark matter* (CDM) depends on the effective annihilation cross section, which contains the annihilation as well as coannihilation cross sections of the CDM and the next heavier particles. The R-parity conserving mSUGRA models provide a promising CDM candidate: the lightest neutralino. The *trilinear scalar coupling* at the GUT scale, A_0, affects this effective neutralino annihilation cross sections through the masses and the couplings of the involved particles. Assuming a vanishing A_0, only mSUGRA models lying on narrow strips in the $m_0 - m_{1/2}$ plane (for fixed $\tan\beta$ values) lead to a relic density within the WMAP constraints. A variation of this coupling within $\pm$ a few TeVs significantly affects this allowed *mSUGRA parameter space.*

6.1 Dark Matter

The nature and the identity of the dark matter in the universe is one of the most challenging problems of modern cosmology. Zwicky studied 1933 the mass-to-light ratios of the Coma cluster [118]. His observations provided first evidence of the existence of invisible matter. In the meanwhile many mass-to-light ratios M/L within galaxies up to clusters of galaxies have been measured. The increase of these ratios with growing distance (Table 6.1) is a strong hint for the existence of DM at large scales.

The expansion rate of the universe is, in the standard Friedmann-Lemaître-Robertson-Walker model [119], expressed by the Friedman equation:

$$H^2 = \frac{\dot{R}(t)^2}{R(t)^2} = \frac{8\pi G_N \rho}{3} - \frac{k}{R^2} + \frac{\Lambda}{3}, \qquad (6.1)$$

distance scale	$(M/L)/(M_\odot/L_\odot)$	Ω_m
solar neighbourhood	$\simeq 2 \pm 1$ solar units	$1 \cdot 10^{-3}$
center of galaxies	$\simeq (10-20)\,h_0$	$1 \cdot 10^{-2}$
small groups of galaxies	$\simeq (60-180)\,h_0$	$1 \cdot 10^{-1}$
clusters of galaxies	$\simeq (200-500)\,h_0$	$3 \cdot 10^{-1}$

Table 6.1: *Mass-to-light ratios (M/L) normalised to the solar $(M_\odot/L_\odot)$ and the corresponding matter relic density Ω_m at different distance scales within galaxies up to clusters of galaxies. $h_0 \approx 0.73$ is the normalised present-day Hubble constant.*

where $H = h_0 \cdot 100\,\mathrm{km\,s^{-1}\,Mpc^{-1}}$, with $h_0 = 0.73^{+0.03}_{-0.03}$, is the present-day Hubble expansion rate[1]. $G_N = 6.6742 \cdot 10^{-11}\,\mathrm{m^3\,kg^{-1}\,s^{-2}}$ is the gravitational constant and $R(t)$ the cosmological scale factor. The three-space curvature $k = 0, +1$ or -1 describes a spatially flat, closed or open universe. The critical energy density is defined by $\rho_c \equiv 3H^2/8\pi G_N = 1.88 \cdot 10^{-29}\,h_0^2\,\mathrm{g\,cm^{-3}}$, in the absence of a cosmological constant Λ. The Friedman equation (6.1) can be converted to:

$$\begin{aligned} \frac{k}{R(t)^2} &= \frac{\rho}{\rho_c} H^2 + \frac{\Lambda}{3} - H^2 \\ &\equiv (\Omega_m + \Omega_\Lambda - 1)\,H^2 \;\equiv\; (\Omega_{tot} - 1)\,H^2, \end{aligned} \tag{6.2}$$

connecting the curvature with the total energy density in the universe Ω_{tot}, which is composed of the matter density Ω_m and the dark energy density Ω_Λ.

Nowadays, there are several additional theoretical and experimental indications that dark matter exists in the universe:

- *Inflation models*: in an adiabatically expanding universe $R(t)$ scales like $R \sim T^{-1}$, with the temperature of the thermal photon background T, leading to a dimensionless constant $\hat{k} = k/(RT)^2$. During inflation one finds $R \sim T^{-1} \sim e^{Ht}$ with a constant expansion rate H. After the inflation period holds $R = R_f \gg R_i$ and $T = T_f \lesssim T_i$. Thus, $R_f T_f \gg R_i T_i$ results in $\hat{k}_f = (\Omega - 1)\,H^2/T_f^2 \ll \hat{k}_i$ and with (6.2) follows that the total abundance of energy in the universe must be very closed to one [120], while measurements show that the baryonic contributions are $\Omega_b \ll 1$.

- *Cosmic Microwave Background (CMB)*: density fluctuations grow in the period of a matter dominated universe. The duration of the epoch of structure formation would have been very short if only the baryonic matter would have been available [121]. Hence, the fluctuations in the CMB would be much larger than observed (Figure 6.1).

- *Rotation curves of spiral galaxies*: in Figure 6.2 the orbital velocity of hydrogen clouds in the spiral galaxy NGC 6503 [123] as a function of the radius is shown. The

[1] The unit of length used in astronomy is parsec with $1\,\mathrm{pc} \approx 3.0857 \cdot 10^{16}\,\mathrm{m} \approx 3.262$ ly. It stands for **par**allax of one arc **sec**ond. At the distance of 1 pc the mean radius of the Earth's orbit around the Sun appears under an angle of one arc second.

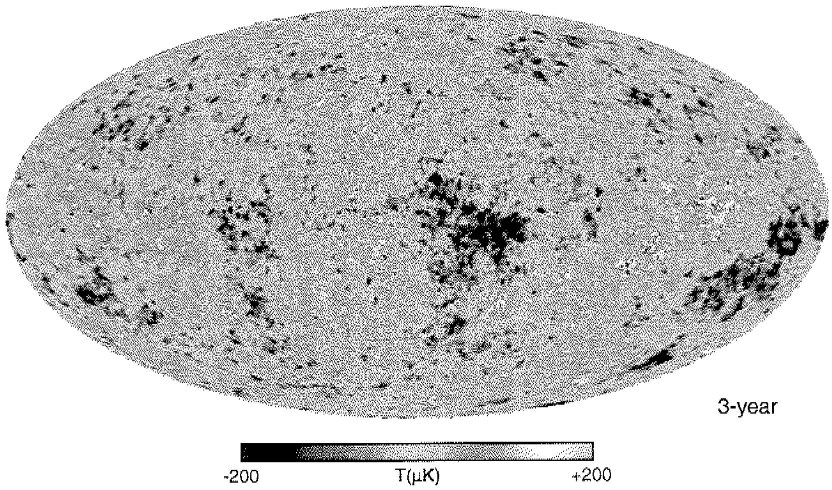

Figure 6.1: *WMAP has produced a new, more detailed picture of the infant universe. The colours indicate "warmer" (red) and "cooler" (blue) spots [122].*

constant speed over a large range of distances indicates that the hydrogen clouds outside the central region move much faster than one would expect from the Newtonian potential, considering only the baryonic mass of the disk and the gas (dashed and dotted lines in Figure 6.2). The rotation velocity is given by:

$$v \quad \propto \quad \sqrt{\frac{M(r)\, G_N}{r}} \qquad \text{with} \qquad M(r) = 4\pi \int \rho(r)\, r^2\, dr.$$

The constant velocity originates in a mass growing proportional to the radius. Thus, even if there is no baryonic matter beyond a certain distance from the center of the galaxy there must be some halo of dark matter increasing the total amount of mass of the galaxy further on.

- *Gravitational lensing*: a mass prediction without relying on dynamics and therefore a complete independent way to measure DM comes from the gravitational lensing effects [124], predicted by general relativity. The *strong lensing* results in clearly visible distortions with multiple images. It is particularly adept in testing the overall geometry of the universe. A cluster which provides multiple lensing of a single background galaxy can be used to determine the total cluster mass. On the other hand from lensing of several background galaxies constraints on the values of the Ω_m and Ω_Λ can be derived [125]. *Weak lensing* of galaxies by galaxies providing single images can probe the nature of galactic halos. Measuring the shapes and orientations of many distant galaxies gives an idea about the shear of the lensing field in any region [126]. Therefrom a background distribution of DM can be obtained.

In Figure 6.3 one of the first unambiguous proofs for the existence of dark matter is shown [127]. By comparing the center of the total mass reconstructed by weak lensing (green and white contours) with the center of baryonic matter (yellow/white

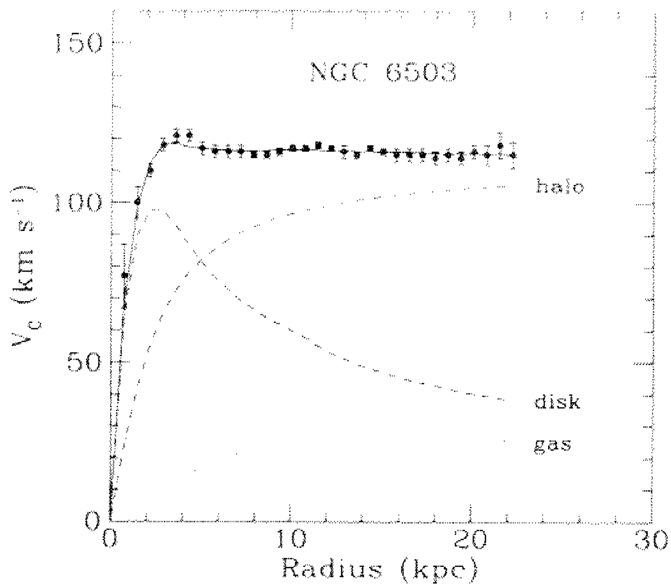

Figure 6.2: *Rotation curve of the spiral galaxy NGC 6503 as a function of the radius. The dashed and the dotted curves show the measured rotational velocity originating in the observed disk and gas distribution, respectively. The dot-dash curve is the predicted contribution from the DM halo to explain the measured flat rotation curve [123].*

region in Figure 6.3b) it is clearly visible that they do not coincide. Thus, there must be some kind of dark matter contributing to the total mass of these galaxies.

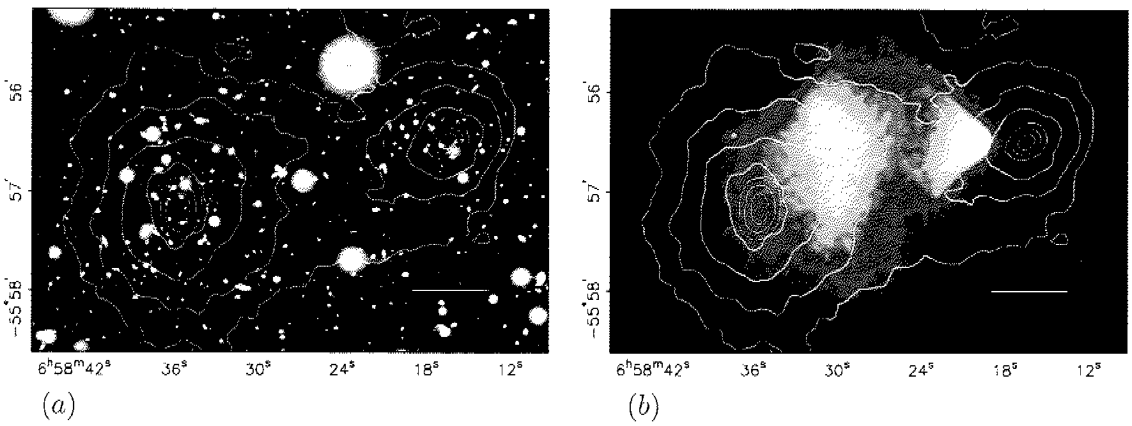

Figure 6.3: *The merging cluster 1E0657-558 is shown in the visible range (a) and the X-ray range (b). The white bars indicates 200 kpc at the distance of the cluster. The green contours in both pictures show the mass distribution reconstruction from the weak lensing, with the white contours show the errors on the mass peak corresponding to 68.3%, 95.5% and 99.7% CL. The blue crosses in (a) show the location of the mass peak of the measured baryonic plasma clouds, shown in (b) as coloured regions [127].*

However, it is not absolutely certain, that the required DM is neither baryonic nor neutrinos (high relativistic and therefore hot). Nevertheless, there exist hints toward a non-baryonic cold (non-relativistic) DM:

- *Large structure formation*: in the hierarchical structure formation small structures, as stars, are collapsing first followed by continuous forming of more and more massive objects like galaxies and clusters of galaxies. The matter heats up by collapsing due to gravitational contraction approaching an hydrostatic pressure balance. Ordinary baryonic matter has too high temperature and too much pressure left over from the big bang to collapse and to form small structures via Jeans instability[2]. On the other hand, in the top-down approach, called hot DM paradigm, flat pancake-like sheets fragment into smaller pieces. Observation of large scale structures strongly disagree with the prediction of this approach obtained by N-body simulations [128], while they coincide very well with the prediction of the bottom-up hierarchical model. Therefore, baryonic as well as hot DM are strongly disfavoured.

- *X-ray observation of hot gas*: from the temperature and density profile of hot X-ray emitting gas of large elliptical galaxies the overall mass distribution needed to bind the hot gas can be determined, assuming of hydrostatic equilibrium. For M87 in the Virgo cluster, e.g., the total mass out to 392 kpc is measured to be $5.7 \cdot 10^{13}\, M_\odot$. The mass of the hot gas is only $2.8 \cdot 10^{12}\, M_\odot$ or 5% of the total mass and the visible mass is expected to contribute with 1% [129]. Thus, the remaining 94% must be non-baryonic DM.

The most precise measurements of the abundance of matter and dark energy result from the satellite born detector WMAP [130], which probes the CMB (Figure 6.4). Of the 4% baryonic matter only a few % are luminous, e.g. stars, hot gas, etc.. A large fraction of it is dark, too, e.g. cold gas, brown dwarfs, etc.. Thus, one should distinguish between visible and invisible baryonic matter (together 4%) and non-baryonic cold dark matter (22%). A vacuum energy density or a cosmological constant, generically called dark energy, contributes the remaining 74% to the total amount of energy in the universe. However, the question concerning the nature of CDM and dark energy still remains unanswered. Potential candidates for CDM are axions, sterile neutrinos and WIMPs (weakly interacting massive particles), whereas, non of them exist in the SM. The axions are pseudo-Goldstone bosons, which arise by solving the strong CP-problem. Through resonant conversion to photons in magnetic fields they would be detectable, if they exist in our galaxy. Sterile neutrinos may mix with ordinary SM neutrinos via a Dirac mass. If both contain also Majorana masses the seesaw mechanism drives the ordinary neutrino mass down and make the sterile neutrinos very heavy. These sterile neutrinos are not completely sterile but the interaction with the left handed neutrinos is very small. The simplest model of sterile neutrinos as the dark matter particle is ruled out since the upper mass limit from their decays is lower than the lower limit from their effect on large scale structures [132]. The most promising candidates are WIMPs. Supersymmetric theories provide several such candidates.

[2]The Jeans instability occurs when internal pressure is no longer strong enough to prevent gravitational collapse of a region filled with matter.

$$\begin{aligned}
\Omega_{\rm tot} &= 1.02^{+0.02}_{-0.02}, \\
\Omega_{\rm m}\, h_0^2 &= 0.135^{+0.08}_{-0.09}, \\
\Omega_{\rm CDM}\, h_0^2 &= 0.1126^{+0.008}_{-0.009}, \\
\Omega_{\rm b}\, h_0^2 &= 0.0224^{+0.0009}_{-0.0009}, \\
\Omega_{\nu}\, h_0^2 &= 0.0076 \text{ at } 95\% \text{ CL},
\end{aligned}$$

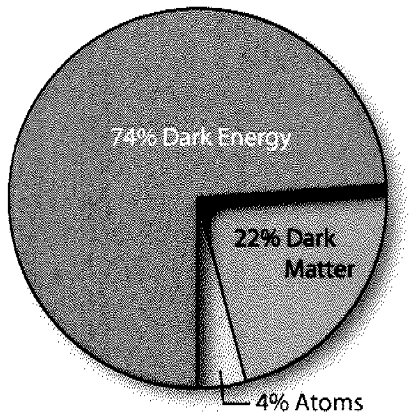

Figure 6.4: *WMAP data reveal that the universe consist of 4% baryonic matter (atoms), the building blocks of stars and planets, of 22% CDM and of 74% dark energy, which is responsible for the present-day acceleration of the universal expansion [131]. Expressed in terms of relic densities × the normalised Hubble constant squared, this leads to the shown numbers for the total (Ω_{tot}), matter (Ω_m), cold dark matter (Ω_{CDM}), baryonic matter (Ω_b) and neutrino (Ω_ν) contributions.*

6.2 Cold Dark Matter in SUSY

In R-parity conserving models sparticles can only be produced and annihilated in pairs resulting in a stable lightest SUSY particle[3] (LSP). The MSSM provides three possible colourless and electrically neutral CDM candidates: sneutrinos, gravitinos and neutralinos. The sneutrinos can be excluded by the results of direct [133] and of indirect [134] searches. The gravitino, which is the LSP in most GMSB models, is very difficult to exclude as a candidate. In mSUGRA models (Chapter 1.4) the lightest neutralino χ_1^0 is the LSP. The further studies presented here concentrate on this scenario.

The relic density of a particle species X can be estimated with the Lee-Weinberg equation [135] to:

$$\Omega_X h_0^2 \approx \frac{3 \cdot 10^{-27}\,\mathrm{cm}^3\,\mathrm{s}^{-1}}{\langle \sigma\, v\rangle_X},$$

with the thermal average of the total annihilation cross section times the velocity of the corresponding particle in the denominator. The neutralino annihilation cross section contains several different channels (Figure 6.5) leading to a non-trivial parameter space dependence of $\Omega_\chi h_0^2$. For example, the trilinear scalar coupling at the GUT scale, A_0, plays a significant role, since the masses and the couplings of the Higgs bosons and of the sfermions depend on it through RGEs and mixing effects. The masses of the gluinos, of the first two squark generations and of the light scalar Higgs boson are nearly independent of A_0 as indicated in Figure 6.6. The third generation squark and leptons, as well as the heavier neutral and the charged Higgs boson H, A and $H^\pm$, respectively show a strong dependence on A_0. The stau masses, e.g., depends quadratically on A_0, while the Higgs masses depend

[3]This is one of the strongest motivation to assume R-parity to be conserved.

linearly as well as quadratically on A_0 [136]. Since these particles appear in the neutralino annihilation channels as virtual particles the annihilation cross section also depends on A_0.

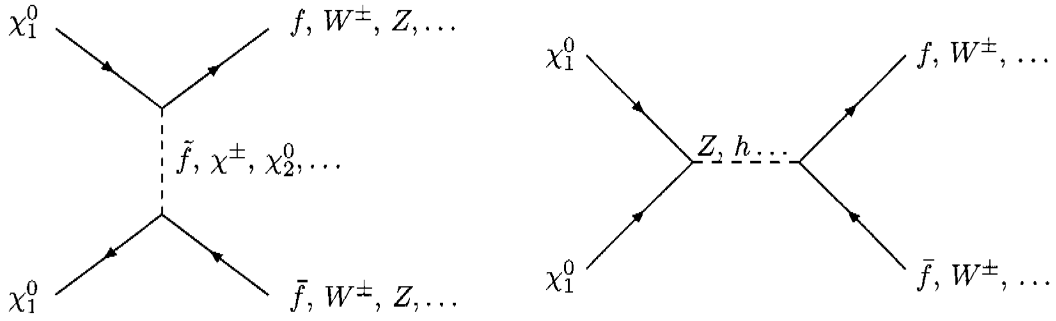

Figure 6.5: *Typical neutralino annihilation processes.*

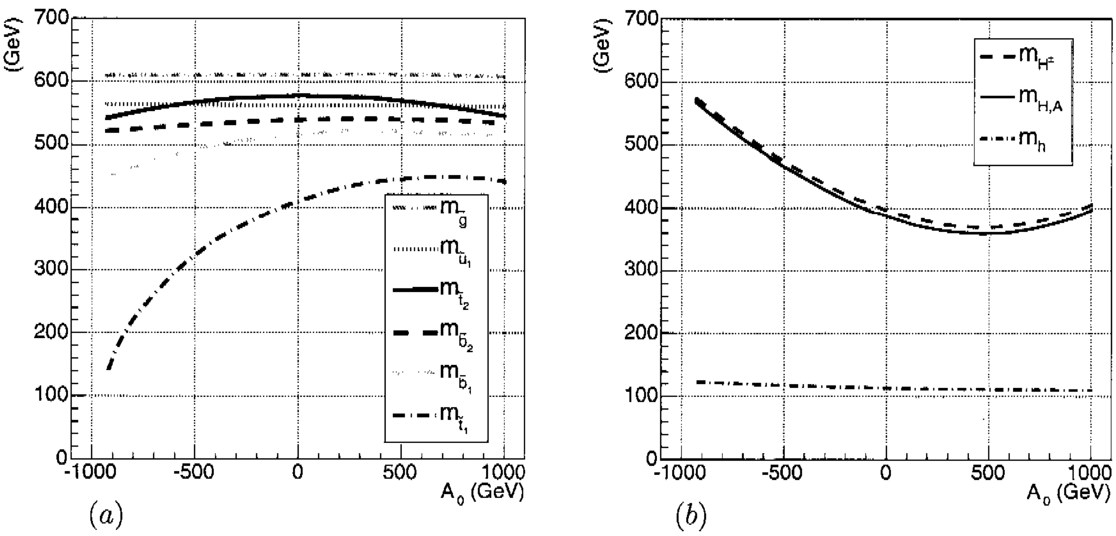

Figure 6.6: *Masses of the squarks, gluinos in (a) and of the Higgs bosons in (b) as functions of the trilinear scalar coupling A_0 for the Snowmass benchmark point SPS1A [105]: m_0 = 100 GeV, $m_{1/2}$ = 250 GeV, $\tan\beta$ = 10, μ > 0 and A_0 varied within $\pm$ 1 TeV. Since the first two squark generations are almost mass degenerated, only $m_{\tilde{u}_1}$ is shown as a representative example.*

Moreover, it is important to include all possible coannihilation processes (Figure 6.7) between the LSP and the next heavier lightest sparticle, the NLSP. Without including coannihilation processes the Snowmass benchmark point SPS1B [105] with A_0 left free within $\pm$ 1 TeV would be excluded (Figure 6.8). Including coannihilation processes results in several allowed models for different A_0 values. Thus, the annihilation cross section must be replaced by an effective cross section:

$$\langle \sigma_{\rm ann}\, v \rangle \longrightarrow \langle \sigma_{\rm eff}\, v \rangle = \frac{1}{n^2} \sum_{ij} \langle \sigma_{ij}\, v_{ij} \rangle\, n_i n_j,$$

with $n_{i,j}$ = number density of particle species $X_{i,j}$ at thermal equilibrium and $n = \sum_i n_i$. The relative particle velocity is given by $v_{ij} = \sqrt{(p_i \cdot p_j)^2 - m_i^2 m_j^2 / E_i E_j}$ with the particle energies $E_{i,j} = p^0_{i,j}$. The total cross section for annihilation into SM particles $\sigma_{ij} = \sum_X \sigma(X_i X_j \to X_{\rm SM})$ contains annihilation processes where $X_{i,j} = \chi_1^0$ as well as coannihilation processes of the LSP $X_i = \chi_1^0$ with the NLSP X_j.

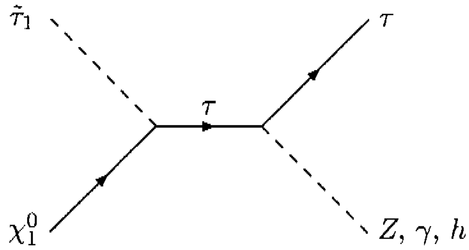

Figure 6.7: *Typical neutralino coannihilation processes. The lightest stau is assumed to be the NLSP in this example.*

Through the dependence of the relic density on this effective cross section the experimental boundaries of the neutralino relic density can constrain the mSUGRA parameter space.

6.3 Monte Carlo Generators

To evolve the mSUGRA input parameters at the GUT scale down to the electroweak scale two different Monte Carlo programs are used:

- `SuSpect 2.2` [137]: this Fortran program calculates the SUSY and Higgs particles spectra within the different constrained scenarios mSUGRA, GMSB and AMSB (Chapter 1.2.2). However, the spectra can also be derived for non-universal MSSM scenarios with conserved R-parity and CP.

- `ISAJET 7.69` [138]: this Monte Carlo event generator is mainly used for pp, $p\bar{p}$ and e^+e^- interactions at high energies. The included `ISASUSY` package calculates the masses and the decay modes in the MSSM. The RGEs are solved iteratively in the constrained mSUGRA, GMSB or AMSB models. If the input parameters are chosen at the electroweak scale, the calculations are performed in the MSSM framework with some assumption concerning mass degenerations.

The two programs lead to slightly different mass spectra for the same set of input parameters, as the implementation of RGEs is not performed in exactly the same way. The mass

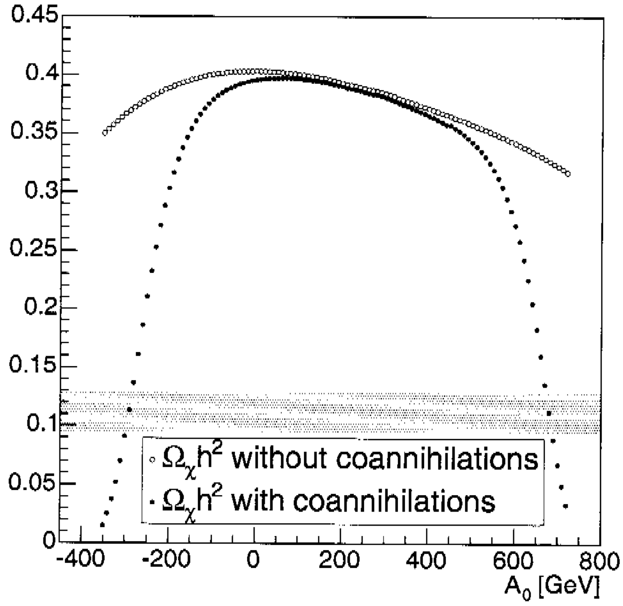

Figure 6.8: *The neutralino relic density $\Omega_\chi h_0^2$ as a function of the trilinear scalar coupling A_0 calculated with (red dots) and without (blue circles) including coannihilation processes. The input parameter are chosen according to the Snowmass point SPS1B (m_0 = 200 GeV, $m_{1/2}$ = 400 GeV, $\tan\beta$ = 30 and $\mu > 0$) [105]. The green shaded area shows the region allowed by the WMAP data within 2σ.*

spectra agree within about 10% for models with m_0 and $m_{1/2}$ of the same order and not too large $\tan\beta$. However, they can differ by a factor of two in the focus point region where m_0 is large and $m_{1/2}$ relatively small.

The neutralino relic density is calculated with the program `DarkSUSY 4.00` [139]. This calculation includes the impact of resonances, pair production thresholds, coannihilation processes and the bounds from accelerators. `DarkSUSY` also computes a large variety of astrophysical signals from neutralino CDM annihilation.

6.4 Impact of A_0 on the mSUGRA Parameter Space

Under the assumption that the CDM consists exclusively of neutralinos, the cosmological bounds on the CDM relic density imply strong constraints on the allowed mSUGRA parameter space. For a vanishing trilinear scalar coupling at the GUT scale and fixed $\tan\beta$ only narrow lines in the $m_0 - m_{1/2}$ plane, the WMAP strips [140], fulfil the WMAP constraints (Figure 6.9a). By varying A_0 within $\pm\,4$ TeV these lines extend to large areas depending on the $\tan\beta$ values (Figure 6.9b). Most of these models range within the LHC discovery reach for an integrated luminosity of 100 and 300 fb^{-1}, respectively, indicated by the brown lines in Figure 6.9b.

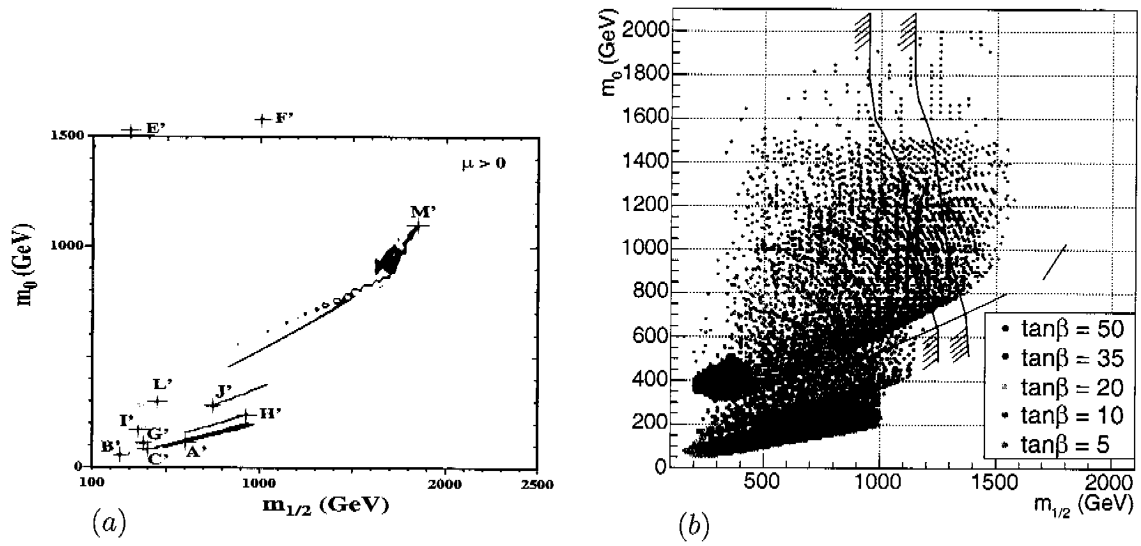

Figure 6.9: *Regions in the $m_0 - m_{1/2}$ plane accounting for 0.094 $< \Omega_\chi h_0^2 <$ 0.129 for different* $\tan\beta$ *between 5 and 50, $\mu > 0$. (a) WMAP strips for A_0 = 0 TeV and m_t = 175 GeV are shown with the post WMAP benchmark points (A'... M') [140]. (b) Allowed models for A_0 within ± 4 TeV obtained with ISAJET. The black lines correspond to the WMAP strips in the left plot. The brown lines indicate the LHC discovery reach for an integrated luminosity of 100 fb^{-1} and 300 fb^{-1}, respectively [46].*

In order to avoid colour and/or charge breaking (CCB) the trilinear scalar couplings at the electroweak scale $A_{t,b,\tau}$ have to be approximately constrained as [141]:

$$\begin{aligned} A_t^2 &\leq 3(m_{H_u}^2 + m_{\tilde{t}_L}^2 + m_{\tilde{t}_R}^2), \\ A_b^2 &\leq 3(m_{H_d}^2 + m_{\tilde{b}_L}^2 + m_{\tilde{b}_R}^2), \\ A_\tau^2 &\leq 3(m_{H_d}^2 + m_{\tilde{\tau}_L}^2 + m_{\tilde{\tau}_R}^2). \end{aligned} \tag{6.3}$$

The consequence of applying these constraints is shown in Figure 6.10 for $\tan\beta = 10$. By far the biggest effect originates from the cut on A_τ due to the light stau masses.

To avoid CCB these cuts are necessary but not sufficient, since the vacuum expectation values of the squarks, the sleptons and the corresponding Higgs boson were assumed to be equal, for simplicity. Moreover the bounds in (6.3) were derived from the tree level scalar potential, while radiative corrections are expected to modify them. The scalar potential may contain global CCB minima in addition to the local electroweak breaking minima. As no CCB has been observed, the universe in its present state may be trapped in a local electroweak breaking minimum. Since this metastable state may have a lifetime longer than the age of the universe due to the small tunnelling probability into the global minimum [142], CCB cannot be excluded. Therefore, these cuts are not applied in the studies described below.

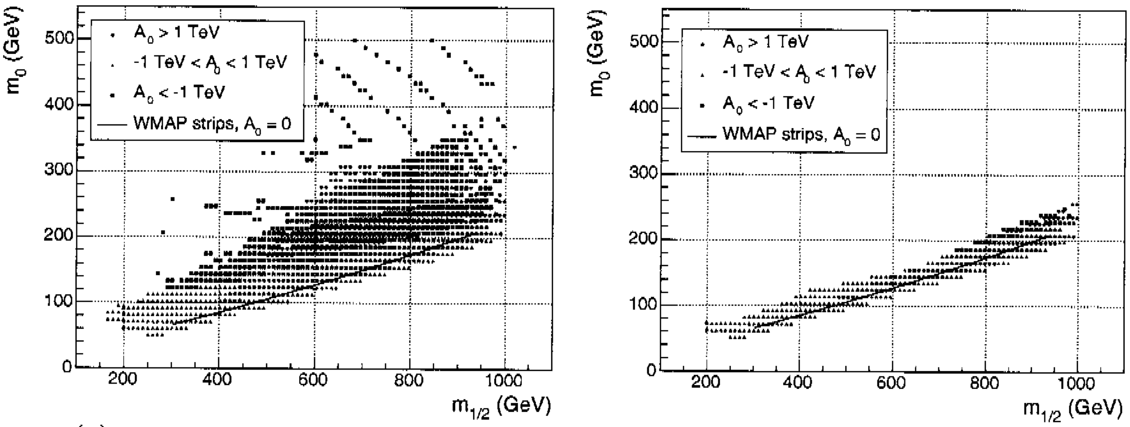

(*a*) (*b*)

Figure 6.10: *Allowed models in the $m_0 - m_{1/2}$ plane for* $\tan\beta$ = *10 and* $\mu > 0$ *obtained with ISAJET. The black lines correspond to the WMAP strip for* A_0 = *0 TeV. In (b) the cuts defined in (6.3) have been applied.*

The mSUGRA models which fulfil the WMAP constraints, lie for fixed values of A_0 and $\tan\beta$ on curves in the $m_0 - m_{1/2}$ plane (Figure 6.11). Because of their smooth narrow shape, they can be fitted by a polynomial of 2nd order:

$$m_0 = a + b \cdot m_{1/2} + c \cdot m_{1/2}^2. \tag{6.4}$$

The parameters, obtained by using the `MINUIT` [143] routines, are given in the Tables 6.2 and 6.3 for $\tan\beta = 10$ and 35 and A_0 varied within ± 4 TeV.

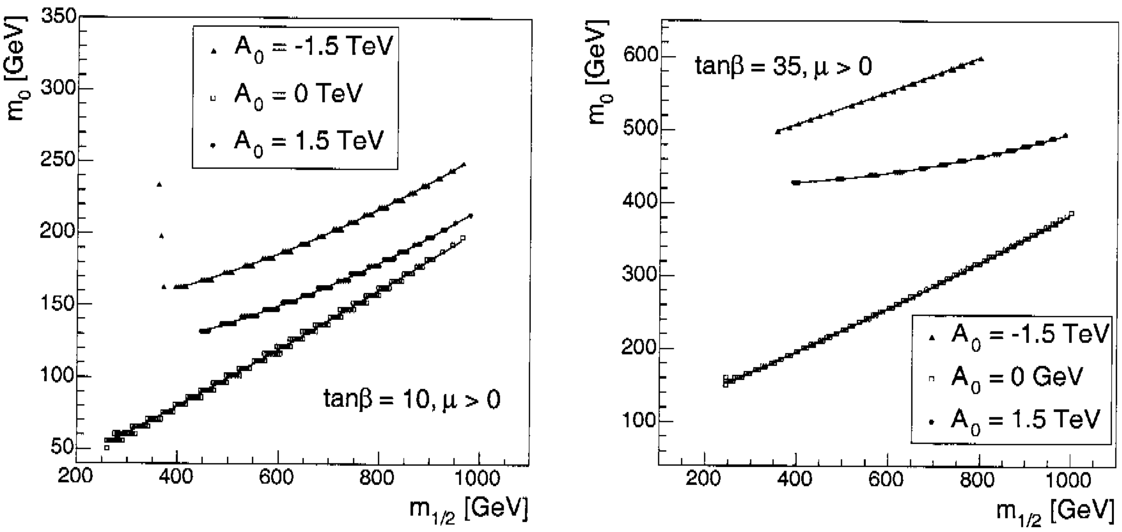

Figure 6.11: *mSUGRA models which fulfil the WMAP constraints in the $m_0 - m_{1/2}$ plane for three different A_0 values. In the left/right plot is* $\tan\beta$ = *10/35 and* μ *is positive in both plots. The black lines are the fits given in Tables 6.2 and 6.3. The "gaps" in the lines originate from the chosen step size for* m_0

The isolated points in the left plot in Figure 6.11 originate from unexpectedly large m_0 values, for small $m_{1/2}$, which lead to $\Omega_\chi h_0^2$ values within the WMAP range. The separation between the lines for different A_0 values becomes larger with increasing tanβ. For negative trilinear scalar couplings the shift in m_0 is larger than for positive values, but always to higher m_0 values so that the minimal m_0 are obtained for vanishing A_0. Thus, the main effect of varying A_0 is a shift of the WMAP strips to higher m_0 values [144].

The dependence of the annihilation cross section on the trilinear scalar coupling leads to an impact of A_0 on the γ−ray flux coming from neutralino annihilations. The analysis of this impact is the subject of the thesis of Luisa Sabrina Stark [145].

A_0	a	b	c $[10^{-5}]$	$m_{1/2}$ domain	m_0 domain
-2 TeV	189 ± 4	-0.02 ± 0.01	11.3 ± 0.9	485 - 965 GeV	208 - 285 GeV
-1.5 TeV	134 ± 2	0.034 ± 0.007	8.8 ± 0.5	400 - 965 GeV	163 - 249 GeV
-1 TeV	96 ± 1	0.045 ± 0.004	9.4 ± 0.3	260 - 954 GeV	117 - 224 GeV
-0.5 TeV	47 ± 1	0.104 ± 0.003	6.6 ± 0.3	260 - 939 GeV	76 - 203 GeV
0 TeV	8 ± 1	0.171 ± 0.003	2.6 ± 0.2	260 - 964 GeV	51 - 198 GeV
0.5 TeV	11 ± 1	0.157 ± 0.004	3.3 ± 0.3	340 - 980 GeV	66 - 198 GeV
1 TeV	53 ± 2	0.081 ± 0.006	7.2 ± 0.4	390 - 984 GeV	97 - 203 GeV
1.5 TeV	105 ± 3	0.016 ± 0.009	9.7 ± 0.6	447 - 980 GeV	132 - 214 GeV
2 TeV	154 ± 4	-0.02 ± 0.01	10.3 ± 0.8	487 - 960 GeV	168 - 229 GeV
2.5 TeV	200 ± 6	-0.05 ± 0.02	10 ± 1	562 - 1000 GeV	208 - 259 GeV

Table 6.2: *Coefficients a, b and c of the parameterisation defined in equations (6.4) for* tanβ *= 10 and discrete values of A_0 between −2 and 2.5 TeV. For larger or smaller A_0 values too few mSUGRA models survive the WMAP constraints to allow a reasonable parameterisation. The last two columns contain the domains for $m_{1/2}$ and m_0, respectively.*

A_0	a	b	c $[10^{-5}]$	$m_{1/2}$ domain	m_0 domain
-1.5 TeV	427 ± 5	0.19 ± 0.02	4 ± 1	356 - 799 GeV	499 - 600 GeV
-1 TeV	301 ± 2	0.190 ± 0.005	5.1 ± 0.4	281 - 995 GeV	358 - 540 GeV
-0.5 TeV	176 ± 1	0.219 ± 0.004	5.4 ± 0.3	245 - 1000 GeV	231 - 448 GeV
0 TeV	88 ± 1	0.251 ± 0.003	4.7 ± 0.2	245 - 1000 GeV	151 - 388 GeV
0.5 TeV	138 ± 1	0.139 ± 0.004	9.7 ± 0.3	311 - 1000 GeV	191 - 373 GeV
1 TeV	282 ± 2	0.001 ± 0.007	13.1 ± 0.5	376 - 995 GeV	302 - 413 GeV
1.5 TeV	432 ± 3	-0.058 ± 0.009	12.2 ± 0.6	391 - 985 GeV	428 - 494 GeV
2 TeV	577 ± 5	-0.08 ± 0.01	10.3 ± 1.0	517 - 980 GeV	565 - 600 GeV

Table 6.3: *Same as in Table 6.2, but for* tanβ *= 35 and A_0 within −1.5 and 2 TeV.*

6.5 Summary

The relic density of neutralino CDM develops a strong dependence on A_0, the trilinear scalar couplings at the GUT scale, through the masses and the couplings of the sparticles. The WMAP data constrains the CDM relic density to lie within $\Omega_{\mathrm{CDM}}\, h_0^2 = 0.1126^{+0.008}_{-0.009}$. Applying these limits on the relic density calculated for mSUGRA models leads to a significant reduction of the allowed mSUGRA parameter space, strongly depending on A_0. For fixed values of A_0 and $\tan\beta$ the allowed regions can be parameterised by lines in the $m_0 - m_{1/2}$ plane, as done for $A_0 = 0$ TeV. The main effect of a non-vanishing A_0 value is a shift of these lines to higher m_0 values.

Chapter 7

Conclusions

The NLO SUSY-QCD corrections to associated neutral MSSM Higgs production with heavy quarks have been calculated for e^+e^- and hadron collisions.

For the leptonic initial state the cross sections and relative corrections are exemplary shown for a linear e^+e^- collider with a center of mass energy of 1 TeV.

For the $At\bar{t}$ final state in e^+e^- collisions the LO cross section is of $\mathcal{O}(10^{-2}\,\text{fb})$ below $m_A \lesssim 350$ GeV. For the heavy scalar Higgs production with top quarks the LO cross section decreases from $\mathcal{O}(1\,\text{fb})$ at $m_H \approx 100$ GeV down to $\mathcal{O}(10^{-1}\,\text{fb})$ at $m_H \approx 350$ GeV. At the $t\bar{t}$ threshold the cross sections increase rapidly to a level of 1 fb due to the resonant $H/A \to t\bar{t}$ in the pair production channel. This dominant channel closes kinematically at $m_A \approx 450$ GeV, hence the cross sections in this region drop down. The cross section of the light scalar Higgs boson production is of $\mathcal{O}(1\,\text{fb})$ in the whole mass range. The NLO SUSY-QCD corrections contribute with about 10–20% for all three neutral Higgs bosons [113]. The previously obtained pure NLO QCD corrections are, apart from the Coulomb singularity around the top threshold, of similar magnitude [104]. Strongly depending on the scenario cancellation or constructive interference between the QCD and SUSY-QCD corrections occurs. Therefore, it is important to include both corrections in future analysis of these processes at linear e^+e^- colliders.

At large values of $\tan\beta$, associated Higgs production with bottom quarks in e^+e^- collisions provides a possibility to measure $\tan\beta$. The LO cross sections are of $\mathcal{O}(10\,\text{fb})$, apart from Higgs masses near the mass bounds of the scalar Higgs bosons. At $m_A \gtrsim 450$ GeV they rapidly decrease due to the kinematical closure of the dominant pair production channel. In the past it has been demonstrated that the bulk of the pure QCD corrections can be absorbed in the running bottom Yukawa couplings, defined at the scale of the corresponding Higgs momentum flows. The running bottom Yukawa couplings are therefore used in the whole calculation. The remaining NLO QCD corrections are of $\mathcal{O}(20\%)$, almost independent of the corresponding Higgs mass [104]. It is shown that the SUSY-QCD corrections are dominated by the non-decoupling Δ_b terms. Those can be absorbed and resummed in the corresponding bottom Yukawa couplings. This absorption reduces the SUSY-QCD corrections from more than 40% to less than 20%. The QCD and SUSY-QCD corrections are of the same order of magnitude and both should be included in studies of these processes at a future ILC.

The numerical results for associated Higgs production with heavy quarks in hadronic collisions are evaluated for the top quark final state at the LHC and for the bottom quark final state at LHC and Tevatron.

At the LHC the LO cross section for associated light scalar Higgs production with top quarks is of $\mathcal{O}(10^2\,\text{fb})$ in the whole mass range. For the heavy scalar it decreases from $\mathcal{O}(10^2\,\text{fb})$ at $m_H \approx 100\,\text{GeV}$ down to $\mathcal{O}(10^{-1}\,\text{fb})$ at $m_H \approx 500\,\text{GeV}$, completely dominated by the gluonic initial state, as expected. The NLO SUSY-QCD corrections range within 20−30% and are of the similar magnitude as the NLO QCD corrections [65]. The LO cross section for the $At\bar{t}$ final states is of $\mathcal{O}(1\,\text{fb})$ in the whole mass range below 500 GeV, and the NLO QCD and SUSY-QCD corrections contribute each with about 20−30%.

For associated light scalar Higgs production with bottom quarks the LO cross section is of $\mathcal{O}(10^5\,\text{fb})$ at the LHC. For the heavy scalar and the pseudoscalar Higgs boson the cross sections decrease from $\mathcal{O}(10^5\,\text{fb})$ at $m_A \approx 100\,\text{GeV}$ to $\mathcal{O}(10^3\,\text{fb})$ at $m_A \approx 500\,\text{GeV}$. The LO cross sections at the Tevatron range about two order of magnitude below the corresponding LHC values. At both colliders they are completely dominated by the gluonic initial state. One may naively expect the $q\bar{q}$ initial state to dominate for a $p\bar{p}$ collider as the Tevatron, but at these energies the gluonic densities for proton and antiproton are larger than the corresponding densities for quarks and antiquark, respectively. The NLO SUSY-QCD corrections are of $\mathcal{O}(50\%)$ for both colliders and the leading contributions can be absorbed by resummation of the bottom Yukawa coupling as for e^+e^- colliders. The bulk of the NLO QCD corrections can be absorbed by the running bottom Yukawa couplings. The remaining QCD corrections vary within 10−80% for the LHC, while they contribute with 60−130% at the Tevatron. Therefore, the NLO QCD [86] and SUSY-QCD [115] corrections are of comparable magnitude and it is important to consider both in further analysis.

The R-parity conserving mSUGRA models provide a promising CDM candidate: the lightest neutralino. The CDM relic density depends on the effective annihilation cross section, which consists of annihilation as well as coannihilation processes of the CDM and the next heavier particles. Among other parameters, the trilinear scalar coupling at the GUT scale, A_0, affects these cross sections through the masses and the couplings of the involved particles. Assuming a vanishing A_0, only mSUGRA models lying on narrow strips in the $m_0 - m_{1/2}$ plane (for fixed tanβ values) lead to a relic density within the WMAP constraints. It is shown, that a variation of this coupling within $\pm$ a few TeVs significantly affects the allowed mSUGRA parameter space [144]. Since the allowed models for fixed values of A_0 and tanβ still lie on lines in the $m_0 - m_{1/2}$ plane they can be fitted by second order polynomials. The main effect of a non-vanishing A_0 value is a shift of these lines to higher m_0 values.

Appendix A

Feynman Rules

Propagators with:

- spinor indices: $\alpha, \beta \ldots$ for fermions,
- colour indices: $i, j \ldots$ for quarks and squarks and $a, b \ldots$ for gluons and gluinos,
- Lorentz indices: $\mu, \nu \ldots$ for vector bosons,
- squark indices: $x, y \ldots = 1, 2$ or L, R.

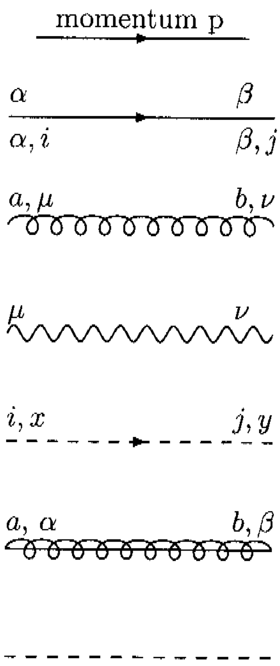

fermion f	$iS^f(p) = i\,\dfrac{\not{p} + m_f}{p^2 - m_f^2}\,\delta_{\alpha\beta}\,(\delta_{ij})$
gluon g	$iS^g(p) = -i\,\dfrac{g_{\mu\nu}}{p^2}\,\delta_{ab}$
vector boson V	$iS^V(p) = -i\,\dfrac{g_{\mu\nu} - \frac{p_\mu p_\nu}{m_V}}{p^2 - m_V^2}$
squark $\tilde{q}$	$iS^{\tilde{q}}(p) = i\,\dfrac{1}{p^2 - m_{\tilde{q}_i}^2}\,\delta_{ij}\,\delta_{xy}$
gluino $\tilde{g}$	$iS^{\tilde{g}}(p) = i\,\dfrac{\not{p} + m_{\tilde{g}}}{p^2 - m_{\tilde{g}}^2}\,\delta_{\alpha\beta}\,\delta_{ab}$
Higgs boson ϕ	$iS^{\phi}(p) = i\,\dfrac{1}{p^2 - m_\phi^2}$

Strong interaction vertices:

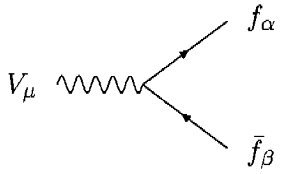

$$\boxed{-ie\left[\gamma_\mu\,(v_V^f - a_V^f\gamma_5)\right]_{\alpha\beta}},$$

$$V = \gamma : \begin{cases} v_\gamma^f = Q_f \\ a_\gamma^f = 0 \end{cases}$$

$$V = Z : \begin{cases} v_Z^f = \dfrac{I_{3,L}^f - 2Q_f \sin^2\theta_W}{2\cos\theta_W \sin\theta_W} \\ a_Z^f = \dfrac{I_{3,L}^f}{2\cos\theta_W \sin\theta_W} \end{cases}$$

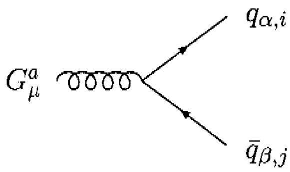

$$\boxed{-ig_s\,T_{ij}^a\,[\gamma_\mu]_{\alpha\beta}}$$

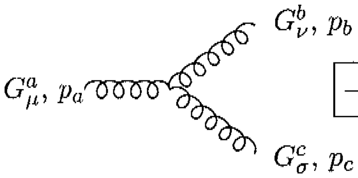

$$\boxed{-g_s\,f^{abc}\left[g_{\mu\nu}(p_a - p_b)_\sigma \;+\; g_{\nu\sigma}(p_b - p_c)_\mu + \;g_{\sigma\mu}(p_c - p_a)_\nu\right]}$$

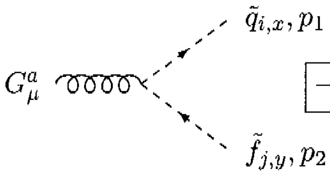

$$\boxed{-ig_s\,T_{ij}^a\,(p_1+p_2)_\mu\,\delta_{xy}}$$

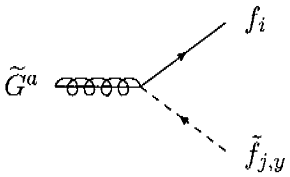

$$\boxed{-i\frac{g_s}{\sqrt{2}}\;T_{ij}^a(v_x + a_x\gamma_5)}$$

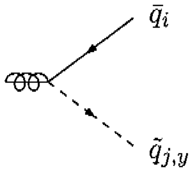

$$\boxed{-i\frac{g_s}{\sqrt{2}}\;T_{ij}^a(v_x - a_x\gamma_5)}$$

$$\begin{aligned} v_{1/2}^Q &= \pm\cos\theta - \sin\theta \\ a_{1/2}^Q &= \quad\cos\theta \pm \sin\theta \\ v_{L/R}^q &= \pm 1 \\ a_{L/R}^q &= \quad 1 \end{aligned}$$

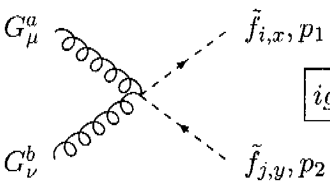

$$\boxed{ig_s^2\,\{T^a,T^b\}_{ij}\,g_{\mu\nu}}$$

Higgs couplings with the coefficients $g^{\phi}_{q,Z}$ and $g^{\phi}_{1,\ldots,4}$, which are defined in Chapter 1.3.4 in Table 1.4 and Table 1.6.

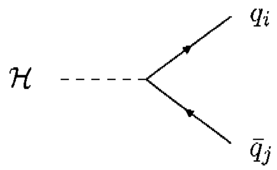

$$\boxed{-i g_q^{\mathcal{H}} \frac{m_q}{v}\, \delta_{ij}}$$

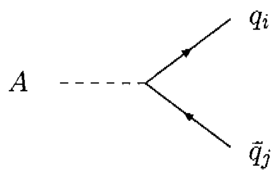

$$\boxed{-i g_q^{A} \frac{m_q}{v}\, [-i\gamma_5]\, \delta_{ij}}$$

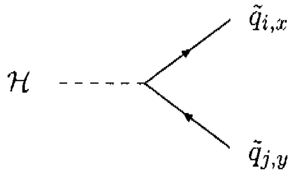

$$\boxed{-i\frac{2}{v}\, G^{\mathcal{H}}_{xy} \delta_{ij}}$$

$$G^{\mathcal{H}}_{11} = g^{\mathcal{H}}_{LL} \cos^2\theta + g^{\mathcal{H}}_{RR} \sin^2\theta + g^{\mathcal{H}}_{LR} \sin(2\theta)$$

$$G^{\mathcal{H}}_{12} = g^{\mathcal{H}}_{LR} \cos(2\theta) + (g^{\mathcal{H}}_{RR} - g^{\mathcal{H}}_{LL}) \sin\theta \cos\theta$$

$$G^{\mathcal{H}}_{22} = g^{\mathcal{H}}_{RR} \cos^2\theta + g^{\mathcal{H}}_{LL} \sin^2\theta - g^{\mathcal{H}}_{LR} \sin(2\theta)$$

$$g^{\mathcal{H}}_{LL} = m_q^2\, g_1^{\mathcal{H}} + m_Z^2\, (I_{3q} - e_q \sin^2\theta_W) g_2^{\mathcal{H}}$$

$$g^{\mathcal{H}}_{RR} = m_q^2\, g_1^{\mathcal{H}} + m_Z^2\, e_q \sin^2\theta_W g_2^{\mathcal{H}}$$

$$g^{\mathcal{H}}_{LR} = -\frac{m_q}{2}\, (\mu\, g_3^{\mathcal{H}} - A_q\, g_4^{\mathcal{H}})$$

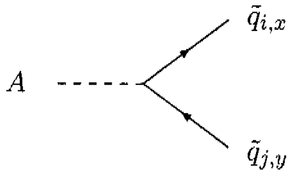

$$\boxed{-\frac{2}{v}\, G^{A}_{xy} \delta_{ij}}$$

$$G^{A}_{11} = G^{A}_{22} = 0$$

$$G^{A}_{12} = \frac{m_q}{2}\, (\mu + A_q\, \tan\beta) = -G^{A}_{21}$$

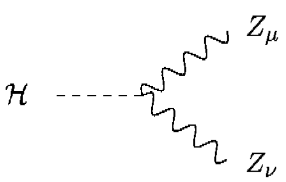

$$\boxed{i\, \frac{2\, m_Z^2}{v}\, g_{\mu\nu}\, g_Z^{\mathcal{H}}}$$

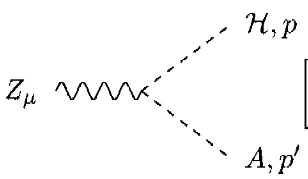

$$\boxed{-i\, \frac{m_Z}{v}\, (p + p')_\mu\, g_Z^{\mathcal{H}}}$$

Seite Leer /
Blank leaf

Appendix B

Scalar One-Loop Integrals

A complete discussion about scalar one-loop integrals can be found in [146] and a summary of tensor reduction and results in [147].

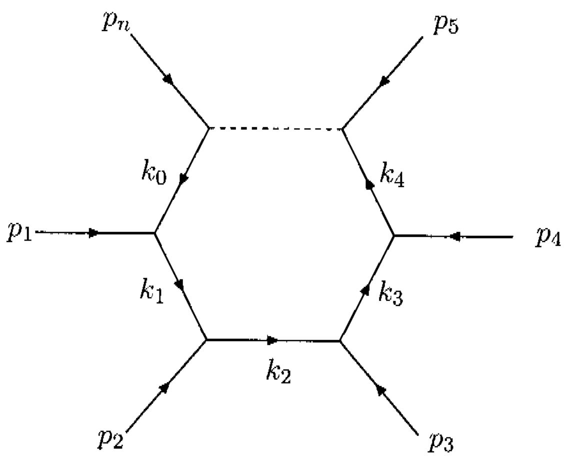

$$\begin{aligned} i &= 1, \ldots, n-1, \\ k_0 &= k_n = \sum_{l=1}^{n} p_l = 0, \\ k_i &= \sum_{l=1}^{i} p_l, \\ d_i &= (k+k_i)^2 - m_i^2 + 0i \end{aligned}$$

The one-loop tensore n-point integrals have the general form:

$$T^{n,\,\mu_1 \ldots \mu_j}(p_1, \ldots, p_{n-1}; m_0, \ldots, m_{n-1}) = \mu^{2\varepsilon} \int \frac{d^D k}{(2\pi)^D} \frac{k^{\mu_1} \cdots k^{\mu_j}}{d_0\, d_1\, d_2 \ldots d_{n-1}}$$

with $n = (1, 2, 3, 4, 5, \ldots) \mathrel{\hat{=}} (A,\, B,\, C,\, D,\, E, \ldots)$.

The tensor decomposition in Lorentz-covariant structures leads to:

$$\begin{aligned} A^{\mu} &= 0, & A^{\mu\nu} &= g^{\mu\nu} A_{00}, \\ T^{n,\,\mu_1} &= \sum_{j=1}^{n-1} p_j^{\mu_1}\, T_j^n, & T^{n,\,\mu_1\mu_2} &= g^{\mu_1\mu_2}\, T_{00}^n + \sum_{j,k=1}^{n-1} p_j^{\mu_1}\, p_k^{\mu_2}\, T_{jk}^n, \\ T^{n,\,\mu_1\mu_2\mu_3} &= \sum_{j=1}^{n-1} g^{[\mu_1\mu_2}\, p_j^{\mu_3]}\, T_{00j}^n + \sum_{j,k,l=1}^{n-1} p_j^{\mu_1} p_k^{\mu_2} p_l^{\mu_3} T_{jkl}^n. \end{aligned}$$

The following notations are use:

$$C_\varepsilon \equiv \frac{\Gamma(1+\varepsilon)}{(4\pi)^2}\left(\frac{4\pi\mu^2}{m_1^2}\right)^\varepsilon \quad \text{with} \quad \frac{\Gamma(1+\varepsilon)}{\varepsilon}(4\pi)^\varepsilon = \frac{1}{\varepsilon} - \gamma_E + \log(4\pi) \equiv \Delta_{UV},$$

$$\alpha_\pm \equiv \frac{p^2+m_1^2-m_2^2}{2(p^2+i\varepsilon)} \pm \sqrt{\left(\frac{p^2+m_1^2-m_2^2}{2(p^2+i\varepsilon)}\right)^2 - \frac{m_1^2}{p^2-i\varepsilon}},$$

$$\rho \equiv \frac{p^2}{m_1^2}, \qquad \beta \equiv \sqrt{1-4/\rho}, \qquad x_b \equiv \frac{1+\beta}{1-\beta}.$$

The scalar 1-point-integrales are result in:

$$A_0(m_1) = iC_\varepsilon m_1^2\left[\frac{1}{\varepsilon}+1+\mathcal{O}(\varepsilon)\right],$$

$$A_0(0) = 0.$$

The scalar 2-point-integrales for general and equal masses reads as:

$$B_0(p;m_1,m_2) = iC_\varepsilon\left[\frac{1}{\varepsilon}+2+\alpha_+\log\left(1-\frac{1}{\alpha_+}\right)+\alpha_-\log\left(1-\frac{1}{\alpha_-}\right) - \log\left(\frac{m_2^2}{m_1^2}\right)+\mathcal{O}(\varepsilon)\right],$$

$$B_0(p;m_1,m_1) = iC_\varepsilon\left[\frac{1}{\varepsilon}+2-\beta\log(-x_b)+\mathcal{O}(\varepsilon)\right].$$

The partial derivative with respect to p^2 of scalar 2-point-integrale is given by:

$$B_0'(p;m_1,m_2) = iC_\varepsilon\left[\frac{(\alpha_+-{\alpha_+}^2)\log(1-1/\alpha_+)-(\alpha_--{\alpha_-}^2)\log(1-1/\alpha_-)}{p^2(\alpha_+-\alpha_-)} - \frac{1}{p^2}+\mathcal{O}(\varepsilon)\right].$$

For higher number of propagators no short analytical results for general energies and masses exist.

Bibliography

[1] S.L. Glashow, *Partial-symmetries of weak interactions,* Nucl. Phys. **22** (1961) 579;
S. Weinberg, *A model of leptons,* Phys. Rev. Lett. **19** (1967) 1264;
A. Salam, *Weak and electromagnetic interactions*, originally printed in *Svartholm: Elementary Particle Theory, proceedings of the Nobel Symposium Held 1968.*

[2] M. Gell-Mann, *A schematic model of baryons and mesons,* Phys. Lett. **8** (1964) 214;
G. Zweig, *An SU(3) model for strong interaction symmetry and its breaking,* published in *Developments in the Quark Theory of Hadrons, Vol.I, 1964-1978, 22*, Editor D.B. Lichtenberg, S.P. Rosen, (Hadronic Press, Nonatum, Massachusetts, 1980) and CERN Report 8182/TH401.

[3] Y.A. Golfand, E.P. Likhtman, *Extension of the algebra of Poincaré group generators and violation of P invariance,* JETP Lett. **13** (1971) 323;
D.V. Volkov, V.P. Akulov, *Is the neutrino a goldstone particle?,* Phys. Lett. **B46** (1973) 109;
J. Wess, B. Zumino, *Supergauge transformations in four dimensions,* Nucl. Phys. **B70** (1974) 39 and *A Lagrangian model invariant under supergauge transformations,* Phys. Lett. **B49** (1974) 52.

[4] N. Arkani-Hamed, S. Dimopoulos, G.R. Dvali, *The hierarchy problem and new dimensions at a millimeter,* Phys. Lett. **B429** (1998) 263, [arXiv:hep-ph/9803315] and *Phenomenology, astrophysics, and cosmology of theories with submillimeter dimensions and TeV scale quantum gravity,* Phys. Rev. **D59** (1999) 086004, [arXiv:hep-ph/9807344];
L. Randall, R. Sundrum, *Large mass hierarchy from a small extra dimension,* Phys. Rev. Lett. **83** (1999) 3370, [arXiv:hep-ph/9905221] and *An alternative to compactification,* Phys. Rev. Lett. **83** (1999) 4690, [arXiv:hep-th/9906064].

[5] E. Witten, *Mass hierarchies in supersymmetric theories,* Phys. Lett. **B105** (1981) 267;
H.P. Nilles, *Supersymmetry, supergravity and particle physics,* Phys. Rep. **110** (1984) 1;
H.E. Haber, G. Kane, *The search for supersymmetry: Probing physics beyond the standard model,* Phys. Rep. **117** (1985) 75;
for review see:
R. Barbieri, *Looking beyond the standard model: the supersymmetric option,* Riv. Nuovo Cim. **11N4** (1988) 1;

J. Wess, J. Bagger, *Supersymmetry and supergravity* (Princeton Univ. Pr., 1991), [ISBN: 0-691-02530-4];
S. Dawson, *SUSY and SUCH*, [arXiv:hep-ph/9612229] and *The MSSM and why it works*, [arXiv:hep-ph/9712464];
S.P. Martin, *A supersymmetry primer*, [arXiv:hep-ph/9709356].

[6] H. Spiesberger, M. Spira, P.M. Zerwas, *The standard model: physical basis and scattering experiments*, published in *Scattering*, Editor P. Sabatier (Academic Press, London, 2000), [arXiv:hep-ph/0011255] and references therein;
F. Halzen, A.D. Martin, *Quarks & Leptons*, (Wiley & Sons, 1984), [ISBN: 0-471-88741-2].

[7] Particle Data Group, `http://pdg.lbl.gov/` and references therein.

[8] C. Itzykson, J.-B. Zuber, *Quantum field theory*, (McGraw-Hill, New York, 1980), [ISBN: 0-07-032071-3];
M. Böhm, A. Denner, H. Joos, *Gauge theories of the strong and electroweak interaction*, (B.G. Teubner Verlage, Stuttgart 3. rev. ed., 2001), [ISBN: 3-519-23045-3];
M.E. Peskin, D.V. Schroeder, *An introduction to quantum field theory*, (Westview Press, 14th print Impressum, 2003), [ISBN: 0-201-50397-2].

[9] G. Arnison et al. (UA1 Collaboration) *Experimental observation of lepton pairs of invariant mass around 95-GeV/c^2 at the CERN SPS collider*, Phys. Lett. **B126** (1983) 398;
P. Bagnaia et al. (UA2 Collaboration) *Evidence for $Z_0 \to e^+e^-$ at the CERN $\bar{p}p$ collider*, Phys. Lett. **B129** (1983) 130.

[10] P.W. Higgs, *Broken symmetries, massless particles and gauge fields*, Phys. Lett. **12** (1964) 132, *Broken symmetries and the masses of gauge bosons*, Phys. Rev. Lett. **13** (1964) 508 and *Spontaneous symmetry breakdown without massless bosons*, Phys. Rev. **145** (1966) 1156;
F. Englert, R. Brout, *Broken symmetry and the mass of gauge vector mesons*, Phys. Rev. Lett. **13** (1964) 321;
G.S. Guralnik, C.R. Hagen, T.W.B. Kibble, *Global conservation laws and massless particles*, Phys. Rev. Lett. **13** (1964) 585;
T.W.B. Kibble, *Symmetry breaking in non-abelian gauge theories*, Phys. Rev. **155** (1967) 1554.

[11] G. 't Hooft, *Renormalizable Lagrangians for massive Yang-Mills fields*, Nucl. Phys. **B35** (1971) 167 and *Renormalization of massless Yang-Mills fields*, Nucl. Phys. **B33** (1971) 173;
G. 't Hooft, M.J.G. Veltman, *Regularization and renormalization of gauge fields*, Nucl. Phys. **B44** (1972) 189 and *Combinatorics of gauge fields*, Nucl. Phys. **B50** (1972) 318.

[12] M. Spira, P.M. Zerwas, *Electroweak symmetry breaking and Higgs physics*, [arXiv:hep-ph/9803257].

[13] S. Weinberg, *Implications of dynamical symmetry breaking,* Phys. Rev. **D13** (1976) 974 and *Implications of dynamical symmetry breaking: an addendum,* Phys. Rev. **D19** (1979) 1277;
L. Susskind, *Dynamics of spontaneous symmetry breaking in the Weinberg-Salam theory,* Phys. Rev. **D20** (1979) 2619.

[14] T. Hambye, K. Riesselmann, *Matching conditions and Higgs boson mass upper bounds reexamined,* Phys. Rev. **D55** (1997) 7255, [arXiv:hep-ph/9610272];
K. Riesselmann, *Limitations of a standard model Higgs boson,* [arXiv:hep-ph/9711456].

[15] N. Cabibbo, L. Maiani, G. Parisi, R. Petronozio, *Bounds on the fermions and Higgs boson masses in grand unified theories,* Nucl. Phys. **B158** (1979) 295;
M. Lindner, *Implications of triviality for the standard model,* Z. Phys. **C31** (1986) 295;
A. Hasenfratz, K. Jansen, C.B. Lang, T. Neuhaus, H. Yoneyama, *The triviality bound of the four-component ϕ^4 model,* Phys. Lett. **B199** (1987) 531;
J. Kuti, L. Lin, Y. Shen, *Upper bound on the Higgs boson mass in the standard model,* Phys. Rev. Lett. **61** (1988) 678;
M. Lüscher, P. Weisz, *Scaling laws and triviality bounds in the lattice ϕ^4 theory (III). N-component model,* Nucl. Phys. **B318** (1989) 705;
M. Sher, *Electroweak Higgs potential and vacuum stability,* Phys. Rept. **179** (1989) 273, *Precise vacuum stability bound in the standard model,* Phys. Lett. **B317** (1993) 159, [arXiv:hep-ph/9307342] and *Addendum-ibid.,* Phys. Lett. **B331** (1994) 448;
G. Altarelli, G. Isidori, *Lower limit on the Higgs mass in the standard model: an update,* Phys. Lett. **B337** (1994) 141;
J.A. Casas, J. Espinosa, M. Quirós, *Improved Higgs mass stability bound in the standard model and implications for supersymmetry,* Phys. Lett. **B342** (1995) 171, [arXiv:hep-ph/9409458] and *Standard model stability bounds for new physics within LHC reach,* Phys. Lett. **B382** (1996) 374, [arXiv:hep-ph/9603227];
J. Espinosa, M. Quirós, *Improved metastability bounds on the standard model Higgs mass,* Phys. Lett. **B353** (1995) 257, [arXiv:hep-ph/9504241].

[16] E. Brubaker et al. (Tevatron Electroweak Working Group), *Combination of CDF and D0 results on the mass of the top quark,* [arXiv:hep-ex/0608032].

[17] G. Abbiendi et al., (ALEP, DELPHI, L3 und OPAL Collaborations, the LEP Working Group for Higgs Boson Searches), *Search for the standard model Higgs boson at LEP,* Phys. Lett. **B565** (2003) 61, [arXiv:hep-ex/0306033].

[18] D. Abbaneo et al., (LEP Electroweak Working Group), A. Chou et al., (SLD heavy flavor and electroweak groups), LEPEWWG/2002-01 and additional updates at `http://lephiggs.web.cern.ch/LEPHIGGS/www/Welcome.html`.

[19] M. Carena, H.E. Haber, *Higgs boson theory and phenomenology,* Prog. Part. Nucl. Phys. **50** (2003) 63, [arXiv:hep-ph/0208209].

[20] R. Haag, J.T. Lopusznski, M. Sohnius, *All possible generators of supersymmetries of the S-matrix,* Nucl. Phys. **B88** (1975) 257.

[21] S. Coleman, J. Mandula, *All possible symmetries of the S matrix,* Phys. Rev. **159** (1967) 1251.

[22] P. Fayet, S. Ferrare, *Supersymmetry,* Phys. Rept. **32** (1977) 249.

[23] W. de Boer, C. Sander, *Global electroweak fits and gauge coupling unification,* Phys. Lett. **B585** (2004) 276, [arXiv:hep-ph/0307049];
M. Carena, S. Mrenna, C.E.M. Wagner, *Complementarity of the CERN LEP collider, the Fermilab Tevatron, and the CERN LHC in the search for a light MSSM Higgs boson,* Phys. Rev. **D62** (2000) 055008, [arXiv:hep-ph/9907422].

[24] H. Georgi, H.R. Quinn, S. Weinberg, *Hierarchy of interactions in unified gauge theories,* Phys. Rev. Lett. **33** (1974) 451.

[25] L.E. Ibañez, G.G. Ross, *Low-energy predictions in supersymmetric grand unified theories,* Phys. Lett. **B105** (1981) 439;
S. Dimopoulos, S. Raby, F. Wilczek, *Supersymmetry and the scale of unification,* Phys. Rev. **D24** (1981) 1681;
J. Ellis, S. Kelley, D.V. Nanopoulos, *Precision LEP data, supersymmetric GUTs and string unification,* Phys. Lett. **B249** (1990) 441;
P. Langacker, M. Luo, *Implications of precision electroweak experiments for m_t, ρ_0, $\sin 2\theta_W$ and grand unification,* Phys. Rev. **D44** (1991) 817;
U. Amaldi, W. de Boer, H. Fürstenau, *Comparison of grand unified theories with electroweak and strong coupling constants measured at LEP,* Phys. Lett. **B260** (1991) 447.

[26] L.E. Ibañez, G.G. Ross, *$SU(2)_L \times U(1)$ symmetry breaking as a radiative effect of supersymmetry breaking in GUTs,* Phys. Lett. **B110** (1982) 215.

[27] S. Deser, B. Zumino, *Consistent Supergravity,* Phys. Lett. **B62** (1976) 335.

[28] H. Goldberg, *Constraint on the photino mass from cosmology,* Phys. Rev. Lett. **50** (1983) 1419;
J.R. Ellis, J.S Hagelin, D.V. Nanopoulos, K.A. Olive, M. Srednicki, *Supersymmetric relics from the Big Bang,* Nucl. Phys. **B238** (1984) 453.

[29] M. Dine, P. Huet, R. Singleton Jr., L. Susskind, *Creating the baryon asymmetry at the electroweak phase transition,* Phys. Lett. **B257** (1991) 351;
M. Dine, P. Huet, R. Singleton Jr., *Baryogenesis at the electroweak scale,* Nucl. Phys. **B375** (1992) 625;
P. Huet, A.E. Nelson, *Electroweak baryogenesis in supersymmetric models,* Phys. Rev. **D53** (1996) 4578, [arXiv:hep-ph/9506477].

[30] W. Pauli, *Scientific Correspondence,* Vol.2, 169 (Springer, New York, 1979).

[31] S. Weinberg, *The cosmological constant problem,* Rev. Mod. Phys. **61** (1989) 1.

[32] J.L. Diaz-Cruz, J. Ferrandis, *Solving the supersymmetric CP problem with flavor breaking F terms,* Phys. Rev. **D72** (2005) 035003, [arXiv:hep-ph/0504094].

[33] S.L. Glashow, J. Iliopoulos, L. Maiani, *Weak interactions with lepton-hadron symmetry,* Phys. Rev. **D2** (1970) 1285.

[34] S. Weinberg, *Cosmological constraints on the scale of supersymmetry breaking,* Phys. Rev. Lett. **48** (1982) 1303;
J.R. Ellis, J.E. Kim, D.V. Nanopoulos, *Cosmological gravitino regeneration and decay,* Phys. Lett. **B145** (1984) 181;
M. Kawasaki, T. Moroi, *Gravitino production in the inflationary Universe and the effects on Big-Bang nucleosynthesis,* Prog. Theor. Phys. **93** (1995) 879, [arXiv:hep-ph/9403364].

[35] S. Ferrara, L. Girardello, F. Palumbo, *General mass formula in broken supersymmetry,* Phys. Rev. **D20** (1979) 403.

[36] A.H. Chamseddine, R. Arnowitt, P. Nath, *Locally supersymmetric grand unification,* Phys. Rev. Lett. **49** (1982) 970;
K. Inoue, A. Kakuto, H. Komatsu, S. Takeshita, *Low energy parameters and particle masses in a supersymmetric grand unified model,* Prog. Theor. Phys. **67** (1982) 1889, *Aspects of grand unified models with softly broken supersymmetry,* Prog. Theor. Phys. **68** (1982) 927, Erratum-ibid. *70,* Prog. Theor. Phys. **1983** (330) and *Renormalization of supersymmetry breaking parameters revisited,* Prog. Theor. Phys. **71** (1984) 413;
L. Alvarez-Gaumé, M. Claudson, M.B. Wise, *Low-energy supersymmetry,* Nucl. Phys. **B207** (1982) 96;
R. Barbieri, S. Ferrara, C.A. Savoy, *Gauge models with spontaneously broken local supersymmetry,* Phys. Lett. **B119** (1982) 343;
J.R. Ellis, D.V. Nanopoulos, K. Tamvakis, *Grand unification in simple supergravity,* Phys. Lett. **B121** (1983) 123.

[37] M. Dine, W. Fischler, *A phenomenological model of particle physics based on supersymmetry,* Phys. Lett. **B110** (1982) 227;
C.R. Nappi, B.A. Ovrut, *Supersymmetric extension of the $SU(3) \times SU(2) \times U(1)$ model,* Phys. Lett. **B113** (1982) 175;
M. Dine, A.E. Nelson, *Dynamical supersymmetry breaking at low energies,* Phys. Rev. **D48** (1993) 1277, [arXiv:hep-ph/9303230];
M. Dine, A.E. Nelson, Y. Shirman, *Low energy dynamical supersymmetry breaking simplified,* Phys. Rev. **D51** (1995) 1362, [arXiv:hep-ph/9408384];
M. Dine, A.E. Nelson, Y. Nir, Y. Shirman, *New tools for low energy dynamical supersymmetry breaking,* Phys. Rev. **D53** (1996) 2658, [arXiv:hep-ph/9507378].

[38] L. Randall, R. Sundrum, *Out of this world supersymmetry breaking,* Nucl. Phys. **B557** (1999) 79, [arXiv:hep-th/9810155];
G.F. Giudice, M.A. Luty, H. Murayama, R. Rattazzi, *Gaugino mass without singlets,* JHEP **9812** (1998) 027, [arXiv:hep-ph/9810442];
T. Gherghetta, G.F. Giudice, J.D. Wells, *Phenomenological consequences of supersymmetry with anomaly induced masses,* Nucl. Phys. **B559** (1999) 27, [arXiv:hep-ph/9904378];
J.L. Feng, T. Moroi, *Supernatural supersymmetry: phenomenological implications*

of anomaly-mediated supersymmetry breaking, Phys. Rev. **D61** (2000) 095004, [arXiv:hep-ph/9907319].

[39] A. Salam, J. Strathdee, *Super-gauge transformations,* Nucl. Phys. **B76** (1974) 477 and *Super-symmetry and non-abelian gauges,* Phys. Lett. **B51** (1974) 353.

[40] P. Fayet, *Supersymmetry and weak, electromagnetic and strong interactions,* Phys. Lett. **B64** (1976) 159.

[41] G.R. Farrar, P. Fayet, *Phenomenology of the production, decay, and detection of new hadronic states associated with supersymmetry,* Phys. Lett. **B76** (1978) 575;
F. Zwirner, *Observable $\Delta B = 2$ transitions without nucleon decay in a minimal supersymmetric extension of the standard model,* Phys. Lett. **B132** (1983) 103;
L.J. Hall, M. Suzuki, *Explicit R-parity breaking in supersymmetric models,* Nucl. Phys. **B231** (1984) 419;
J.R. Ellis, G. Gelmini, C. Jarlskog, G.G. Ross, J.W.F. Valle, *Phenomenology of supersymmetry with broken R-parity,* Phys. Lett. **B150** (1985) 142;
G.G. Ross, J.W.F. Valle, *Supersymmetric models without R parity,* Phys. Lett. **B151** (1985) 375;
S. Dawson, *R-parity breaking in supersymmetric theories,* Nucl. Phys. **B261** (1985) 297.

[42] D. Cavalli et al., *The Higgs Working Group: summary report,* [arXiv:hep-ph/0203056].

[43] M. Carena, S. Heinemeyer, C.E.M. Wagner, G. Weiglein, *Suggestions for improved benchmark scenarios for Higgs boson searches at LEP-2,* [arXiv:hep-ph/9912223].

[44] ALEP, DELPHI, L3 und OPAL Collaborations, the LEP Higgs Working Group, *Searches for the neutral Higgs bosons of the MSSM: preliminary combined results using LEP data collected at energies up to 209-GeV,* [arXiv:hep-ex/0107030] and *Search for charged Higgs bosons: preliminary combined results using LEP data collected at energies up to 209-GeV,* [arXiv:hep-ex/0107031], `http://lephiggs.web.cern.ch/LEPHIGGS/www/Welcome.html`.

[45] W. de Boer, *Search for SUSY and Higgs particles,* [arXiv:hep-ph/9808448].

[46] `http://cmsinfo.cern.ch/outreach/CMSdocuments/CMSplots/CMSplots.html`.

[47] CMS Collaboration, *Technical Proposal Report 8.2,* CERN-LHCC 2006-021 (June 2006), `http://cmsdoc.cern.ch/cms/cpt/tdr/`;
ATLAS Collaboration, *Technical Design Report,* CERN-LHCC 99-14/15 (Mai 1999), `http://atlas.web.cern.ch/Atlas/GROUPS/PHYSICS/TDR/access.html`.

[48] `http://www-bdnew.fnal.gov/tevatron/`.

[49] `http://www.linearcollider.org/cms/`.

[50] *Technical Design Report, part III*, Editors: R.D. Heuer, D. Miller, F. Richard, P. Zerwas, `http://tesla.desy.de/new_pages/TDR_CD/PartIII/physic.html`.

[51] A. Djouadi, *The anatomy of electro-weak symmetry breaking. I: the Higgs boson in the standard model*, [arXiv:hep-ph/0503172].

[52] A. Djouadi, *The anatomy of electro-weak symmetry breaking. II: the Higgs boson in the minimal supersymmeric model*, [arXiv:hep-ph/0503173].

[53] M. Spira, *QCD effects in Higgs physics,* Fortschr. Phys. **46** (1998) 203, [arXiv:hep-ph/9705337].

[54] M. Spira, *Higgs boson production and decay at the Tevatron*, [arXiv:hep-ph/9810289];
M. Carena, J.S. Conway, H.E. Haber, J.D. Hobbs, *Report of the Tevatron Higgs working group, Part 6*, [arXiv:hep-ph/0010338].

[55] K.-i. Hikasa, *Heavy Higgs production in e^+e^- and e^-e^- collisions,* Phys. Lett. **B164** (1985) 385 and Erratum-ibid., Phys. Lett. **195B** (1987) 623;
W. Kilian, M. Krämer, P.M. Zerwas, *Higgs-strahlung and WW fusion in e^+e^- collisions,* Phys. Rev. **B373** (1996) 135, [arXiv:hep-ph/9512355].

[56] H.M. Georgi, S.L. Glashow, M.E. Machacek, D.V. Nanopoulos, *Higgs bosons from two-Gluon annihilation in proton-proton collisions,* Phys. Rev. Lett. **40** (1978) 692.

[57] A. Djouadi, M. Spira, P.M. Zerwas, *Production of Higgs bosons in proton colliders. QCD corrections,* Phys. Lett. **B264** (1991) 440;
S. Dawson, *Radiative corrections to Higgs boson production,* Nucl. Phys. **B359** (1991) 283;
D. Graudenz, M. Spira, P.M. Zerwas, *QCD corrections to Higgs-boson production at proton-proton colliders,* Phys. Rev. Lett. **70** (1993) 1372;
S. Dawson, R.P. Kauffman, *QCD corrections to Higgs boson production: nonleading terms in the heavy quark limit,* Phys. Rev. **D49** (1994) 2298, [arXiv:hep-ph/9310281] and *Higgs boson production at the LHC,* Nucl. Phys. **B453** (1995) 17, [arXiv:hep-ph/9504378];
A. Ghinculov, J.J. van der Bij, *The Higgs resonance shape in gluon fusion: heavy Higgs effects,* Nucl. Phys. **B482** (1996) 59, [arXiv:hep-ph/9511414];
M. Krämer, E. Laenen, M. Spira, *Soft gluon radiation in Higgs boson production at the LHC,* Nucl. Phys. **B511** (1998) 523, [arXiv:hep-ph/9611272].

[58] R.V. Harlander, W.B. Kilgore, *Next-to-next-to-leading order Higgs production at hadron colliders,* Phys. Rev. Lett. **88** (2002) 201801, [arXiv:hep-ph/0201206];
C. Anastasiou, K. Melnikov, *Higgs boson production at hadron colliders in NNLO QCD,* Nucl. Phys. **B646** (2002) 220, [arXiv:hep-ph/0207004];
V. Ravindran, J. Smith, W.L. van Neerven, *NNLO corrections to the total cross section for Higgs boson production in hadron-hadron collisions,* Nucl. Phys. **B665** (2003) 325, [arXiv:hep-ph/0302135];
S. Catani, D. de Florian, M. Grazzini, P. Nason, *Soft-gluon resummation for Higgs boson production at hadron colliders,* JHEP **07** (2003) 028, [arXiv:hep-ph/0306211].

[59] A. Djouadi, P. Gambino, *Leading electroweak correction to Higgs boson production at proton colliders,* Phys. Rev. Lett. **73** (1994) 2528, [arXiv:hep-ph/9406432];
A. Ghinculov, J.J. van der Bij, *The Higgs resonance shape in gluon fusion: heavy Higgs effects,* Nucl. Phys. **B482** (1996) 59, [arXiv:hep-ph/9511414];
A. Djouadi, P. Gambino, B.A. Kniehl, *Two-loop electroweak heavy-fermion corrections to Higgs-boson production and decay,* Nucl. Phys. **B523** (1998) 17, [arXiv:hep-ph/9712330].

[60] R.N. Cahn, S. Dawson, *Production of very massive Higgs bosons,* Phys. Lett. **B136** (1984) 196 and Erratum-ibid., Phys. Lett. **B138** (1984) 464;
G. Altarelli, B. Mele, F. Pitolli, *Heavy Higgs production at future colliders,* Nucl. Phys. **B287** (1987) 205.

[61] D. Rainwater, D. Zeppenfeld, *Searching for $H \to \gamma\gamma$ in weak boson fusion at the LHC,* JHEP **12** (1997) 005, [arXiv:hep-ph/9712271], *Observing $H \to W^{(*)}W^{(*)} \to e^{\pm}\mu^{\mp}$ p_T in weak boson fusion with dual forward jet tagging at the CERN LHC,* Phys. Rev. **D60** (1999) 113004 and Erratum-ibid., Phys. Rev. **D61** (1999) 099901, [arXiv:hep-ph/9906218];
D. Rainwater, D. Zeppenfeld, K. Hagiwara, *Searching for $H \to \tau\tau$ in weak boson fusion at the CERN LHC,* Phys. Rev. **D59** (1999) 014037, [arXiv:hep-ph/9808468];
T. Plehn, D. Rainwater, D. Zeppenfeld, *Method for identifying $H \to \tau\tau \to e^{\pm}\mu^{\mp}$ p_T at the CERN LHC,* Phys. Rev. **D61** (2000) 093005, [arXiv:hep-ph/9911385];
N. Kauer, T. Plehn, D. Rainwater, D. Zeppenfeld, *$H \to WW$ as the discovery mode for a light Higgs boson,* Phys. Lett. **B503** (2001) 113, [arXiv:hep-ph/0012351].

[62] T. Han, G. Valencia, S. Willenbrock, *Structure-function approach to vector-boson scattering in pp collisions,* Phys. Rev. Lett. **69** (1992) 3274, [arXiv:hep-ph/9206246].

[63] T. Figy, C. Oleari, D. Zeppenfeld, *Next-to-leading order jet distributions for Higgs boson production via weak-boson fusion,* Phys. Rev. **D68** (2003) 073005, [arXiv:hep-ph/0306109].

[64] R. Raitio, W.W. Wada, *Higgs-boson production at large transverse momentum in quantum chromodynamics,* Phys. Rev. **D19** (1979) 941;
J.N. Ng, P. Zakarauskas, *QCD-parton calculation of conjoined production of Higgs bosons and heavy flavors in $p\bar{p}$ collisions,* Phys. Rev. **D29** (1984) 876;
Z. Kunszt, *Associated production of heavy Higgs boson with top quarks,* Nucl. Phys. **B247** (1984) 339;
W.J. Marciano, F.E. Paige, *Associated production of Higgs bosons with $t\bar{t}$ pairs,* Phys. Rev. Lett. **66** (1991) 2433.

[65] S. Dawson, L. Reina, *QCD corrections to associated Higgs boson production,* Phys. Rev. **D57** (1998) 5851, [arXiv:hep-ph/9712400];
W. Beenakker, S. Dittmaier, M. Krämer, B. Plümper, M. Spira, P.M. Zerwas, *Higgs radiation off top quarks at the Tevatron and the LHC,* Phys. Rev. Lett. **87** (2001) 201805, [arXiv:hep-ph/0107081] and *NLO QCD corrections to $t\bar{t}H$ production in hadron collisions,* Nucl. Phys. **B653** (2003) 151, [arXiv:hep-ph/0211352];
S. Dawson, L.H. Orr, L. Reina, D. Wackeroth, *Next-to-leading order QCD*

corrections to $pp \to t\bar{t}h$ at the CERN Large Hadron Collider, Phys. Rev. **D67** (2003) 071503, [arXiv:hep-ph/0211438].

[66] S.L. Glashow, D.V. Nanopoulos, A. Yildiz, *Associated production of Higgs bosons and Z particles,* Phys. Rev. **D18** (1978) 1724;
J.F. Gunion, *Associated $t\bar{t}$−Higgs production as a large source of WH events: implications for Higgs detection in the $l\nu\gamma\gamma$ final state,* Phys. Lett. **B261** (1991) 510;
Z. Kunszt, Z. Trocsanyi, W.J. Stirling, *Clear signal of intermediate mass Higgs boson production at LHC and SSC,* Phys. Lett. **B271** (1991) 247.

[67] T. Han, S. Willenbrock, *QCD correction to the $pp \to WH$ and ZH total cross sections,* Phys. Lett. **B273** (1991) 167.

[68] O. Brein, A. Djouadi, R. Harlander, *NNLO QCD corrections to the Higgs-strahlung processes at hadron colliders,* Phys. Lett. **B579** (2004) 149, [arXiv:hep-ph/0307206].

[69] M.L. Ciccolini, S. Dittmaier, M. Krämer, *Electroweak radiative corrections to associated WH and ZH production at hadron colliders,* Phys. Rev. **D68** (2003) 073003, [arXiv:hep-ph/0306234].

[70] A. Djouadi, J. Kalinowski, M. Spira, *HDECAY: a program for Higgs boson decays in the standard model and its supersymmetric extension,* Comput. Phys. Commun. **108** (1998) 56, [arXiv:hep-ph/9704448].

[71] E. Braaten, J.P. Leveille, *Higgs-boson decay and the running mass,* Phys. Rev. **D22** (1980) 715;
N. Sakai, *Perturbative quantum-chromodynamic corrections to the hadronic decay width of the Higgs boson,* Phys. Rev. **D22** (1980) 2220;
T. Inami, T. Kubota, *Renormalization group estimate of the hadronic decay width of the Higgs boson,* Nucl. Phys. **B179** (1981) 171;
S.G. Gorishnii, A.L. Kataev, S.A. Larin, *The width of Higgs boson decay into hadrons: three loop corrections of strong interactions,* Sov. J. Nucl. Phys. **40** (1984) 329;
M. Drees, K.-i. Hikasa, *Heavy-quark thresholds in Higgs-boson physics,* Phys. Rev. **D41** (1990) 1547 and *Note on QCD corrections to hadronic Higgs decay,* Phys. Lett. **B240** (1990) 455 and Erratum-ibid., Phys. Lett. **B262** (1991) 497;
K.G. Chetyrkin, B.A. Kniehl, M. Steinhauser, *Virtual top-quark effects on the $H \to b\bar{b}$ decay at next-to-leading order in QCD,* Phys. Rev. Lett. **78** (1997) 594, [arXiv:hep-ph/9610456] and *Three-loop $\mathcal{O}(\alpha_s^2 G_F M_t^2)$ corrections to hadronic Higgs decays,* Nucl. Phys. **B490** (1997) 19, [arXiv:hep-ph/9701277];
K.G. Chetyrkin, *Correlator of the quark scalar currents and $\Gamma_{tot}(H \to hadrons)$ at $\mathcal{O}(\alpha_s^3)$ in pQCD,* Phys. Lett. **B390** (1997) 309, [arXiv:hep-ph/9608318].

[72] J. Fleischer, F. Jegerlehner, *Radiative corrections to Higgs-boson decays in the Weinberg-Salam model,* Phys. Rev. **D23** (1981) 2001;
D.Y. Bardin, B.M. Vilensky, P.K. Khristova, *Calculation of the Higgs boson decay width into fermion pairs,* Sov. J. Nucl. Phys. **53** (1991) 152;

A. Dabelstein, W. Hollig, *Electroweak corrections to the fermionic decay width of the standard Higgs boson,* Z. Phys. **C53** (1992) 507;
B.A. Kniehl, *Electroweak corrections to the fermionic decay width of the standard Higgs boson,* Nucl. Phys. **B376** (1992) 3.

[73] J. Dai, J. F. Gunion, R. Vega, *Using b tagging to detect $t\bar{t}-$Higgs-boson production with $H \to b\bar{b}$,* Phys. Rev. Lett. **71** (1993) 2699, [hep-ph/9306271].

[74] H. Zheng, D. Wu, *First-order QCD corrections to the decay of the Higgs boson into two photons,* Phys. Rev. **D42** (1990) 3760;
A. Djouadi, M. Spira, J.J. van der Bij, P. M. Zerwas, *QCD corrections to $\gamma\gamma$ decays of Higgs particles in the intermediate mass range,* Phys. Lett. **B257** (1991) 187;
S. Dawson, R.P. Kauffman, *QCD corrections to the Higgs-boson decay $H \to \gamma\gamma$,* Phys. Rev. **D47** (1993) 1264;
A. Djouadi, M. Spira, P. M. Zerwas, *Two-photon decay widths of Higgs particles,* Phys. Lett. **B311** (1993) 255, [arXiv:hep-ph/9305335];
K. Melnikov, O. Yakovlev, *Higgs-two-photon interaction in the standard model. The QCD radiative correction,* Phys. Lett. **B312** (1993) 179, [arXiv:hep-ph/9302281];
M. Inoue, R. Najima, T. Oka, J. Saito, *QCD corrections to two photon decay of the Higgs boson and its reverse process,* Mod. Phys. Lett. **A9** (1994) 1189;
M. Spira, A. Djouadi, D. Graudenz, P.M. Zerwas, *Higgs boson production at the LHC,* Nucl. Phys. **B453** (1995) 17, [arXiv:hep-ph/9504378];
M. Steinhauser, *corrections of $\mathcal{O}(\alpha_s^2)$ to the decay of an intermediate mass Higgs boson into two photons*, [arXiv:hep-ph/9612395].

[75] A. Djouadi, P. Gambino, B.A. Kniehl, *Two-loop electroweak heavy-fermion corrections to Higgs-boson production and decay,* Nucl. Phys. **B523** (1998) 17, [arXiv:hep-ph/9712330];
U. Aglietti, R. Bonciani, G. Degrassi, A. Vicini, *Two-loop light fermion contribution to Higgs production and decays,* Phys. Lett. **B595** (2004) 432, [arXiv:hep-ph/0404071];
G. Degrassi, F. Maltoni, *Two-loop electroweak corrections to the Higgs-boson decay $H \to \gamma\gamma$,* Nucl. Phys. **B724** (2005) 183, [arXiv:hep-ph/0504137].

[76] B.W. Lee, C. Quigg, H.B. Thacker, *Weak interactions at very high-energies: the role of the Higgs boson mass,* Phys. Rev. **D16** (1977) 1519.

[77] M. Dittmar, H. Dreiner, *How to find a Higgs boson with a mass between 155 and 180 GeV at the CERN LHC,* Phys. Rev. **D55** (1997) 167, [arXiv:hep-ph/9608317].

[78] J. Fleischer, F. Jegerlehner, *Radiative corrections to Higgs-boson decays in the Weinberg-Salam model,* Phys. Rev. **D23** (1981) 2001;
B.A. Kniehl, *Radiative corrections for $H \to ZZ$ in the standard model,* Nucl. Phys. **B352** (1991) 1 and *Radiative corrections for $H \to W^+W^-(\gamma)$ in the standard model,* Nucl. Phys. **B357** (1991) 439.

[79] M. Spira, A. Djouadi, D. Graudenz, P.M. Zerwas, *SUSY Higgs production at proton colliders,* Phys. Lett. **B318** (1993) 347;

R.P. Kauffman, W. Schaffer, *QCD corrections to production of Higgs pseudoscalars,* Phys. Rev. **D49** (1994) 551, [arXiv:hep-ph/9305279].

[80] R.V Harlander, W.B. Kilgore, *Production of a pseudo-scalar Higgs boson at hadron colliders at next-to-next-to-leading order,* JHEP **10** (2002) 017, [arXiv:hep-ph/0208096].

[81] S. Dawson, A. Djouadi, M. Spira, *QCD corrections to supersymmetric Higgs boson production: the role of squark loops,* Phys. Rev. Lett. **77** (1996) 16, [arXiv:hep-ph/9603423].

[82] R.V. Harlander, M. Steinhauser, *Hadronic Higgs production and decay in supersymmetry at next-to-leading order,* Phys. Lett. **B574** (2003) 258, [arXiv:hep-ph/0307346], *Effects of supersymmetric QCD in hadronic Higgs production at next-to-next-to-leading order,* Phys. Rev. **D68** (2003) 111701, [arXiv:hep-ph/0308210] and *Supersymmetric Higgs production in gluon fusion at next-to-leading order,* JHEP **09** (2004) 066, [arXiv:hep-ph/0409010];
R.V. Harlander, F. Hofmann, *Pseudo-scalar Higgs production at next-to-leading order SUSY-QCD,* JHEP **03** (2006) 050, [arXiv:hep-ph/0507041].

[83] T. Plehn, D. Rainwater, D. Zeppenfeld, *Probing the MSSM Higgs sector via weak boson fusion at the LHC,* Phys. Lett. **B454** (1999) 297, [arXiv:hep-ph/9902434].

[84] A. Djouadi, M. Spira, *Supersymmetric QCD corrections to Higgs boson production at hadron colliders,* Phys. Rev. **D62** (2000) 014004, [arXiv:hep-ph/9912476].

[85] P. Wu, M. Wen-Gan, H. Hong-Sheng, Z. Ren-You, H. Liang, J. Yiet, *NLO supersymmetric QCD corrections to $t\bar{t}h^0$ associated production at hadron colliders,* [arXiv:hep-ph/0505086].

[86] S. Dittmaier, M. Krämer, M. Spira, *Higgs radiation off bottom quarks at the Fermilab Tevatron and the CERN LHC,* Phys. Rev. **D70** (2004) 074010, [arXiv:hep-ph/0309204];
S. Dawson, C.B. Jackson, L. Reina, D. Wackeroth, *Exclusive Higgs boson production with bottom quarks at hadron colliders,* Phys. Rev. **D69** (2004) 074027, [arXiv:hep-ph/0311067].

[87] J.F. Gunion, G.L. Kane, J. Wudka, *Search techniques for charged and neutral intermediate-mass Higgs bosons,* Nucl. Phys. **B299** (1988) 231.

[88] S. Heinemeyer, W. Hollik, J. Rosiek, G. Weiglein, *Neutral MSSM Higgs-boson production at e^+e^- colliders in the Feynman-diagrammatic approach,* Eur. Phys. J. **C19** (2001) 535, [arXiv:hep-ph/0102081].

[89] A. Denner, T. Sack, *The top width,* Nucl. Phys. **B358** (1991) 46;
G. Eilam, R.R. Mendel, R. Migneron, A. Soni, *Radiative corrections to top-quark decay,* Phys. Rev. Lett. **66** (1991) 3105;
H. Murayama, Y. Sumino, *Axial-vector-coupling contribution to toponium resonances,* Phys. Rev. **D47** (1993) 82;

K. Fujii, T. Matsui, Y. Sumino, *Physics at $t\bar{t}$ threshold in e^+e^- collisions,* Phys. Rev. **D50** (1994) 4341;
P. Comas, R. Miquel, M. Martinez, S. Orteu, *the Physics of the $e^+e^- \to t\bar{t}$ threshold scan*, published in *e^+e^- Linear Collisions* (1995) 57.

[90] S.H. Zhu, *Supersymmetric QCD corrections to Higgs boson associated production with top quark pair at linear colliders* [arXiv:hep-ph/0212273].

[91] J.A. Coarasa, R.A. Jiménez, J. Solà, *Strong effects on the hadronic widths of the neutral Higgs bosons in the MSSM,* Phys. Lett. **B389** (1996) 312, [arXiv:hep-ph/9511402].

[92] G. t'Hooft, M.J. Veltman, *Regularization and renormalization of gauge fields,* Nucl. Phys. **B44** (1972) 189;
C.G. Bollini, J.J. Giambriagi, *Dimensional renormalization: the number of dimensions as a regularizing parameter,* Nuovo Cim. **B12** (1972) 20;
J.F. Ashmore, *A method of gauge invariant regularization,* Lett. Nuovo Cim. **4** (1972) 289;
G. t'Hooft, *Dimensional regularization and the renormalization group,* Nucl. Phys. **B61** (1973) 455.

[93] J.C. Taylor, *Ward identities and charge renormalization of the Yang-Mills field,* Nucl. Phys. **B33** (1971) 436;
A.A. Slavnov, *Ward identities in gauge theories,* Theor. Math. Phys. **10** (1972) 99.

[94] J.C. Ward, *An identity in quantum electrodynamics,* Phys. Rev. **78** (1950) 182;
Y. Takahashi, *On the generalized Ward identity,* Nuovo Cim. **6** (1957) 371.

[95] D.A. Ross, J.C. Taylor, *Renormalization of a unified theory of weak and electromagnetic interactions,* Nucl. Phys. **B51** (1973) 125, Erratum-ibid., Nucl. Phys. **B58** (1973) 643;
K.-i. Aoki, Z. Hioki, R. Kawabe, M. Konuma, T. Muta, *One-loop corrections to $\nu - e$ scattering in Weinberg-Salam theory: neutral current processes,* Prog. Theor. Phys. **64** (1980) 707, *Electroweak radiative corrections to high-energy $\nu - e$ scattering,* Prog. Theor. Phys. **65** (1981) 1001 and *Electroweak theory. Framework of on-shell renormalization and study of higher order effects,* Prog. Theor. Phys. Suppl. **73** (1982) 1.

[96] W.A. Bardeen, A.J. Buras, D.W. Duke, T. Muta, *Deep-inelastic scattering beyond the leading order in asymptotically free gauge theories,* Phys. Rev. **D18** (1978) 3998.

[97] J.C. Collins, F. Wilczek, A. Zee, *Low-energy manifestations of heavy particles: application to the neutral current,* Phys. Rev. **D18** (1978) 242.

[98] A.D Martin, R.G. Roberts, W.J. Stirling, *Parton distributions: a study of the new HERA data, α_s, the gluon and $p\bar{p}$ jet production,* Phys. Lett. **B387** (1996) 419, [arXiv:hep-ph/9606345];
D. Wegener, H1 and Zeus Collaborations, *The parton structure of protons and photons measured at the ep storage ring HERA,* Nucl. Phys. **A680** (2000) 184.

[99] J.C. Collins, D.E. Soper, G. Sterman, *Factorization of hard processes in QCD,* Adv. Ser. Direct. High Energy Phys. **5** (1988) 1, [arXiv:hep-ph/0409313].

[100] V.N. Gribov, L.N. Lipalov, *Deep inelastic ep scattering in perturbation theory,* Sov. J. Nucl. Phys. **15** (1972) 438 and e^+e^- *pair annihilation and deep inelastic ep scattering in perturbation theory,* Sov. J. Nucl. Phys. **15** (1972) 675;
L.N. Lipatov, *The parton model and perturbation theory,* Sov. J. Nucl. Phys. **20** (1975) 94;
G. Altarelli, G. Parisi, *Asymptotic freedom in parton language,* Nucl. Phys. **B126** (1977) 298;
Y.L. Dokshitzer, *Calculation of the structure functions for deep inelastic scattering and* e^+e^- *annihilation by perturbation theory in quantum chromodynamics,* Sov. Phys. JETP **46** (1977) 641.

[101] P. Nogueira, *Automatic Feynman graph generation,* J. Comput. Phys. **105** (1993) 279, `http://cfif.ist.utl.pt/~paulo/qgraf.html`.

[102] J.A.M. Vermaseren, NIKHEF-00-032, *New features of FORM,* [arXiv:math-ph/0010025], `http://www.nikhef.nl/~form`.

[103] J.J. Gunion, T. Han, J. Jiang, S. Mrenna, A. Sopczak, *Determination of* $\tan\beta$ *at a future* e^+e^- *linear collider,* eConf C010630 (2001) 120, [arXiv:hep-ph/0112334];
J.F. Gunion, T. Han, J. Jiang, A. Sopczak, *Overview of* $\tan\beta$ *determination at a linear* e^+e^- *collider,* [arXiv:hep-ph/0211123].

[104] S. Dittmaier, M. Krämer, Y. Liao, M. Spira, P.M. Zerwas, *Higgs radiation off quarks in supersymmetric theories at* e^+e^- *colliders,* Phys. Lett. **B478** (2000) 247, [arXiv:hep-ph/0002035].

[105] B.C. Allanach et al., *The Snowmass points and slopes: benchmarks for SUSY searches,* Eur. Phys. J. **C25** (2002) 113, [arXiv:hep-ph/0202233].

[106] M. Carena, M. Quirós, C.E.M. Wagner, *Effective potential methods and the Higgs mass spectrum in the MSSM,* Nucl. Phys. **B461** (1996) 407, [arXiv:hep-ph/9508343];
H.E. Haber, R. Hempfling, A.H. Hoang, *Approximating the radiatively corrected Higgs mass in the minimal supersymmetric model,* Z. Phys. **C75** (1997) 539, [arXiv:hep-ph/9609331];
S. Heinemeyer, W. Hollik, G. Weiglein, *QCD corrections to the masses of the neutral CP-even Higgs bosons in the MSSM,* Phys. Rev. **D58** (1998) 091701, [arXiv:hep-ph/9803277].

[107] T. Hahn, M. Pérez-Victoria, *Automated one-loop calculations in four and D dimensions,* Comput. Phys. Commun. **118** (1999) 153, [arXiv:hep-ph/9807565] and for updates `http://www.feynarts.de/looptools/`.

[108] H.E. Haber, M.J. Herrero, H.E. Logan, S. Penaranda, S. Rigolin, D. Temes, *SUSY QCD corrections to the MSSM* $h^0b\bar{b}$ *vertex in the decoupling limit,* Phys. Rev. **D63** (2001) 055004, [arXiv:hep-ph/0007006].

[109] L.J. Hall, R. Rattazzi, U. Sarid, *Top quark mass in supersymmetric SO(10) unification,* Phys. Rev. **D50** (1994) 7048, [arXiv:hep-ph/9306309];
R. Hempfling, *Yukawa coupling unification with supersymmetric threshold corrections,* Phys. Rev. **D49** (1994) 6168;
M. Carena, M. Olechowski, S. Pokorski, C.E.M. Wagner, *Electroweak symmetry breaking and bottom-top Yukawa unification,* Nucl. Phys. **B426** (1994) 269, [arXiv:hep-ph/9402253];
D.M. Pierce, J.A. Bagger, K.T. Matchev, R.-j. Zhang, *Precision corrections in the minimal supersymmetric standard model,* Nucl. Phys. **B491** (1997) 3, [arXiv:hep-ph/9606211].

[110] M. Carena, D. Garcia, U. Nierste, C.E.M. Wagner, *Effective Lagrangian for the $\bar{t}bH^+$ interaction in the MSSM and charged Higgs phenomenology,* Nucl. Phys. **B577** (2000) 88, [arXiv:hep-ph/9912516].

[111] J. Guasch, P. Häfliger, M. Spira, *MSSM Higgs boson decays to bottom quark pairs reexamined,* Phys. Rev. **D68** (2003) 115001, [arXiv:hep-ph/0305101].

[112] S. Dittmaier, M. Krämer, Y. Liao, M. Spira, P.M. Zerwas, *Higgs radiation off top quarks in e^+e^- collisions,* Phys. Lett. **B441** (1998) 383, [arXiv:hep-ph/9808433].

[113] P. Häfliger, M. Spira, *Associated Higgs boson production with heavy quarks in e^+e^- collisions: SUSY-QCD corrections,* Nucl. Phys. **B719** (2005) 35, [arXiv:hep-ph/0501164].

[114] S. Kretzer, H.L. Lai, F.I. Olness, W.K. Tung, *CTEQ6 parton distributions with heavy quark mass effects,* Phys. Rev. **D69** (2004) 114005, [arXiv:hep-ph/0307022].

[115] S. Dittmaier, P. Häfliger, M. Krämer, M. Spira, M. Walser, paper in preparation.

[116] S.K. Jones, C.H. Llewellyn Smith, *Leptoproduction of supersymmetric particles,* Nucl. Phys. **B217** (1983) 145;
H.E. Haber, G.L. Kane, *The search for supersymmetry: probing physics beyond the standard model,* Phys. Rept. **117** (1985) 75;
A. Denner, H. Eck, O. Hahn, J. Küblbeck, *Feynman rules for fermion-number-violating interactions,* Nucl. Phys. **B387** (1992) 467.

[117] W.H. Furry, *A symmetry theorem in the positron theory,* Phys. Rev. **51** (1937) 125.

[118] F. Zwicky, *Spectral displacement of extra galactic nebulae,* Helv. Phys. Acta **6** (1933) 110.

[119] G.F.R. Ellis, H. van Elst, *Cosmological models: Cargese lectures 1998,* [arXiv:gr-qc/9812046].

[120] for reviews see: A.D. Linde, *Particle physics and inflationary cosmology,* Contemp. Concepts Phys. **5** (2005) 1, [arXiv:hep-th/0503203];
K.A. Olive, *Inflation,* Phys. Rept. **190** (1990) 307;
D.H. Lyth, A. Riotto, *Particle physics models of inflation and the cosmological density perturbation,* Phys. Rept. **314** (1999) 1, [arXiv:hep-ph/9807278].

[121] M. Kamionkowski, D.N. Spergel, *Large-angle cosmic microwave background anisotropies in an open Universe,* Astrophys. J. **432** (1994) 7, [arXiv:astro-ph/9312017];
M. Kamionkowski, D.N. Spergel, N. Sugiyama, *Small scale cosmic microwave background anisotropies as a probe of the geometry of the Universe,* Astrophys. J. **426** (1994) L57, [arXiv:astro-ph/9401003].

[122] G. Hinshaw et al., *Three-year wilkinson microwave anisotropy probe (wmap) observations: temperature analysis.*, [arXiv:astro-ph/0603451].

[123] K.G. Begeman, A.H. Broeils, R.H. Sanders, *Extended rotation curves of spiral galaxies: dark haloes and modified dynamics*, Mon. Not. Roy. Astron. Soc. **249** (1991) 523.

[124] J.A. Tyson, F. Valdes, R.A. Wenk, *Detection of systematic gravitational lens galaxy image alignments - mapping dark matter in galaxy clusters,* Astrophys. J. **349** (1990) 1.

[125] R.D. Blandford, R. Narayan, *Cosmological applications of gravitational lensing*, Annual Review of Astronomy and Astrophysics, **30** (1992) 311.

[126] L. van Waerbeke, Y. Mellier, M. Radovich, *Cosmic shear statistics and cosmology,* Astron. Astrophys. **374** (2001) 757, [arXiv:astro-ph/0101511].

[127] D. Clowe, M. Bradac, A.H. Gonzalez, M. Markevitch, S.W. Randall, C. Jones, D. Zaritsky, *A direct empirical proof of the existence of dark matter*, [astro-ph/0608407].

[128] S.D.M. White, C.S. Frenk, M. Davis, *Clustering in a neutrino dominated Universe,* Astrophys. J. **274** (1983) L1.

[129] D. Fabricant, P. Gorenstein, *Further evidence for M87's massive, dark halo,* Astrophys. J. **267** (1983) 535;
G.C. Stewart, A.C. Fabian, P.E.J. Nulsen, C.R. Canizares, *The mass profile and gas content of M87,* Astrophys. J. **278** (1984) 536.

[130] C. Bennett et al., *First year Wilkinson Microwave Anisotropy Probe (WMAP) observations: preliminary maps and basic results*, Astrophys. J. Suppl. **148** (2003) 1, [arXiv:astro-ph/0302207];
D.N. Spergel et al. [WMAP Collaboration], *First year Wilkinson Microwave Anisotropy Probe (WMAP) observations: determination of cosmological parameters*, Astrophys. J. Suppl. **148** (2003) 175, [arXiv:astro-ph/0302209].

[131] `http://map.gsfc.nasa.gov/m_mm.html`.

[132] U. Seljak, A. Makarov, P. McDonald, H. Trac, *Can sterile neutrinos be the dark matter?*, [astro-ph/0602430].

[133] S. Ahlen, et al., *Limits on cold dark matter candidates from an ultralow background germanium spectrometer,* Phys. Lett. **B195** (1987) 603;

D.O. Caldwell, et al., *Laboratory limits on galactic cold dark matter,* Phys. Rev. Lett. **61** (1988) 510;
M. Beck, et al., *Searching for dark matter with the enriched Ge detectors of the Heidelberg-Moscow $\beta\beta$ experiment,* Phys. Lett. **B336** (1994) 141.

[134] K.A. Olive, M. Srednicki, *Solar neutrino searches and cold dark matter,* Phys. Lett. **B205** (1988) 553.

[135] G. Jungman, M. Kamionkowski and K. Griest, *Supersymmetric dark matter,* Phys. Rept. **267** (1996) 195, [arXiv:hep-ph/9506380].

[136] V. Bertin, E. Nezri, J. Orloff, *Neutrino indirect detection of neutralino dark matter in the CMSSM,* Eur. Phys. J. **C26** (2002) 111, [arXiv:hep-ph/0204135];
J.R. Ellis, S. Heinemeyer, K.A. Olive, G. Weiglein, *Indirect sensitivities to the scale of supersymmetry,* JHEP **0502** (2005) 013, [arXiv:hep-ph/0411216].

[137] A. Djouadi, J.-L. Kneur, G. Moultaka, *SuSpect: a Fortran code for the supersymmetric and Higgs particle spectrum in the MSSM,* [arXiv:hep-ph/0211331].

[138] F.E. Paige, S.D. Protopopescu, H. Baer, X. Tata, *ISAJET 7.69: a Monte Carlo event generator for pp, $\bar{p}p$, and e^+e^- reactions,* [arXiv:hep-ph/0312045].

[139] P. Gondolo, J. Edsjö, P. Ullio, L. Bergström, M. Schelke, E.A. Baltz, *DarkSUSY: computing supersymmetric dark matter properties numerically,* JCAP **0407** (2004) 008, [arXiv:astro-ph/0406204].

[140] J.R. Ellis, K.A. Olive, Y. Santoso, V.C. Spanos, *Supersymmetric dark matter in light of WMAP,* Phys. Lett. **B565** (2003) 176, [arXiv:hep-ph/0303043].

[141] L. Alvarez-Gaumé, J. Polchinski, M.B. Wise, *Minimal low-energy supergravity,* Nucl. Phys. **B221** (1983) 495;
J.M. Frère, D.R.T. Jones, S. Raby, *Fermion masses and induction of the weak scale by supergravity,* Nucl. Phys. **B222** (1983) 11;
M. Claudson, L.J. Hall, I. Hinchliffe, *Low-energy supergravity: false vacua and vacuous predictions,* Nucl. Phys. **B228** (1983) 501;
C. Kounnas, A.B. Lahanas, D.V. Nanopoulos, M. Quirós, *Low-energy behaviour of realistic locally-supersymmetric grand unified theories,* Nucl. Phys. **B236** (1984) 438;
J.-P. Derendinger, C.A. Savoy, *Quantum effects and $SU(2) \times U(1)$ breaking in supergravity gauge theories,* Nucl. Phys. **B237** (1984) 307.

[142] A. Riotto, E. Roulet, *Vacuum decay along supersymmetric flat directions,* Phys. Lett. **B377** (1996) 60, [arXiv:hep-ph/9512401].

[143] F. James, *Minuit - a system for function minimization and analysis of the parameter errors and correlations,* Comput. Phys. Commun. **10** (1975) 343, `http://wwwasdoc.web.cern.ch/wwwasdoc/WWW/minuit/minmain/minmain.html`.

[144] L.S. Stark, P. Häfliger, A. Biland, F. Pauss, *New allowed mSUGRA parameter space from variations of the trilinear scalar coupling A_0,* JHEP **0508** (2005) 059, [arXiv:hep-ph/0502197].

[145] Thesis of L.S. Stark, in preparation.

[146] G. 't Hooft, M. Veltman, *Scalar one-loop integrals,* Nucl. Phys. **B153** (1979) 365.

[147] A. Denner, *Techniques for calculation of electroweak radiative corrections at the one loop level and results for W physics at LEP-200,* Fortschr. Phys. **41** (1993) 307; A. Denner, S. Dittmaier, *Reduction of one loop tensor five point integrals,* Nucl. Phys. **B658** (2003) 175, [arXiv:hep-ph/0212259].

List of Tables

List of Figures

Acknowledgements

I would like to thank Felicitas Pauss, for accepting me as her PhD student four years ago. It was a great pleasure to work in her group and I profited a lot from the "experimental" environment. We "suffered" many hours together during the examination periods but I enjoyed the dinners we had afterwards a lot.

Many thanks to my supervisor, Michael Spira, for proposing me very interesting projects, for his help and his encouragement during the time we were working together.

I am very grateful to my co-PhD student Manuel Walser for fruitful discussions and patience in comparing number by number and also to my collaborator Stefan Dittmaier from the Max Planck Institute in Munich. It was not always easy to compare results over hundreds of kilometers, but always successful. I am also very grateful to Babis Charalampos Anastasiou for introducing me into MAPLE and QGRAF and for very enlightening discussions. It is a pity that we did not meet earlier. I am grateful to Heidi Rzehak for proofreading parts of my thesis and to Ansgar Denner for providing me with very helpful programs to evaluate the scalar integrals.

I would like to thank Luisa Sabrina Stark for very interesting discussions and for the enjoyable and intense time during writing a paper together. It was great to have you (and since more than a year also Ambra) often in my office.

Finally, I will always remember the time I had with my colleagues at the IPP and at the PSI. Special thanks goes to Günther Dissertori and Christoph Grab for proofreading parts of my thesis and answering all my questions about experimental particle physics and to Adrian Biland for solving almost all my computer problems.

A very special thanks go to my boyfriend Simon Schwarz for every minute we spent and will spend with and without physics together.

Finally, I would like to thank my parents Theres and Toni Häfliger for always supporting me.

Curriculum vitae

Petra Häfliger

Date and place of birth	13th of July 1976 in Luzern, LU
Nationality	Swiss
Address	Clausiusstrasse 38, 8006 Zürich
Email	petra.haefliger@alumni.ethz.ch

Education

1/2003 – 12/2006	PhD thesis in Theoretical Physics at the Institute for Particle Physics, ETH Zürich and at the Paul Scherrer Institut, Villigen, under supervision of Prof. Dr. F. Pauss and PD Dr. M. Spira about *Associated Higgs Production with Heavy Quarks: SUSY-QCD Corrections and Impact of A_0 on the mSUGRA Parameter Space*
5/2002 – 9/2002	Dipl. Phys. ETH Diploma thesis at the Institute for Particle Physics, ETH Zürich under supervision of Prof. Dr. F. Pauss and PD Dr. M. Spira about *Higgsboson-Zerfall $H \to b\bar{b}$: supersymmetrische QCD-Strahlungskorrekturen* Specifications: Cryptography, Particle Physics
9/1998 – 6/1999	Exchange year at the Università degli Studi di Milano, Italy
6/1996	Schweizerische Eidgenössische Matura, Typus C (mathematical scientific field)
8/1989 – 6/1996	Gymnasium Kantonsschule Alpenquai, Luzern

Professional Experience

1/2003 – 12/2006	Scientific assistant at the Institute for Particle Physics, ETH Zürich, tutor and support of the lecture homepages
10/2002 – 11/2002	Visiting researcher at the Imperial College London
10/1999 – 7/2002	Assistant at the Department of Mathematics, ETH Zürich
10/2000	Design of data bases at SwissOnline AG, Otelfingen
7/1999 – 10/1999	Administration assistance at MAZ · Management auf Zeit AG, Luzern